



UNIVERSIDADE D
COIMBRA

José Carlos Ferreira Sousa

**DEVELOPMENT OF A HIGH-ENERGY
ASTROPHYSICS TRACKER FOR THE
SPACE RIDER ORBITAL MAIDEN FLIGHT**

**Dissertação no âmbito do Mestrado em Engenharia Física
orientada pelo Professor Doutor Rui Miguel Curado da Silva e
pelo Professor Doutor Jorge Manuel Maia Pereira,
apresentada ao Departamento da Física da Faculdade de
Ciências e Tecnologia da Universidade de Coimbra.**

Setembro de 2023



Faculty of Sciences and Technology

UNIVERSITY OF COIMBRA

Development of a High-Energy Astrophysics Tracker for the Space Rider Orbital Maiden Flight

José Carlos Ferreira Sousa

Supervisor:

Rui Curado Silva

(LIP and University of Coimbra)

Co-supervisor:

Jorge Maia Pereira

(LIP and University of Beira Interior)

Thesis submitted to the
University of Coimbra for the degree of
Masters in Engineering Physics

September 2023

Esta cópia da tese é fornecida na condição de que quem a consulta reconhece que os direitos de autor são pertença do autor da tese e da Universidade de Coimbra e que nenhuma citação ou informação obtida a partir dela pode ser publicada sem a referência apropriada.

This copy of the thesis has been supplied on condition that anyone who consults it, is understood to recognize that its copyright rests with its author and with the University of Coimbra that no quotation from the thesis and no information derived from it may be published without proper reference.

The studies presented in this thesis were carried out at the Laboratory of Instrumentation and Experimental Particle Physics at the Physics Department, Faculty of Sciences and Technology, University of Coimbra, Portugal and with the financial support from:

- BIL grant, LIP_C/BIL-3/2022, within the project 'Ciência e Monitorização de Flashes de Raios Gama Terrestres para a Segurança na Aviação' – ref. EXPL/FIS-PAR/0333/2021' from Fundação para a Ciência e Tecnologia;
- BIL grant, LIP_C/BIL-4/2023, within the project 'THOR-SR - TGF and High-energy astrophysics Observatory for gamma-Rays on board the Space Rider' ref. PEA4000141332 from the ESA PRODEX program.



*"Cada um vai brincar à sua maneira, vai jogar e explorar como sabe.
Criar com diversidade para gerar melhor devia ser a regra."*

Fernando Carvalho Rodrigues

Abstract

The detection of gravitational waves (GW) in 2015 by the LIGO facilities gave new strength to the Multimessenger Astrophysics. A novel way of observing the Universe can now be performed by combining several types of messengers: multi wavelength light, neutrinos, cosmic rays and also GW. This is particularly relevant for the high-energy astrophysics domain where the study of the non-thermal universe, e.g., gamma-ray bursts (GRBs), supernovae, physics of neutrons stars and black holes, compact object mergers, active galactic nuclei and so on, has now multiple messengers to help understand the physics behind such objects/events. The mission presented in this dissertation aims to give the Multimessenger Astrophysics another observable, the gamma-ray light polarization in the energy band $100\text{ keV} - 10\text{ MeV}$, an area that has not yet been properly explored. Light polarization can provide information about the emission mechanisms as well as the source magnetic field geometry. In this work, we present the preliminary design of THOR-SR mission which will be on orbit for 2 months, on board the new reusable vehicle from the European Space Agency (ESA), the Space Rider (SR). A concept of operations is presented together with a detailed timeline of operations which take into account strict observation times that allow the mission to detect GRB, monitor the Crab nebula and record Terrestrial Gamma-ray Flashes (TGF), a still to be understood phenomena. A comprehensive in orbit scientific operation plan that ensures the mission achieves its scientific objectives is defined. Also an in-depth description of the payload products is given together with the demonstration of the Gamma-ray and Particle detectors' capabilities. Our study of the expected orbital gamma-ray and particle environment verified that the main mission objectives can be achieved with the data to be downlinked via the SR communication services, despite the limit imposed by the SR team. A preliminary version of the Assembly, Integration, Verification and Testing plan is presented as well as the results of the tests already performed. The tests conducted on the first development model of the detector showcased an energy resolution of $5.97 \pm 0.10\%$ at 511 keV and an intrinsic peak efficiency of $1.6 \pm 0.9\%$ at 511 keV .

Keywords: Space Instrumentation, System Engineering, High-energy Astrophysics, Space Rider, Gamma-ray Polarimetry.

Resumo

A detecção de ondas gravitacionais em 2015 pelas instalações LIGO deu um novo folego à Astrofísica Multimessageira. Pode-se agora observar o Universo de uma nova maneira combinando dados de diferentes observáveis: luz em vários comprimentos de onda, neutrinos, raios cósmicos e também ondas gravitacionais. Isto é particularmente interessante para o domínio da astrofísica de altas energias, onde o estudo do universo não térmico, por exemplo, explosões de raios gama (GRBs), super novas, física da estrelas de neutrões e buracos negros, fusão de objetos compactos, núcleos ativos de galáxias, tem agora à sua disposição múltiplos observáveis para ajudar a entender a física por de trás destes objetos/eventos. A missão apresentada nesta dissertação tem como objetivo dar à Astrofísica Multimessageira ainda outro observável, a polarização da luz de raios gama na banda de energia $100\text{ keV} - 10\text{ MeV}$, uma área que ainda não foi devidamente explorada. A polarização da luz pode fornecer informações sobre os mecanismos de emissão, bem como a geometria do campo magnético da fonte. Nesta dissertação, apresentamos o desenho preliminar da missão THOR-SR, que estará em órbita durante 2 meses a bordo do novo veículo reutilizável da Agência Espacial Europeia (ESA), o Space Rider (SR). Apresentamos o conceito de operações juntamente com uma detalhada sequencia temporal de operações, que leva em consideração tempos de observação estritos que permitem que a missão detete GRBs, monitorize a nebulosa do Caranguejo e registre Flashes de Raios Gama Terrestres (TGFs). É apresentado um plano operacional científico em órbita que garante que a missão atinja seus objetivos científicos. Também é dada uma descrição detalhada dos componentes da experiência, juntamente com a demonstração das capacidades dos detetores de Raios Gama e Partículas. O nosso estudo sobre o ambiente esperado de raios gama e partículas em órbita verificou que os principais objetivos da missão podem ser alcançados com os dados a serem descarregados através dos serviços de comunicação do SR, apesar do limite imposto pela equipa do SR. Uma versão preliminar do plano de Montagem, Integração, Verificação e Teste é apresentada, bem como os resultados dos testes já realizados. Os testes realizados no primeiro modelo de desenvolvimento do detetor mostraram uma resolução de energia de $5.97 \pm 0.10\%$ a 511 keV e uma eficiência de pico intrínseca de $1.6 \pm 0.9\%$ a 511 keV .

Keywords: Instrumentação para o Espaço, Engenharia de Sistemas, Astrofísica das Altas Energias, Space Rider, Polarimetria de Raios Gama

Acknowledgements

First and foremost I want to express gratitude to my supervisors, Professor Rui Curado Silva and Professor Jorge Maia Pereira for giving me this unique opportunity. Its been a challenging journey, the expertise and knowledge transfer that is taking place has been paramount for the growth of space instrumentation for high-energy astrophysics in Coimbra. I am honored to be a part of making the vision come true.

A special thanks to Professor Filomena Santos that went out of her way and helped me proofreading this dissertation. Also to Alexandre Trindade, Prof. Filipa Borges, Afonso Marques and José Escada for their kind welcome to the laboratory.

I would also thank the LIP team, namely Elisabete Neves, Margarida Rodrigues, João Silva, Nuno Carolino, Luís Lopes and Américo Pereira for their availability whenever I decided to poke them.

Would also like to thank SAC/AAC and everyone that is SAC, namely Henrique Neves for being a great Leader and source of inspiration.

Also my Family, Mãe, Pai, Irmão, Avó, agradeço a vossa paciência e compreensão que tiveram durante todo este meu percurso. Muitas vezes coloquei o trabalho em primeiro e não estive presente, é algo que tenho de melhorar. Agradeço do fundo do coração, sem vocês nada disto seria possível.

Last but surely not least to ALL the friends that Coimbra gave me, especially, Miguel Carvalho, Barbara Matos, André Neves, Edson Pontes, Hugo Costa, Rita Barradas, Mario Cristovão, , for all the shared unforgettable/forgettable moments! A special remark to my special friend Ana Sofia for the interesting and colourful voyage through life.

Contents

| | |
|---|--------------|
| Abstract | vii |
| Resumo | ix |
| Acknowledgements | xi |
| List of Figures | xvii |
| List of Tables | xxiii |
| Abbreviated Terms | xxv |
| 1 Introduction | 1 |
| 1.1 Context | 2 |
| 1.1.1 Motivation | 2 |
| 1.1.2 Role in THOR-SR | 2 |
| 1.2 Thesis Overview | 3 |
| 1.3 Author Contributions | 4 |
| 2 High-Energy Astrophysics | 5 |
| 2.1 General Description | 5 |
| 2.2 Gamma-Ray Emission Sources | 6 |
| 2.2.1 Supernova | 6 |
| 2.2.2 Compact Object Collision | 7 |
| 2.3 Emission Mechanisms | 7 |
| 2.4 Gamma-ray Measurement Techniques | 8 |
| 2.5 Charged Particles Interacting with Matter | 11 |
| 2.5.1 Heavy Particles | 11 |
| 2.5.2 Electrons and Positrons | 12 |
| 2.6 Gamma-Ray Polarimetry | 13 |
| 2.6.1 Gamma-ray Polarimetry Measurements | 14 |
| 2.7 Current Gamma-ray Telescopes | 16 |
| 2.7.1 INTEGRAL | 16 |
| 2.7.2 Fermi Gamma-ray Telescope | 17 |
| 2.7.3 POLAR | 19 |
| 2.8 Multimessenger Astrophysics Era | 20 |

| | | |
|----------|---|-----------|
| 3 | THOR-SR Mission | 23 |
| 3.1 | Mission Statement | 23 |
| 3.2 | THOR-SR Design Overview | 24 |
| 3.3 | Organizational Consortium | 26 |
| 3.3.1 | Internal Project organization - WBS | 27 |
| 3.3.2 | Sub-contractors | 30 |
| 3.4 | Space Rider Vehicle | 32 |
| 3.4.1 | Main integration requirements | 34 |
| 3.5 | Requirements | 36 |
| 3.6 | Operations | 37 |
| 3.6.1 | Concept of operations | 37 |
| 3.6.2 | Mission Profile and Timeline | 39 |
| 3.6.3 | Commissioning description | 42 |
| 3.6.4 | Housekeeping Mode description | 44 |
| 3.6.5 | Observational Mode description | 46 |
| 3.6.6 | OBC Science Operations | 48 |
| 3.7 | Function Description | 58 |
| 3.7.1 | Function Definition | 58 |
| 3.8 | Product Description | 58 |
| 3.8.1 | Detector Unit - THOR_DET | 59 |
| 3.8.2 | Gamma Tracker Array - THOR_DET_GAM | 61 |
| 3.8.3 | Particle Detector Array - THOR_DET_PAR | 69 |
| 3.8.4 | OnBoard Computer - THOR_OBC | 70 |
| 3.8.5 | Power Distribution Unit - THOR_PDU | 73 |
| 3.8.6 | Payload Enclosure - THOR_ENC | 80 |
| 3.8.7 | Ground Segment - THOR_GS | 84 |
| 3.9 | Interfaces | 84 |
| 3.9.1 | Internal Electrical Interfaces | 85 |
| 3.10 | Orbital Environment | 87 |
| 3.10.1 | Gamma-ray Environment | 87 |
| 3.10.2 | Electron Environment | 90 |
| 3.10.3 | Proton Environment | 92 |
| 3.11 | Scientific Data Architecture Definition | 95 |
| 3.11.1 | RAW Data | 95 |
| 3.11.2 | Enhanced Pre-Processed Data | 96 |
| 3.11.3 | Scientific Data String Architecture | 97 |
| 3.12 | Budgets | 98 |
| 3.12.1 | Scientific RAW Data Budget | 98 |
| 3.12.2 | Enhanced Pre-Processed Data Budget | 106 |
| 3.12.3 | Scientific Data Budget | 107 |
| 3.12.4 | Data Budget | 109 |
| 3.12.5 | Mass Budget | 109 |
| 3.12.6 | Power Budget | 110 |
| 3.13 | Risk Management | 112 |

| | | |
|----------|---|------------|
| 4 | Assembly, Integration, Verification and Testing | 115 |
| 4.1 | Payload Model Philosophy | 115 |
| 4.1.1 | Payload Level Development Models | 115 |
| 4.2 | Product Level Development Philosophy | 117 |
| 4.2.1 | Detector Unit Development Models | 119 |
| 4.2.2 | PDU Development Models | 122 |
| 4.2.3 | OBC Development Models | 124 |
| 4.2.4 | Enclosure Development Models | 124 |
| 4.3 | Test Descriptions | 125 |
| 4.3.1 | Payload Level Tests | 125 |
| 4.3.2 | Detector Unit Tests | 128 |
| 4.3.3 | PDU Tests | 139 |
| 5 | Conclusions | 141 |
| | References | 145 |
| | Appendix A Function Description | 149 |
| A.1 | Scientific Data Collection - THOR_F_SCI | 149 |
| A.2 | Data Processing - THOR_F_DP | 151 |
| A.3 | Data Storage - THOR_F_DS | 156 |
| A.4 | Power Distribution - THOR_F_PDU | 159 |
| A.5 | Control - THOR_F_CTR | 159 |
| A.6 | Hold Components - THOR_F_STR | 162 |
| A.7 | User Operations Control - THOR_F_OP | 163 |
| | Appendix B List of Requirements | 165 |
| | Appendix C Electrical Interfaces Block Diagram | 191 |
| | Appendix D Connectors' location on THOR products | 193 |
| D.1 | GAM Finger Board - THOR_DET_GAM_RO.x.FB.x | 193 |
| D.2 | GAM Read Out Board - THOR_DET_GAM_RO.x | 194 |
| D.3 | PAR board - THOR_DET_PAR_B.x | 194 |
| D.4 | Onboard Computer Carrier Board - THOR_OBC_CB | 195 |
| D.5 | Power Distribution Unit - THOR_PDU | 195 |
| | Appendix E THOR-SR Gantt Chart | 197 |
| | Appendix F PDR Enclosure design LIP comments | 199 |
| | Appendix G LIP-AST meeting PDR design discussion | 225 |

List of Figures

| | | |
|------|---|----|
| 2.1 | Mechanisms of gamma-ray radiation interacting with matter. Credit: Jonathan Flunger. | 9 |
| 2.2 | Compton scattering diagram | 10 |
| 2.3 | Scattered photon and electron energies as a function of the photon scattering angle. For energy >300 keV the energy of the outgoing photon has a lower limit of around 200 keV. | 10 |
| 2.4 | Total and partial attenuation coefficient as a function of main gamma-ray interaction mechanisms in CdTe versus the incoming gamma-ray photon. The two peaks in the total attenuation are relative to the k-absorption edges of the Cd(27 keV) and Te(32 keV). Credit: Jonathan Flunger | 11 |
| 2.5 | Visual representation of the Compton Scattering taking into account the relation between the direction of the scattered photon and the incoming photon electric field. | 14 |
| 2.6 | A Compton event scattered through a two-layer pixelized polarimeter. | 15 |
| 2.7 | INTEGRAL SPI instrument. | 16 |
| 2.8 | INTEGRAL IBIS instrument. | 17 |
| 2.9 | LAT detector configuration and geometry diagram. | 18 |
| 2.10 | Location of one set of 3xNaI(Tl) 1xBGO detectors. The location of the second BGO detector is on the opposite side. The remainder 9 NaI(Tl) detectors are distributed in sets of 3, diagonally as seen by the blue squares in the figure. | 19 |
| 2.11 | POLAR instrument geometry. | 20 |
| 3.1 | THOR-SR Flight segment simple block diagram showcasing electrical interfaces. | 25 |
| 3.2 | Left: THOR PDR configuration showcasing the hoisting points for assembly purposes, 295x230x163 mm ³ . Right: THOR inside view: colour green is the PDU, in blue the Onboard Computer, red the CdTe and Si detectors and in white the detector's read-out boards. | 25 |
| 3.3 | Diagram showcasing the entities involved in the development of THOR as well as the interfaces. | 26 |
| 3.4 | THOR Work Breakdown Structure. | 27 |
| 3.5 | Showcase the institutions working on THOR. | 30 |
| 3.6 | Diagram showcasing team composition for the development of the DET, ENC and Environmental Tests. | 32 |
| 3.7 | Artist representation of the Space Rider in orbit. Source ³ | 33 |
| 3.8 | P/L possible locations inside the SR vehicle. | 33 |
| 3.9 | Space Rider System ground segment architecture, simplified. | 34 |
| 3.10 | In-flight operation mode of the THOR-SR payload. | 37 |

| | |
|---|----|
| 3.11 THOR-SR operations timeline and major events. | 39 |
| 3.12 Commission Mode concept operation philosophy. | 43 |
| 3.13 Housekeeping Mode concept operation philosophy. | 45 |
| 3.14 Test sub-Mode concept operation philosophy. | 46 |
| 3.15 Observational Mode concept operation philosophy. | 47 |
| 3.16 Debug sub-Mode concept operation philosophy. | 48 |
| 3.17 Scientific data collection flow chart. For a detailed description of the function codes see Appendix A. | 49 |
| 3.18 Factory calibration flow chart. For a detailed description of the function codes see Appendix A | 50 |
| 3.19 Visual representation of the parameters that characterize a proton/heavy particle interaction. | 51 |
| 3.20 Identification and characterization of physics events flow chart. For a detailed description of the function codes see Appendix A | 52 |
| 3.21 Background environment characterization flow chart. For a detailed description of the function codes see Appendix A | 53 |
| 3.22 GRB/TGF identification and characterization flow chart. For a detailed description of the function codes see Appendix A | 54 |
| 3.23 Compton source localization visual representation within CdTe DET geometry. For every Compton recorded an elliptical perimeter of possible gamma-ray source position is created on to a projected plane. The intersection of multiple elliptical projections represents the localization of the source. | 55 |
| 3.24 Illustration of the moving detector geometry projecting elliptical perimeters of possible gamma-ray source positions on to a fixed projected plane over several passes. | 56 |
| 3.25 Gamma-ray source localization flow chart upon receiving attitude data from SR. For a detailed description see Appendix A. | 57 |
| 3.26 THOR Function Tree as defined in ECSS-E-ST-10C Annex H. | 58 |
| 3.27 THOR Product Tree as defined in ECSS-M-ST-10 Annex B. | 59 |
| 3.28 a) Geometric configuration of the THOR_DET_GAM - Gamma Tracker Array, b)The distance between the successive CdTe detector planes (DPs). | 62 |
| 3.29 GAM readout electronics and communications configuration block diagram. | 62 |
| 3.30 Showcase of some physics events on the GAM Tracker Array. Event γ_A showcases a Compton double event where the incoming photon, γ_A^1 , suffers Compton scattering in the first plane and the scattered photon, γ_A^2 , get absorbed by the photoelectric effect on the third plane. Event γ_B is also a Compton double event but within the same DP. Event C showcases a multiple (triple) Compton event, where the scattered primary photon, γ_C^2 , undergoes a second Compton scattering in the third plane that finally gets absorbed by photoelectric effect on the forth plane. The event H^+ showcases a highly energetic proton crossing every plane of the GAM. | 63 |
| 3.31 Data visualization from Timepix3 ASIC. | 64 |

| | | |
|------|---|----|
| 3.32 | Diagram representing a proton interacting with the CdTe (left) and a gamma-ray photon undergoing photoelectric effect (right). The electrons/holes drifts in material due to the electric field applied, being collected in the anode and cathod electrodes, respectively (center). The charge collected on the anode represents the energy deposited in the detector by particle/photon and will be read out by the Timepix3 ASIC. | 65 |
| 3.33 | Charge drift time as a function of the drift distance within a CdTe detector. | 66 |
| 3.34 | Representation of Compton event within the same FB CdTe. For the simultaneity of the γ interactions in the CdTe the electrons trails start the migration to the anode at the same instant. Measuring the time of arrival of each electron cloud/trail, t_1 and t_2 one can get the relative distance Δz at which the events happened. | 67 |
| 3.35 | Timepix3 ASIC pixel schematics | 68 |
| 3.36 | GAM readout board with the representation of the TBD modification. | 69 |
| 3.37 | Particle detectors geometry alongside GAM. | 69 |
| 3.38 | THOR Onboard computer. | 71 |
| 3.39 | ELTON Carrier board selected for the OBC design. Manufacturer: Diamond Systems | 72 |
| 3.40 | Adaptation board to redirect 2x USB2.0 via the PCIe interface. To be developed by LIP. | 73 |
| 3.41 | PDU block diagram representing the design needs. | 73 |
| 3.42 | PDU detailed block diagram. | 75 |
| 3.43 | Detailed PDU housekeeping block diagram. | 75 |
| 3.44 | Left: THOR front view and dimensions. The fixation M6 hole are horizontally spaced by 275mm and vertically space by 210mm. Right: THOR bottom view and dimensions. | 80 |
| 3.45 | Expected shock environment on THOR. | 81 |
| 3.46 | Power connector to be placed on the outside of the enclosure. To receive the 28V from the SR. | 82 |
| 3.47 | Communication connector to be placed on the outside of the enclosure. To secure RS422 electrical interface. | 83 |
| 3.48 | Testing connector to be placed on the outside of the enclosure, to ensure the ETHERNET electrical interface. | 83 |
| 3.49 | Kill switch parallel design. | 84 |
| 3.50 | LIP ground segment block diagram. | 84 |
| 3.51 | Simulated orbit geometry overlapped with globe map. Source SPENVIS. | 87 |
| 3.52 | Photon background flux for a 400km 6° inclination. Up until ± 200 keV Cosmic photons re the predominant ones, whilst from 200keV-100MeV the Albedo photons become the predominant background source. Data collected from the github database ⁴ | 88 |
| 3.53 | Cosmic Photons with 1mm Al attenuation. | 89 |
| 3.54 | THOR orbital exposure to trapped electrons versus orbit position. Source SPENVIS. | 90 |
| 3.55 | Trapped electron integral and differential average flux in the THOR orbit, calculated with SPENVIS platform. | 91 |

| | | |
|------|---|-----|
| 3.56 | THOR orbital electron exposure simulated for 3 days versus the time in orbit, calculated with SPENVIS platform. | 92 |
| 3.57 | THOR orbital exposure to trapped protons versus orbit position. The proton integral flux was calculated using the SPENVIS platform. | 93 |
| 3.58 | Proton Flux for 400km, 6°. Simulated on the SPENVIS platform. | 93 |
| 3.59 | THOR orbital Proton exposure simulated for 3 days versus the time in orbit, calculated with SPENVIS platform. | 94 |
| 3.60 | Photon interaction highlighted in green circle. Event captured with the first detector development model - THOR_DET_DM.1 | 98 |
| 3.61 | Number of activated pixels per event as a function of the incoming photon energy. Credit: Jonathan Flunger | 99 |
| 3.62 | Electron interaction highlighted in green. Event captured with the first detector development model - THOR_DET_DM.1 | 100 |
| 3.63 | Proton interaction highlighted in green. Event captured with the first detector development model - THOR_DET_DM.1 | 102 |
| 3.64 | Maximum possible distance travelled by a proton in the GAM geometry. . . | 103 |
| 3.65 | Geometry of the incident proton beam, CdTe Scenario A. Only one DP presented in the figure for simplicity. | 103 |
| 3.66 | Geometry of the incident proton beam, CdTe Scenario B. Only one DP presented in the figure for simplicity. | 104 |
| 3.67 | Geometry of the incident proton beam, Si Scenario A | 105 |
| 3.68 | Risk Index and magnityde scheme, from ECSS-M-ST-80C. | 113 |
| 3.69 | Risk magnitude designations and proposed actions for individual risks, from ECSS-M-ST-80C. | 113 |
| 4.1 | Product level development flow chart. | 117 |
| 4.2 | Picture of the detector unit first development model, THOR_DET_DM.1. . . | 119 |
| 4.3 | Configuration of the detector unit second development model, THOR_DET_DM.2. | 120 |
| 4.4 | Configuration of the detector unit third development model, THOR_DET_DM.3. | 121 |
| 4.5 | Block diagram of the first development model of the PDU, THOR_PDU_DM.1. | 123 |
| 4.6 | Expected random environment to be applied to THOR interface with the SR base plate , | 126 |
| 4.7 | Expected shock environment to be applied to THOR interface with the SR base plate. The amplitude of shock is expressed in units of gravity acceleration, $g=9.8\text{ m/s}^2$ | 126 |
| 4.8 | EMC environment that THOR shall withstand (right) and emit (left). | 127 |
| 4.9 | Timeline of the pre-integration test. | 128 |
| 4.10 | Calibration curve of the first detector unit development model. Credit: Jonathan Flunger. | 130 |
| 4.11 | Measured energy resolution of the first detector unit development model. Credit: Jonathan Flunger. | 130 |
| 4.12 | Example of two Compton events detected with the preliminary Compton finder algorithm. | 132 |
| 4.13 | Left, example of an electron with 2352keV. Right, example of a proton with 1964keV. | 134 |

| | | |
|------|---|-----|
| 4.14 | Left, example of an alpha with 4595keV. Right, example of a muon with a 2859keV. | 134 |
| 4.15 | Setup in the LIP laboratory. Hot surface in contact with metal table to dissipate the heat. Image credit: Jonathan Flunger. | 135 |
| 4.16 | Test setup at ICNAS, ^{154}Eu | 136 |
| 4.17 | Muon captured, CdTe polarized with -500V. Electron charge drift time $t_{drift} = 44.75ns$ | 137 |
| 4.18 | Set-up available in the LAB. | 138 |
| | | |
| A.1 | This is the ID data format for the Physics Event data. | 157 |
| A.2 | This is the ID data format for the Source event data. | 157 |
| A.3 | This is the Id data format for the Analysis data. | 157 |
| | | |
| C.1 | Detailed Electrical Interfaces block diagram of the THOR P/L. | 192 |
| | | |
| D.1 | Finger Board connector location. | 193 |
| D.2 | GAM RO connector location. | 194 |
| D.3 | Particle detector connector location. | 194 |
| D.4 | OBC Carrier Board connector location. | 195 |
| D.5 | Power Distribution Unit connector location. | 195 |
| | | |
| E.1 | Last updated on September 2023. | 198 |

List of Tables

| | | |
|------|---|-----|
| 3.2 | SR integration driving requirements, PDR status. | 35 |
| 3.4 | Integration to launch phase resource consumption. | 39 |
| 3.6 | Commissioning phase resource consumption. | 40 |
| 3.8 | Observational Phase resource consumption. | 41 |
| 3.9 | Parameters to be sent to the LIP-GS. | 44 |
| 3.11 | Parameters that characterize a Proton/Ion event | 51 |
| 3.13 | GAM main characteristics | 60 |
| 3.15 | PAR main characteristics | 61 |
| 3.16 | CdTe physics characteristics. | 65 |
| 3.17 | Si physics characteristics. | 70 |
| 3.18 | OBC flight model configuration | 71 |
| 3.20 | Radiation hardness tests with the Jetson AGX Xavier. | 72 |
| 3.21 | Low frequency and random environment of THOR. | 81 |
| 3.22 | Electrical interfaces between THOR products. Location of the connector within each product is showcased on Appendix D. | 85 |
| 3.24 | Electrical interface description. | 86 |
| 3.25 | Space Rider expected orbit. | 87 |
| 3.26 | Orbit used on the simulations. | 87 |
| 3.28 | Gamma-ray background estimated for the THOR GAM within the energy range of 100keV – 1MeV. | 90 |
| 3.30 | Electron, $0.04 \text{ MeV} < E_e < 4 \text{ MeV}$, background estimated for the THOR orbit. | 91 |
| 3.32 | Electron, $0.04 \text{ MeV} < E_e < 4 \text{ MeV}$, background estimated for the THOR detectors | 91 |
| 3.33 | Total electron orbital exposure. | 92 |
| 3.35 | Proton background estimated for the THOR orbit. | 94 |
| 3.37 | Proton background estimated for the THOR detectors. | 94 |
| 3.38 | Total proton orbital exposure. | 95 |
| 3.40 | Output of the functions THOR_F_SCI.G and THOR_F_SCI.P. | 95 |
| 3.42 | RAW DATA format to be saved on THOR_MMU. | 96 |
| 3.44 | Enhanced Pre-Processed Proton Data format to be saved on THOR_MMU. | 97 |
| 3.45 | Current design of the THOR scientific data strings. | 97 |
| 3.46 | Orbital gamma-ray scientific RAW data generated by GAM detector. | 99 |
| 3.47 | Characteristics of an electron, $E_{electron} = 4\text{MeV}$, interacting with GAM. | 100 |
| 3.48 | Characteristics of an electron, $E_{electron} = 4\text{MeV}$, interacting with PAR | 101 |
| 3.49 | Orbital Electron Scientific Data generated by each detector. | 101 |
| 3.50 | Characteristics of a proton, $E_{proton} = 300\text{MeV}$, interacting with GAM. | 102 |

| | | |
|------|--|-----|
| 3.51 | Characteristics of a proton, $E_{proton} = 300\text{MeV}$, interacting with PAR. | 102 |
| 3.52 | Maximum possible energy detected per proton interaction. | 103 |
| 3.54 | Orbital Proton Scientific Data generated by each detector, CdTe Scenario A. | 104 |
| 3.56 | Orbital Proton Scientific Data generated by CdTe Scenario B. | 105 |
| 3.58 | Orbital Proton Scientific Data generated by Si Scenario A. | 106 |
| 3.60 | Orbital Proton Scientific Data generated by each detector, Si Scenario B. | 106 |
| 3.61 | Total Orbital Proton Scientific Data generated by each detector. | 106 |
| 3.62 | EPPD Gamma-ray data rate. | 107 |
| 3.63 | EPPD Electron data rate. | 107 |
| 3.64 | EPPD Poton/Ion data rate. | 107 |
| 3.66 | Summary of the RAW Scientific Data generated by THOR_DET. | 108 |
| 3.68 | Summary of the EPPD generated by THOR_DET. | 108 |
| | | |
| 4.1 | Tests to be performed by each development model. | 118 |
| 4.2 | Expected low frequency mechanical environment to be applied to THOR interface with the SR baseplate. The design loads are expressed in units of gravity acceleration, $g=9.8\text{ m/s}^2$ | 126 |
| 4.4 | Radioactive sources used as well as the used peaks on the calibration and energy resolution tests. Source [Bé et al., 2016] | 129 |
| 4.5 | Measured resolution of key energies measured with the first development model of the detector unit, THOR_DET_DM.1. | 131 |
| 4.6 | Detection efficiency measured with the first development model of the detector unit, THOR_DET_DM.1. | 136 |
| | | |
| A.1 | Data type identifier. | 157 |
| A.2 | Data source identifier. | 157 |
| A.3 | Event type identifier. | 158 |

Abbreviated Terms

| | |
|-------------|--|
| ADV | Advacam. |
| AGN | Active Galactic Nuclei. |
| AI | Artificial Intelligence. |
| API | Application Programming Interface. |
| ASIC | Application Specific Integrated Circuit. |
| CB | Carrier Board. |
| CDR | Critical Design Review. |
| CdTe | Cadmium Telluride. |
| CoG | Center of Gravity. |
| COM | Communication. |
| COTS | Component Off the Shelf. |
| CPU | Central Processing Unit. |
| CSDA | Continuous-Slowing-Down Approximation. |
| DAC | Digital to Analogue Converter. |
| DET | Detector. |
| DP | Detector Plane. |
| EME | Electromagnetic Environment. |
| ENC | Payload Enclosure. |
| EPPD | Enhanced Pre-Processed Data. |
| ESA | European Space Agency. |
| ESRF | European Synchrotron Radiation Facility. |
| FB | Finger Board. |
| FEM | Finite Element Model. |
| FoV | Field of View. |
| FPGA | Field Programmable Gate Array. |
| FToA | Fast Time of Arrival. |
| GAM | Gamma Tracker Array. |
| GPU | Graphics Processing Unit. |
| GRB | Gamma-Ray Burst. |
| GW | Gravitational Wave. |
| HK | Housekeeping. |
| HV | High Voltage. |

| | |
|---------------|--|
| I/F | Interface. |
| LEO | Low Earth Orbit. |
| LIP | Laboratório de Instrumentação e Física Experimental de Partículas. |
| MMU | Mass Memory Unit. |
| MPCB | Multi Purpose Cargo Bay. |
| OBC | OnBoard Computer. |
| OBSW | OnBoard Software. |
| P/L | Payload. |
| PAR | Particle Detector Array. |
| PCB | Printed Circuit Board. |
| PDOR | Payload Direct Operation Request. |
| PDR | Preliminary Design Review. |
| PDU | Power Distribution Unit. |
| PGCC | Payload Ground Control Centre. |
| POV | Point of View. |
| PRODEX | PROgramme de Développement d'Expériences scientifiques. |
| REQ | Requirement. |
| RO | Readout Board. |
| SAA | South Atlantic Anomaly. |
| SCI | Scientific. |
| Si | Silicon. |
| SPI | Serial Peripheral Interface. |
| SR | Space Rider. |
| SR-RM | SpaceRider Reentry Module. |
| TBC | To be Confirmed. |
| TBD | To be Done. |
| TC | Telecommand. |
| TGF | Terrestrial Gamma-ray Flash. |
| ToA | Time of Arrival. |
| ToT | Time over Threshold. |
| TRL | Technology Readiness Level. |
| UPOC | User Payloads Operation Centre. |
| VCC | Vehicle Control Centre. |
| WBS | Work Breakdown Structure. |

Chapter 1

Introduction

Recently Astronomy has been subject to exciting new discoveries. In 2015 the first gravitational wave was detected by LIGO facilities which unveiled a new chapter in multimessenger astrophysics [Abbott et al., 2016]. This new chapter provides new and exciting opportunities in this very old discipline. Particularly in high-energy astrophysics where the study of the non-thermal universe, e.g., super novae, physics of neutron stars and black holes, compact object collisions (neutron star - neutron star merger, neutron star - black hole merger and black hole - black hole merger), origin of cosmic rays, has now a new observable to help on the understanding of the physics of such objects/events [Mészáros et al., 2019]. Already this new era in multimessenger astrophysics brought the scientific community a joint detection of GW and Gamma-Ray Burst (GRB) with an arrival coincidence time of just ~ 1.7 seconds [Abbott et al., 2017]. Just based on this fact, some cosmological theories that were trying to justify the rate at which the universe is expanding by modifying general relativity were instantly ruled out [Creminelli and Vernizzi, 2017].

Within the high energy astrophysics, the energy band 100 keV–10 MeV is of particular interest since future instruments may provide gamma-ray light polarization, which is an observable that is not currently measured as in the rest of the light spectrum. Taking advantage of the fact that for this energy band the predominant mechanism of light interacting with matter is Compton scattering, and that the scattered photons new direction depends on the incoming light polarization angle [Lei et al., 1997], dedicated Compton instruments' configurations allow to measure the polarized status of celestial objects' gamma-ray emissions. These can provide the scientific community with gamma-ray polarization measurements of Super Novae remnants (pulsars), Gamma-Ray Burst (GRB), Active Galactic Nuclei (AGN), binary black hole systems, solar flares and Terrestrial Gamma-ray Flash (TGF). This observation parameter will contribute to understand the emission mechanisms, source magnetic field geometries as well as structure of GRBs, as a few examples [Lei et al., 1997, Bellazzini and Muleri, 2010, Baring et al., 2019].

1.1 Context

To date there were only a few missions that performed polarimetric measurements within the 100keV – 10MeV range. The most successful being the POLAR mission that in 2016 confirmed that GRB in fact come polarized [Kole, 2018]. The mission described in this dissertation is a pathfinder to develop future instruments with improved performances to measure cosmic gamma-rays’ polarization.

The Space Instrumentation for Astrophysics (i-Astro) group of the Laboratory of Instrumentation and Experimental Particle Physics (LIP) have been studying and developing different detectors and configurations to provide polarimetric, spectroscopic, time variability and imaging capabilities.

In 2021 i-Astro group had a project approved by the Portuguese Space Agency, THOR-SR, whose objective was to develop a high-energy astrophysics tracker to be integrated on the maiden flight of the Space Rider. This dissertation presents the development status of the payload at the PDR level.

1.1.1 Motivation

Prior involvement in projects¹ within the research field of LIP, specifically the i-Astro group, allowed me to really understand what LIP does. Turns out that the instrumentation developed at LIP meets my long held dream of being part of this machine that its trying to understand it self. Also, the balance between topics such as physics, electronics, space, the universe, programming, management and the fact we are going to observe events that happened billions of years in the past got me hooked to the project.

1.1.2 Role in THOR-SR

Within the project I act as a System Engineer carrying out the following tasks: Perform the necessary function breakdown for the payload. Collaborate with subcontractors to determine expected performance of each product and characteristics of the interfaces. Conceived the payload’s operation concept and monitored resource usage throughout the mission timeline.

Work together with the scientific team to understand the required functions to be implemented on-board in order to achieve the mission objectives. Design the detector geometry taking into account the scientific objectives, their mechanical limitations as well as the assembly process. Perform scientific and housekeeping data characterization as well as their production rates. Develop a detailed on-orbit operations plan for the OBC. Perform the

¹SAC, Stratospolca

selection of a Commercial-Off-The-Shelf (COTS) carrier board suitable for our OBC, considering various requirements (interface and environmental). Despite exploring COTS power distribution units, the need arose for a custom-made unit tailored to our specifications, which I oversaw from conception to execution.

Furthermore, manage interfaces within the payload products as well as with the Space Rider cargo bay, by regularly meeting with the ESA team to ensure seamless integration with the SR vehicle. Devise a development plan strategy for the payload, including comprehensive tests and development stages for each sub-system. Carry out verification and performance tests on the first detector unit development model, by developing Python scripts for its communication via the detector's API as well as develop data processing algorithms.

Extra curricular activities such as, STRATOSPOLCA, POLLUX and ANTAEUS gave me guidance throughout this journey. During the development of the THOR, knowledge in space systems, project management, electronics design and manufacturing, PCB assembly, space system testing, requirements, CAD design (and many others) came in handy. Knowledge developed from the above mentioned extra curricular activities. Summarizing: my role in THOR is to make everything work as intended.

1.2 Thesis Overview

Chapter 1 - Introduction A brief introduction of the scope of the thesis where it is presented the description of the main objectives of the THOR project. Also an explanation of my motivation of being in the project. An overview of my role in the THOR project is presented.

Chapter 2 - High-Energy Astrophysics Provides a brief description of the sources we aim to detect. Also, a theoretical introduction of the physics behind gamma-ray and particle detection is provided. A brief description of the current main telescope missions that operate on the same energy range is provided.

Chapter 3 - THOR-SR Mission A detailed flight operations plan is presented as well as the detailed description of the scientific operations to be carried out by the OBC. A detailed description of the current THOR design is provided. Also, preliminary simulations of the on-orbit environment (gamma-rays, electrons and protons) is presented. These simulations are then used to calculate the maximum expected scientific data that THOR is going to generate in orbit. At the end of the chapter we present some risks that lead to design changes.

Chapter 4 - Assembly, Integration, Verification and Testing In this chapter the development and qualification logic of the payload is presented. The model philosophy

of either the P/L and the products is presented and described. Also, the description of the qualification and validation tests of either the P/L and the products are presented. The validation tests to be performed on the payload products is presented as well as a short description of the scope and rationale. Preliminary results of the test already performed are showcased.

Chapter 5 - Conclusions In this Chapter a brief summary of the major conclusions of the work is presented as well as some actions to be taken in the future.

1.3 Author Contributions

National Oral Communications

- R. M. Curado da Silva, J. M. Maia, José Sousa, P. Póvoa, J. Gonçalves, G. Falcão, A. Neves, M. Abreu, A. Mendonça, J. Flunger, J. Campos, C. Granja, J. Jakubek, L. Marek, F. Castanheira, G. Salgado, M. Moita, 'TGF and High-energy astrophysics Observatory for gamma-Rays on board the Space Rider (THOR-SR)', XXXIII ENNA- Encontro Nacional de Astronomia e Astrofísica, 7-9 September 2023, University of Coimbra, Portugal
- J. Santos, J.Sousa, 'ANTAEUS - Fases do Projeto', Jornadas do Espaço do Laboratório para Órbita, 28 February 2023, University of Beira Interior, Covilhã, Portugal.
- J.Sousa, 'Development of a High-Energy Astrophysics Tracker for a SpaceRider Orbital Flight', Seminários de Engenharia Física, 17 February 2023, University of Coimbra, Coimbra, Portugal.

International Oral Communications

- J.Sousa et al., 'Astrophysical Nanosatellite for Technological Advancement and high-Energy Universe Studies - Workshop Pitch', Fly Your Satellite Design Booster 2022, 7-11 September 2022, ESA-ESTEC, Noordwijk, The Netherlands.

Chapter 2

High-Energy Astrophysics

This chapter is dedicated to introducing the High-Energy Astrophysics domain as well as its implications in other research fields. It gives a brief introduction of the gamma-ray sources in the universe and their non-thermal emission mechanisms. This chapter also presents to the reader some physics principles in order to understand the scope in which the mission THOR will operate. It explains the main mechanisms of how radiation interacts with matter in this energy and gives insight on how one can measure gamma-ray polarization. In the end of the chapter a design description of the INTEGRAL and Fermi telescopes is given, as well as a short description of the mission that made the best gamma-ray polarization measurements to date, the POLAR mission. Finally, the chapter finalizes with an overview of what is the multimessenger astrophysics.

2.1 General Description

High-energy astrophysics is a multidisciplinary field that encompasses many sub-disciplines of physics, including relativistic astrophysics, particle physics, and nuclear physics. At its core, high-energy astrophysics involves the study of large quantities of energy, often associated with relativistic matter, and the rapid release of this energy in events of extreme violence, such as supernovae explosions and the merger of compact objects. These events can sometimes completely destroy the underlying source and result in the emission of high fluxes of gamma-rays. [Murase and Bartos, 2019]

In addition to the study of energy release and emission, high-energy astrophysics also involves the investigation of the interaction of matter and radiation under extreme conditions of superstrong gravity and magnetic fields, such as those found in the vicinity of black holes and neutron stars. These extreme environments offer a unique opportunity to test fundamental theories, such as general relativity, and study physical phenomena that cannot be replicated in the laboratory or even within the solar system.

As an instrumentation and observational science, high-energy astrophysics requires the use of specialized telescopes and instruments, such as X-ray and gamma-ray telescopes, to detect and measure high-energy radiation.

2.2 Gamma-Ray Emission Sources

The universe is home to numerous processes that result in the generation of gamma-rays. In the spectral domain emission processes are mostly non-thermal. Through the examination of massive star explosions and compact object mergers, it is possible to probe complex physics at play. Gamma-rays emitted during these phenomena are an exceptional tool for exploring the boundaries of physics.

2.2.1 Supernova

Stars with a stellar mass of $\geq 8M_{\odot}$ lead to a supernova explosion. When this occurs, the star's interior is comprised of several concentric shells, each representing the remnants of previous burning phases (hydrogen, helium, carbon, neon, oxygen, and silicon). The final burning phase involves the production of iron, and once the iron core reaches a mass of approximately 1.44 solar masses (the Chandrasekhar limit), gravity dominates and weak interaction processes become more relevant and processes such as β decay and electron capture by a proton take over. [Janka et al., 2007].

The gamma-ray burst (GRB) associated with supernovae is connected to the collapse of rapidly rotating massive stars that form a disk accretion. This releases energy, creating ultra-relativistic jets along the rotation axis. These jets of accelerated matter are the source of the GRB and subsequent afterglow across the entire electromagnetic spectrum [Murase and Bartos, 2019, Macfadyen and Woosley, 1999]. Furthermore, analysis of the light curves GRB has enabled their classification into two distinct categories: long and short GRBs. Long GRBs, which have a duration longer than 2 seconds, have been linked to the collapse of massive stars [Branchesi, 2016, Kole et al., 2022].

2.2.1.1 Crab Nebula

The Crab Nebula is the remnant of the supernova SN1054, which was observed and recorded in 1054 A.D. The explosion left behind a rapidly rotating pulsar that emits a continuous wind of magnetized plasma composed of electron-positron pairs. Photon polarization measurements suggest that synchrotron radiation is responsible for the generation of light up to an energy of 100 keV [Tavani et al., 2011]. These synchrotron photons may also interact with relativistic electrons through Inverse Compton scattering.

As the most well-studied object in the universe, the Crab Nebula serves as an excellent calibration source for instruments during orbital observations.

2.2.2 Compact Object Collision

The coalescence of binary systems composed of a neutron star is expected to produce the central engine responsible for powering short gamma-ray bursts (GRBs). These bursts are characterized by brief (less than 2 seconds) and intense flashes of high-energy radiation (keV to MeV), which are released through the accretion of matter onto a black hole or magnetar, surrounded by an accretion disk [Branchesi, 2016].

For instance, the joint detection of GW and GRB transient, GW/GRB170817, confirmed that a neutron star merger produces a short GRB [Burns et al., 2019]. Although there is still much debate regarding the emission mechanism of the GRB it is believed that when two neutron stars approach each other, some of their mass becomes disrupted, forming a disk around the newly formed compact object. The accretion to this newly formed compact object drives a relativistic outflow [Murase and Bartos, 2019]. The possible observation of a short GRB by Fermi-GBM, not yet officially confirmed, in coincidence with a binary black hole merger, GW150914, could be the first hint that BlackHole - BlackHole merger also emits GRB [Murase and Bartos, 2019].

2.3 Emission Mechanisms

Multiple mechanisms contribute to the generation of gamma radiation, with a significant portion being of a non-thermal nature and tied to chaotic events, particularly in the context of intense magnetic field environments.

Compton Scattering

The generation of gamma-ray photons due to the Compton Scattering mechanism always involves the interaction of a photon with an electron. There are two instances of interest: the general Compton Scattering in which a gamma-ray photon collides with an electron, the electron gains kinetic energy and the photon is scattered with lower energy; and the Inverse Compton Scattering in which low energy photons interact with relativistic electrons and the electron transfers some of its kinetic energy to the photon [Knoll, 2010, W.R.Leo, 1994].

Bremsstrahlung

The gamma-ray photon generation by Bremsstrahlung is due to the interaction of charged particles with strong electric fields. Since the Bremsstrahlung cross-section varies with the

inverse square of the particle mass, the particles that are often associated with this process are protons, electrons and positrons [W.R.Leo, 1994].

Synchrotron Emission

The Synchrotron-like emission is the relativist limit of the magneto-Bremsstrahlung radiation. Due to the chaotic environment around the extreme cosmic events, described in section 2.2, some charged particles accelerate to relativistic velocities. As these particles pass a strong magnetic field they are deflected and thus generate photons. This process is more relevant for electrons than for protons as their lighter nature is more prone to deflections [Angelis and Mallamaci, 2018].

Synchrotron emission can also happen inside the GRB jets, as the collisionless shocks formed in the jet may produce sizable magnetic fields with random directions that lead to the creation of polarized photons. [Kole et al., 2022]

Cyclotron Emission

The Cyclotron Emission occurs when a non-relativistic charged particle is accelerated in a magnetic field.

2.4 Gamma-ray Measurement Techniques

Gamma rays interact with matter by three main mechanisms: *photoelectric absorption*, *Compton scattering* and *pair production* [W.R.Leo, 1994], we ignore the coherent scattering mechanism since it does not 'produce' electrons. All of these processes lead to the partial or complete transfer of the photon energy to an electron/positron: either the photon disappears completely (is absorbed) or is scattered through a significant angle.

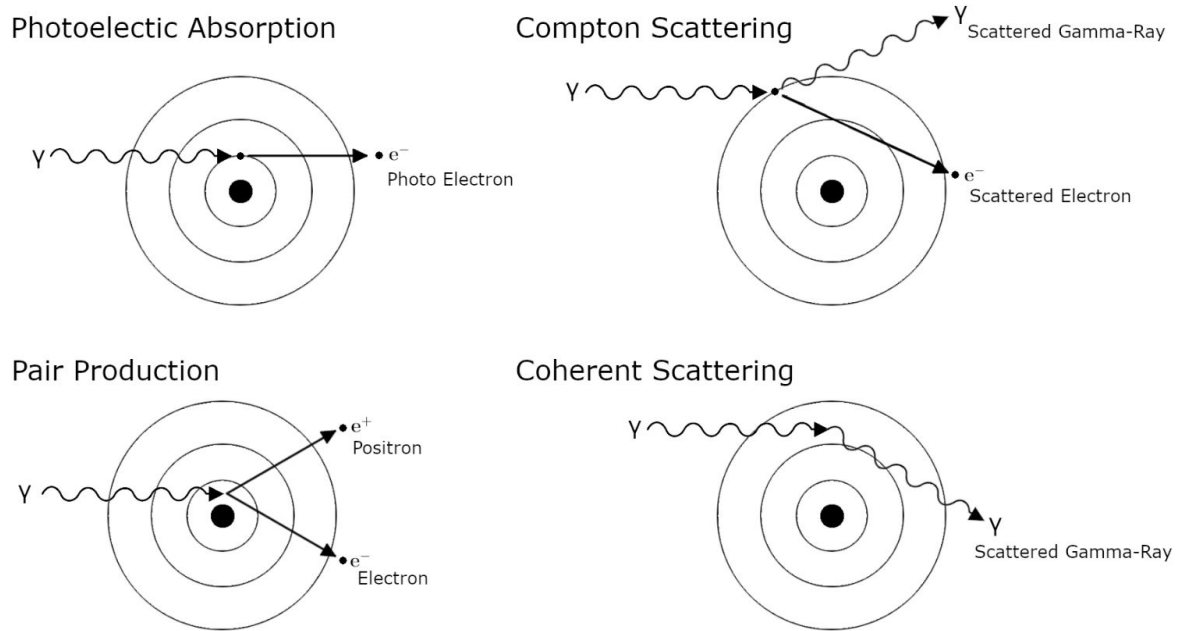


Figure 2.1: Mechanisms of gamma-ray radiation interacting with matter. Credit: Jonathan Flunger.

In the Photoelectric Absorption process, the incoming gamma ray photon is completely absorbed by the atom, with the highest probability of interaction being with the K shell, for which typical binding energies range from few keV for materials with low atomic number (Z) to tens of keV for materials with high Z . This process cannot take place with free electrons. The ejected electron carries off the excess of the incoming photon's energy,

$$E_e = E_\gamma - E_b \quad (2.1)$$

where E_e is the energy of the ejected electron, E_γ the energy of the incoming photon and E_b the binding energy of the electron in the atom, see Figure 2.1. Upon electron emission the unpopulated shell can be repopulated by either free electrons or electrons from other shells more external. As the electrons fall into this lower energy state the excess of energy can be released in the form of characteristic X-ray photons, or in the ejection of electron from the outermost shells (Auger electrons). The escape of this x-ray is known as the fluorescence. The fluorescence has very distinct energy lines as one can see in Figure 2.4.

The Compton Scattering takes place between an incoming gamma-ray photon and an electron present in the target material. The photon transfers a portion of its energy to the electron and is deflected through an angle of θ with respect to its original direction.

The deflection angle θ is related to the energy lost by the incoming photon, as eq.2.2 shows,

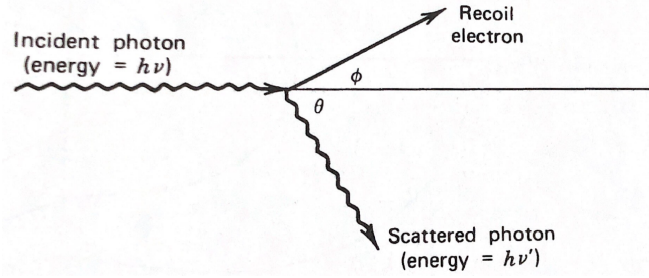


Figure 2.2: Compton scattering diagram

$$E' = \frac{E}{1 + \frac{E}{m_0c^2}(1 - \cos\theta)} \tag{2.2}$$

where E' is the energy of the outgoing photon, E the energy of the incoming photon, m_0c^2 the rest-mass energy of the electron (0.511 MeV). Figure 2.3 showcases the behaviour of the Equation 2.2.

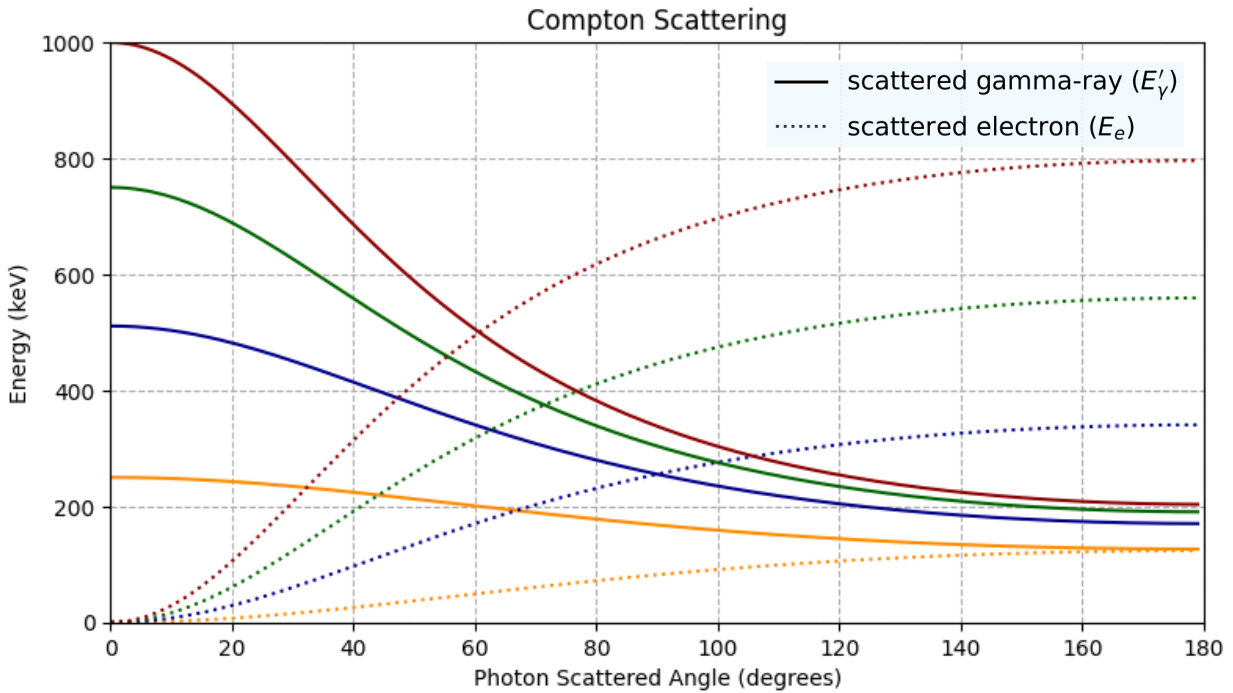


Figure 2.3: Scattered photon and electron energies as a function of the photon scattering angle. For energy >300 keV the energy of the outgoing photon has a lower limit of around 200 keV.

The Pair Production mechanism is predominantly confined to high-energy gamma-rays since it only becomes energetically possible if the incoming gamma-ray equals or exceeds $2m_0c^2$ (1.022 MeV). This process takes place predominantly in the coulomb field of a nucleus where the gamma-ray photon disappears originating an electron-positron pair. In case the energy of the incoming photon is greater than 1.022 MeV the extra energy is converted to kinetic energy distributed between the positron and the electron. It is interesting to note that

the positron after slowing down in the medium, annihilate with an electron which creates two secondary photons emitted at 180° , each with 511 keV .

The probability of these three mechanisms is dependent on the incident photon energy and the material's atomic number (Z). Figure 2.4 showcases the absorption mechanisms applied to the CdTe material. The two peaks in the graph represent the K-absorption edges of both Cadmium (27 keV) and Tellurium (32 keV).

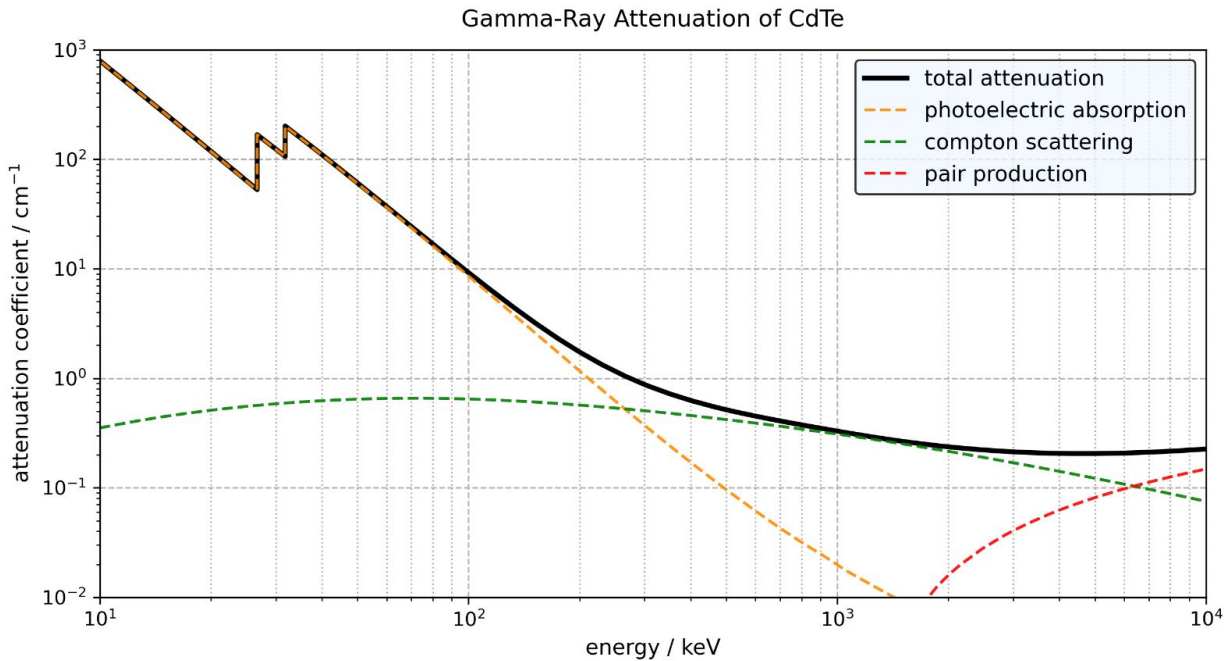


Figure 2.4: Total and partial attenuation coefficient as a function of main gamma-ray interaction mechanisms in CdTe versus the incoming gamma-ray photon. The two peaks in the total attenuation are relative to the k-absorption edges of the Cd(27 keV) and Te(32 keV). Credit: Jonathan Flunger

2.5 Charged Particles Interacting with Matter

2.5.1 Heavy Particles

Heavy charged particles, e.g.. protons, alpha particles, ions, when travelling through matter mainly interact with the Coulomb forces between their positive charge and the negative charge of the electrons present in the material. Interactions with the nuclei are also possible (Rutherford scattering) but such events occur very rarely and don't represent significant importance on the mean path of the charged particle within the medium. These interactions are typically, for each material, described by the *Stopping Power* which represents the energy loss for a particle within a material divided by the corresponding differential path length, expressed in mass thickness units MeVcm^2/g [Knoll, 2010].

$$-\frac{dE}{dx} = \frac{4\pi e^4 z^2}{m_0 v^2} N Z \left[\ln \frac{2m_0 v^2}{I} - \ln \left(1 - \frac{v^2}{c^2} \right) - \frac{v^2}{c^2} \right] \quad (2.3)$$

In the Equation 2.3 v is the particle velocity, z the charge of the incoming particle, N the number density of the absorber atoms, Z is the atomic number, m_0 is the electron rest mass, e the electron charge and I represents the average excitation and ionization potential of the absorber. The *Beth* formula, 2.3 showcases that for materials with a higher atomic number a particle will deposit its energy in the medium at a higher rate, which in turn results on a lower range inside the material. Also, for different charged particles, for instances protons $z_{proton} = +1$ and alpha $z_{alpha} = +2$, the rate at which the alpha particle losses energy to the medium is 4x greater than for protons. Also it is important to note that for a highly energetic particle, e.g. proton 300 MeV, its path within a material is mostly straight because, as discussed earlier, the proton mainly interacts with the Coulomb forces of the electrons. As the mass of the proton is way greater than of the electrons, the proton suffers minimal scattering effects.

2.5.2 Electrons and Positrons

Like heavy particles, electrons and positrons¹ also interact with the Coulomb forces from the electrons on the material. In this case, as the mass of the interacting particle is the same as the mass of the orbiting electrons the incoming particles suffer deviations when traveling within the material. Also, the electrons and positrons may also interact with the nuclei which can abruptly change the electron direction (due to different charge and difference on mass). Because of these two mechanisms *Beth* derived two equations to describe these mechanisms.

$$-\left(\frac{dE}{dx}\right)_c = \frac{2\pi e^4 N Z}{m_0 v^2} \left(\ln \frac{m_0 v^2 E}{2I^2(1-\beta^2)} - (\ln 2)(2\sqrt{1-\beta^2}-1+\beta^2) + (1-\beta^2) + \frac{1}{8}(1-\sqrt{1-\beta^2})^2 \right) \quad (2.4)$$

Where the symbols have the same meaning as in 2.3 and $\beta = v/c$.

$$-\left(\frac{dE}{dx}\right)_r = \frac{NEZ(Z+1)e^4}{137m_0^2c^4} \left(4\ln \frac{2E}{m_0c^2} - \frac{4}{3} \right) \quad (2.5)$$

Equation 2.4 is relative to the Coulomb interactions with the atomic electrons and the equation 2.5 is relative to the interactions with the nuclei electric field, *bremstrahlung* (radiative process). The total linear stopping power for the electrons/positrons is then:

¹The only difference between electrons and positrons is the charge values. $z_{electron} = -1$ while $z_{positron} = +1$.

$$\frac{dE}{dx} = \left(\frac{dE}{dx}\right)_c + \left(\frac{dE}{dx}\right)_r \quad (2.6)$$

2.6 Gamma-Ray Polarimetry

Polarization is a property of electromagnetic waves that describes the relative oscillation orientation of the electric and magnetic field of the photon. Measuring and analysis GRBs' polarization might greatly contribute to understand the mechanisms responsible for such emissions [Kole et al., 2022]. Although light can have several types of polarization such as Linear polarization, Circular polarization and Elliptical polarization, with the current space instrumentation it is only possible to detect linear polarization in the gamma-ray domain. Therefore linear polarization will be, from here on referred to as "polarization".

The measurement of the relative number of photons polarized in the same direction within a given photon flux is related to the conditions present when the gamma-ray jet beam were generated. The measurement of this property gives information about the magnitude and orientation of the magnetic fields acting on the source and through which information can be taken [Toma et al., 2009]. If, for example, a gamma-ray jet is found to be polarized one can infer the presence of a strong magnetic field acting on the emission mechanism, being the emission characterized by synchrotron emission. On the other hand, if the gamma-ray jet is found not to be polarized one can infer that magnetic fields have not played an important role in the process and therefore one can restrict the emission mechanism to inverse-Compton scattering process [Kole et al., 2022]

The parameters related to the polarization measurements that one must take into account are the Polarization Degree (PD), defined as the percentage of the gamma-rays polarized in a non-random direction, and the Polarization Angle (PA), the preferred angle of the polarization vectors of the gamma-rays as measured against the north celestial pole.

Several instruments have been built with the objective of detecting some properties of the incoming gamma-rays, such as the spectrum, source localization and time of arrival. Missions such as the International Gamma-Ray Astrophysics Laboratory (INTEGRAL), Fermi Gamma-ray Space Telescope and the Compton Gamma-ray Observatory (CGRO) were the first big missions to achieve these objectives. However, they were not designed to measure polarization. Even though INTEGRAL was not designed to perform polarimetry, after its deployment in orbit, limited polarimetric measurements were possible thanks to extensive simulation work combined with observational data.

In recent years efforts have been made to develop space instrumentation to perform some polarimetric measurements of the strongest gamma-ray emitters in the sky, GRB, active pulsars (crab neutrons star pulsar). Among those, one can mention the POLAR payload

launched in 2016 on the Chinese module Tiangong2, the AstroSAT-CZTI launched in 2015 and the Gamma-ray Burst Polarimeter (GAP) onboard IKAROS.

2.6.1 Gamma-ray Polarimetry Measurements

Gamma-ray polarimetry measurements rely on the Compton scattering, photons' energy within the 100 keV–10 MeV range. The photons' electric field orientation is related to the scattered photon direction. Gamma-ray polarimetry measurements don't allow a measurement of the polarization of each individual photon, but only of a cumulative flux of detected photons, and therefore determine the PD and PA. Compton scattering follows the Klein-Nishina angular differential cross section which is dependent of the incoming photons polarization.

$$\frac{d\sigma}{d\Omega} = \frac{r_0^2}{2} \left(\frac{E'}{E} \right)^2 \left[\frac{E'}{E} + \frac{E}{E'} - 2\sin^2\theta\cos^2\varphi \right] \quad (2.7)$$

In the equation $r_0 = 2.818 \times 10^{-13} \text{cm}$ which is the classic electron radius, E is the energy of the incoming photon, E' the energy of the outgoing photon, φ is the angle between the scattering plane (defined by the incoming and outgoing photon) and the polarisation plane of the incident photon, and the θ is the photon scattering angle defined on the equation 2.2.

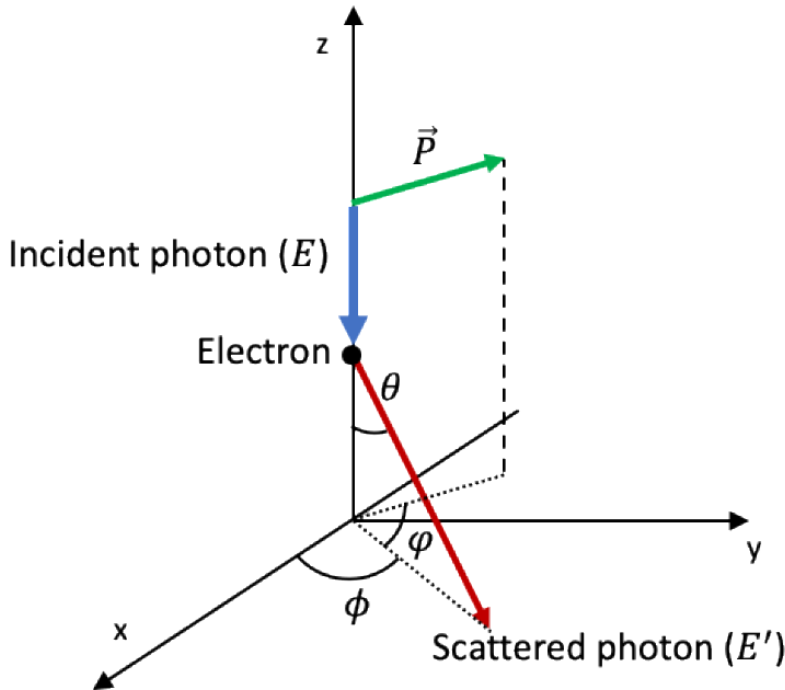


Figure 2.5: Visual representation of the Compton Scattering taking into account the relation between the direction of the scattered photon and the incoming photon electric field [Moita, 2019].

Analysing Equation 2.7 one can see that the cross-section has a maximum value for

photons scattered at an azimuthal angle of $\varphi = \frac{\pi}{2}$. For an azimuthal angle = 0, the cross-section reaches a minimum. Thus, fixing all the parameters in Equation 2.7, an asymmetry can be detected by modulating the planar angular distribution, ϕ , that in turn is related to the modulation of the φ .

Depending on the detector's geometry one can have access to different θ values and therefore have more precise polarimetric measurements.

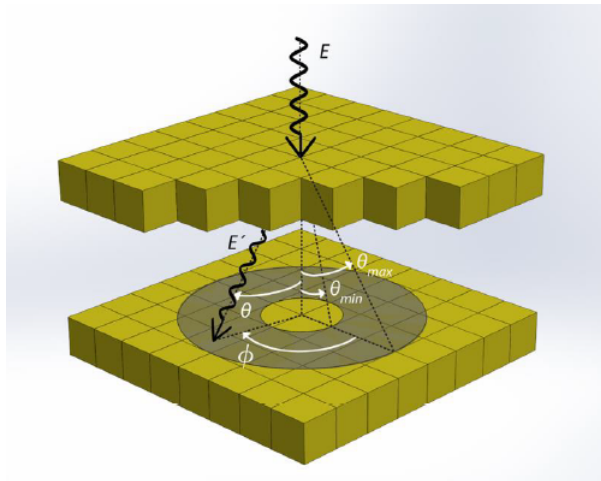


Figure 2.6: A Compton event scattered through a two-layer pixelized polarimeter. Adapted from [Moita, 2019].

The polarimetric performance of an instrument can be evaluated taking into account two parameters which are Minimum Detectable Polarization (MDP) and the modulation factor (Q_{100}) for a 100% polarized source. In general, the modulation factor Q is a useful parameter to evaluate the performance of a scattering polarimeter which gives us a measure of how the instrument sees the modulation in the double-event azimuthal angular distribution around a central irradiated pixel, expressed as [Caroli et al., 2018]:

$$Q = \frac{N_{\parallel} - N_{\perp}}{N_{\parallel} + N_{\perp}} \quad (2.8)$$

where N_{\parallel} and N_{\perp} are the numbers of double-events integrated over the orthogonal directions of a planar detector. In case the irradiation beam is 100% polarized its called the Q_{100} .

The MDP metric provides the polarimetric sensitivity of an instrument for a certain celestial object and under a certain background, quantifying the lowest linear polarization that can be obtained for a certain observation time. The $MDP_{99\%}$ gives a measure, with 99% confidence level, of the minimum detectable polarization fraction for a gamma-ray source; for instance if the reconstructed polarization fraction is equal to the MDP value, then there is only a 1% probability that it comes from statistical fluctuations and not from a real polarized incident beam. It is described as:

$$MDP_{99\%} = \frac{4.29}{S_F Q_{100} \epsilon A} \sqrt{\frac{S_F \epsilon A + B}{\Delta T}} \quad (2.9)$$

where S_F is the source flux (photons/s/cm²), ϵ is the double event detection efficiency, A the detection area in cm², B the background count rate (counts/s) and ΔT (s) is the observational effective time.

2.7 Current Gamma-ray Telescopes

2.7.1 INTEGRAL

The European Space Agency's INTEGRAL (International Gamma-Ray Astrophysics Laboratory) observatory was launched on October 17, 2002 from Baikonur, Kazakhstan. INTEGRAL was designed to observe the gamma-ray sky in the 15keV – 10MeV energy range. The telescope instrumentation have an energy resolution of 2keV @ 1MeV and performs imaging with a resolution of 12'. The Scientific payload consists of two main gamma-ray instruments: the Spectrometer SPI and the Imager IBIS.

The SPI is composed of an array of 19 hexagonal Germanium detectors that, in order to reduce leakage currents and the electronic noise has to work with an operation temperature of 85K. The total geometric detection area is of 500 cm². Above the detector is located a mask that gives the detector a clear FOV of 16° with a resolution of 2°.

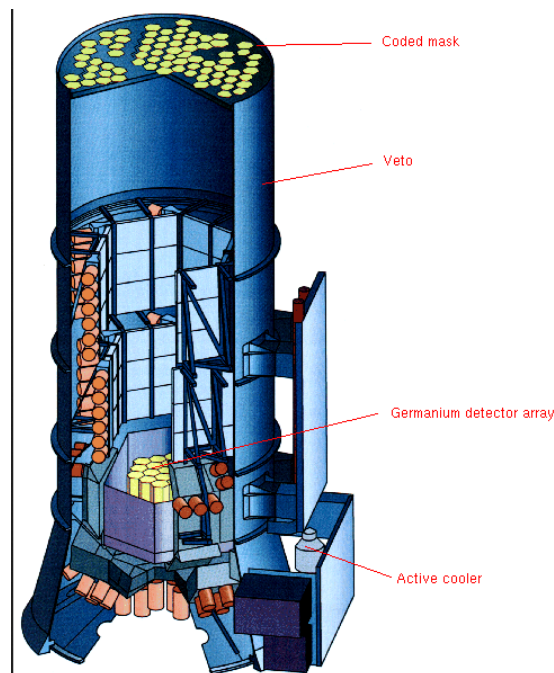


Figure 2.7: INTEGRAL SPI instrument. Adapted from ².

The IBIS imager is composed of two detection planes. The top one composed of a pixelated ($4 \times 4 \times 2 \text{ mm}^3$) cadmium-telluride (CdTe) semiconductor matrix with a total detection area of 2600 cm^2 . The bottom one made of a pixelated ($9 \times 9 \times 30 \text{ mm}^3$) cesium iodide (CsI) matrix with a 3100 cm^2 of detection area. The two-layers are separated by 94 mm and allows photons to be 3D-tracked (Compton), giving the INTEGRAL telescope photon traceability thus revealing the photon's source localization as well as polarimetry capabilities.

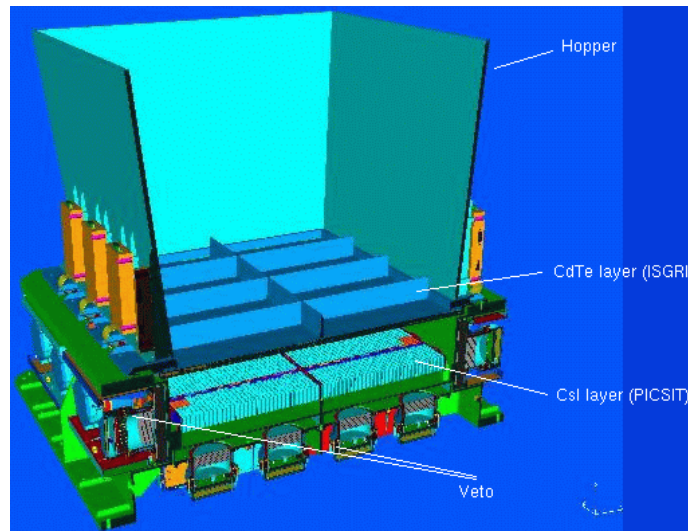


Figure 2.8: INTEGRAL IBIS instrument. Adapted from ².

The telescope was deployed into a geosynchronous, highly eccentric orbit, with a perigee of 9000 km and apogee of 154000 km , which enables extended periods of continuous observation, up to 90% payload availability, with minimal background noise due to the trapped radiation near the Earth.

The telescope was designed to have a nominal lifetime of 2 years but it is still working as of today. [Winkler, 1998]

2.7.2 Fermi Gamma-ray Telescope

The Fermi Gamma-ray Space Telescope was launched in June of 2008 with the objective to monitor the gamma-ray sky in the $8 \text{ keV} - 300 \text{ GeV}$ energy range. It was launched into a circular low earth orbit (LEO) with an inclination of 25.6° and altitude of 565 km . The sensitivity range is split into two main instruments, The Large Area Telescope (LAT), which covers the energy range from 20 MeV to 300 GeV , and the Gamma-ray Burst Monitor (GBM), which covers the complementary energy range $8 \text{ keV} - 40 \text{ MeV}$.

The Large Area Telescope (LAT) consists of three detector subsystems:

²<https://www.cosmos.esa.int/web/integral/instruments>

Tracker/convertor (TKR): 18 layers of silicon-strip detectors (SSD) with a total area of 70m^2 . The main purpose is to measure the direction of incident particles/photons. The underlying detection mechanism is pair-production.

Calorimeter (CAL): composed of a 8 layer CsI(Tl) scintillation crystal (1536 individual crystals) that provides imaging capabilities as well as energy measurements. The scintillator crystal converts incoming radiation into lower energy light, proportional to the incoming photon's energy. The light is then detected with photodiodes.

Anti-coincidence detector (ACD): composed by a plastic scintillator that surrounds the TKR in order to ensure background rejection of cosmic rays. It was designed to detect cosmic rays and not gamma rays and does a very good job at it having over 99% of rejection efficiency.

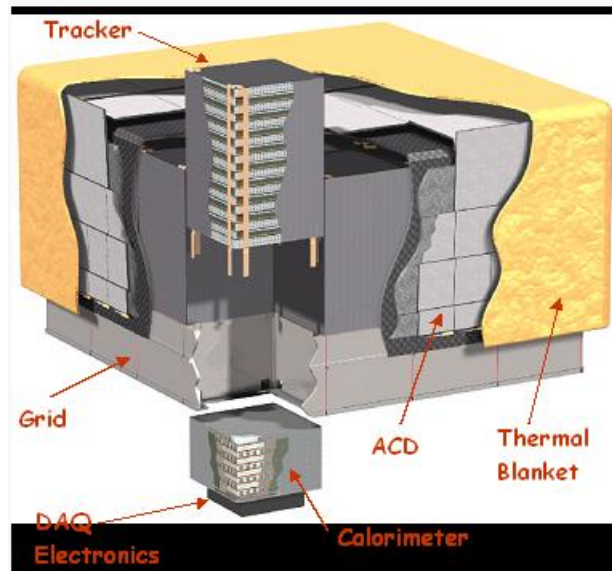


Figure 2.9: LAT detector configuration and geometry diagram.

Using the LAT's 3 instruments one can differentiate source events from background. For instances if an event is both detected in the ACD, TKR and CAL (within a coincidence time window) one can assume it is from a particle, and depending on the energy deposited on each detector (dE/dx) and the particle path (which crystals are activated) one can differentiate the type of particle and if it is from a Cosmic source (particle with very high energy) or from trapped particles (usually don't arrive to the CAL). Combining these factors, coincidence time, energy deposited while travelling in the detector, spacial distribution of interactions (on which crystal the particle interacted) and what detectors the event activated one can characterize the events detected.

The Gamma-ray Burst Monitor (GBM) is composed of two subsystems:

The first one has 12 thin NaI(Tl) plates which are sensitive in the energy range between 8keV and 1MeV . Each NaI(Tl) detector is composed of a cylindrical crystal disk with a

diameter of 12.7cm and 1.27cm thickness.

The second one is composed of 2 cylindrical BGO scintillator detectors which detect gamma-rays between 150keV and 40MeV . Each detector has 12.7cm of diameter and 12.7cm length.

Both subsystems are connected to photomultiplier tubes [McEnery et al., 2012].

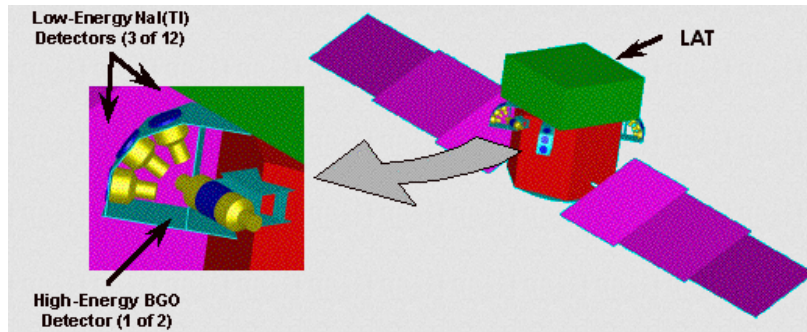


Figure 2.10: Location of one set of 3xNaI(Tl) 1xBGO detectors. The location of the second BGO detector is on the opposite side. The remainder 9 NaI(Tl) detectors are distributed in sets of 3, diagonally as seen by the blue squares in the figure.

The combination of the FOV, geometrical distribution and orientation of the NaI(Tl) and the BGO detectors, allows the Fermi telescope to have 9.5 sr of FOV².

2.7.3 POLAR

The POLAR mission, launched in 2016 on the Chinese Tiangong 2 space laboratory had the objective of measuring light polarization of GRB. To do so the detector was sensitive to the $50\text{keV} - 500\text{keV}$ energy range and relied on Compton scattering to perform polarization measurements. The detector was composed of 1600 plastic scintillators, each having $5.8 \times 5.8 \times 176\text{ mm}^3$ of dimension, resulting on 300cm^2 geometrical area. The generated light signals are read in groups of 64 scintillators by 25 Multi-Anode PhotoMultiplier Tubes. [Kole, 2018] This configuration gives a high detection efficiency but when performing Compton reconstruction it assumes the scattering angle is always 90° . This assumption induces errors on the PA and PD calculations, yet the POLAR mission has the best measured PA's and PD's of GRB's until this date.

²<https://gammaray.nsstc.nasa.gov/gbm/instrument/>

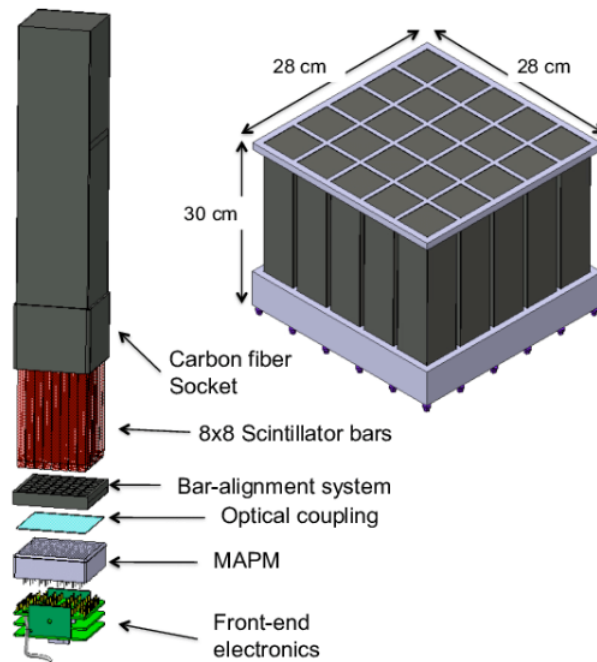


Figure 2.11: POLAR instrument geometry [Hulsman et al., 2021].

The POLAR mission was active for 6 months and took polarimetry measurements of 55 GRB allowing the confirmation that GRB, in fact, come polarized. From the 55 GRB measured, 4 were classified as short GRBs, and can therefore likely be associated to Black-Hole Neutron Star mergers. These 4 GRBs were GRB170101A, GRB170127C, GRB170206A and GRB170305A. Out of this four, the brightest one was GRB170206A, which allowed to produce a measurement of PD of $13.5^{+7.5}_{-8.6}\%$, whereas GRB170305A was an order of magnitude weaker and only allowed to provide an upper limit for the PD of around 65% [Kole et al., 2022].

2.8 Multimessenger Astrophysics Era

Until recent decades astrophysics was limited to the observation of electromagnetic waves (EM). However, the discovery of astrophysical neutrinos from the SN1987, [Hirata et al., 1987], the scientific community have put an effort on building sophisticated detectors to detect, not only neutrinos, but gravitational waves and cosmic rays which can all be generated from the same astrophysical events. Astrophysics has now at its disposal the direct detection of the four fundamental forces to study the distant Universe (electromagnetic force, gravity, weak and strong nuclear forces) [Mészáros et al., 2019]. The joint observation of two or more observables from the same source is considered a multimessenger astrophysics observation. Large-scale international joint efforts have been made by the scientific community united, be able to study the chaotic universe.

Among these we may refer the ICECUBE neutrino detector, a cubic-kilometre detector located at the South Pole and the ANTARES neutrino detector, in the Mediterranean. Scientists can detect emissions of extragalactic neutrinos. As an example, we have IceCube-170922A emitted by the TXS 0506+056 AGN (Active Galactic Nuclei) [Aartsen et al., 2018] which lead to follow-up observations on different wavelengths, in particular by the Chandra Telescope (X-ray) and the Hubble Telescope (visible).

The LIGO gravitational wave observatory in the United States lead to the first detection of a GW in 2015 [Abbott et al., 2016]. The addition of the VIRGO observatory lead to the detection of the neutron star merger GW170817 in 2017 which became the first joint detection of a GW transient and a GRB. The optical kilonova emission of the merger was discovered within less than 11 hours of the event, initially detected by the Swift Telescope. However, it was observed that the X-ray and radio emission from the GRB afterglow was only detected with a substantial delay, with the Chandra X-ray Observatory detecting X-ray emission 9 days after the merger and the Jansky Very Large Array detecting radio emission 16 days post-merger [Murase and Bartos, 2019]. There is also the prospect of the future of a space-based system for gravitational waves, the LISA observatory to be launched in 2037. In 2015 it was launched the LISA pathfinder mission whose scientific objectives were to test future technologies for the next generation of space-based gravitational wave detection [Armano et al., 2015].

The Pierre Auger Observatory is an international effort to cover a 3000 km² with detectors to measure the result of the cosmic-rays air showers produced by the interaction of high-energy cosmic rays with atoms in the atmosphere [Kampert et al., 2019].

Chapter 3

THOR-SR Mission

This chapter is dedicated to the current design description of the mission THOR. Here the reader can find the mission objectives as well as the description of how we intend to achieve them. The consortium that is involved on the development of THOR is presented along with their responsibilities in the project. A short description of the vehicle that is going to deploy THOR in orbit is given, along with the main requirements that THOR shall be compliant with in order to be integrated in the space vehicle. The mission concept of operations is presented, as well as a detailed description of the scientific operations to be performed on orbit. A detailed analysis of the expected orbital environment (photon and particle flux) is presented as well as its impacts on the scientific data generated on orbit. Also, a detailed description of each of the flight segment products is given with an emphasis on the scientific capabilities of the gamma-ray detector. In the end of the chapter the data, mass and power budget is presented as well as the risk matrix.

3.1 Mission Statement

TGF and **H**igh-energy astrophysics **O**bservatory for gamma-**R**ays on-board **S**pace **R**ider, shortly THOR-SR, is a pathfinder mission developed by the iAstro group at Laboratório de Instrumentação e Física Experimental de Partículas (LIP) Coimbra to be launched on the maiden flight of the Space Rider, the ESA new reusable shuttle. THOR aims to address the high-energy astrophysics domain as well as space weather and Terrestrial Gamma-ray Flash (TGF) science. The mission aims to be a proof of concept to showcase the potential of a high density pixel detector to study gamma-ray polarimetric properties of celestial gamma-ray sources. THOR focuses on the the 100keV to 1MeV energy range and performs spectroscopy, time variability measurements, imaging and polarimetry of continuum and transient gamma-ray sources (e.g. Crab Nebula pulsar, GRBs, solar flares).

Additionally it will monitor TGF emissions from Earth and the space radiation envi-

ronment in LEO. The SR program from ESA provides a platform to test the operation of scientific instruments in space at the highest TRL's (> 7) up to 2 months. THOR has the following scientific objectives:

1. High-energy astrophysics: spectroscopy, imaging, polarimetry and time variability of the most intense gamma-ray sources in the sky (Crab Nebula and GRB). An instrument operating in all-sky mode as a polarimeter will be a premiere in a space mission;
2. Terrestrial Gamma-ray Flash (TGF) science: record TGF's emissions (spectroscopy, imaging and time variability) to evaluate the potential of CdTe pixelated detector as a TGF monitor. The ultimate goal is the development of a commercial product for aviation safety to alert and assess the risks associated with TGF emissions for passengers and crew members;
3. Space radiation in Low Earth Orbit (LEO) and space weather: to record protons and electrons around the Van Allen belts, and the protons from solar proton events. Study of the orbital environment (radiation and temperature) effects on the performance of CdTe detectors for high-energy astrophysics telescopes' detection planes, with the goal of projecting future telescope solutions that provide better radiation hardness.

3.2 THOR-SR Design Overview

THOR is composed of four main products that form of the space segment: Detector Unit; Onboard Computer; Power Distribution Unit and Enclosure, as well as two products that are part of the ground segment: Ground Server; Ground support Equipment.

Detector Unit: To carry out the scientific measurements that allows the achievement of the scientific objectives. Composed of 2 units, the CdTe Gamma-ray Tracker Array and the Si Particle Detector Array.

Onboard Computer: To readout the scientific measurements from the Detector Unit and manage the scientific data. To monitor the housekeeping data from DET and PDU and manage the operations. Communicate with THOR_GS via SR_MMU, send SCI and HK data as well as P/L health status.

Power Distribution Unit: To receive the power from space rider and convert it to usable voltage levels that THOR products require to operate.

Enclosure: To hold THOR products taking into account the mechanical environment characteristics of the launch phase. Also, it ensures that the heat generated by the P/L electronics is transferred, via conduction, to the SR base plate.

Ground Server: To receive and monitor the SCI and HK data sent by the OBC via the SR ground segment. Surveys THOR behaviour.

Ground Support Equipment: To test all aspects of operation and performance of THOR on ground. It can be electronic devices, mounting structures or support equipment for ground tests.

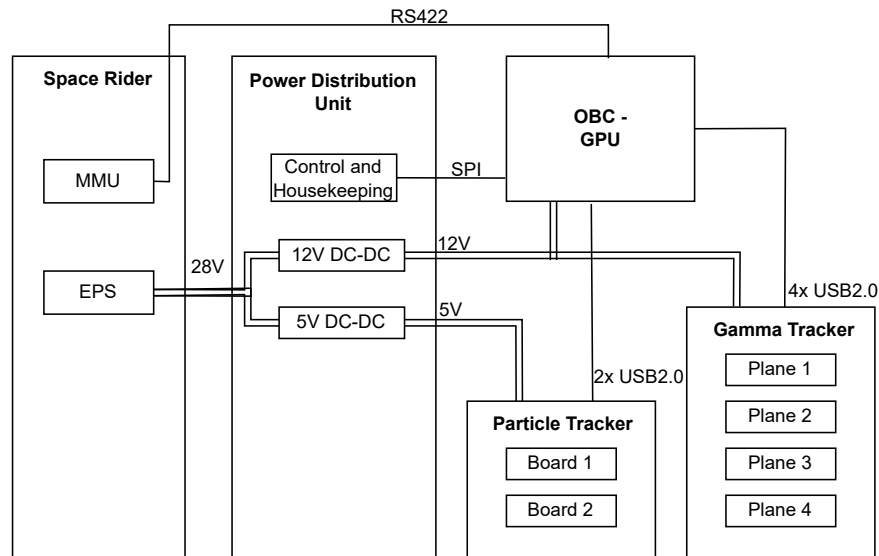


Figure 3.1: THOR-SR Flight segment simple block diagram showcasing electrical interfaces.

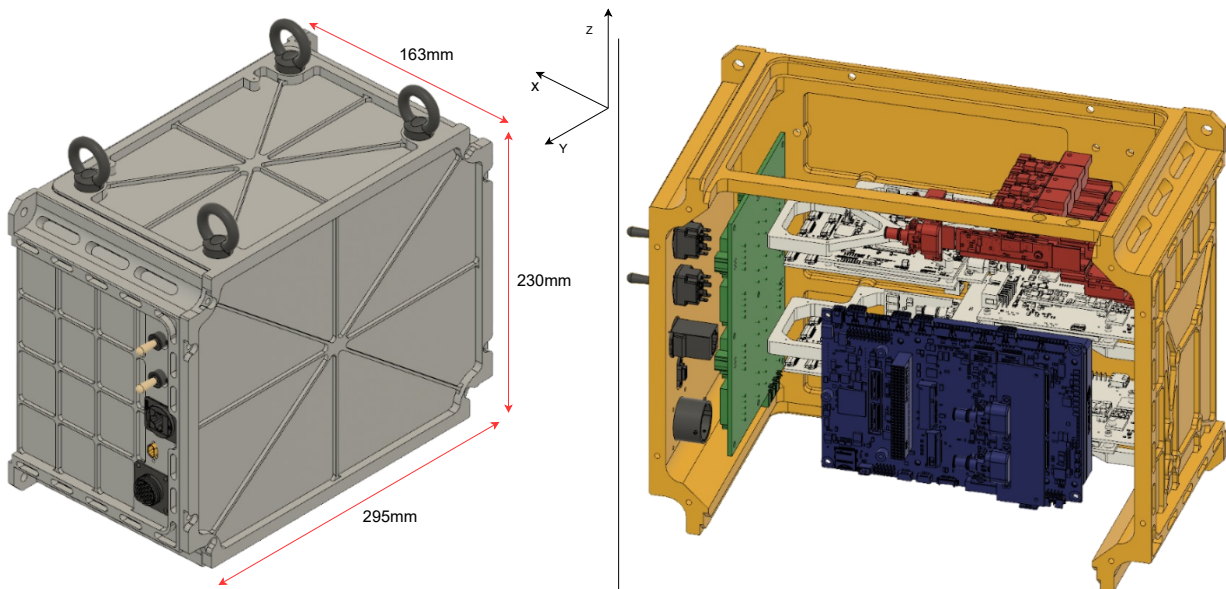


Figure 3.2: Left: THOR PDR configuration showcasing the hoisting points for assembly purposes, 295x230x163 mm³. Right: THOR inside view: colour green is the PDU, in blue the Onboard Computer, red the CdTe and Si detectors and in white the detector's read-out boards.

3.3 Organizational Consortium

The THOR-SR project is led by LIP iAstro group and receives financial support from PRODEX-ESA, which in turn is funded by the Portuguese Space Agency. To meet specific project needs, LIP has subcontracted Active Space Technologies. Their role is to design a custom enclosure solution that meets the thermal, electrical, mechanical, and detector geometry requirements. LIP has also partnered with ADVACAM to supply customized gamma-ray detectors that are fit for space deployment. In addition to these partnerships, LIP is outsourcing several testing facilities, including a TVAC chamber, a shaker table, an EMC/EMI test facility, a proton beam line, and gamma-ray beam lines.

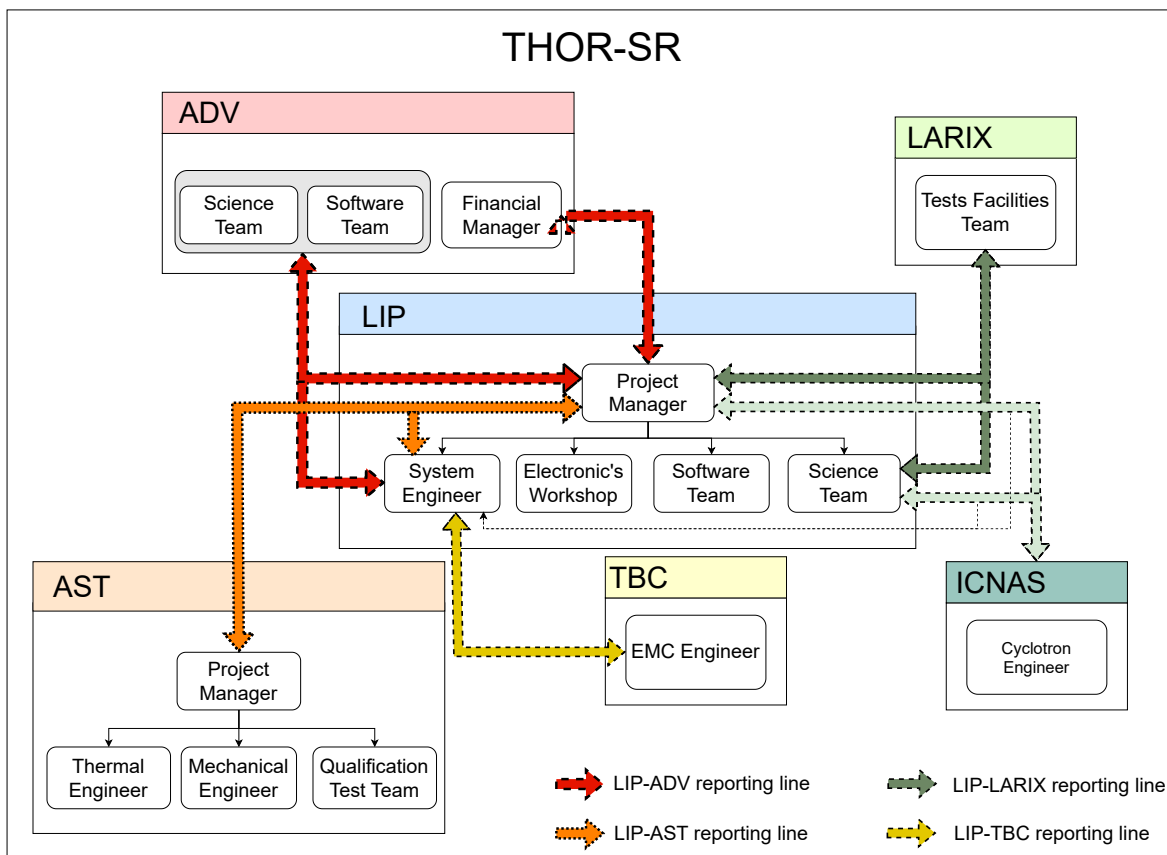


Figure 3.3: Diagram showcasing the entities involved in the development of THOR as well as the interfaces.

3.3.1 Internal Project organization - WBS

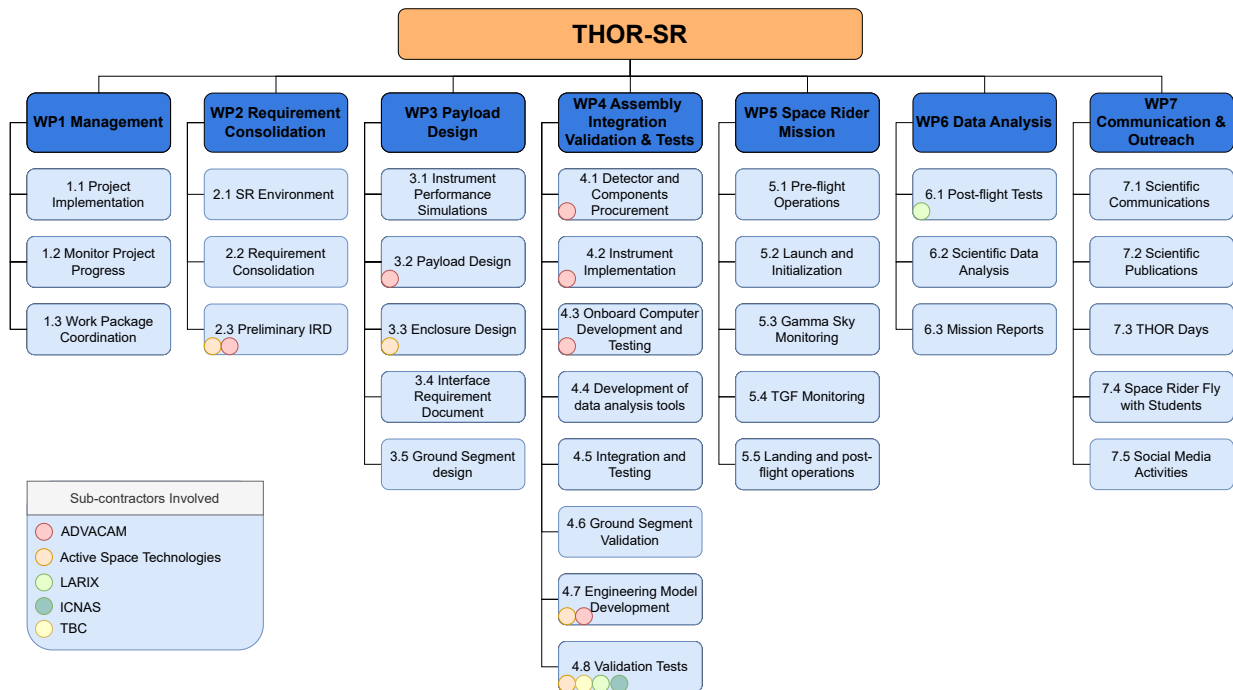


Figure 3.4: THOR Work Breakdown Structure.

WP1 Management : The Management work package, comprising the Principal Investigator (PI), Co-Investigator (Co-PI), and LIP Project Manager, is entrusted with achieving the project’s objectives within budget. The board ensures task timelines, interactions among stakeholders, and budget allocation, while also aggregating essential data for milestones like financial summaries and progress reports. The LIP Project Manager handles daily administration and makes the liaison with ESA. Progress oversight is jointly performed by the PI and Co-PI, through meetings to discuss and resolve issues, document decisions, and monitor project progress. They also work closely with internal and external stakeholders, disseminating results through international meetings to both the scientific community and the general public. On a granular level, each work package (WP) has a Coordinator who is responsible for implementing the action plan, tracking scientific and technical achievements, and reviewing task results.

WP2 Requirements Consolidation : The project involves a multi-step approach to align with the SpaceRider environment and services. In the first phase, a thorough analysis of the Space Rider’s expected thermal, electrical, and mechanical conditions is conducted. This extends to an evaluation of the services offered by Space Rider. Preliminary scientific simulations are performed to gauge outputs like photon and particle fluxes, data generation, heat dissipation, and mass. All this information is then consolidated

to provide a cohesive understanding of the project's environmental landscape. Building on the initial analysis, the next phase involves refining the project's requirements. The insights from the environmental and service analysis of Space Rider are used to revisit and revise the project's initial requirements, as well as to create new ones that align with the initial insights. Finally, these refined and newly-established requirements are incorporated into a preliminary version of the Interface Requirements Document (IRD) that is shared with the SR team. This initial IRD establishes the ground rules for how various project components will interact, ensuring compatibility and functionality within the Space Rider framework.

WP3 Payload Design : Initial simulations with the MEGAlib toolkit will test detector configurations for celestial and terrestrial gamma-ray sources. The payload's design will be guided by scientific mission requirements and taking into account ADVACAM modules limitations. This is an iterative process to ensure all requirements are implemented and risks are taken into consideration and minimized. Multiple reviews and meetings are going to take place until a Critical Design Review (CDR) locks in the final setup. Active Space Technologies will design the enclosure, considering all payload specifications. An Interface Requirement Document, developed with ESA, will outline the mission and system requirements where LIP team will include internal I/F's. A specialized ground segment will be established for secure command uplinks, interfacing with the PGCC via Internet. Throughout this process, meticulous safety analysis will evaluate and mitigate potential risks, particularly focusing on human safety while in ground operations. This comprehensive methodology ensures that both the payload and its enclosure are functionally and safely optimized.

WP4 Assembly Integration Validation and Testing : Procurement of the Detector Unit, OBC and PDU. The initial setup will involve a single CdTe module coupled with a readout board for characterization and performance tests. These tests will utilize either laboratory gamma-ray sources or the LARIX beamline at the University of Ferrara, Italy. The onboard computer (OBC) development will be a collaborative effort involving ADVACAM at the detector level. Software integration will focus on facilitating seamless communication between the payload OBC and the Space Rider's (SR) onboard systems. Concurrently, a data analysis tool leveraging the MEGAlib toolkit will be created to process scientific data generated by the Detector Unit. An engineering model will be crafted for further validation, consisting of operating and non-operating components to simulate the flight model. Finally, a series of validation tests—including thermal, vibration, and electromagnetic compatibility checks—will be performed by AST, culminating in a Qualification Review submission to the European

Space Agency (ESA).

WP5 Space Rider Mission : Once completed, the flight model is sent to ESA's ESTEC, then to the Kourou launch site in French Guiana for final checks. It will be launched into Low Earth Orbit via a Vega-C rocket. Two key mission events follow: Deep Sky Monitoring and Terrestrial Gamma-ray Flashes Monitoring. The first focuses on collecting gamma-ray data from celestial sources like the Crab Nebula, while the second targets TGF emissions from Earth. 'Real-time' adjustments are made based on LIP ground station analysis. Just before landing, the experiment powers down, and upon landing at Kourou, the payload is recovered for analysis.

WP6 Post-Flight Tests and Data Analysis : Post-recovery, the THOR-SR payload, specifically the Detector Unit and electronics, will be examined and tested to evaluate performance alterations or degradation due to exposure to LEO and descending phase. This analysis will contribute to a scientific publication on the ageing of CdTe detector modules and electronics. Simultaneously, the collected flight data, encompassing observations of the Crab Nebula, GRBs, TGFs, and charged particles, will be processed, compared with simulations, and integrated with existing literature and ongoing missions' data. This comprehensive analysis will facilitate the interpretation of the collected data, validate the simulation models, and culminate in a series of mission reports and scientific publications, concluding the data analysis and performance evaluation phase.

WP7 Communication and Outreach : The THOR-SR project will disseminate its scientific findings through international conferences and peer-reviewed journals. Special outreach events at universities and live-streaming activities targeting students will enhance educational engagement. A multi-platform digital strategy, including social media, will ensure broader public interaction, making the project's scientific contributions accessible to diverse audiences.

For a detailed view of the project timeline see the Appendix E.

3.3.2 Sub-contractors

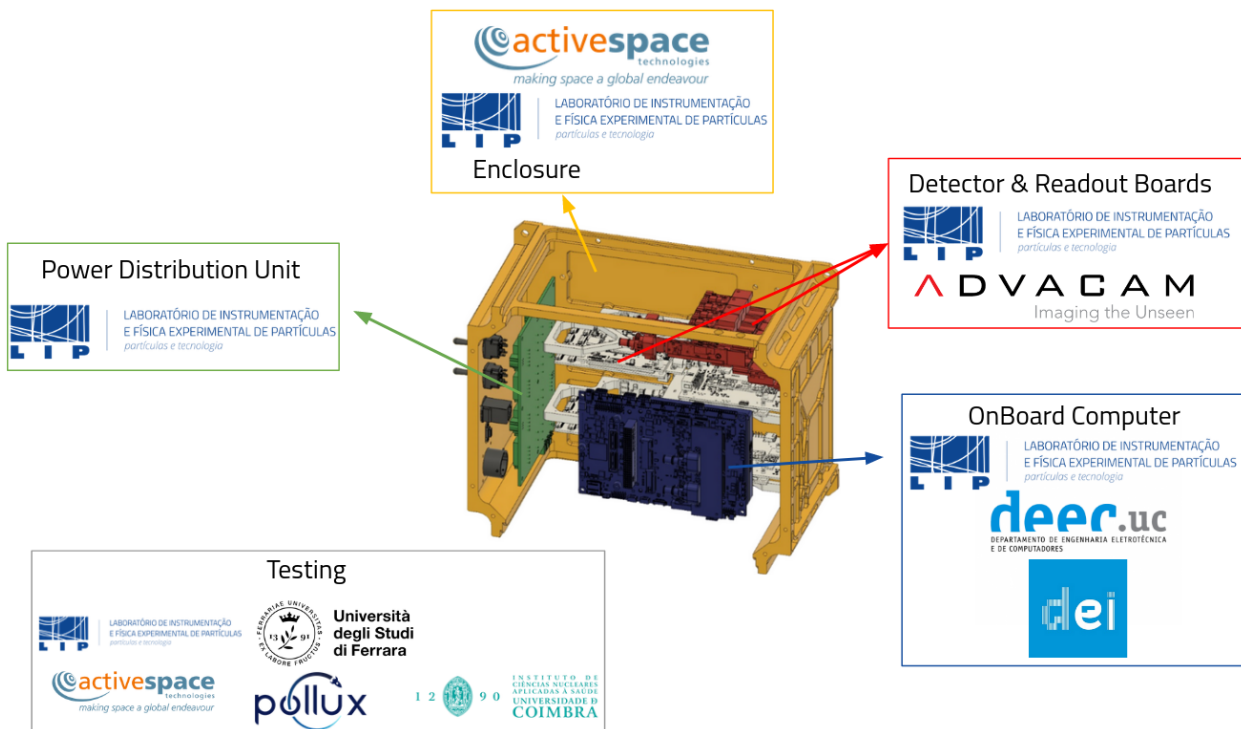


Figure 3.5: Showcase the institutions working on THOR.

Department of Electrotechnical Engineering and Computer, University of Coimbra

- Responsible to develop the OnBoard Software (OBSW) as well as the ground software. Collaborate with LIP to integrate high demanding computational calculations on the OBSW.

Department of Engineering Informatics, University of Coimbra

- Collaborate with LIP to develop IA algorithms for active particle identification and pre-processing of data.

ADVACAM

- Responsible for supplying the CdTe sensor matrices, including the back-end electronics with the required design modification (e.g. the FingerBoards of the Detector Unit), and the two Si matrices. Collaboration with LIP on the development and integration of the software between the Detector Unit and the OBC.

Deliverables:

- Development Model 1 - Minipix3 (CdTe 2mm);
- Development Model 2 - 1xQuad Advapix (CdTe 2mm);
- Development Model 3 - 1xQuad Advapix (CdTe 2mm);

- Engineering Model - 1x Custom CdTe Finger Board + 1x Custom Readout Board;
- Flight Model - 16x Custom CdTe Finger Boards + 4x Custom Readout Boards.

Active Space Technologies - Development, manufacturing and testing of the experiment's enclosure. Perform thermal simulations of THOR taking into account THOR operation cycle, power consumption of the products and the thermal conditions imposed by the SR (e.g. temperature range of support plates, radiation emission requirements, etc). Responsible for carrying out the validation tests: TVAC and Vibration/Shock tests.

Deliverables/activities:

- CAD Model;
- FEM Thermal Model;
- Engineering Model - 1x Enclosure;
- Flight Model - 1x Enclosure FM;
- TVAC test;
- Shaker test.

ICNAS - Provide access to the proton cyclotron at ICNAS facilities.

Activities:

- 16MeV proton beamline.

LARIX - Provide access to the gamma-ray beamline.

Activities:

- Up to 320keV photon Beam.

ESRF Grenoble - Provide access to the polarized gamma-ray beamline. Upon acceptance via a competitive call.

- ID-15A beamline, 20keV-500keV 99% polarized

Pollux - Launch a stratospheric Balloon up to 25km where environmental conditions, temperature and pressure, are similar to the ones on space.

- Stratospheric balloon launch to validate the PDU to TRL6.

TBD - Provide access to the EMC/EMI Test facility.

Activities:

- Electromagnetic emissivity test;
- Electromagnetic susceptibility test.

The interfaces between LIP and external contractors are organised in work team groups as described in Figure 3.6.

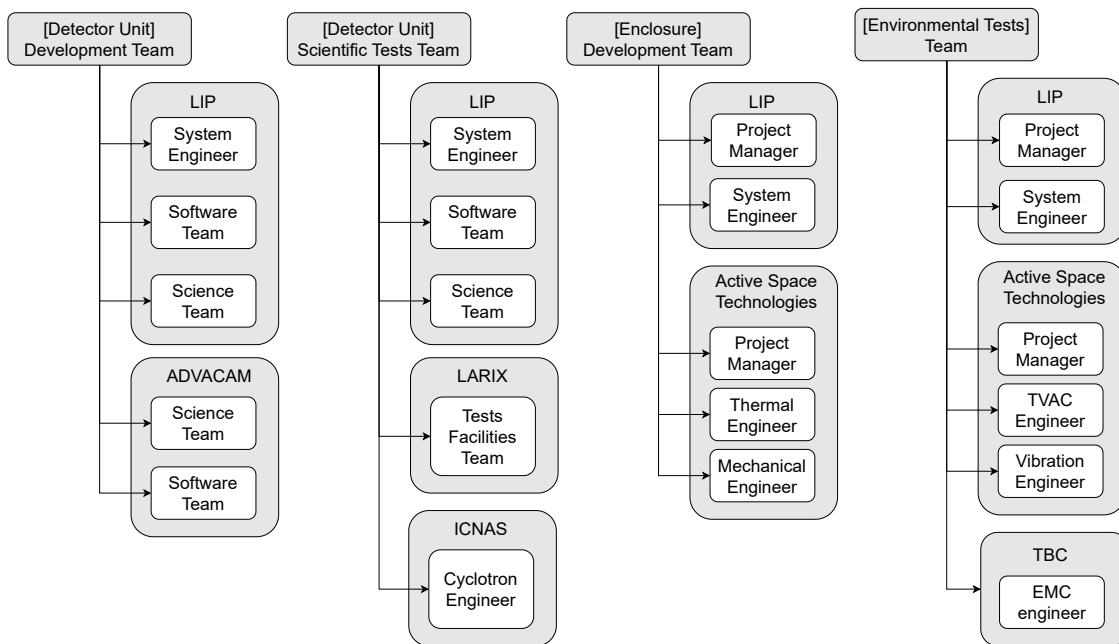


Figure 3.6: Diagram showcasing team composition for the development of the DET, ENC and Environmental Tests.

3.4 Space Rider Vehicle

The Space Rider is the new reusable shuttle from ESA that will allow companies, research centers and students quick and frequent access to space and back. After each flight the SR system is refurbished for further flights with a down time of months. Each flight the SR will stay in orbit during 2 months allowing up to 600kg of payloads to perform their missions in LEO conditions.



Figure 3.7: Artist representation of the Space Rider in orbit. Source ³

The SR will be launched to orbit by the Vega-C rocket from Kourou. The maiden flight is expected to happen in 2025 and the SR will be deployed on a 400km orbit with 5° of inclination. The SR system⁴ offers power (28V/600W), temperature controlled support plates (15°C to 40°C), downlink (2Gbyte/day) and uplink (600kb/orbit) communication capabilities, onboard data storage (5.6 Gbyte/day) as well as direct access to space for the payloads on either plate 1 or 6 via opening of the MPCB door, see Figure 3.8.

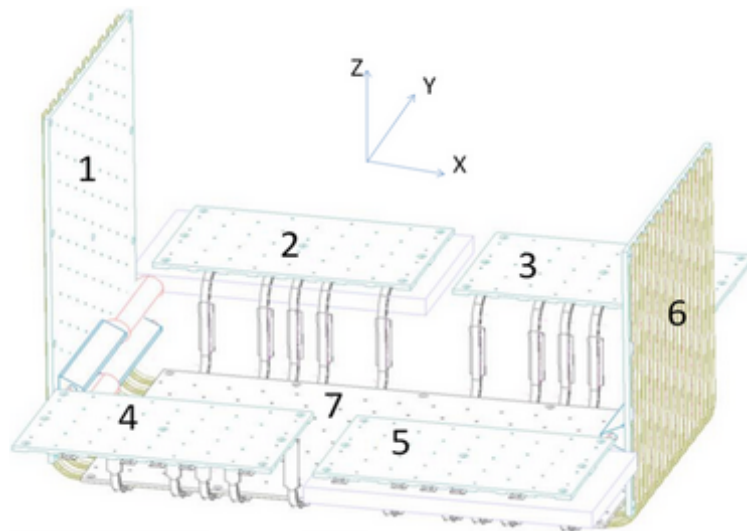


Figure 3.8: P/L possible locations inside the SR vehicle [ESA, 2021].

The fact that the vehicle returns to Earth after flight enables the payloads to fit a lot of memory storage that can later be retrieved after landing. 'Live data' is available to the

³https://www.esa.int/esatv/Videos/2022/11/To_orbit_and_back_with_Space_Rider/Space_Rider_-_Mission_animation

⁴Budgets for all payloads

payload operators. The SR ground segment is divided into two main systems, the Vehicle Control Centre (VCC) and the Payload Ground Control Centre (PGCC). The VCC is in charge to monitor and control the SR vehicle and redirects THOR related data to the PGCC. The PGCC oversees the payload’s operations and interfaces the experiments with the end-users, the User Payloads Operation Centre (UPOC). The UPOC receives the downlink data via Internet to monitor THOR operations and scientific data. Also, the end-user has access to data processing and archive system at the PGCC level upon request [ALTEC, 2021]. See Figure 3.9 for a simplified ground segment architecture.

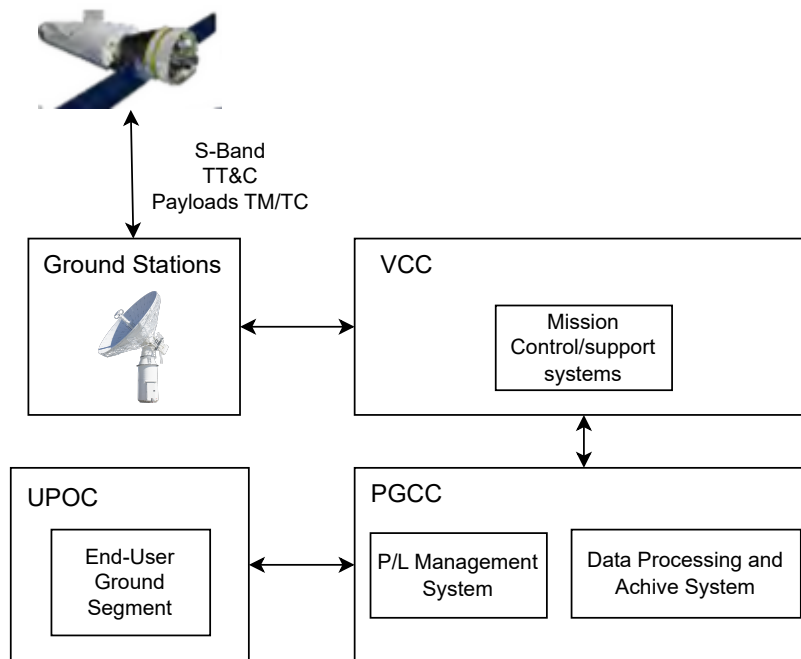


Figure 3.9: Space Rider System ground segment architecture, simplified.

The end-user upon receiving the downlink data from the respective P/L is able to send TM commands. The end-user, when required, shall request a PDOR custom modified message, in case its an action overruling the nominal operations. The PGCC will redirect the TM to the VCC to be sent to the SR.

3.4.1 Main integration requirements

In order for THOR to be integrated in the SR vehicle the payload shall be compliant with the available interfaces of the vehicle (electrical and mechanical), compliant with the resource consumption budget that the SR team attributes to the P/L (power and communication) and finally, with the pre-determined mass limit. In the Table 3.2 we present the current status of the main integration requirements. The requirement compliance is subject to change with the further development of the P/L design.

| Requirement ID | Requirement Text | PDR Design Compliance | Comments |
|----------------|--|-----------------------|--|
| REQ-017 | The experiment shall weigh less than 3kg. | Not compliant | PDR design = 5.8kg with 15% margin. Already identified action items to implement between PDR and CDR. See Appendix F and Appendix G. |
| REQ-030 | The total data transferred to the SR storage system shall not be greater than 300MByte/day. | Compliant | PDR design = 340MB/day with 25% margin. Assumptions made in Section 3.10 are unrealistic. More detailed simulations will showcase a lower flux and therefore lower data generated. |
| REQ-035 | The maximum power consumption shall be of 50W. | Compliant | PDR design = 50.3W with 25%. It is foreseen that the power drawn by the DET can be managed. Confident that the power consumption will decrease when verification takes place. |
| REQ-093 | The experiment housing shall have the connector 340105601B06-15-19PN for the power interface. | Compliant | See Section 3.8.6.3 |
| REQ-094 | The experiment housing shall have the connector 3401/001 D-SUB 9 pins, Male for the RS422 communication. | Compliant | See Section 3.8.6.3 |
| REQ-095 | The PDU shall have an input voltage of 22-38V that interfaces with the Power Connector. | Compliant | The document [ESA, 2021] states 26-33V. For that we are compliant. But on ECSS-E-ST-20-20C states that 28V unregulated is 22-38V. That's why the requirement has a higher voltage range than the SR user manual. |
| REQ-157 | The experiment shall be mounted to the Aluminium adaptor using M6 drill with 58mmx58mm spacing. | Not Compliant | See 3.44. Between PDR and CDR the THOR volume will decrease and the M6 hole layout will be compliant with the requirement. See item SU36 from the document in the Appendix G |

Table 3.2: SR integration driving requirements, PDR status.

3.5 Requirements

Requirements are a set of sentences that state what is necessary for the mission to achieve its scientific objectives. Some of the requirements are directly linked to the mission objectives, the mission requirements, while other are there to meet the mission technical needs to achieve the objectives, such as the design and operational requirements. The full list of requirements can be found on the Appendix B. The requirements presented bellow follow the format presented on the ECSS-E-ST-10-06C:

Shall A requirement with the word 'shall' is of mandatory compliance. In case the requirement is not achieved a good justification shall be presented to the THOR-SR team and the acceptance or decline of the non-conformity shall be stated.

Should Although not used in the list bellow, a 'should' requirement states a desirable feature to be implemented. It is not of mandatory implementation.

The requirements can be divided into several types for easier attribution to either products, entities or mission phases. The THOR-SR requirements were divided into Mission Requirements, Design Requirements, Operational Requirements, Interface Requirements and Environmental Requirements

Mission Requirements This requirements relate directly to the mission objectives. This requirements state a task, function, constraint or action to be taken to achieve the THOR mission objective.

Design Requirements This requirements state an imposed constraint regarding the performance/property of a product.

Operational Requirements This requirements state operations that a product/system must be capable of performing.

Interface Requirements These requirements state physical, electrical, protocol, operations interfaces that THOR has with the SR system.

Environmental Requirements This requirements state the environmental conditions that the THOR P/L must be cable to withstand.

Also, for each requirement a verification method is assigned in order to, further down the project, assess the compliance with the proposed requirements. The methods of verification are the following:

Review of Design(RoD) Using approved or known facts that unambiguously show that said requirement is met.

Testing(T) Measuring performance of said requirement under representative deployment conditions.

Inspection(I) Visual determination of some physical characteristic.

Analysis/Similarity(A) Verify the requirement performing theoretical or empirical evaluation with the aid, if needed, of specialized software.

3.6 Operations

3.6.1 Concept of operations

After the integration of the THOR-SR payload into the SpaceRider Reentry Module (SR-RM) MPCB the operator shall remove a pull-pin kill switched that will be properly identified with a red ‘Remove Before Flight’ tag. THOR is only able to boot if this pull-pin is removed. The Figure 3.10 showcases the operations modes defined for the OBC.

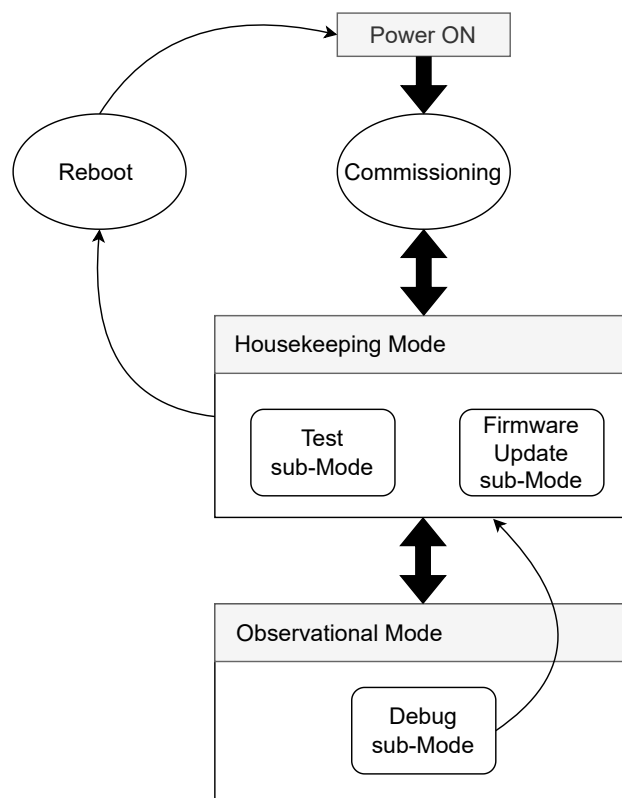


Figure 3.10: In-flight operation mode of the THOR-SR payload.

Upon reaching orbit THOR will autonomously boot when the SR turns on the power supply. THOR will boot up and perform the commissioning procedure. THOR OBC will check the operationality of the PDU and the Detector Unit. The commissioning procedure will take about 2 hours and have a peak power consumption of 17.3W. At the end of this procedure THOR OBC will enter the Housekeeping mode and produce a report of THOR status to be included in the HK data. If the results of the report are as expected THOR OBC will autonomously enter the Observational Mode, if not THOR OBC will remain on Housekeeping Mode waiting for ground intervention (waiting for TC).

Upon entering the Observational Mode THOR OBC will fully turn on the Detector Unit and begin gathering scientific data. In this mode THOR will nominally consume 43W with peak power consumption of 50.3W during high intensity calculations. For each event detected THOR OBC will time stamp it and save it to the internal memory. THOR will continuously gather scientific data regardless of the SR orientation. The SR-OBC shall update the associated THOR-SR P/L MMU with attitude data every 24h (SR altitude and orientation). With the attitude data and the cumulative gamma-ray detection, THOR OBC can identify the gamma-ray sources (GRB, crab nebula, other) and perform the required scientific calculations. During the observation time, it is expected to have 18 days of deep sky pointing, in which 5 days are of Crab Nebula observation for calibration and scientific purposes (polarization measurements). It is also expected to have 7 days of Earth pointing to detect TGF's as well as a total of 12h of Sun observation to monitor solar activity (solar flares). During the Observation Mode THOR OBC will update the SR MMU with HK data every 3.5h, to be sent to the LIP-GS. Upon performing scientific calculations THOR OBC will update the SR MMU with scientific data, every 24h. THOR OBC will operate in this mode with 95% availability. In case THOR OBC identifies an anomaly in the normal functioning of THOR subsystems (ex.: overheating, over-current consumption, noisy pixels in the Detector Unit), it autonomously switches to the Debug sub-Mode where it will solve the issue at hand while still taking scientific data. If it is an unknown error, THOR OBC will switch to Housekeeping Mode and include in the HK data an error message explaining the problem to the LIP-GS. THOR OBC will wait for ground intervention. When the ground TC message arrives to THOR OBC, it will enter the Test Sub-mode where it will test the new software patch. Before testing the new software version, THOR OBC saves the current version on the internal memory. If the test is successful THOR OBC enters the Firmware Update sub-Mode to update the OBSW.

THOR will be ready, at any give time, for an emergency power cut-off. THOR OBC shall start the shutdown of THOR 1h before the power cut, to prepare for the SR reentry.

3.6.2 Mission Profile and Timeline

A list of the THOR-SR payload mission phases, from integration on the vehicle until retrieval after landing, is summarised below (see Figure 3.11). The payload will be fully autonomous on the execution of the timeline, except when an unexpected error/event occurs, as explained below in the Observational phase paragraph. This will require an uplink UPOC message to the payload OBC.



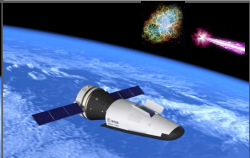


| Integration to launch phase | | Commissioning Phase | | Observational phase | | Landing and retrieval phases | | | |
|---|-----|---|-----------|---|------------------|--|------------------|---|-----|
|  | |  | |  | |  | |  | |
| | | ↔ 2 hour | | ↔ 18 days | | ↔ 7 days | | | |
| Payload ready to be switched ON OBC will boot when power is turned ON | | Payload boot Payload Health check. | | Deep sky Observation Crab 5 days, GRB's, AGN | | Earth Pointing TGF's | | End of Operations T-1h power cut the experiment will be turned OFF. | |
| TM | N/A | TM | 28 Mbytes | TM | 344 Mbytes/orbit | TM | 344 Mbytes/orbit | TM | N/A |
| TC | N/A | TC | N/A | TC | Emergency | TC | Emergency | TC | N/A |
| Power | N/A | Power | 17.3 W | Power | 50.3 W | Power | 50.3 W | Power | N/A |

Figure 3.11: THOR-SR operations timeline and major events.

Integration to launch phase : At this stage the critical operation to be performed by the integration operator is to remove the Red 'Remove Before Flight' pull-pin kill switch. At this stage there is no power supplied to the experiment, so the heat dissipation requirement is 0W, see Table 3.4 for the THOR resource consumption during this phase. No data is to be stored in the SR storage system nor are there any communication requirements. THOR will remain in this state during the launch phase until the SR system turns ON THOR power lines. For the time being there are no requirements regarding the heating of THOR support plates. This may change upon further specific thermal simulations regarding a delayed power ON of THOR.

| Operation Mode | Communications | Power (Max) |
|----------------|----------------|-------------|
| THOR OFF | N/A | 0W |

Table 3.4: Integration to launch phase resource consumption.

Commissioning Phase: Upon entering orbit, THOR is waiting and ready to be powered up by the SR power supply. Once that happens THOR boots into the commissioning

procedure. The THOR resource consumption during this phase is presented in Table 3.8. The OBC performs the following critical operations:

- Time synchronisation with SR MMU;
- Detector Unit Health check;
- PDU health check.

This phase will take approximately 2 h.

| Operation Mode | Communications | Power (Max) |
|-------------------------|----------------|-------------|
| Commissioning Procedure | 28.7 MB | 17.3W |

Table 3.6: Commissioning phase resource consumption.

At the end of the commissioning phase the results of THOR health check will be included in the HK data, without affecting the maximum data packet size.

Observational Phase: Having completed the commissioning phase successfully, the OBC switches to the Observational mode in which the Detector Unit is fully operational, taking scientific measurements independently of the SR orientation. At this stage THOR OBC is making scientific calculations and crunching the data to be sent to the SR MMU as well as to THOR memory unit. THOR OBC will update the SR MMU every 3.5h with Housekeeping data and every 24h with Scientific data. THOR will be cumulatively collecting gamma-ray events that are over layered with the SR attitude data in order to map the gamma-ray sky and identify gamma-ray continuum and transient sources. The THOR resource consumption during this phase is presented in Table 3.8. Whenever there is an anomaly detected on the normal functioning of the experiment THOR OBC can either switch to ‘Debug’ mode, in case of a predictable anomaly; or to ‘Housekeeping’ mode to request ground intervention. In case the Housekeeping data that arrives to the LIP-GS shows signs of an irregularity on the normal operation of THOR subsystems, the LIP-GS shall send a PDOR emergency command to the PGCC @ALTEC via Internet to be delivered to the THOR-SR P/L with no more than 3.5h delay, REQ-143. This Emergency Command shall be used in the following situations (or others still not identified):

1. Incongruity on the scientific data (problem related to the malfunctioning of the Gamma Array or Particle Array of the Detector Unit, e.g: noisy pixels);
2. Thermal Control System is activated due to overheating of any of the payload components;

3. Unexpected cosmic event that may saturate or damage the Detector Unit, e.g high intensity solar storms, etc;
4. Unpredictable anomaly on the normal functioning of the payload's components (e.g: software bug).;
5. Loss of communication between THOR and the SR MMU.

The procedure in the sequence of the occurrence of one, or more, of the events summarised above is:

- If either problem 1. or 2. occur, the payload OBC will try to manage the problem without the need of an intervention from the Ground. At this stage the Housekeeping mode can be activated if needed;
- If problem 3. occurs, the LIP Ground Segment shall be able to send a PDOR Emergency Command to the payload OBC in order to change the operational mode to Housekeeping. Also, if during the flight, a supernova or another relevant cosmic (unexpected) event occurs, an uplink command shall be sent to the OBC in order to adjust the Detector Unit's threshold to capture these events;
- If problem 4. occurs the OBC shall send a warning message inside the Health Monitor Data package. The LIP Ground Segment shall be able to send an Emergency Command to mitigate the issue at hand.
- If problem 5. occurs the OBC shall carry out the scientific observations autonomously, saving the useful data on the internal memory until the power cut.

| Operation Mode | Predicted availability | Communications | Power Nominal | Power Max |
|----------------|------------------------|----------------|---------------|-----------|
| Observational | 95% | 344 MB/day | 43W | 50.3W |
| Housekeeping | 5% | 0.13 MB/day | 10.5W | 10.5W |

Table 3.8: Observational Phase resource consumption.

During this phase the SR shall comply with specific pointing requirements to achieve the scientific objectives of the mission. It is required that the SR performs deep sky observations, earth observations and Sun observation as stated in REQ-169, REQ-170, REQ-171 and REQ-172:

Deep sky Pointing : REQ-170 states that in order to achieve the scientific objectives of the mission the SR Z-axis, according to the SR-RM Geometric Body Fixed Reference Frame,

shall be oriented towards the deep sky (ideally to the Zenith), to preferentially record gamma-ray astrophysical emission sources (GRBs, Crab, AGN's or others). Due to the small effective area of the detector, THOR-SR requires a cumulative 18 days observational time to deep space, considering that Earth doesn't obstruct more than 20% of the Detector 2π FoV. During this pointing mode the SR shall also comply with REQ-169 in order to observe the Crab Nebula for a cumulative 5 days of observational time to perform imaging, spectroscopy and polarimetric measurements.

Earth Pointing : REQ-171 states that in order to achieve the scientific objectives regarding TGF observation the SR Z-axis, according to the SR-RM Geometric Body Fixed Reference Frame, shall be oriented towards the Earth (ideally to nadir), to preferentially record gamma-ray's emitted from cumulonimbus clouds (TGF). Due to the unpredictability of the TGF emissions, both in frequency of events and correct spacial location, to detect the event 7 cumulative days of observational time are required.

Sun Pointing : REQ-172 states that in order to study the sun activity and possibly make a x-ray and proton observation from a solar flare THOR requires 12h of cumulative Sun pointing.

End of Operation phase: With Time -1 h from the power cut THOR OBC will proceed with the shutdown of the experiment. At this stage, the OBC and the PDU are on standby ready for the power cut.

Landing and Retrieval Phase: There are no special requirements regarding the retrieval of the payload. A 1 month of THOR retrieval delay is acceptable.

3.6.3 Commissioning description

When the SR turn on THOR power supply, THOR boots up and the commissioning procedure takes place. At this stage the OBC is powered ON as soon as the SR supplies power to THOR. The OBC then starts to perform several health checks that guarantee the normal operations of the payload. The OBC starts to check the communications with the SR_MMU by creating dummy data labeled as HK data. Upon confirmation that the connection is established the OBC performs the clock sync sequence that will later allow a seamless integration of the SCI data with the attitude data of the SR. Afterwards the OBC checks the access to the OBC_MMU that may have become loose during launching. Being done with the OBC related checks the OBC proceeds to check the health status of the PDU. It checks the ON/OFF capabilities of the PDU outputs while monitoring the voltage and currents

levels of said outputs and temperature of the PDU temperature sensors. Upon checking the normal operation of the PDU the OBC starts to monitor and record the current, voltage and temperature of the PDU in order to be actively evaluating the PDU behaviour during the Detector Unit health check. The OBC then starts to check the Detector Unit's health status. It starts to evaluate the GAM by turning one detector plane at the time¹. The OBC checks if the current drawn, voltage levels and temperature are nominal and proceeds to look for potential dead pixels due to the harsh launch mechanical environment. Upon performing this procedure on the GAM the OBC does the same to the PAR. When the Detector Unit health check ends the OBC produces a report of the health check of THOR. The report shall contain the information present on Table 3.9. In the Figure 3.12 the reader can find a diagram representing this operation mode.

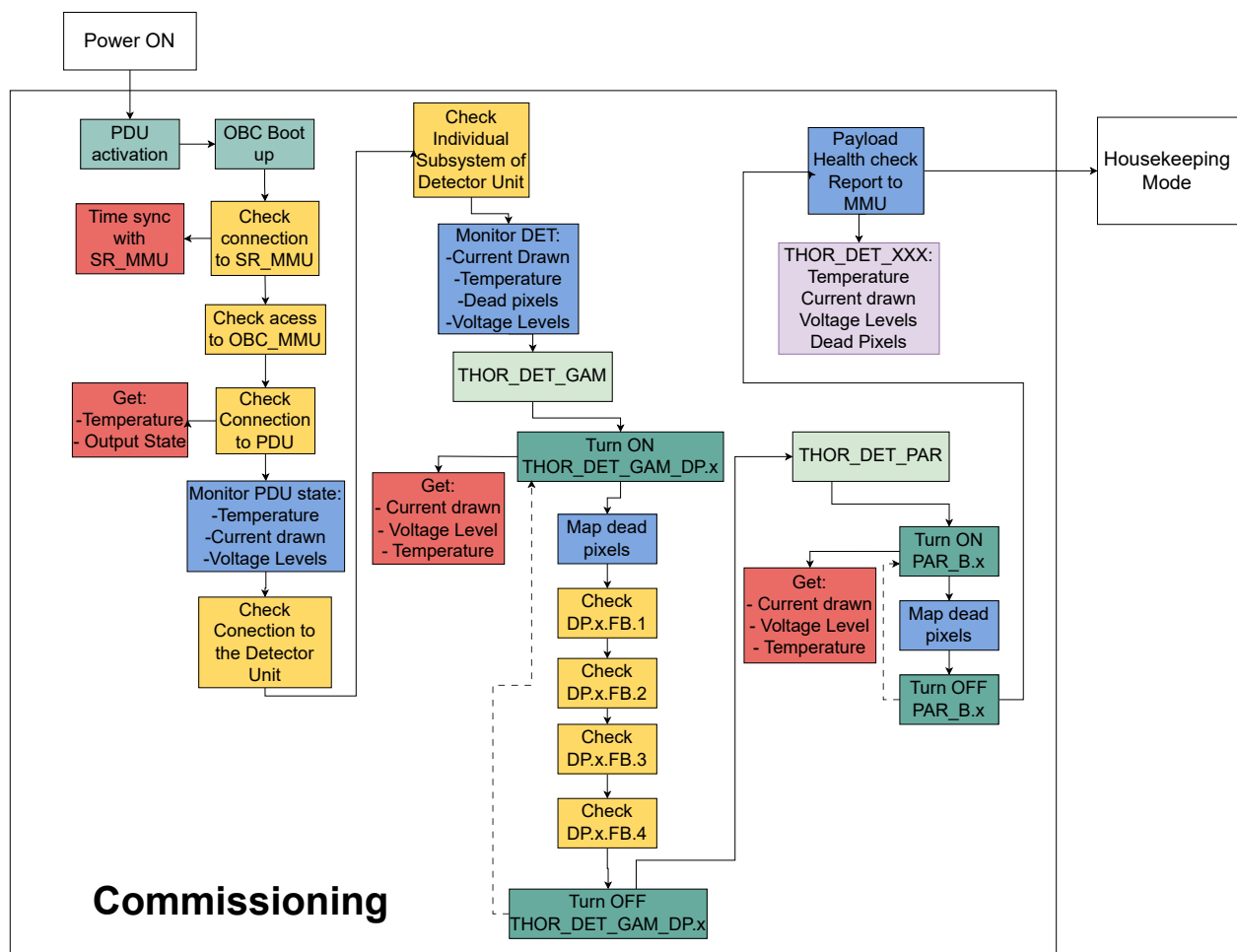


Figure 3.12: Commission Mode concept operation philosophy.

¹At this stage the PDU can only activate the 2 DP's at a time. A design change may be implemented in order to control DP's individually.

| Parameter | Value |
|---------------------------------|-----------------------------|
| SR_MMU access status | Nominal or Non-nominal |
| OBC_MMU access status | Nominal or Non-nominal |
| Clock Sync status | Nominal or Non-nominal |
| SR input voltage | Nominal or Non-nominal |
| PDU output ID ON/OFF capability | Nominal or Non-nominal |
| PDU temperature ID | Nominal or Non-nominal |
| DET power I/F ID (Voltage) | Nominal or Non-nominal |
| DET power I/F ID (Current) | Nominal or Non-nominal |
| DET FB ID temperature | Nominal or Non-nominal |
| DET FB ID noisy pixels | n ^o noisy pixels |

Table 3.9: Parameters to be sent to the LIP-GS.

3.6.4 Housekeeping Mode description

Upon entering the Housekeeping Mode the OBC turns the DET completely OFF by shutting down the voltage outputs of the PDU². At this stage the OBC continues to monitor the HK data from either the OBC and PDU. The Housekeeping Mode can be activated by several other operation modes/sub-modes. In case it is activated by a scheduled reboot sequence the Housekeeping Mode redirects the operation to the reboot sequence. In case the Housekeeping Mode is activated by the Test sub-Mode it is assumed that THOR is nominal and can proceed to Observational Mode. If the Housekeeping Mode is activated by the Commissioning procedure, the Housekeeping Mode can either directly enter the Observational Mode, in case the Commissioning procedure is nominal. If an error occurs during Commissioning it shall be transmitted to the LIP-GS with the label 'Emergency Message'. If the error is manageable, e.g. DCDC that activates the DP.1 does not respond, the OBC treats that error as manageable since the other DCDC works fine. In this case the OBC may enter the Observational Mode taking into account the limitations imposed by the error at hand. In case the error is unmanageable, e.g. SPI interface with PDU wont respond, the OBC shall wait for ground intervention. When the TM is received the OBC may proceed to the Test sub-Mode to test the proposed solution from LIP-GS operators. In the Figure 3.13 the reader can find a diagram representing this operation mode.

²At this stage the OBC has available a lot more power budget and therefore it is still under discussion using the available power budget to implement a data processing algorithm that requires more power

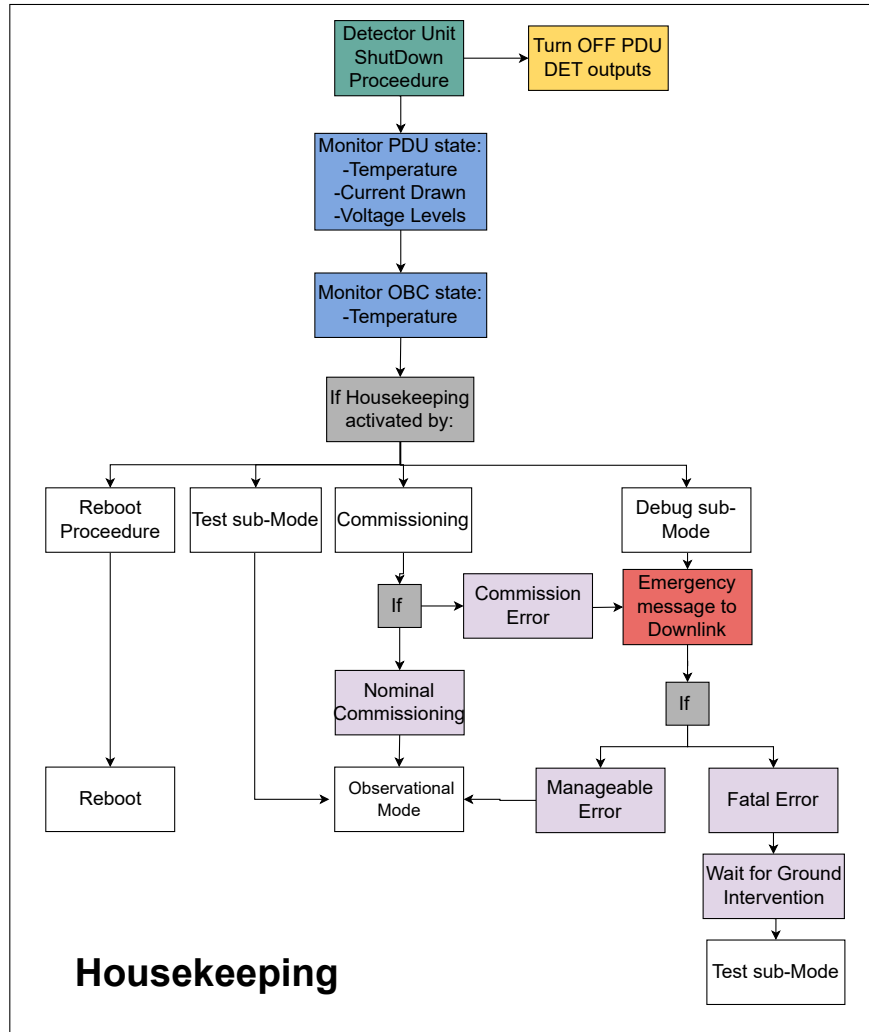


Figure 3.13: Housekeeping Mode concept operation philosophy.

3.6.4.1 Test sub-Mode description

The Test sub-mode can be accessed either from a LIP-GS TC request or from the end of the firmware update. If this mode is activated by a ground intervention, the OBC saves the current firmware of the payload on a bootable section of the memory, in case the tests to be performed induce a critical error. Upon performing this, the OBC can commence the implementation of the new software sent from ground. If the tests are successful, THOR can proceed to the Firmware Update mode. In case they are unsuccessful the OBC firmware shall return to its initial state and do a reboot procedure. In the Figure 3.14 the reader can find a diagram representing this operation sub-mode.

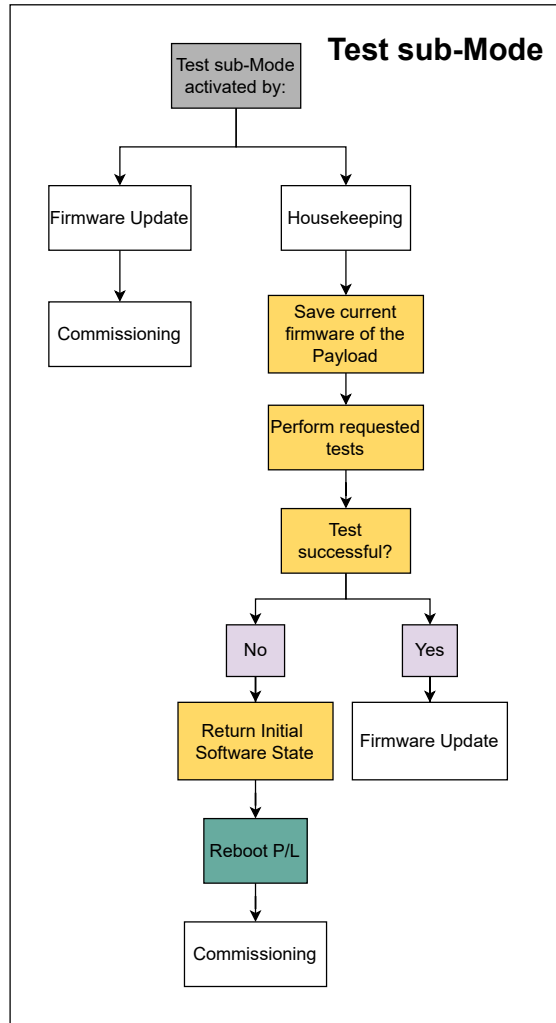


Figure 3.14: Test sub-Mode concept operation philosophy.

3.6.4.2 Firmware Update sub-Mode description

THOR enters this mode whenever new software patches are to be implemented. The software architecture will be designed taking into account that most of the software modifications are parameter adjustments in the kernel. It is also foreseen the possibility of updating the particle identification neural network.

3.6.5 Observational Mode description

During Observational Mode THOR is fully operational, having the DET fully turned ON and THOR producing scientific data. When THOR enters this mode the OBC turns ON the PDU outputs that power each sub-product of the DET. At this point the OBC monitors the HK data related to the power supply of the DET (voltage and current levels) as well as the HK data from DET itself (temperature, bias voltage, leakage current). During this mode the OBC is actively evaluating the HK data. In case the OBC detect an anomaly,

e.g. detector over heating or arc discharge on the detector, the OBC acts on the problem and introduces a report message on the HK data. Whenever possible the OBC tries to go back into nominal operations by turning ON the affected products. If the problem persists it is identified as a bug and THOR may switch to Debug sub-Mode. Whenever THOR is operating nominally the OBC + DET perform scientific data collection, data processing and data storage on either the internal MMU and on the SR_MMU. It is foreseen that THOR will be in Observational Mode during 95% of its online time. In the Figure 3.15 the reader can find a diagram representing this operation mode.

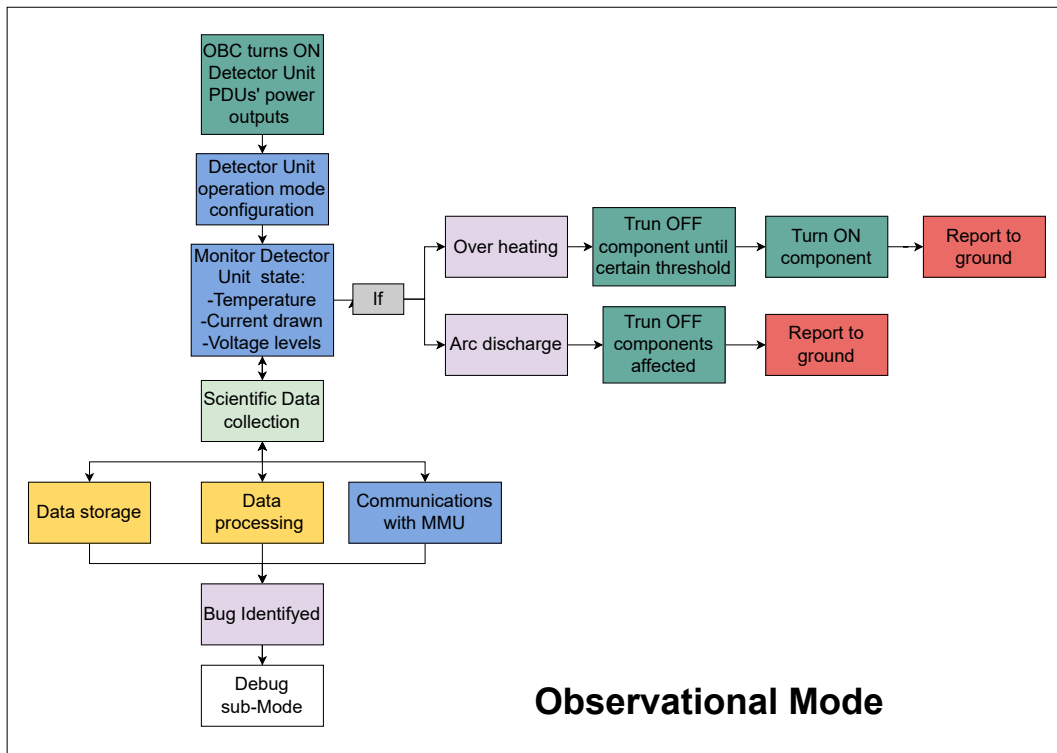


Figure 3.15: Observational Mode concept operation philosophy.

3.6.5.1 Debug sub-Mode description

The Debug sub-Mode is activated whenever an error occurs or persists during the Observational mode. Upon Debug sub-Mode activation the OBC continues to monitor the HK data from the PDU, DET and OBC. If a known error activates this sub-mode, the OBC will evaluate if it affects the SCI operations, e.g. over heating of a FB. In case it affects the SCI operations the OBC it will judge, upon pre-determined failure modes, if THOR can proceed with SCI data collection - allowing THOR to continue operating with a lower scientific potential e.g. DP needs to be shutdown due to overheating. - and therefore may enter the Observational Mode. If the error is not bearable, e.g. DCDC_GAM shutdown and ON/OFF capability doesn't respond, the OBC will generate an Emergency message to be sent to LIP-GS and switch to Housekeeping Mode. In case the error does not affect SCI

operations, e.g. PDU temperature sensor not responding, THOR can go back to the Observational mode. If the sub-Mode is activated by an unknown error the OBC will evaluate if the error affects the nominal operations of THOR. If it affects, e.g. OBC loses the ability to receive SCI data from DET, the OBC generates an emergency message to ground and switches to housekeeping mode, waiting for ground intervention. If the error does not affect the nominal operations of THOR and its a bearable error, the OBC sends an Emergency message to ground and proceeds with the SCI data gathering by switching to Observational Mode. In case the error is not bearable the OBC notifies the ground also via an emergency message and switches to housekeeping mode until ground intervention. In the Figure 3.16 the reader can find a diagram representing this operation sub-mode.

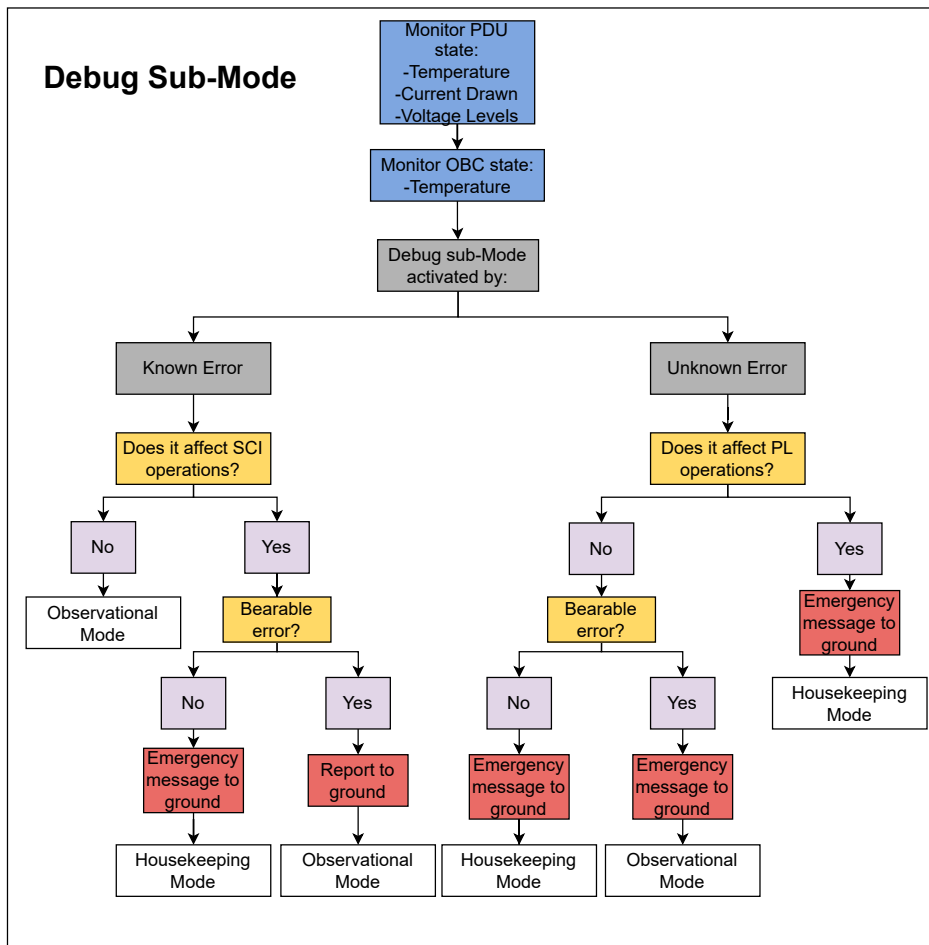


Figure 3.16: Debug sub-Mode concept operation philosophy.

3.6.6 OBC Science Operations

3.6.6.1 Scientific Data Collection

While in Observational Mode, the OBC is responsible to perform the scientific data collection from either the PAR and GAM. The OBC uses the API developed by ADV to communicate

with the detectors. The API allows the OBC to request a fixed time of acquisition (TBD) during which the detectors will be acquiring SCI data (ToT, ToA, FToA) for every physics event. After each SCI acquisition the OBC puts the ToA+FToA value as a reference of the SR time for easier integration with the attitude data. In parallel the OBC does the routine housekeeping procedure where it gets the temperature of operation of both the ASIC and CPU of the detectors and if a noisy pixel is identified it is masked. See Figure 3.17 for a detailed flow chart of this operation.

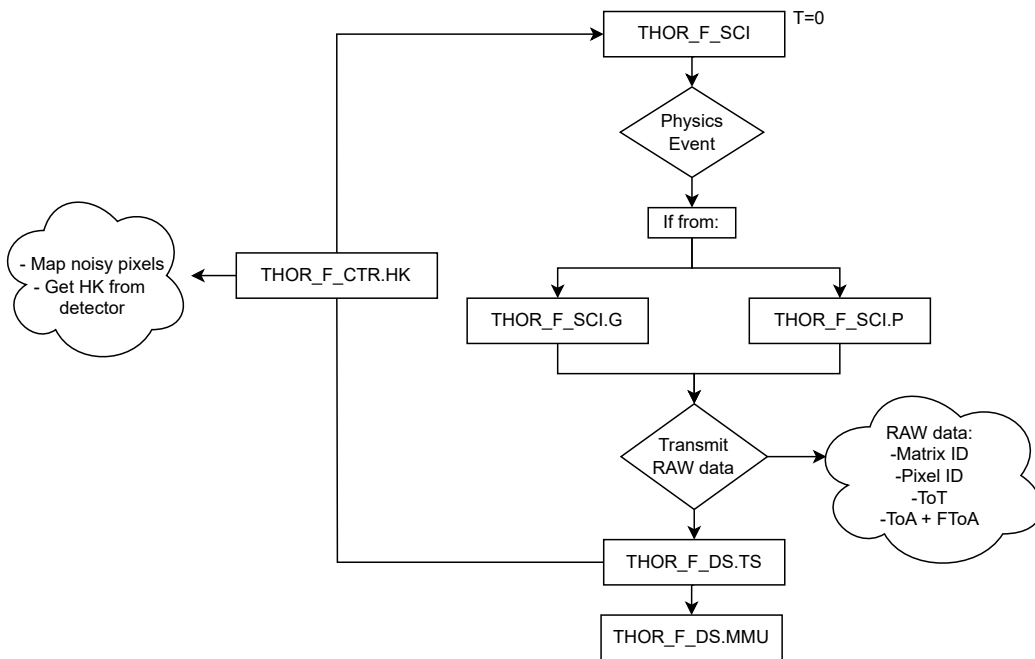


Figure 3.17: Scientific data collection flow chart. For a detailed description of the function codes see Appendix A.

3.6.6.2 Scientific Data Factory Calibration

After each SCI data acquisition, the OBC is going to apply the factory calibration. For each pixel there are a combination of 4 parameters a, b, c, t that allows us to transform the ToT into energy (keV) value. Figure 3.18 is a flowchart representing this function.

$$E[\text{keV}] = \frac{ta - b + \text{ToT}}{2a} + \sqrt{\left(\frac{ta - b + \text{ToT}}{2a}\right)^2 - \frac{t(\text{ToT} - b) - c}{a}} \quad (3.1)$$

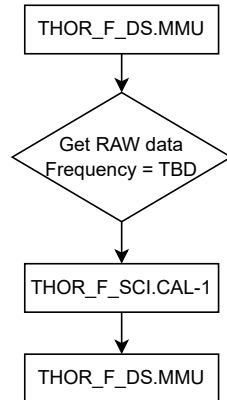


Figure 3.18: Factory calibration flow chart. For a detailed description of the function codes see Appendix A

3.6.6.3 Event Identification

Once available on the OBC_MMU, the RAW scientific data, already with the energy in keV, physics events are identified by an artificial intelligence algorithm implemented by the OBC. The algorithm separates the events into two categories:

- Single Event/Compton: These events are related to photon and electron interactions with the detectors. Since there is no direct way to differentiate an electron interaction from a single photon event, the algorithm groups these two interactions into just one, the Single Event. The Compton events can be differentiated by creating a coincidence time window (typically of $2 \mu s$ width) encompassing at least two interactions: Compton-photoelectric or Compton-Compton. Also, by evaluating the energy and angular distribution of the interactions, applying Compton kinematics formula, one can confirm if it really was a Compton event.
- Proton/Heavy Ion: These events are related to heavy particles interacting with the detectors. They leave similar energy/charge patterns on the 2D pixels matrix of the detectors (typically straight lines) that can easily be differentiated between one another on post processing. This event type also undergoes a characterization with 5 parameters that represent the interaction. These parameters are explained on Table 3.11, see Figure 3.19 for a visual representation.

| Parameter | Description |
|---------------------------------|---|
| Hit Pixel | Per interaction it must be saved the pixel that first interacted with the particle. |
| Energy Deposited | The sum of the ToT value of all the activated pixels. |
| N ^o activated pixels | The total number of activated pixels that represents the range projection onto the direction plane inside the detector. |
| Phi | The azimuthal angle between the XY plane and the direction at which the particle travels inside the detector volume. |
| Theta | The polar angle(from the Z axis) at which the particle travels inside the detector volume. |

Table 3.11: Parameters that characterize a Proton/Ion event

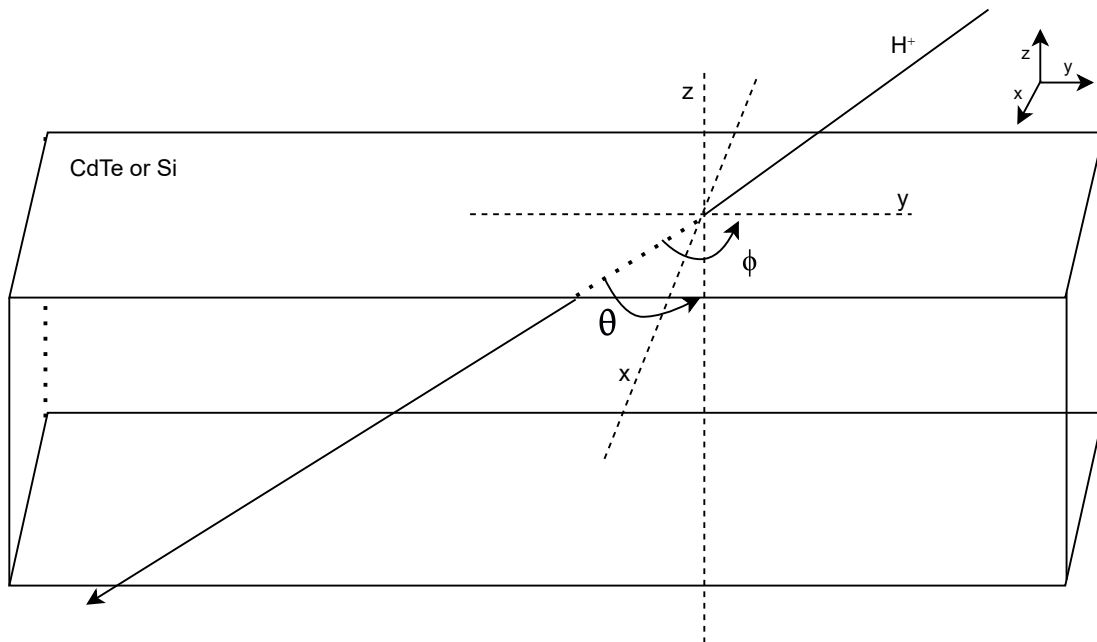


Figure 3.19: Visual representation of the parameters that characterize a proton/heavy particle interaction.

Once the algorithm identifies single particles, the OBC shall also implement the second and third stage of energy calibration. After having the physics event characterized by the right energy the OBC will add to the event an unique, incremental, numerical identifier and a header representing the type of physics event. See Figure 3.20 for a detailed flow chart of this operation.

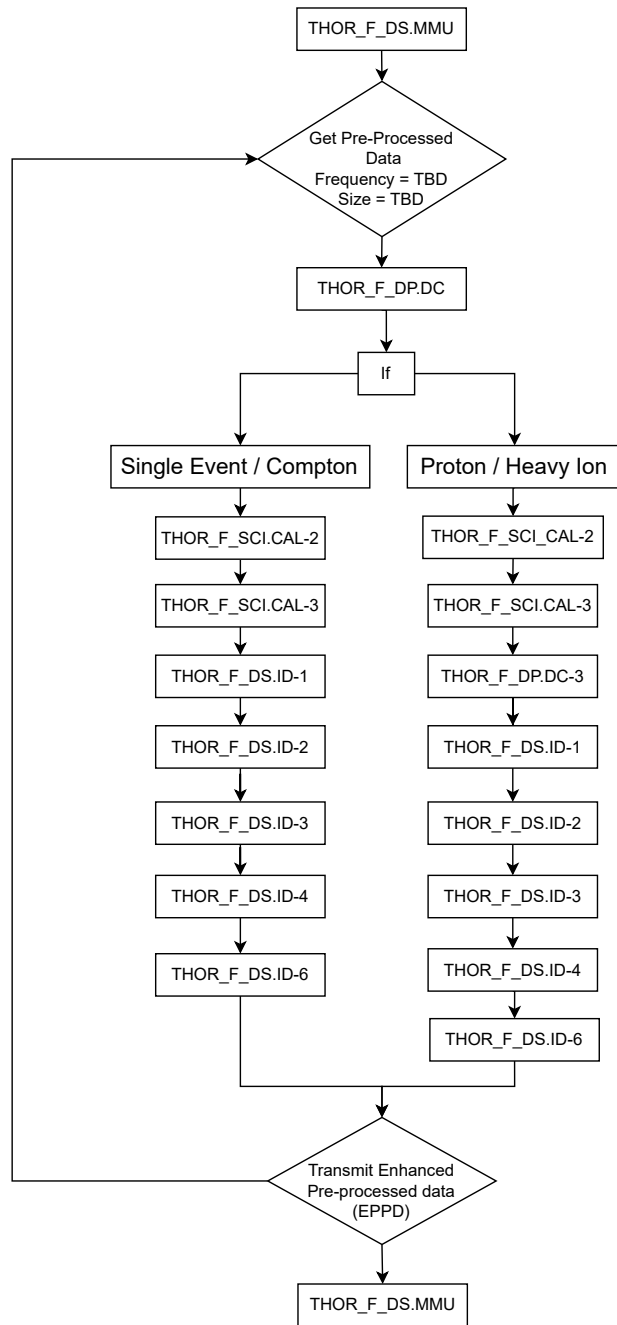


Figure 3.20: Identification and characterization of physics events flow chart. For a detailed description of the function codes see Appendix A

At this stage the OBC_MMU has the data that scientific calculations require. From here the data can be used to perform scientific calculations on orbit or to be transmitted to the LIP-GS as is.

3.6.6.4 Background Characterisation

The OBC performs a background characterization for every celestial gamma-ray source. The OBC grabs the events from the MMU that relate of TBD% of the orbit. The OBC

identifies the number of counts vs energy detected by the detectors on that % of orbit. This results must later be related with the attitude data of the SR for a characterization of the background on exact position of the orbit. To relate this data, a time stamp shall be attributed to this analysis to further relate with the attitude data. See Figure 3.21 for a detailed flow chart of this operation.

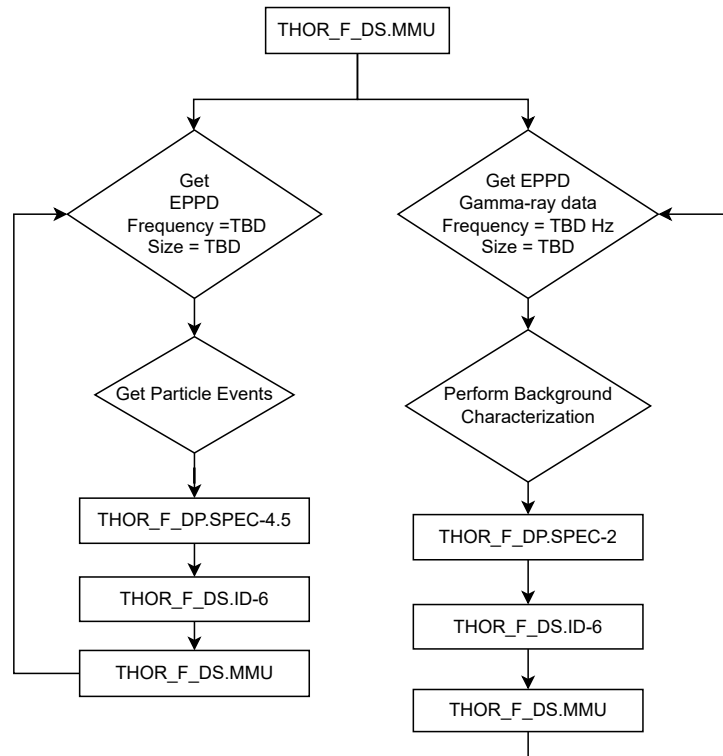


Figure 3.21: Background environment characterization flow chart. For a detailed description of the function codes see Appendix A

3.6.6.5 GRB/TGF Identifier

The OBC regularly checks the Pre-processed data for GRBs/TGFs. Both GRBs and TGFs are transient events in which the photon count rate rises rapidly. To identify such events one shall compare the new data with the background characterization. The OBC shall perform an FFT of the counts vs time and search for peaks. Peaks represent a rapid increase of counts that indicate the detection of a gamma-ray transient. Upon detecting a transient, the OBC will select the events related to the transient and give them a set of unique identifiers. The transients also go through a spectral analysis, polarization degree (PD) and angle (PA) determination. The data related to the transient, as well as the result of the analysis, are saved on the OBC_MMU. See Figure 3.22 for a detailed flow chart of this operation.

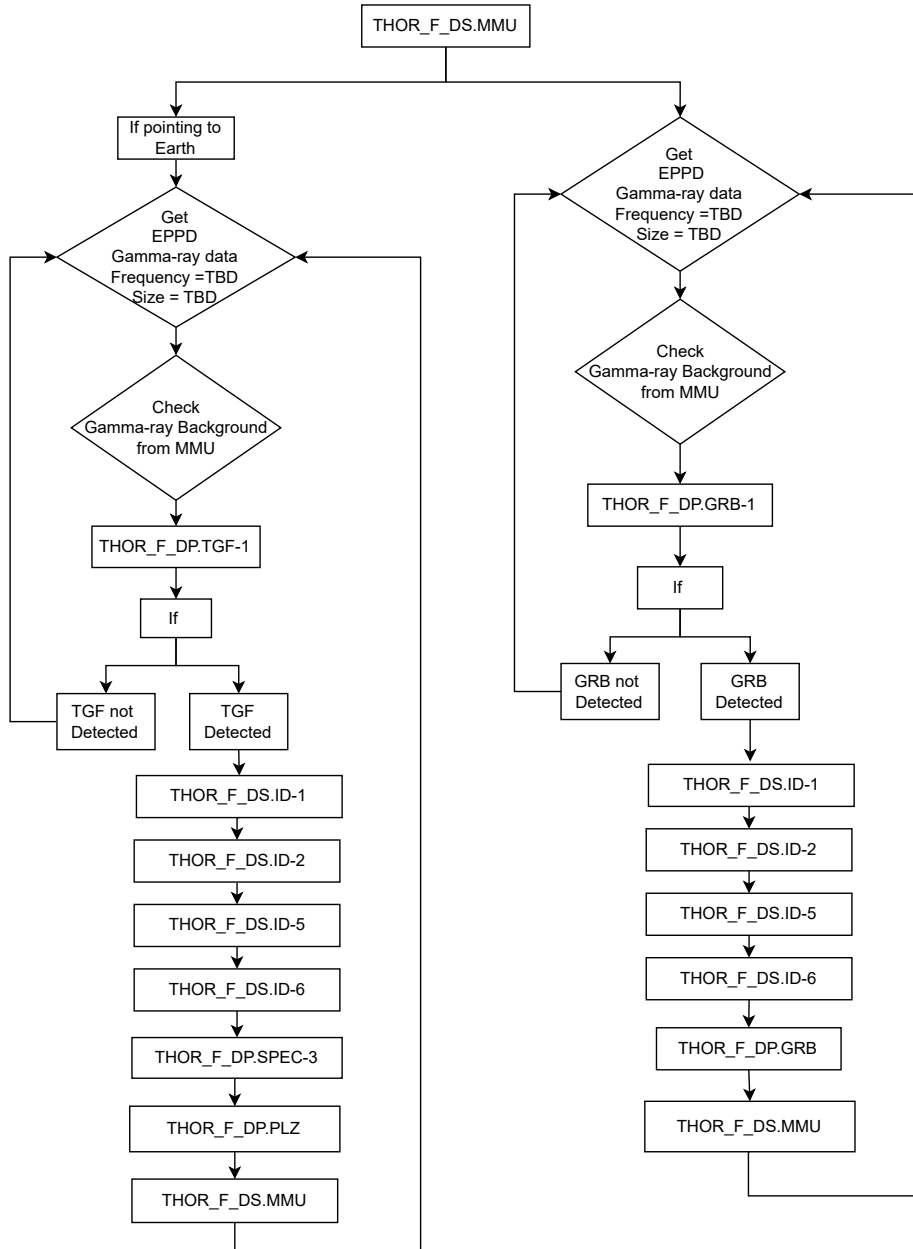


Figure 3.22: GRB/TGF identification and characterization flow chart. For a detailed description of the function codes see Appendix A

3.6.6.6 Source Localization

To identify the source location one uses only the recorded Compton events. Using the Compton kinematics Formula, 2.2, and the data available on the MMU, the energy deposited and the geometric location of the events in the detector, one can create a hypothetical cone from where the source could possibly be. For different Compton events, the area of intersection of these cones, on a projected plane, is the location of the source, see Figure 3.23 for a visual representation.

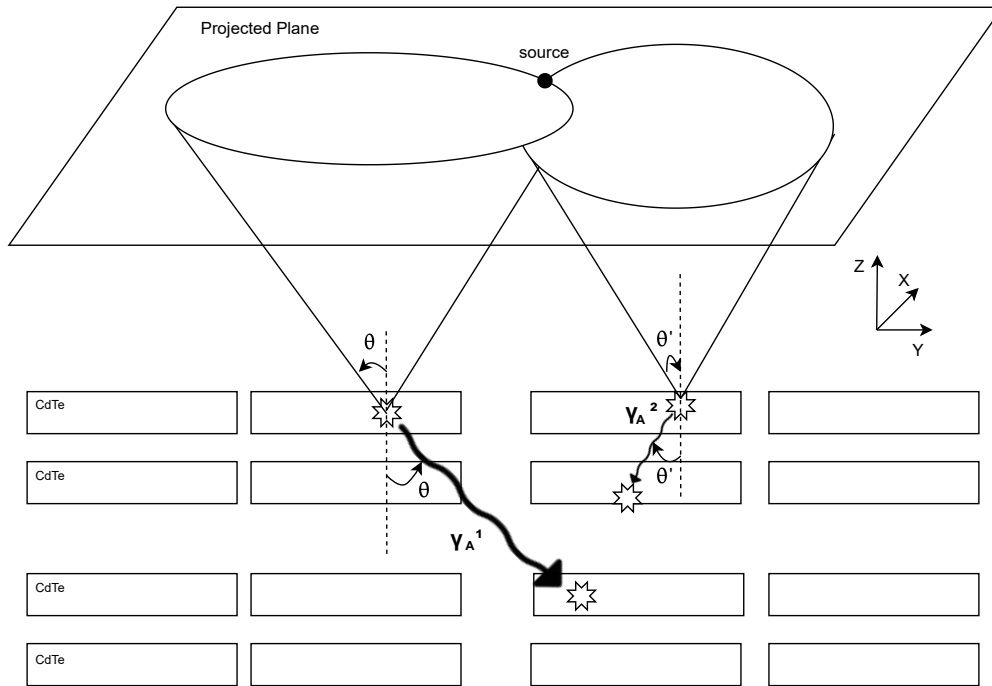


Figure 3.23: Compton source localization visual representation within CdTe DET geometry. For every Compton recorded an elliptical perimeter of possible gamma-ray source position is created on to a projected plane. The intersection of multiple elliptical projections represents the localization of the source.

To do a characterization of continuous sources of the whole universe one can imagine a fixed projection plane and the detector geometry traveling parallel to the plane with \vec{v} velocity (orbit velocity). This projected plane is fixed on the galactic reference frame. The initial position of the detector geometry corresponds to the T0 of an orbit. The final position of the detector geometry corresponds to the end of the orbit. Once the detector geometry reaches that value its goes back to the zero position and starts a new 'scan'. While the detector geometry travels parallel to the projected plane, when a Compton event is detected, an ellipse representing the possible location of the source is projected to the plane. The overlap of the projections gathered from all the scans gives us the location of continuum sources, see Figure 3.24 for a visual representation. To implement the source localization algorithm one must have access to the attitude data of the SR to normalize for orbit and orientation of the THOR reference frame . When the SR sends the record of its attitude data to the OBC (via SR_MMU) the OBC can then implement the source localization algorithm to localize continuum sources as well as transient sources. Also with the attitude data the OBC can then transform the PA and PD of the recorded transients from the THOR coordinate system to the galactic coordinate system. See Figure 3.25 for a detailed flow chart of this operation.

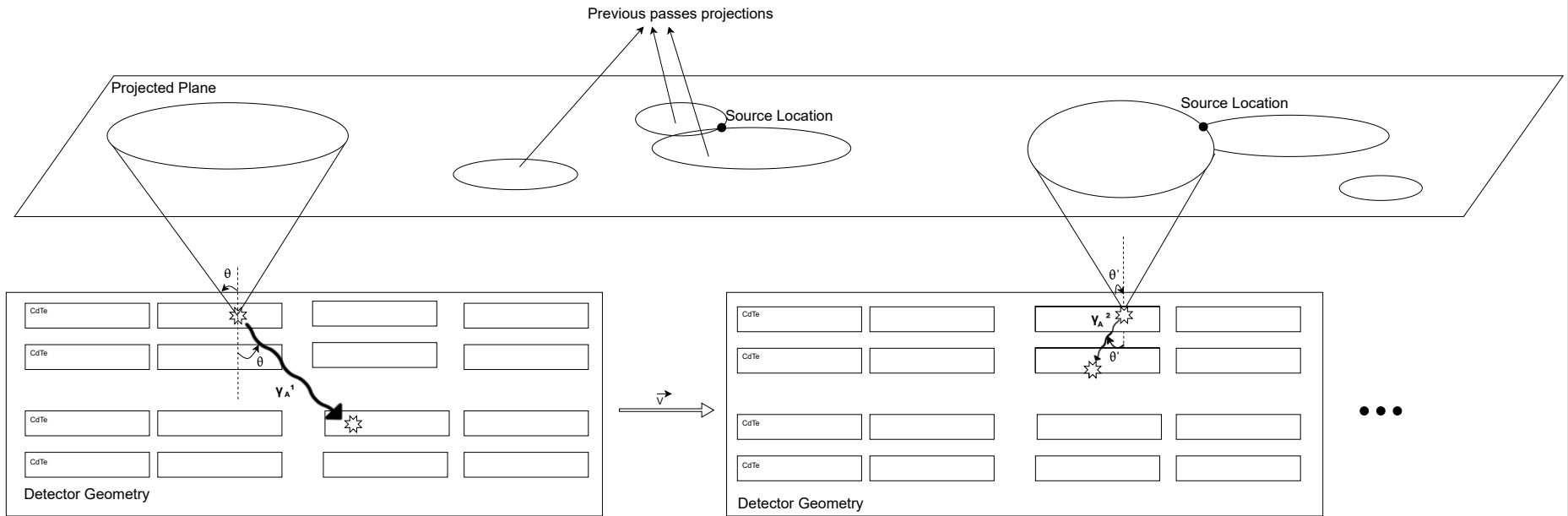


Figure 3.24: Illustration of the moving detector geometry projecting elliptical perimeters of possible gamma-ray source positions on to a fixed projected plane over several passes.

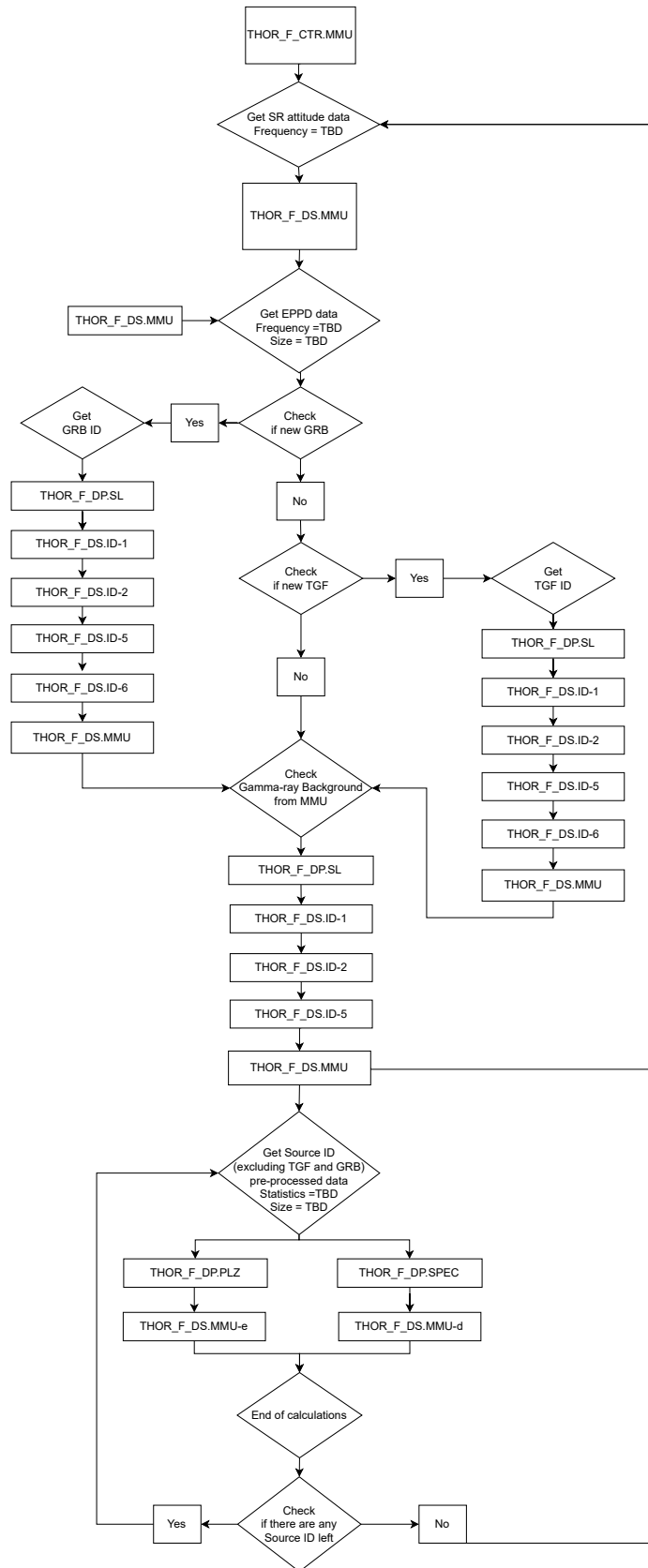


Figure 3.25: Gamma-ray source localization flow chart upon receiving attitude data from SR. For a detailed description see Appendix A.

3.7 Function Description

From the concept of operations it is then defined key function that the payload shall perform. These functions are presented in a function tree, see Figure 3.26 for an easy visualization of the hierarchical decomposition of the P/L capabilities.

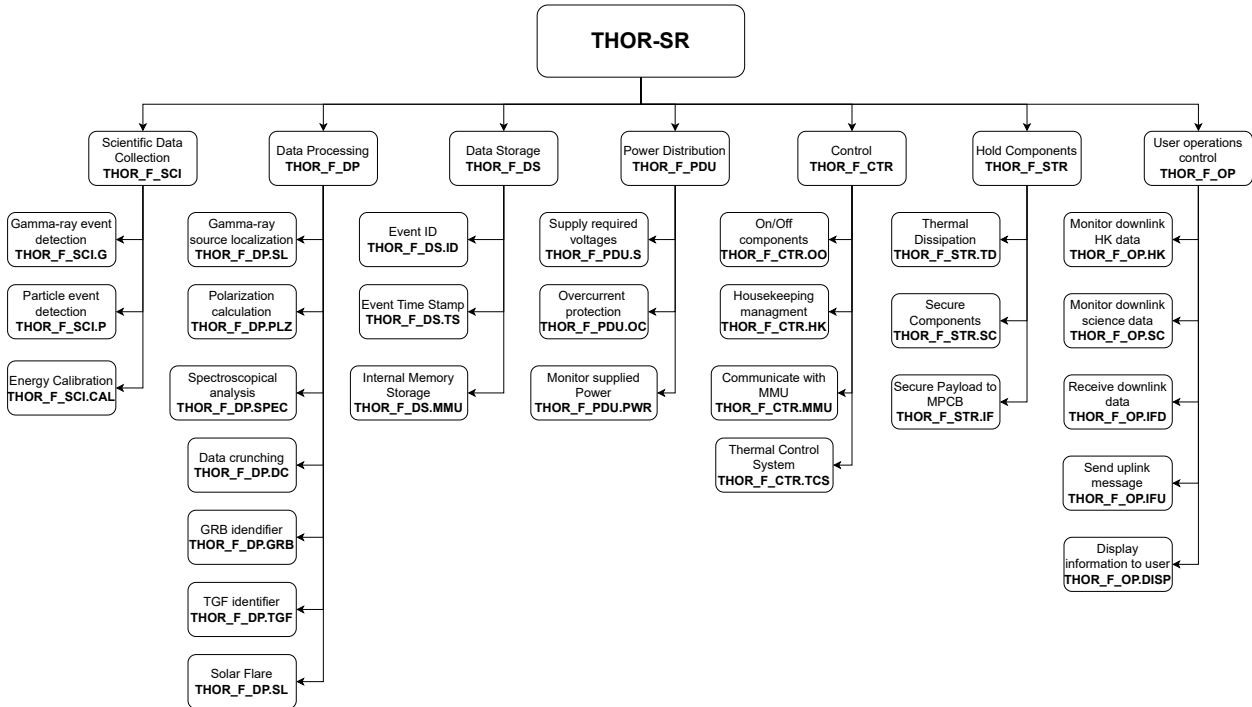


Figure 3.26: THOR Function Tree as defined in ECSS-E-ST-10C Annex H.

3.7.1 Function Definition

In this section it is presented the iteration after the basic definition of the function tree. The first iteration of the function tree helped to formulate the required hardware needed, as well as the functions to be performed on orbit to achieve the scientific objectives. This iteration was developed to help the software team, providing them with an extensive description of each function taking into account the products selected. A detailed description of the functions can be found on the Appendix A.

3.8 Product Description

With the functions outlined is now very easy to understand what components should be used to carry out the operations outline in Section 3.6. Now diving the payload into products and lower level sub-products that constitute a physical deliverable product. The function tree allows a characterization of products for an easy selection of configuration items. Also

the product tree, Figure 3.27, establishes the foundation of the work breakdown structure which allows to allocate human resources/teams/sub-contractors for the development of the products.

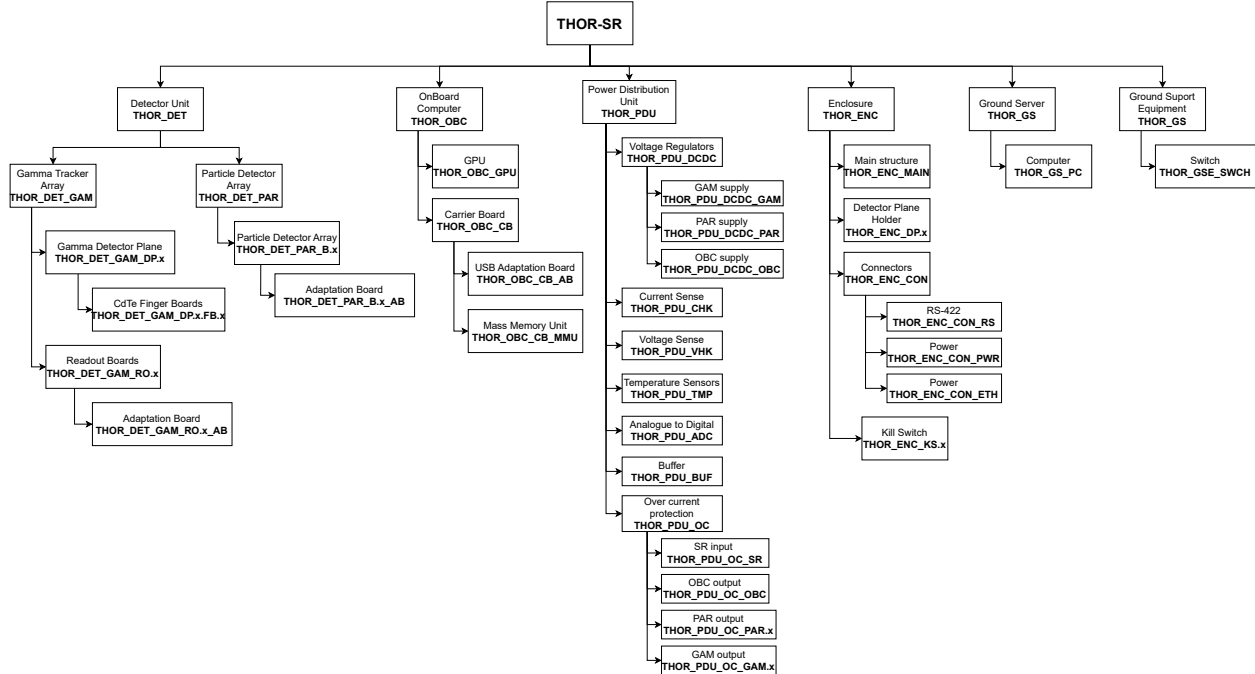


Figure 3.27: THOR Product Tree as defined in ECSS-M-ST-10 Annex B.

From the product tree one can identify 4 main products on the Flight Segment and 2 on the Ground Segment. The products within the Flight Segment; Detector Unit, Onboard Computer, Power Distribution Unit and Enclosure are those to be integrated into the SR unit and are responsible for the achievement the mission objectives, whilst the Ground Segment products have a supporting role within the mission and are not critical for its success. Therefore in this thesis I will mainly focus on the development of the Flight Segment.

3.8.1 Detector Unit - THOR_DET

The THOR-SR will be composed by two main Arrays. The Gamma Tracker Array (GAM) that will be mainly used to measure photons with energy between 20 keV and 10MeV, and the Particle Detector Array (PAR) which will be used to monitor radiation environment on-orbit, photons (x-rays), electrons, protons and heavy ions. GAM is going to be composed of 16 individual 256x256 pixels CdTe matrices, 2 mm thickness that will give us a geometrical front active area of 7.84 cm^2 , a total of 6.27 cm^3 of sensitive volume and a theoretical FoV of 4π sr. It is important to note that, although it is not its primary function, this detector will also be detecting orbital particles that can also be used to characterize the particle background environment. Due the high atomic number, $Z=50$, and density, $\rho = 5.86 \text{ g/cm}^3$,

of the CdTe the detector is sensitive to more energetic particles than the PAR detector. The main characteristics of the GAM are presented in Table below:

| GAM - Gamma Tracker Array main characteristics | |
|---|--|
| Energy range | Photons: 20 keV - 10 MeV; Electron: 20keV - 10MeV; Protons: 20keV - 100MeV |
| Detector Material | CdTe (Cd $Z=48$, Te $Z=52$): $\rho=5.86$ g/cm^3 |
| Single Matrix Characteristics | 256x256 pixels; pixels: $55 \times 55 \mu m^2$; $1.4 \times 1.4 cm^2$; 2 mm thick |
| Geometric configuration | $16 \times FB$; $4 \times (1 \times 4)$ |
| Number of pixels | $> 10^6$ |
| Front active area | $7.84 cm^2$ |
| Total active volume | $6.27 cm^3$ |
| Theoretical Field of view (FoV) | 1.5π sr |
| Effective area (total) | $\sim 5.8 cm^2$ (30keV); $\sim 7.5 cm^2$ (100keV); $\sim 2.6 cm^2$ (500keV); $\sim 1.8 cm^2$ (1MeV); $\sim 1.3 cm^2$ (10MeV) |
| Threshold | 5keV |
| Time Resolution | 1.6ns |
| Dead time per pixel | 475 ns |

Table 3.13: GAM main characteristics

The PAR is composed of 2 individual 256x256 pixel Si matrices, $500 \mu m$ thickness, oriented in two orthogonal directions to monitor the radiation environment giving with 2π FoV. The PAR front end readout electronics is similar to the one in the GAM. The PAR geometric configuration gives us a $2.03 cm^2$ of front active area and a total of $0.196 cm^3$ of sensitive volume. The main characteristics of the PAR are presented in the Table 3.15 below:

| PAR - Particle Detector Array Main characteristics | |
|--|--|
| Energy Range | Photons: 10keV - 60keV; Protons: 20keV - 10MeV; Electrons: 20keV - 500keV |
| Detector Material | Si, $Z=14$; $\rho=2.33 \text{ g/cm}^3$ |
| Single Matrix Characteristics | 256x256 pixels; pixels: $55 \times 55 \mu\text{m}^2$; $1.4 \times 1.4 \text{ cm}^2$; 500 μm thick |
| Geometric configuration | 2xmatrix; (1+1) orthogonal |
| Front active area | 2.03 cm^2 |
| Total active volume | 0.196 cm^3 |
| Theoretical Field Of view (FoV) | $2\pi \text{ sr}$ |
| Threshold | 3keV |
| Time Resolution | 1.6ns |
| Dead time per pixel | 475 ns |

Table 3.15: PAR main characteristics

3.8.2 Gamma Tracker Array - THOR_DET_GAM

The Gamma Tracker array is composed of 4 individual DP assembled in a stack configuration. In [Moita, 2019, Moita et al., 2019, Moita et al., 2020] it was showed that having different detector planes stacked improves the measurement of the polarization of the gamma-rays so the same approach was followed. Also this configuration allows us to have a Compton camera [Cree and Bones, 1994, Turecek et al., 2018] that will be useful to map the gamma-ray sky and identify gamma-ray sources via Compton reconstruction. Each of the DP is going to be composed by 4 horizontally aligned individual CdTe Finger Boards. Limitations regarding physical contact between the DP physical volume the mounting procedure were discussion topics with ADV, and led us to the present configuration, that is presented in Figure 3.28a).

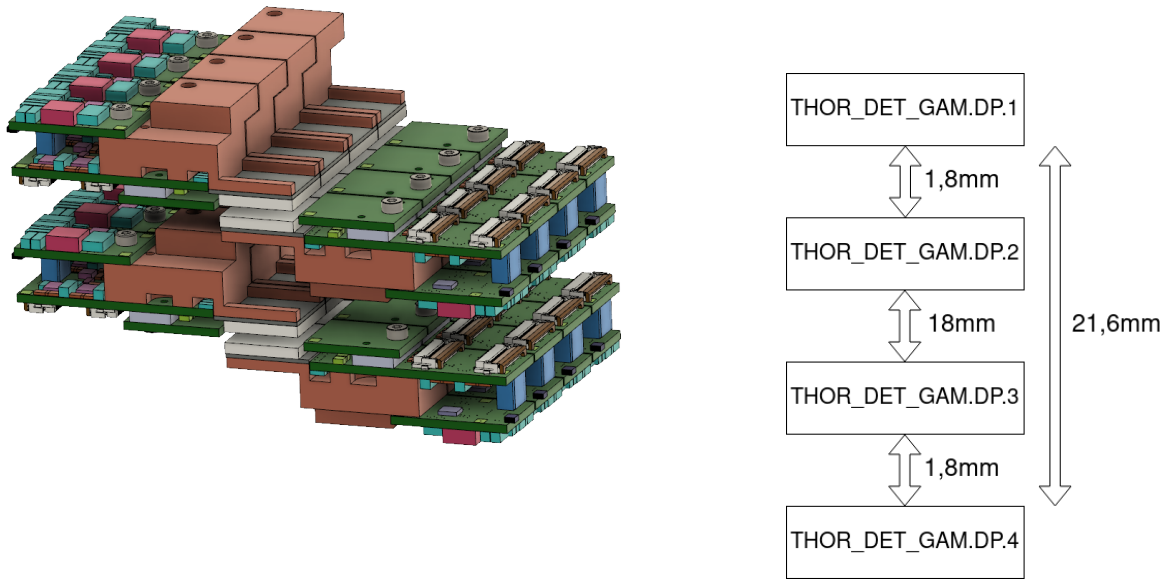


Figure 3.28: a) Geometric configuration of the THOR_DET_GAM - Gamma Tracker Array, b) The distance between the successive CdTe detector planes (DPs).

In Figure 3.29 is depicted the block diagram with the GAM readout electronics and communications configuration. for details see the next sections below.

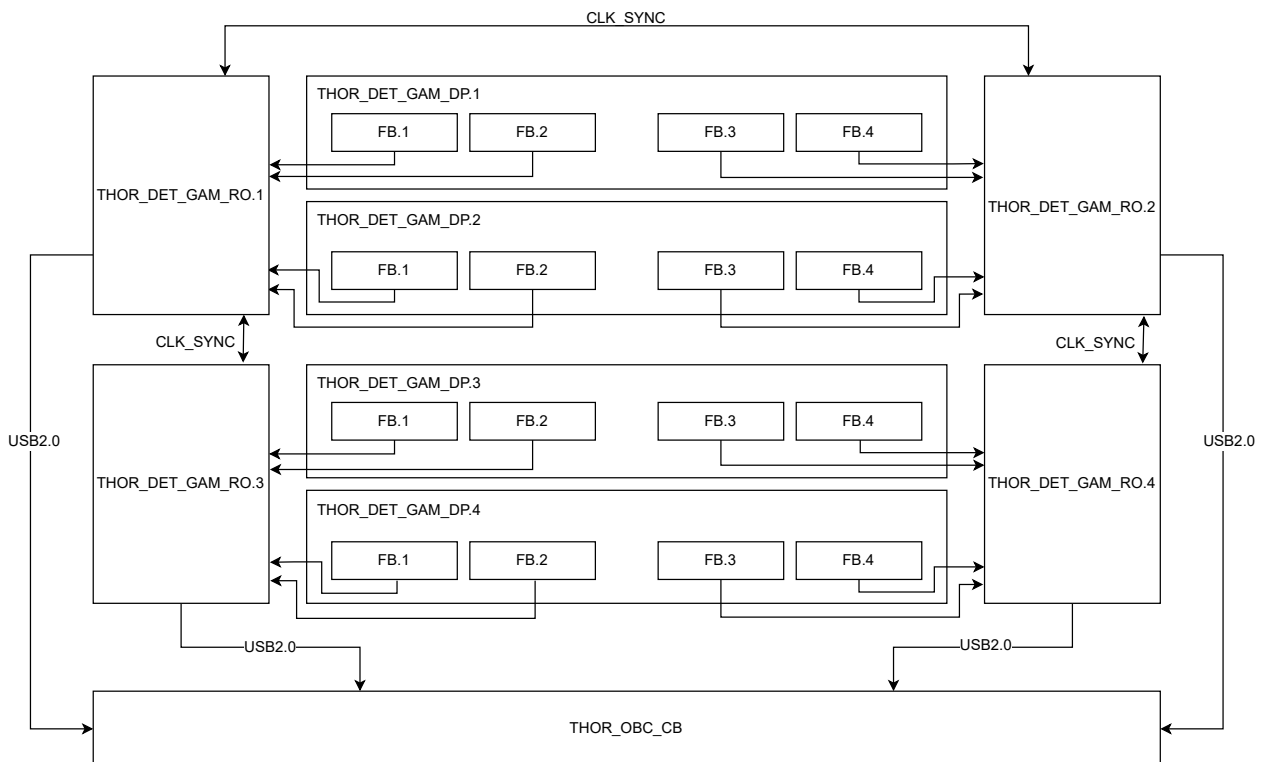


Figure 3.29: GAM readout electronics and communications configuration block diagram.

3.8.2.1 Gamma Detector Plane - THOR_DET_GAM_DP.x

Each DP is composed by 4 CdTe matrices, 4 Finger Board (FB), horizontally aligned in a 1×4 configuration. Half of the DP, will be controlled by one Readout Board (RO) and the other half by other Readout Board (RO), meaning that half of the plane can be ON and the other half can be OFF, see Figure 3.29 above. Thus a spacing of 5mm between the middle finger boards is required to avoid electrical discharge arcs between FBs. This configuration allows for a variety of possible physical interactions with the detector. In the Figure 3.30 is depicted some of the interactions, that we will record during flight. In order to understand the interaction pattern that the physics events leave on the GAM we only need to ensure that the readout electronics of the 16 individual FBs of the detector are in sync within $2\mu s$ (as a first approach we use a $2\mu s$ coincidence windows to identify two signals as coming from the same physics interaction). This is achieved with the use of a 32 pin connector present on the RO boards that share the 40MHz clock.

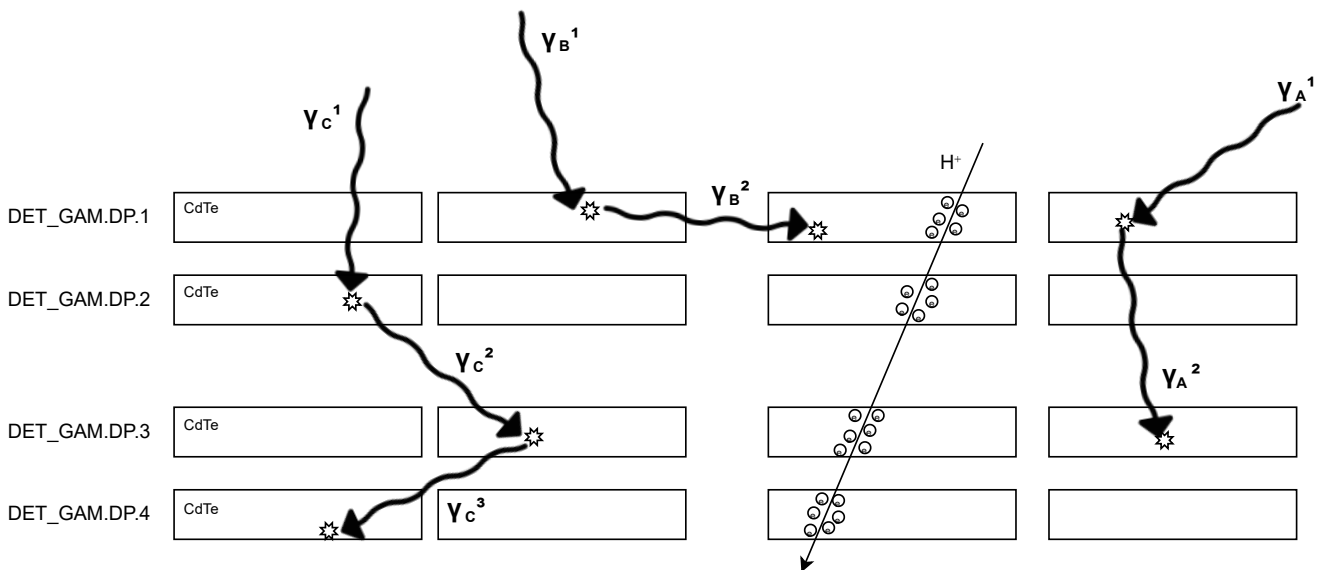


Figure 3.30: Showcase of some physics events on the GAM Tracker Array. Event γ_A showcases a Compton double event where the incoming photon, γ_A^1 , suffers Compton scattering in the first plane and the scattered photon, γ_A^2 , get absorbed by the photoelectric effect on the third plane. Event γ_B is also a Compton double event but within the same DP. Event C showcases a multiple (triple) Compton event, where the scattered primary photon, γ_C^2 , undergoes a second Compton scattering in the third plane that finally gets absorbed by photoelectric effect on the fourth plane. The event H^+ showcases a highly energetic proton crossing every plane of the GAM.

3.8.2.2 Gamma Finger Board - THOR_DET_GAM_DP.xFB.x

Each Finger Board (FB) is composed by the CdTe crystal and front end electronics, a Timepix3 ASIC, that reads the analog current signal generated by an interaction on the semiconductor and converts it to digital. The data sent to the RO boards is already digital and needs to be further characterized by the FPGA present on the RO boards. For every physics event, and per pixel activated, the FB chip gives us the Time over Threshold (ToT) value provided by a 10 bit 40MHz counter (25 ns step) that counts the number of clock pulses the analog pre-amplified voltage signal stays over a threshold value, the Time of Arrival (ToA) a 14 bit value representing the charge time of arrival to the anode of the detector using a 40MHz clock counter (25ns step). The ToA value is complemented with the Fast Time of Arrival (FToA), a 4 bit 640MHz (1.6ns step) clock counter that counts the number of clocks from the time at which the analog pre-amplified voltage signal crossed the threshold and the next ToA clock pulse (see Figure 3.31). The FB attributes the ToT, ToA and FToA values to the respective pixel that collected the charge induced by the physics event.

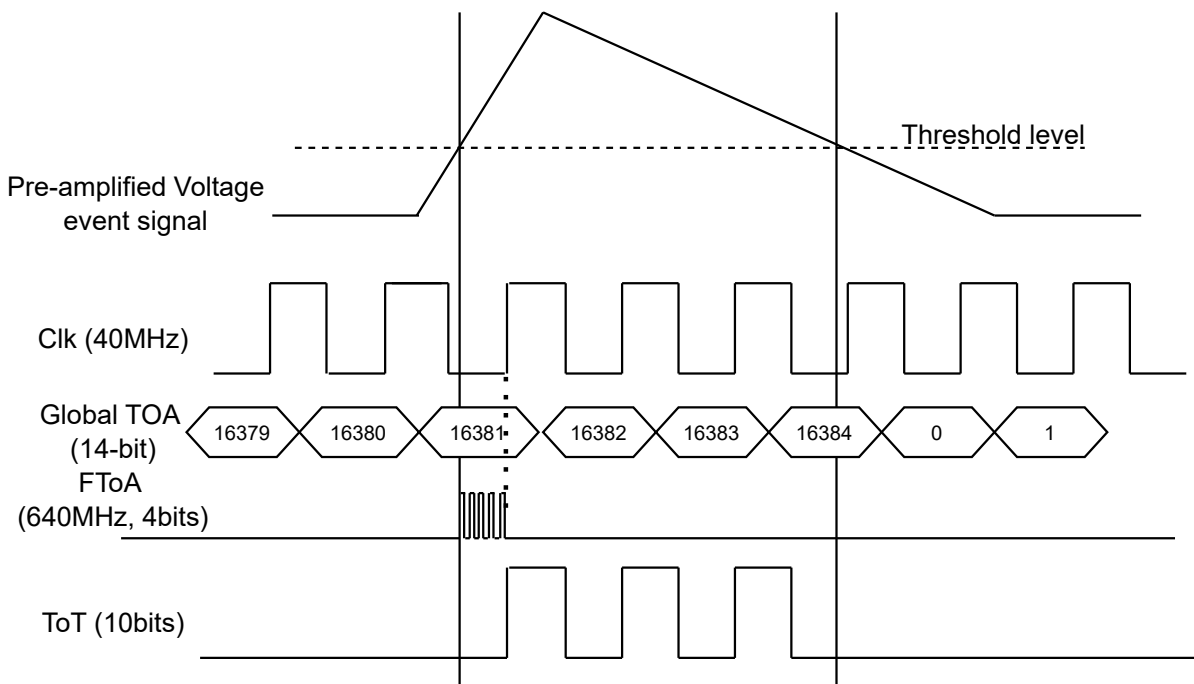


Figure 3.31: Data visualization from Timepix3 ASIC . Adapted from [Brezin et al., 2014].

When an ionizing particle (photons, electrons, protons, heavy ions) arrives to the CdTe semiconductor, the particle transfers part or all of its energy to the medium. This energy is mainly transferred to the orbiting electrons of the cadmium and tellurium atoms, leading to its ejection. These high-energy electrons will then travel in the medium and produce a trail of electron-hole pairs, as represented in the Figure3.32 on the right.

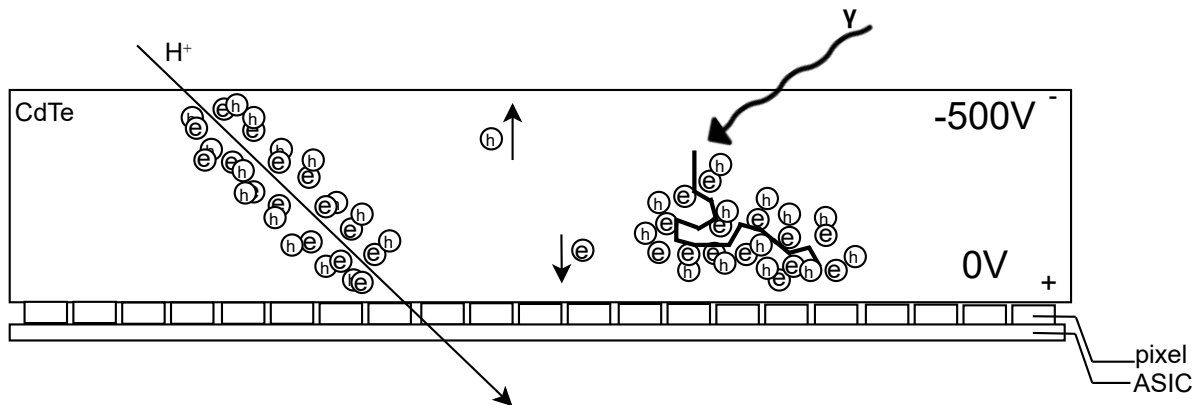


Figure 3.32: Diagram representing a proton interacting with the CdTe (left) and a gamma-ray photon undergoing photoelectric effect (right). The electrons/holes drifts in material due to the electric field applied, being collected in the anode and cathod electrodes, respectively (center). The charge collected on the anode represents the energy deposited in the detector by particle/photon and will be read out by the Timepix3 ASIC.

For a given material the energy necessary to produce an electron-hole pair is largely independent of the type of incident radiation and energy [Knoll, 2010]. Therefore the energy deposited by the primary electron in the medium (CdTe) is directly related to the number of electron-holes created and therefore to the energy deposited by the incident radiation in the CdTe. The Table 3.16 outlines the main characteristics of the CdTe semiconductor.

| Parameter | Value | Units |
|----------------------|--------|--------------------|
| Density | 5.85 | $\frac{g}{cm^3}$ |
| Atomic Number | 48, 52 | |
| Band Gap | 1.44 | eV |
| Pair creation energy | 4.43 | eV |
| Electron Mobility | 1100 | $cm^2V^{-1}s^{-1}$ |
| Hole Mobility | 100 | $cm^2V^{-1}s^{-1}$ |

Table 3.16: CdTe physics characteristics.

The electron-hole pairs produced are submitted to the electric field created by the bias voltage applied to the CdTe, cathod electrode, typically -500V fr CdTe 2mm thick. This electric field conducts the electron-hole pairs to the charge collection electrodes, anode and cathode respectively. The intensity of the electric field applied determines the electrons and holes drift time within the CdTe as the equation below shows,

$$electron : v_e(t) = \frac{dx_e}{dt} = \mu_e E(z) \quad (3.2)$$

$$\text{hole} : v_h(t) = \frac{dx_h}{dt} = \mu_h E(z) \quad (3.3)$$

where μ_e and μ_h are the electron and hole mobility, respectively, in the CdTe - see Table 3.16 for the values. The electric field inside the CdTe semiconductor can be approximated by [Filipenko et al., 2014]:

$$E_z(z, U) = U(f_2 + f_1 z + f_3 \exp(-f_4 U z)) \quad (3.4)$$

where U is the bias voltage applied, z the distance to the detector cathode, and the variable f_1 to f_4 are; $f_1 = (5.8 \pm 0.09) * 10^5 m^{-2}$, $f_2 = (228.0 \pm 7.5) m^{-1}$, $f_3 = (540 \pm 144) m^{-1}$ and $f_4 = 479 \pm 216) V^{-1} m^{-1}$

The charge drift time vs drift distance is presented in the Figure 3.33 for different applied voltage levels.

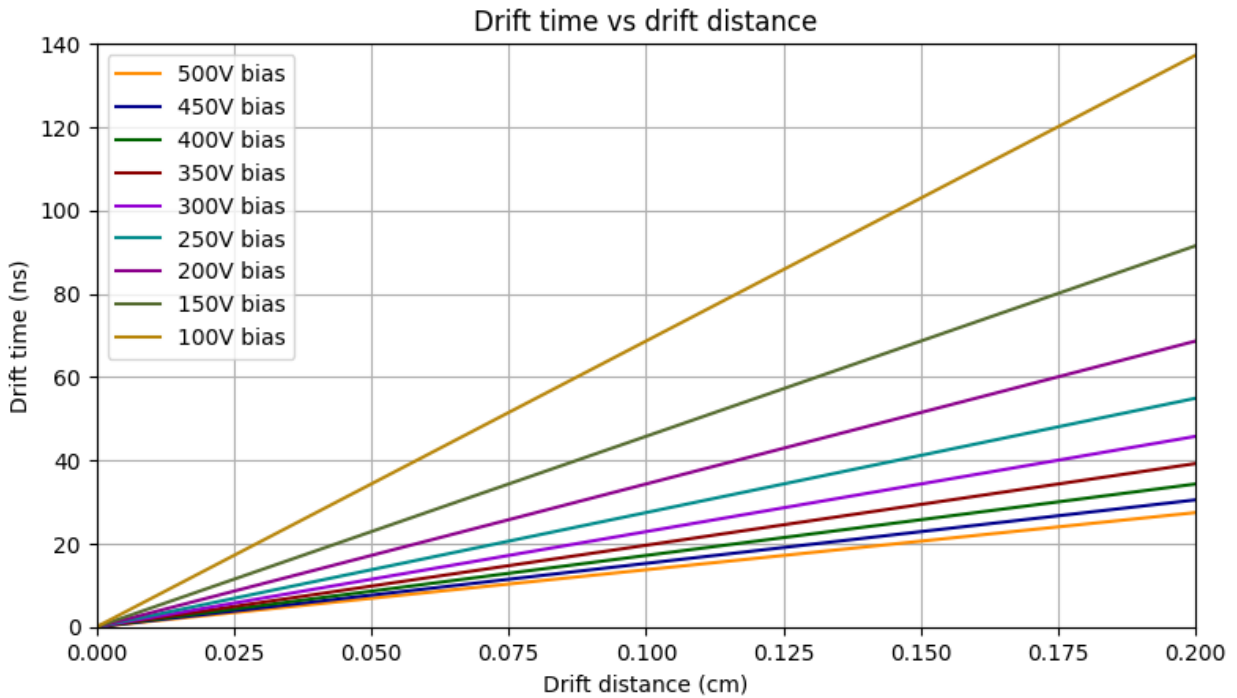


Figure 3.33: Charge drift time as a function of the drift distance within a CdTe detector.

The fast electrons undergo electron-electron interactions and create an electron trail that travels to the anode, see Figure 3.32 right for a visual representation. This charge generates a small current signal at the anode - it is only considered the electrons signal because not only the hole mobility is 10 times lower than the electron mobility but also because the induced signal on the anode pixels by the holes is minimal compared to the signal generated by the electrons and therefore can be neglected [Filipenko et al., 2014]. The electron trail at

the anode may extend over several pixels due to their small size, $55\mu\text{m} \times 55\mu\text{m}^3$. The 1.6ns time resolution due to the combination of ToA+FToA values allows a precise measurement of the time of the event detection, using the following expression:

$$\text{Time}(ns) = \text{ToA} \times 25 - \text{FToA} \times 1.5625 \quad (3.5)$$

This allows the charge drift time inside the CdTe crystal to be characterized. For an event that activates more than one pixel it is then possible to compare the ToA+FToA value for each activated pixel and get the relative depth distance at which the actual interactions took place. This is particularly interesting because it allows us to use each DP as a Compton camera [Turecek et al., 2020].

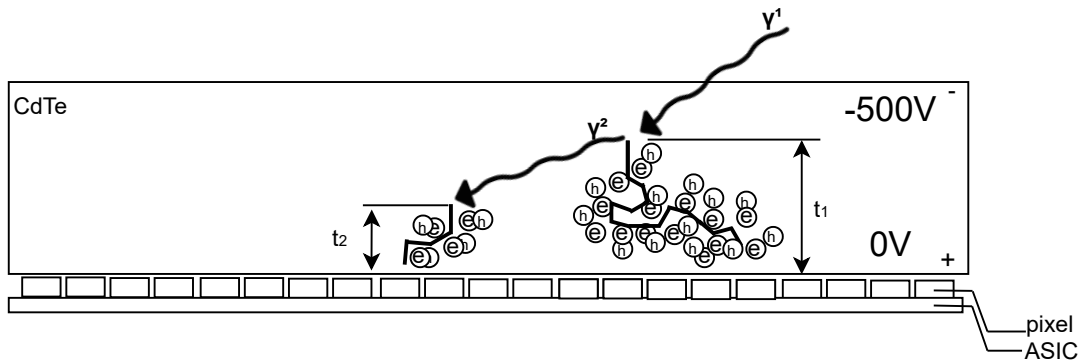


Figure 3.34: Representation of Compton event within the same FB CdTe. For the simultaneity of the γ interactions in the CdTe the electrons trails start the migration to the anode at the same instant. Measuring the time of arrival of each electron cloud/trail, t_1 and t_2 one can get the relative distance Δz at which the events happened.

The Figure 3.34 showcases a Compton interaction in the CdTe. It can be assumed that the absorption of the γ^2 happens at the same instant as the Compton scattering event γ^1 , $t=0$. For practical matters this means that electrons begin their journey to the anode at the same instant. As the γ^2 photon was absorbed closer to the anode the charge will arrive earlier than the charge produced by the scattering of the γ^1 . By considering the 1.6ns time resolution, showcased by Equation 3.5, and an appropriate choice of bias voltage one can maximize the detector depth (z coordinate) determination resolution in order to use a singular DP as a Compton camera.

The signal that is actually measured by the front end electronics is the amount of charge

³The electron cloud can become so diffuse that for the outer perimeter of the cloud the induced charge on the pixels pads may no be sufficient to overcome the threshold of the detector. At this stage of design this hasn't been a problem but is something that we are taking into consideration during tests with the THOR_DET_DM.1

that is induced in the pixel electrode by the charge cloud of secondary electrons during their drift through the CdTe detector. This analog current signal is then readout by the Timepix3 ASIC where for each pixel the signal passes through a charge pre-amplifier that amplifies the signal ($50mV/ke^-$) and transforms it into a voltage signal with a rise time of $<25ns$. After the pre-amplification the signal is routed to a comparator that receives an analog reference voltage, supplied by a DAC, known to misbehave with the changes in temperature. After the analog circuitry the data is converted to digital and ToT, ToA and FToA are acquired as showed in the digital circuitry of the Figure 3.35.

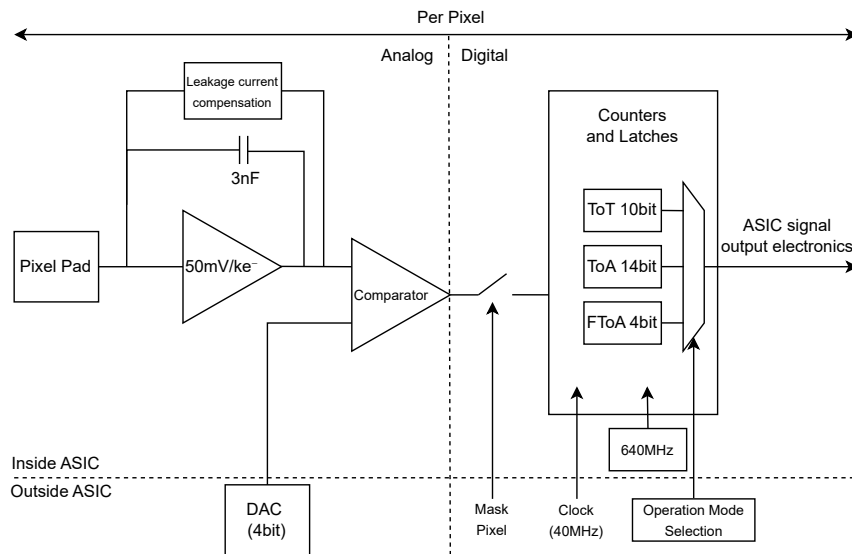


Figure 3.35: Timepix3 ASIC pixel schematics

3.8.2.3 Readout Boards - THOR_DET_GAM_RO.x

The Readout Board (RO) is responsible to interface with the FB to collect the ToT, ToA and FToA whenever an event occur. The system will operate in data driven mode so the RO will be always collecting the SCI data generated by the Timepix3 ASIC. Each RO can interface with up to 4 FB and the configuration that we have at the moment is presented on the Figure 3.29. For each pixel activated, the RO will also add an identifier that represents the ID of which FB the signal came from. The ROs will also share a 32 pin connector that will ensure that the 40MHz clock used to measure the ToT and ToA is in sync. This means that the DP's will be in sync within a 25ns time, REQ-146. The RO will communicate the SCI data with the OBC via USB2.0 protocol. Since the USB2.0 protocol is not a differential protocol the THOR_RSK_005 was identified and the mitigation method lead us to force ADV the redesign of the RO to include proper shielded connectors and harness, to isolate the electrical interface from the EME of the SR. At this stage, still to be reviewed in PDR, the Harwin G125-MH10605M4P was selected due to its space heritage and also to fulfill the mitigation method of the THOR_RSK_006. Also the Power connector had to be changed to

the IPL1-102-01-L-D-RA-K to also fulfill the mitigation procedure of this same risk. In the Figure 3.36 a representation of the redesign, still to be implemented (design change between PDR and CDR) by ADVACAM can be seen.

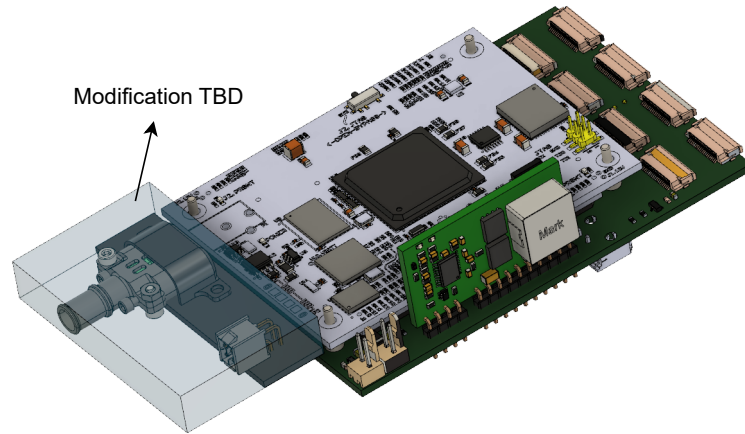


Figure 3.36: GAM readout board with the representation of the TBD modification.

3.8.3 Particle Detector Array - THOR_DET_PAR

PAR will be composed of two Minipix3 detectors that will mainly be used to detect the electron and proton environment on-orbit. For an effective monitoring of the particle radiation that allows for a seamless integration with the GAM's data, the detectors are going to be placed alongside the GAM array as showed in the Figure 3.37. The detectors will monitor the radiation environment in two orthogonal directions.

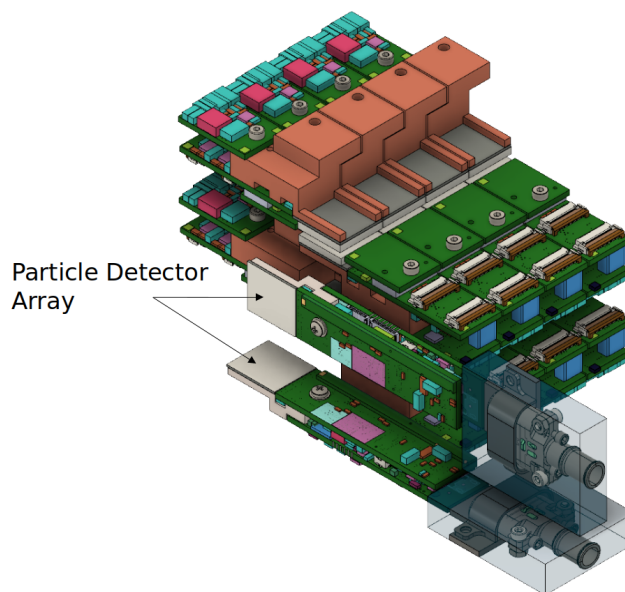


Figure 3.37: Particle detectors geometry alongside GAM.

3.8.3.1 Particle Detector Board - THOR_DET_PAR.Bx

Similar to the GAM the PAR also has a timepix3 ASIC to readout the induced signals from the semiconductor detector, with a similar operation mode. But now, the detector material is Si. Due to the lower stopping power than CdTe hence for a particle with the same energy interacting in both detectors, the mean path inside the Si material is greater than the one on CdTe. In practical terms this means that the particle will activate more pixels on the Si detector than on the CdTe detector and therefore we are able to detect lower energy particles. The Table 3.17 showcases the main characteristics of the Si semiconductor.

| Parameter | Value | Units |
|----------------------|-------|--------------------|
| Density | 2.33 | $\frac{g}{cm^3}$ |
| Atomic Number | 14 | |
| Band Gap | 1.12 | eV |
| Pair creation energy | 3.6 | eV |
| Electron mobility | 1000 | $cm^2V^{-1}s^{-1}$ |
| Hole Mobility | 450 | $cm^2V^{-1}s^{-1}$ |

Table 3.17: Si physics characteristics.

The PCB board of the detectors has already integrated a FPGA that handles the data from the ASIC. It reads out the ToT, ToA and FToA value, organizes them (attributing the pixel id) and sends it to the OBC via USB2.0 protocol.

3.8.4 OnBoard Computer - THOR_OBC

The Onboard Computer (OBC) is responsible for retrieving the data from the DET, pre-processed the data as described on Section 3.11. As the detectors operate in data-driven mode, the OBC will continually be retrieving data from the DET via 6x USB2.0 ports present on the Carrier Board (CB). The OBC performs scientific calculations such as spectroscopy, polarimetry, source localization and identification, and source time variability measurements. In addition to data collection and calculations, the OBC retrieves housekeeping data from each detector's sub-components to monitor their health state. The OBC also controls the functions of the PDU, turning its outputs on/off and monitoring the PDU's housekeeping data. The OBC organizes and characterizes the collected scientific and housekeeping data and saves it to the internal memory OBC_MMU. The relevant data is then transferred to the SR_MMU to be sent to the ground segment. The OBC is based on the NVIDIA Jetson AGX Xavier module, see Figure 3.38, and its characteristics in Table 3.18.

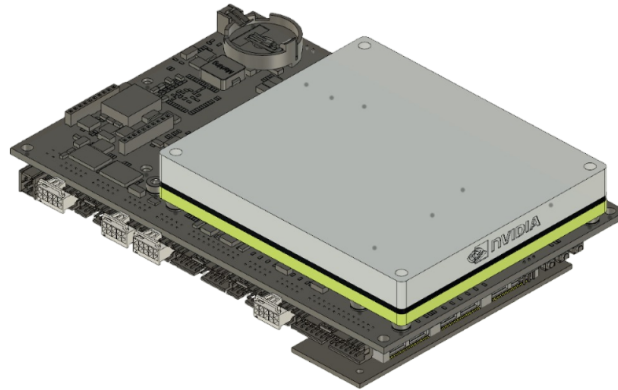


Figure 3.38: THOR Onboard computer.

The module has an ARM v8.2 64 bit CPU with 8 cores with a total of 16Mbyte of cache memory and a GPU with 512 Volta cores and internal memory of 32GB LPDDR4x. Also the Carrier Board will have available a M.2 PCIe SSD Socket 2242 eMMC. The OBC has the capability of limiting its power consumption. In flight mode the consumption will be limited to 10W.

| OBC flight configuration | |
|--------------------------|---------------------------------|
| Model | Jetson AGX Xavier |
| CPU | 2 Cores @2.26GHz, 16Mbyte cache |
| GPU | 512 Volta cores @1377MHz |
| Memory | 32GB |
| Power | 10W |
| Performance | 32 Tera operations s^{-1} |

Table 3.18: OBC flight model configuration

The high performance of this unit is mainly going to be explored by the particle identification and characterization AI algorithms, as well as to perform on-orbit Compton reconstruction.

The use of GPU's in space is an on-going discussion topic [Kosmidis et al., 2022, Kosmidis et al., 2021] where preliminary conclusions indicate that an adoption of such hardware on LEO orbits for short duration of time is viable. Nonetheless, the single-event-effects induced by ionizing radiation on the silicon present on the chip's circuitry is still a problem. Radiation hardness tests on the Jetson AGX Xavier have been performed [Hiemstra et al., 2020], where a 105 MeV proton beam was used in the irradiation of the CPU/GPU and the single-event-effects on the normal operation of the system was studied. The major results are summarized in the Table 3.20 below.

| Test subject | Description | Proton Fluence (<i>protons/cm²</i>) | THOR Exposure Time (days) | Single Event Count | Single Event Description |
|--------------|--------------------------|---|---------------------------|--------------------|--------------------------|
| CPU | Cache ON, Single core | 7.94×10^8 | ~ 101.8 | 4 | System Reboot |
| | | 1.63×10^8 | 20.9 | 1 | System Frozen |
| | | 5.20×10^8 | 66.7 | 1 | Software Error + Reboot |
| GPU | Cache L1 Full Size | 3.73×10^8 | 47.8 | 4 | System Reboot |

Table 3.20: Radiation hardness tests with the Jetson AGX Xavier [Hiemstra et al., 2020].

Taking into account the peak of integral proton flux, with 50% margin, presented below (see Table 3.35) of $7.8 \times 10^6 \text{ proton cm}^{-2} \text{ day}^{-1}$ it also presents the equivalent exposure time of the THOR. It should be highlighted that also electrons may induce single-event-effects. However this is a preliminary approach to estimate the impact of radiation on the OBC.

3.8.4.1 Onboard Computer Carrier Board - THOR_OBC_CB

The carrier board selected is a COTS. The main selection criteria was having an RS-422 interface, 6 x USB2.0 interfaces and the device be industrial grade. The use of an external USB HUB was considered, but the addition of another component would introduce another possible source of failure modes. The selected device is the ELTON carrier board from Diamond Systems, see Figure 3.39. The board is compatible with MIL-STD-202G shock and vibration test and an operating temperature within $-25 - 80^\circ\text{C}$ range.

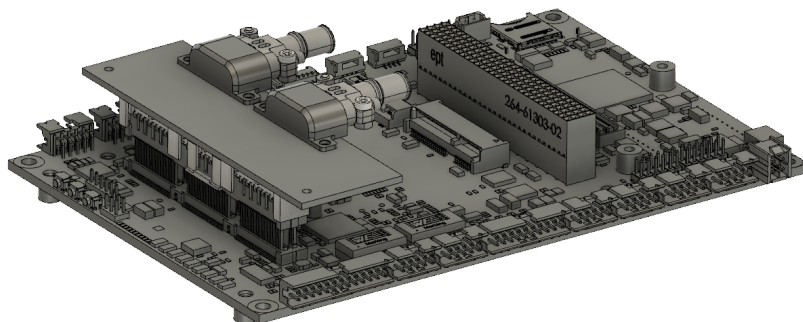


Figure 3.39: ELTON Carrier board selected for the OBC design. Manufacturer: Diamond Systems

The board's PCB is 2.6mm thick and has positive latching connectors to avoid disconnection during the launch phase. To access the $6 \times$ USB2.0 present in the board a custom PCB will need to be developed in order to get the USB's of the vertical ASP-142781-03 PCIe interface, see Figure 3.40.

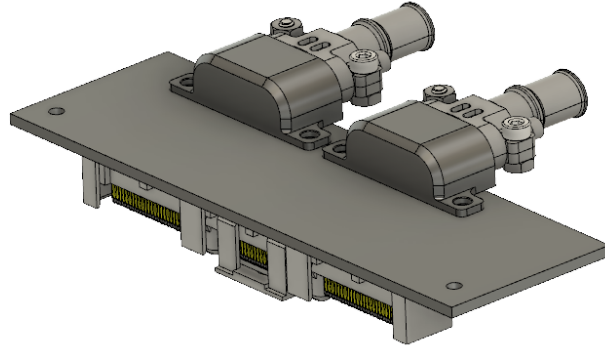


Figure 3.40: Adaptation board to redirect 2x USB2.0 via the PCIe interface. To be developed by LIP.

3.8.5 Power Distribution Unit - THOR_PDU

The power Distribution Unit will be fully developed at LIP and custom designed to fulfil the required needs. In this section a description and a preliminary design of the PDU is presented. The design was achieved by keeping in mind the needs of the P/L. The decision to develop a custom PDU was based on a trade-off study of the available COTS PDU's. Figure 3.41 showcases a block diagram representing THOR's needs/requirements. To check the requirements see Appendix B.

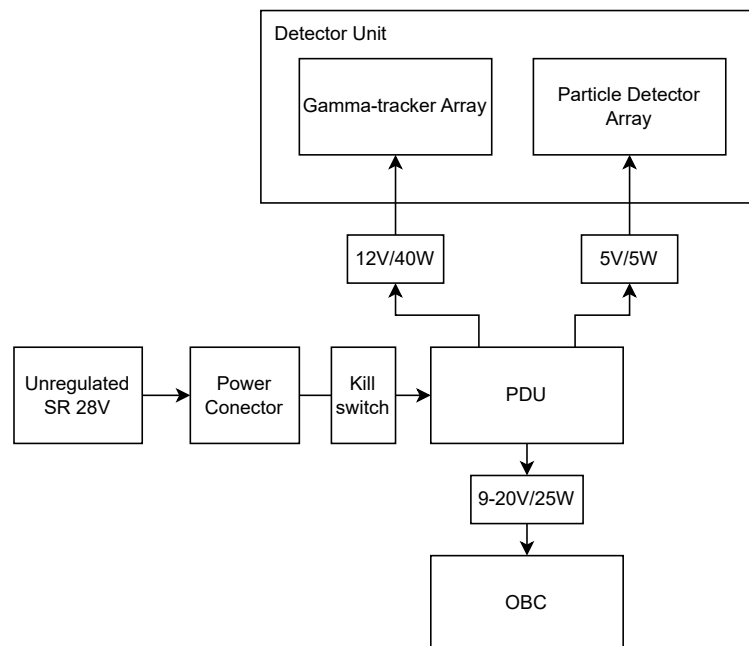


Figure 3.41: PDU block diagram representing the design needs.

The Gamma Tracker Array and Particle Detector Array have specific requirements for their voltage supplies and maximum power consumption. The PDU must be designed to provide controllable voltage supplies within the required ranges and handle the maximum power consumption of each array. The PDU must have a voltage output named VS_GAM that provides a controllable voltage supply of 12V and a maximum power consumption of 40W to the GAM. The output VS_GAM shall be subdivided into 4 individual controllable VS_GAM.x that supply the Readout Boards. Each VS_GAM.x shall be limited to a peak 12W power supply and be limited to a $0.83A \pm 5\%$ continuous current. The PDU must also have a voltage output named VS_PAR that provides a voltage supply of 4.8 to 5.2V and a maximum peak power consumption of 4W. VS_PAR is subdivided into 2 individual controllable VS_PAR.x that supply the particle detectors. Each of the VS_PAR.x output shall be limited to a $0.5A \pm 5\%$ to ensure that if an anomaly happens on the PAR boards, ex. short circuit, the power is cut before any damage is propagated to other P/L products.

The OBC requires a voltage supply of 9V-20V with a maximum power consumption of 25W. From experience it is wise to choose standard voltage levels like 12V since there plenty of options to choose from on the market. The output that supplies the OBC shall always be ON and be able to handle up to a peak of 25W. On the voltage output line it shall also be installed an overcurrent limiter of $2A \pm 5\%$.

The PDU must handle an input voltage range of 22-38V that comes from the SR power system, I/F ID: SR_PWR, and a maximum of 50W - as agreed with the SR team. The PDU must have an input overcurrent protection of 2.5A as a safety provision to ensure that if there is an electrical problem inside the THOR P/L the problem is not propagated to the rest of the SR spacecraft. In addition, it is still unknown if the THOR P/L will share the SR power line with other P/L, in that case, this protection system is paramount in order not to electrically damage neighboring P/L. In order to meet this requirement the PDU must meet specific requirements for input and output overcurrent protection. The input overcurrent protection must be compliant with the ECSS-E-HB-20-20A circuit standard.

In order to reduce the risk of a P/L product becoming nonoperational due to a faulty DC-DC converter, the PDU must have dual modular redundancy at the power converters. Also, to keep the OBC updated on the P/L health status, the PDU must give feedback to the OBC if the outputs are active within a $\pm 10\%$ normal operational voltage, this requirement can be achieved my means of providing the OBC with the ability to continuously monitor the output voltage levels. Current monitor is also required, as the OBC shall be able to monitor each of the current outputs from the PDU with a resolution of 10 bits.

Finally, the PDU must have an external pull-pin kill switch and an external redundant mechanical kill switch on a parallel connection. These switches provide a safety mechanism for shutting down the system in case of an emergency. In addition it gives the test operators

a mechanical switch to turn ON and OFF the payload without needind to connect and disconnect the power plug.

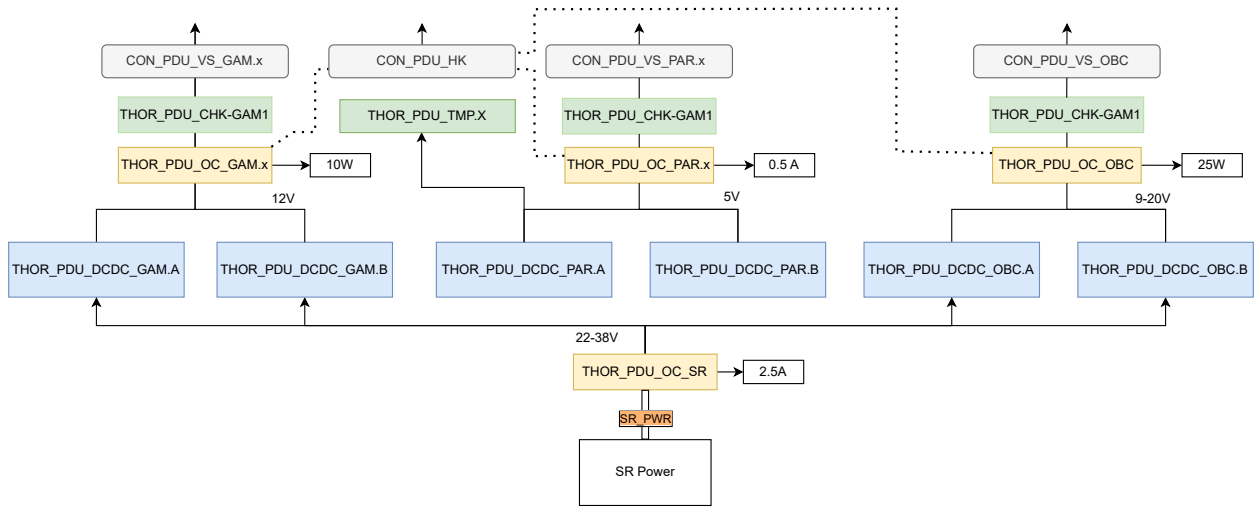


Figure 3.42: PDU detailed block diagram.

The detailed diagram of the housekeeping sensors is presented in Figure 3.43.

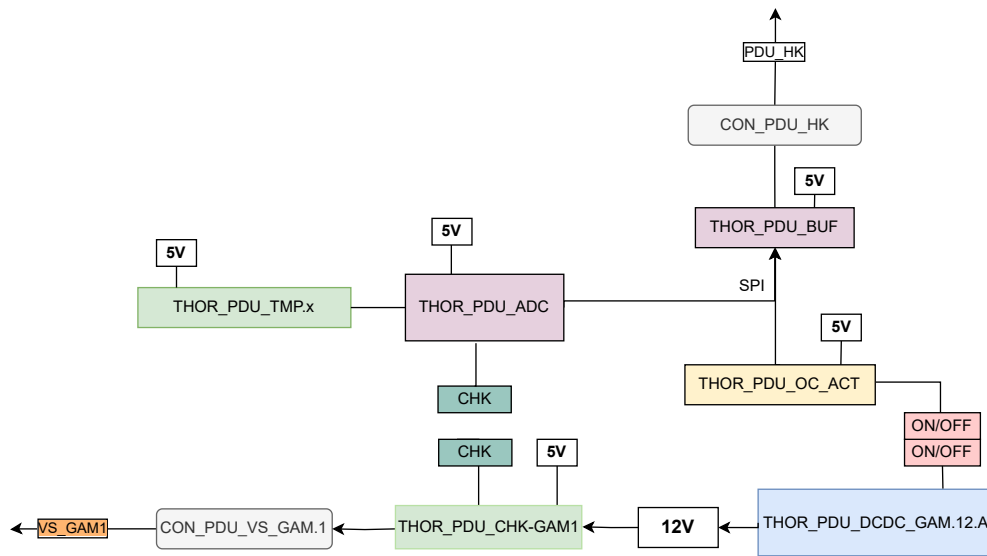


Figure 3.43: Detailed PDU housekeeping block diagram.

3.8.5.1 DCDC Converters - THOR.PDU_DCDC

THOR.PDU_DCDC_GAM

Objective: To supply the correct voltage level to GAM. To convert the unregulated 28V available from SR system to 12V.

Applicable Requirements: REQ-088, REQ-103, REQ-174, REQ-175

Current Design: The selection of this model was based on heritage. The STRATOSPOLCA project used DC-DC from the same series. The components were tested on a TVAC test as well as on a high altitude balloon flight, at 27km. Dual modular redundancy. 4 units in total. 2 sets of 2 parallel connected DC-DC's.

- Model: UWS-12/4.5-Q12P
- Input Voltage: 9-36V
- Output Voltage: 12V
- Output Power: 54W
- Efficiency: 91%
- ON/OFF voltage levels: ON (10-15V), OFF(0V)
- Temperature: -40°C to +85°C
- Storage Temperature: -55°C to 125°C

THOR_PDU_DCDC_OBC

Objective: To supply the correct voltage level to OBC. To convert the 28V from SR system to 12V. Has to be always in ON state. When the PDU turns ON the OBC also turns ON.

Applicable Requirements: REQ-088, REQ-103, REQ-174, REQ-175

Current Design: The selection of this model was based on heritage. The STRATOSPOLCA project used DC-DC from the same series. The components were tested on a TVAC test as well as on a high altitude balloon flight, at 27km. Dual modular redundancy. 2 units in parallel.

- Model: UWS-12/4.5-Q12N
- Input Voltage: 9-36V
- Output Voltage: 12V
- Output Power: 54W
- Efficiency: 91%
- ON/OFF voltage levels: ON (10-15V), OFF(0V)
- Temperature: -40°C to +85°C
- Storage Temperature: -55°C to 125°C

Comments: It might be useful to use the UWS-12/4.5-Q12N since the ON state requires a pin to be connected to GND. Its easier to achieve the Always On functionality.

THOR_PDU_DCDC_PAR

Objective: To supply the correct voltage level to PAR. To convert the 28V from SR system to 5V.

Applicable Requirements: REQ-089, REQ-090, REQ-099

Current Design: The selection of this model was based on heritage. The STRATOSPOLCA project used DC-DC from the same component. The components were tested on a TVAC test as well as on a high altitude balloon flight, at 27km. Dual modular redundancy. 2 units in parallel.

- Model: UWS-5/10-Q12P-C
- Input Voltage: 9-36V
- Output Voltage: 5V
- Output Power: 50W
- Efficiency: 91%
- ON/OFF voltage levels: ON (10-15V), OFF(0V)
- Temperature: -40°C to +85°C
- Storage Temperature: -55°C to 125°C

3.8.5.2 Over Current Protection - THOR_PDU_OC

Objective: When the electrical current intensity on the power supply line exceeds a TBD% value of the nominal value by TBD seconds, the power line is cut.

Applicable Requirements: REQ-097; REQ-102; REQ-103; REQ-106; REQ-107; REQ-176.

Current Design: The present design of the Over current protection circuit is software based. The OBC shall use the HK electrical current intensity data from the PDU outputs and if the current sense value exceeds TBD% of the nominal current by TBD seconds the OBC communicates a command via SPI to the THOR_PDU_OC_ACT to turn off the respective DC-DC. See Figure 3.43

THOR_PDU_OC_ACT

- Model: MCP23s17
- Input Voltage: 5V
- Output I/O: 16 × GPIO, 0-5V
- COM I/F: SPI
- Temperature: -40°C to +125°C
- Storage Temperature: -65°C to +150°C

Comments: This component shall control the ON/OFF state of the DC/DC. The voltage levels are not compatible. A voltage amplifier shall be introduced in this interface (e.g. transistor being supplied by the 12V from THOR_PDU_DCDC_OBC). Also, at this stage we haven't yet decided the design for the THOR_PDU_OC_SR. We want to prevent any fault on our system to propagate to the SR power delivery system. However, we want this process to be reversible, so we don't want to use a fuse as a misfire would render THOR inoperable during the rest of the flight. We want a system that can be managed by the OBC, or a Logic circuit that tries TBD times to reconnect the system to the SR power supply. If the problem continues, it cuts the power for good.

3.8.5.3 Current Sensors - THOR_PDU_CHK

Objective: To measure the current that is being drawn by a power line.

Applicable Requirements: REQ-038, REQ-108.

Current Design: The circuit is based on sensing the voltage at the end of a small resistor, amplifying the signal and feeding it to an ADC.

- Model: INA139
- Input Voltage: 5V
- Output: Current
- Temperature: -40°C to $+125^{\circ}\text{C}$
- Storage Temperature: -65°C to $+150^{\circ}\text{C}$

Comments: If a resistor is placed on the output of the current signal, it can be converted to voltage with the desirable gain.

3.8.5.4 Voltage Sensors - THOR_PDU_VHK

Objective: To measure the voltage level on power line.

Applicable Requirements: REQ-039, REQ-105.

Current Design: At this stage this functionality is not implemented in the design. However, using the INA139 one could also monitor voltage by means of a big sensing resistor.

3.8.5.5 Analogue to Digital Converters - THOR_PDU_ADC

Objective: To readout the analog signal coming from the THOR_PDU_CHK and THOR_PDU_TMX to turn it to digital in ourder to be readout by the OBC.

Applicable Requirements: N/A

Current Design: A 12bit ADC that communicates via SPI with a controller. Acquisition frequency is not a requirement.

- Model: MCP3208T-CI/SL
- Input Voltage: 5V
- Input Frequency: 100kSamples/s
- Bit: 12
- Channels: 8
- Temperature: -40°C to $+185^{\circ}\text{C}$
- Output protocol: SPI

3.8.5.6 SPI Buffer - THOR_PDU_BUF

Objective: Increase the power of the SPI line. The SPI signals need to travel from the PDU to the OBC without beeing affected by EMI.

Applicable Requirements: N/A

Current Design: A buffer circuit that just gives power to the signal.

- Model: SN74LVC2G34DBVR
- Input Voltage: 5V
- Input $\Delta t/\Delta v$: $20\text{ns}/\text{V}$
- Temperature: -40°C to $+125^{\circ}\text{C}$
- Storage Temperature: -65°C to $+150^{\circ}\text{C}$

3.8.5.7 Temperature Sensors - THOR_PDU_TMP

Objective: To monitor the temperature of the DC-DC converters.

Applicable Requirements: N/A

Current Design: A buffer circuit that just gives power to the signal.

- Model: LM19
- Input Voltage: 5V
- Package: TO-92
- Output: Analog voltage, linear
- Temperature: -55°C to 130°C

Comments: Might have to change the temperature sensor depending on the TEST_PDU_001. TO-92 package shall be in contact with the DC-DC for a reliable heat transfer interface.

3.8.6 Payload Enclosure - THOR_ENC

The THOR_ENC system is composed of several sub-products that perform specific functions. The main function of the payload enclosure is to contain the internal THOR P/L products as well as to thermally decouple the heat generated by THOR P/L products. THOR_ENC can be sub-divided into several sub-products, as shown in the product tree, Figure 3.27. The Figure 3.2 left shows the reference frame of THOR and Figure 3.44 showcases the enclosure dimensions and the fixation holes position. The reference frame of the THOR P/L coincides with the reference plane of the Reentry Module of the SR and it is presented on Figure 3.2.

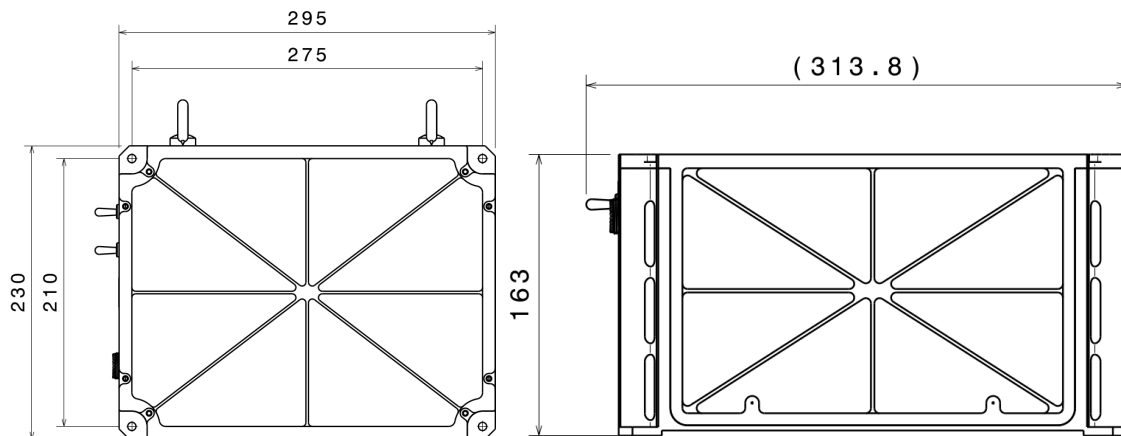


Figure 3.44: Left: THOR front view and dimensions. The fixation M6 hole are horizontally spaced by 275mm and vertically space by 210mm. Right: THOR bottom view and dimensions.

3.8.6.1 Main Structure - THOR_ENC_MAIN

The THOR_ENC_MAIN is the mechanical part that is will hold the THOR_PDU, THOR_OBC and THOR_ENC_DP.x to the Space Rider. The THOR_ENC_MAIN shall ensure that the heat generated by THOR systems is properly dissipated to the SR Support Plates. So, the SR team will provide a thermal filler to improve the heat transfer between THOR and the

base plates (thermal conductivity TBC). The SR Support Plates will be thermally controlled ensuring a temperature within 15 – 40°C range (TBD). Additionally, the THOR enclosure will be covered with a thermal blanket to ensure the P/L's are radiatively decoupled from the MPCB IR environment.

During launch the interface with the SR support plates must support the following mechanical vibration environment:

| Low Frequency Environment | |
|---------------------------|----------------------|
| Axis | Load (g) |
| X | 15 |
| Y | 3.75 |
| Z | 12.5 |
| Random Environment | |
| Frequency (Hz) | Qualification (G/Hz) |
| 20 | 0.0010 |
| 150 | 0.0900 |
| 600 | 0.0900 |
| 2000 | 0.0010 |
| Overall g_{rms} | 7.98 |

Table 3.21: Low frequency and random environment of THOR.

Regarding the shock environment three shocks were identified by the SR team

- Launcher separation shock events, Vega-C first stage separation, and SR separation;
- Parachute mortar shock event, during reentry;
- Parachute strap cutter sock events, during reentry;

The amplitude of the shocks is presented in the Figure 3.45 but still TBC by the SR team.

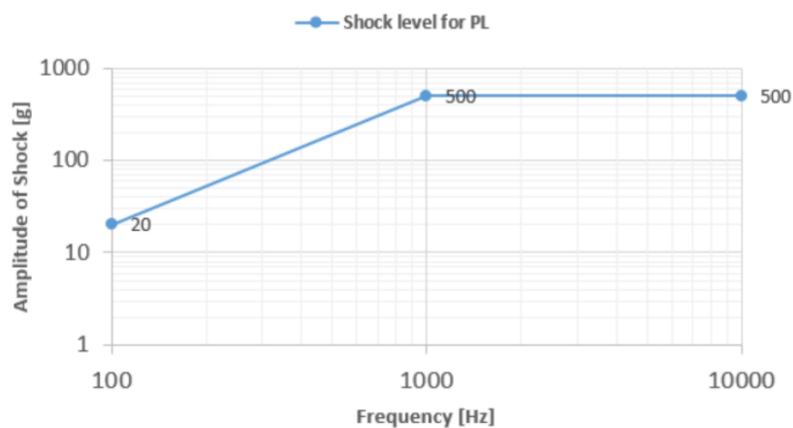


Figure 3.45: Expected shock environment on THOR.

3.8.6.2 Detector Plane Structure - THOR_ENC_DP.x

For easier integration purposes, the structure holding the Detector Unit, THOR_DET, shall be modular. Each of the Detector Planes shall have a corresponding enclosure module, nominated by THOR_ENC_DP.x, with *x* the plane number ID. The Detector Planes will be assembled by Advacam.

3.8.6.3 External Connectors - THOR_ENC_CON

Power Connector, THOR_ENC_CON_PWR - The Power connector to be used is

340105601B06-15-19PN, male, with the characteristics presented on the Figure 3.46. The connector ensures a Ground connection to THOR structure (due to the highlighted **06** code, 340105601B06-15-19PN). The single-point connection to ground shall be on the connector.

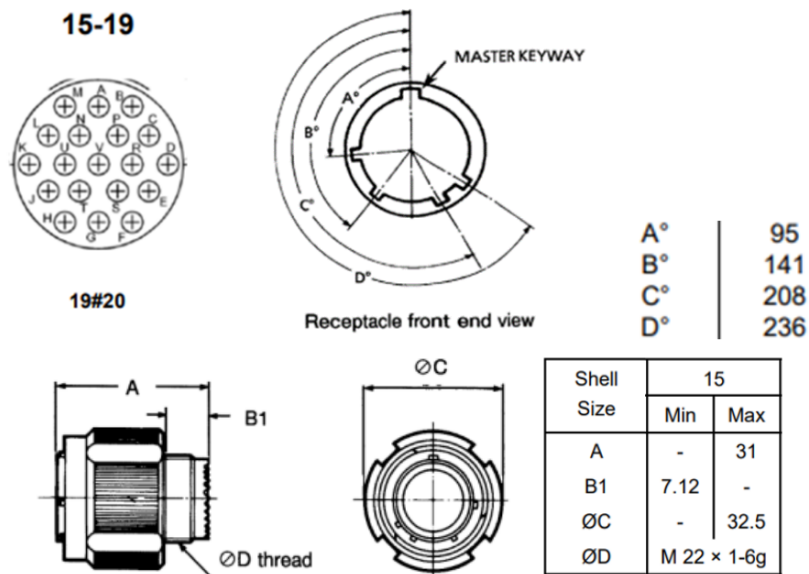


Figure 3.46: Power connector to be placed on the outside of the enclosure. To receive the 28V from the SR.

Communication Connector, THOR_ENC_CON_RS - The Communications connector to be used is 340107702B MDMA-9S-FO female receptacle plug, with the following characteristics, Figure 3.47:

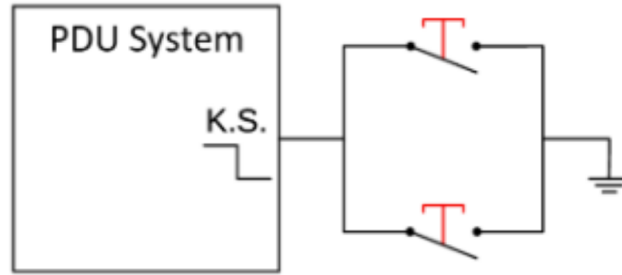


Figure 3.49: Kill switch parallel design.

3.8.7 Ground Segment - THOR_GS

The LIP Ground Segment shall be connected permanently to the PGCC to receive the payload downlink data (TM) and also to send uplink commands (TC) whenever required. The LIP Ground Segment will be analysing the Scientific Data on a daily basis in order to check if the Detector Unit is operating properly. In case of an unforeseen error, the LIP Ground Segment shall be able to send a command to the SR Ground Segment in order to re-transmit it to the payload OBC and also in case of a solar or transient celestial event that can either be of great scientific value (e.g. supernova explosion, strong X-ray emitter, etc.) or critical to the Detector Unit. In both cases, an uplink message to the OBC shall be sent to either adjust the Detector’s threshold or to turn-off the Detector Unit. Figure 3.50 showcases the LIP ground segment architecture.

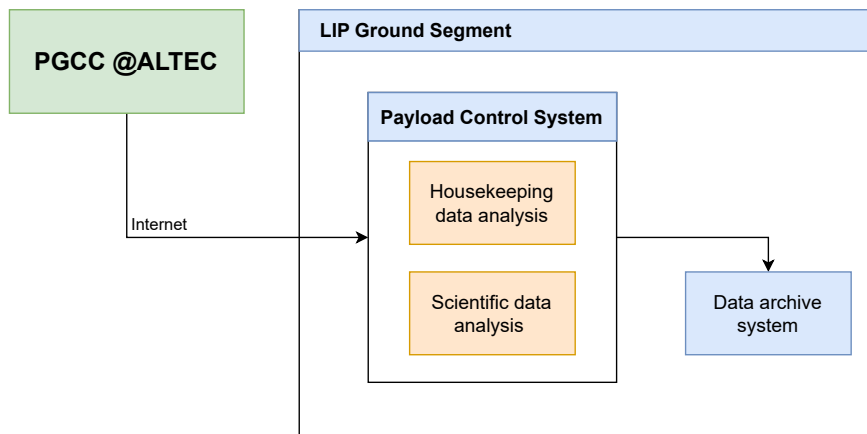


Figure 3.50: LIP ground segment block diagram.

3.9 Interfaces

On the Table 3.22 we present the electrical interfaces of the P/L. On Table 3.24 a brief description is given regarding the functions and interface type.

3.9.1 Internal Electrical Interfaces

The Appendix C showcases a detailed diagram of the electrical interfaces between the P/L products.

| Electrical Interfaces | | | | |
|------------------------|------------------|----------------------|---|----------------------------|
| Product A ID | Connector ID | Interface ID | Connector ID | Product B ID |
| THOR_DET_GAM_DP.x.FB.x | CON_DET_GAM_FBRO | GAM_FLATCABLE | CON_DET_GAM_ROFB | THOR_DET_GAM_RO.x |
| THOR_DET_GAM_RO.x | CON_VS_GAM_RO.x | VS_GAMx | CON_PDU_VS_GAM.x | THOR_PDU |
| THOR_DET_GAM_RO.x | CON_DET_GAM_RO.x | USB2_GAMx | CON_OBC_CB_USB_GAMx | THOR_OBC_CB |
| THOR_DET_PAR_B.x | CON_DET_PAR_B.x | USB2_PARx VS_PARx | CON_OBC_CB_USB_PARx CON_PDU_VS_PAR.x | THOR_OBC_CB_AB THOR_PDU |
| THOR_OBC_CB_AB | CON_AB_PCIE_USB | PCIE_USB | CON_CB_PCIE_USB | THOR_OBC_CB |
| THOR_OBC_CB | CON_VS_OBC_CB | VS_OBC | CON_PDU_VS_OBC | THOR_PDU |
| THOR_OBC_CB | CON_OBC_PDU_HK | PDU_HK | CON_PDU_HK | THOR_PDU |
| THOR_OBC_CB | CON_OBC_CB_RS | SR_RS422 | THOR_ENC_CON_RS | THOR_ENC_CON_RS |
| THOR_PDU | CON_PDU_SR_PWR | SR_PWR | THOR_ENC_CON_PWR | THOR_ENC_CON_PWR |
| THOR_PDU | CON_PDU_SR_KS.x | SR_KS.X | THOR_ENC_KS.x | THOR_ENC_KS.1 |
| THOR_OBC_CB | CON_OBC_CB_ETH | OBC_ETH | THOR_ENC_CON_ETH | THOR_ENC_CON_ETH |

Table 3.22: Electrical interfaces between THOR products. Location of the connector within each product is showcased on Appendix D.

| Electrical Interfaces Description | | | | |
|--|--|---------------|-----------------|-----------------------|
| Interface ID | Function | Type | Protocol | Cable Type |
| GAM_FLATCABLE | Transmit data from front end electronics to the RO.x. Supply power to the front end electronics. Supply HV to polarize the CdTe. | Data + Power | N/A | Flat Cable (30cm max) |
| USB2_GAMx | SCI+HK data transmission from gamma detector (CdTe) from the respective planes (x). | Data | USB2.0 | Shielded |
| USB2_PARx | SCI+HK data transmission from particle detector (Si) from respect planes (x). | Data | USB2.0 | Shielded |
| PCIE_USB | Redirect the 2xUSB2.0 present on the PCIe 3 Bank on the THOR_OBC_CB | Data | USB2.0 | N/A |
| VS_GAMx | Supply power to THOR_DET_GAM_RO.x | Power | 12V | Normal |
| VS_PAR | Supply power to the THOR_DET_PAR_B.x | Power | 5V | Normal |
| VS_OBC | Supply power to the THOR_OBC | Power | 12V | Normal |
| PDU_HK | Transmit HK data from the THOR_PDU to the THOR_OBC. Allow control ON/OFF of voltage outputs | HK | SPI | Twisted |
| SR_RS422 | Communication between THOR_OBC and SR_MMU | HK+SCI +TM+TC | Serial - RS422 | Twisted |
| SR_PWR | Power delivery from the SR Power Supply System. | Power | 28V unregulated | Normal |
| SR_KS.x | External ON/OFF control status of THOR | ON/OFF | Binary | Normal |
| OBC_ETH | Allow the User full control of the THOR_OBC during ground tests. | Data | Ethernet | Normal |

Table 3.24: Electrical interface description.

3.10 Orbital Environment

The SpaceRider is expected to be launched into a stable 400km and 5.3° inclination orbit with a 2 months nominal mission lifetime. The launch is expected to be on the 3Q 2025, which coincides with the forecast for the maximum solar activity [Petrovay, 2020]. The objective of this chapter is to predict the gamma-ray and particle environment in orbit. It was considered the worse-case scenario which is used as a baseline to predict the SCI data generated by the THOR. It is well known that the trapped particle environment in orbit depends strongly from its inclination and altitude. Figure 3.51 depicts the representation of the simulated orbit overlapped with the globe map.

| SR Orbit | |
|--------------------|-------|
| Orbit Inclination: | 5.3° |
| Altitude: | 400km |

Table 3.25: Space Rider expected orbit.

| Simulated Orbit | |
|--------------------|-------|
| Orbit Inclination: | 6° |
| Altitude: | 400km |

Table 3.26: Orbit used on the simulations.

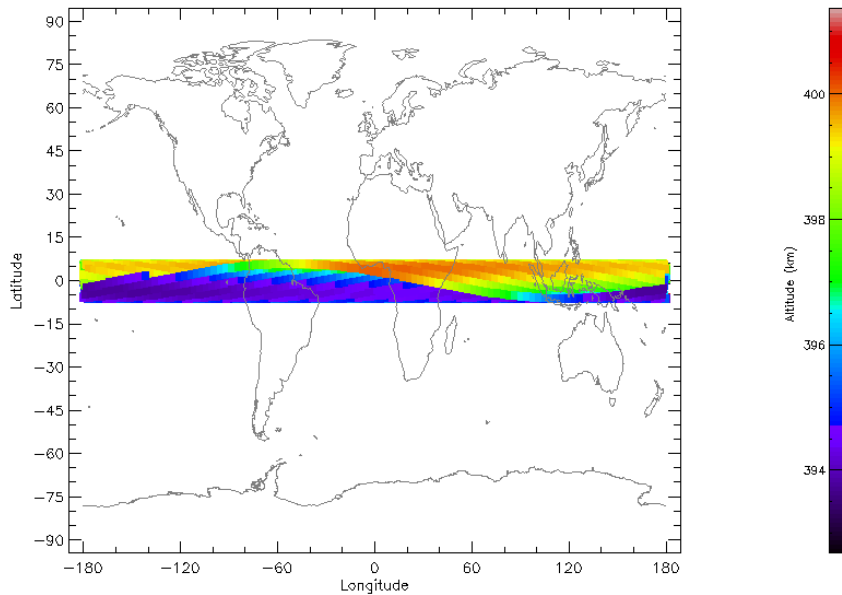


Figure 3.51: Simulated orbit geometry overlapped with globe map. Source SPENVIS.

In the simulation of the particle environmental conditions in LEO, the SPENVIS platform was used [Kruglansky et al., 2009].

3.10.1 Gamma-ray Environment

For this study the background gamma-rays between the energies of 100keV to 1MeV were considered. This subsection was based on the work of [Cumani et al., 2019] in which a GitHub

repository⁴ with the simulations made is available. There are several sources of gamma-rays’ in the universe: i) extragalactic photons (isotropic) coming far from the galactic plane, ii) albedo photons created in the Earth atmosphere due to the interaction of cosmic rays or reflection of the cosmic X-ray background, and iii) galactic photons that come from the galactic plane of the Milky Way.

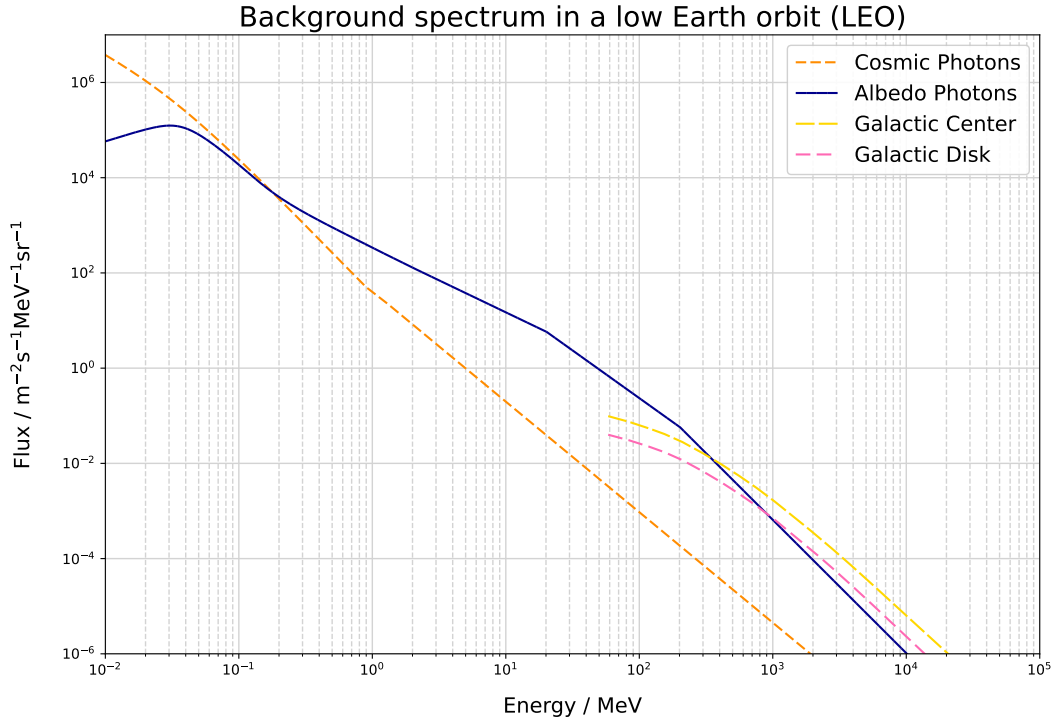


Figure 3.52: Photon background flux for a 400km 6° inclination. Up until ±200keV Cosmic photons re the predominant ones, whilst from 200keV-100MeV the Albedo photons become the predominant background source. Data collected from the github database⁴.

The photons from the galactic plane can be neglected because they are too energetic for the energy range of interest. As a preliminary study we only consider the Cosmic Photons as a source of background events because we assumed that the SR is always zenith pointing⁵. The absorption of the 1mm thick Al of the enclosure was not considered although, in fact, it will reduce the flux for lower energies as shown in the Figure 3.53. But as we are interested in the worst case scenario this wont impact the outcome of this assessment.

⁴<https://github.com/pcumani/LEOBackground>

⁵in reality it will comply with REQ-171 but using a 50% margin on the expected flux this change should fall within the error margin.

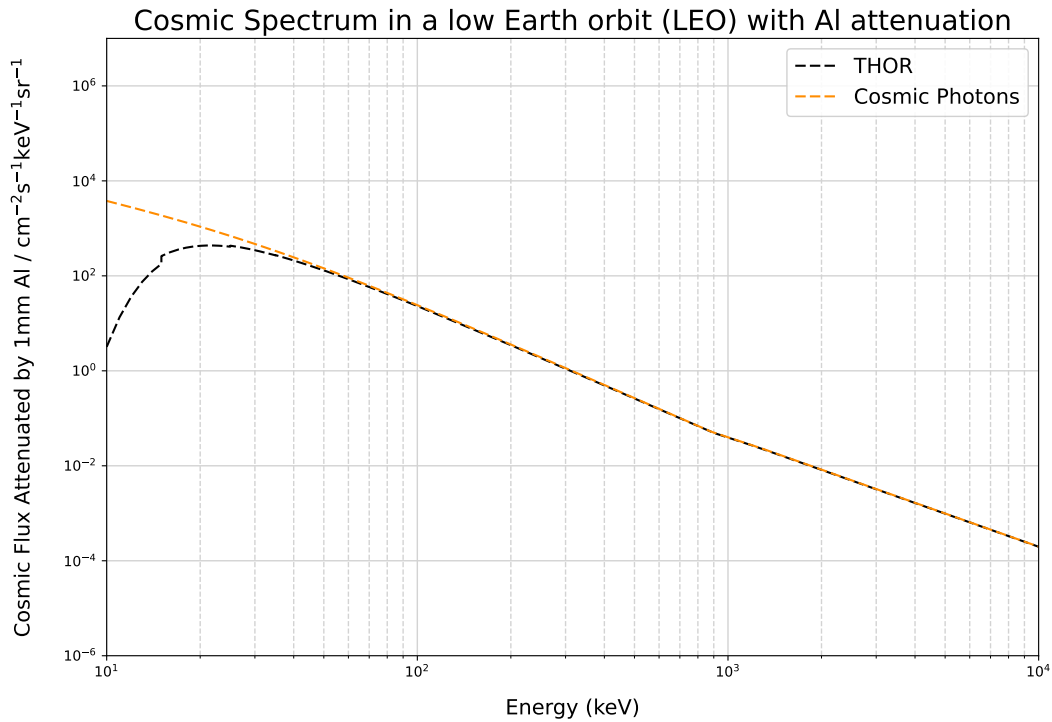


Figure 3.53: Cosmic Photons with 1mm Al attenuation.

For energies $E < 890 \text{ keV}$ the Cosmic gamma-ray background flux can be modeled as:

$$F = \frac{0.109}{(E/28 \text{ keV})^{1.4} + (E/28 \text{ keV})^{2.88}} \quad (3.6)$$

and for $E \geq 890 \text{ keV}$ by:

$$F = 0.95 \times 10^{-10} \left(\frac{E}{100 \text{ MeV}} \right)^{-2.32} \exp\left(\frac{-E}{279 \times 10^3 \text{ MeV}} \right) \quad (3.7)$$

Equations 3.6 and 3.7 have the units: $\text{keV}^{-1} \text{ cm}^{-2} \text{ s}^{-1} \text{ sr}^{-1}$. Thus integrating the equations numerically and setting the correct units an integral flux of $0.154 \text{ photons cm}^{-2} \text{ s}^{-1}$ is estimated. Taking into account the detection efficiency measured with the DET_DM.1 on the test THOR_DET_DM.1 and the detection area of the GAM, 7.84 cm^2 , the expected integral gamma-ray background integral count rate is presented in the Table 3.28, also considering a 50% margin applied on the flux value.

| | | |
|-------------------------|-----------------|-------------------------|
| Photon flux | integral | 0.154 ($cm^2 s^{-1}$) |
| THOR-SR rate | count | 5.25 (s^{-1}) |
| THOR-SR rate 50% | count | 7.89 (s^{-1}) |

Table 3.28: Gamma-ray background estimated for the THOR GAM within the energy range of 100keV – 1MeV.

3.10.2 Electron Environment

The trapped electron environment in the THOR orbit was estimated using the SPENVIS⁶ platform from ESA. The model selected was the AE-8 MAX using the solar maximum version. Figure 3.54 showcases the THOR orbital exposure to electrons along the position in the orbit. It was assumed that the flux is omnidirectional: 4π sr

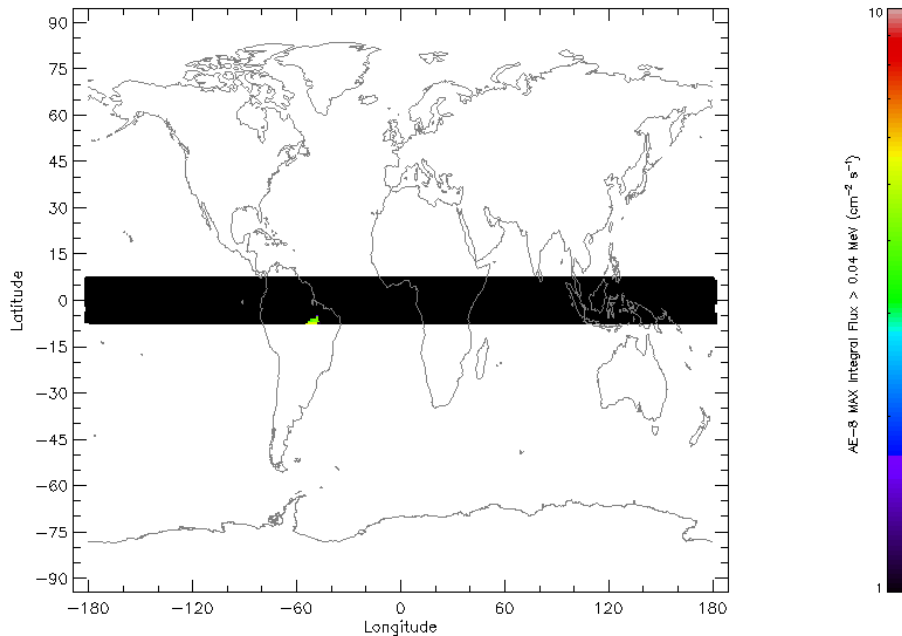


Figure 3.54: THOR orbital exposure to trapped electrons versus orbit position. Source SPENVIS.

⁶<https://www.spennis.oma.be/>

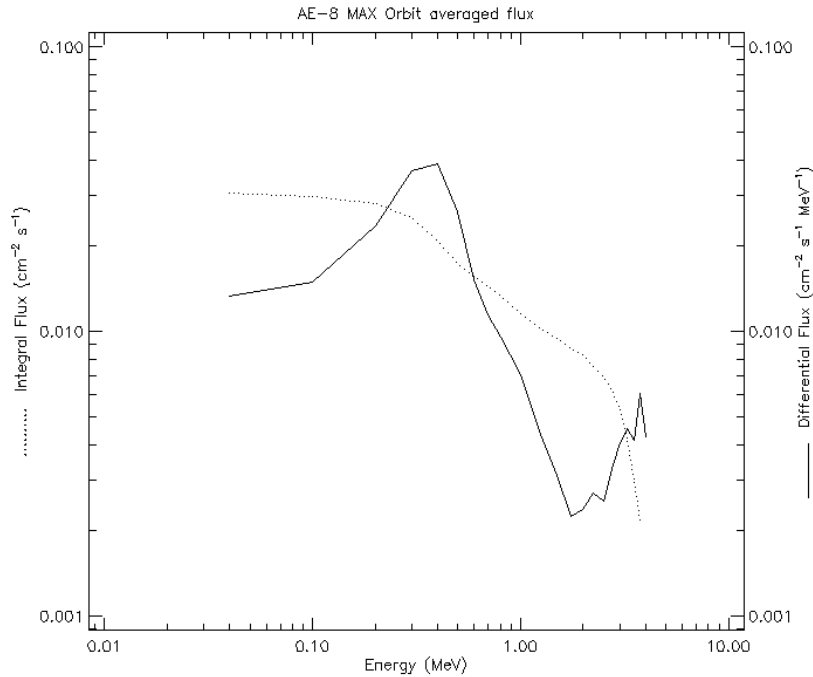


Figure 3.55: Trapped electron integral and differential average flux in the THOR orbit, calculated with SPENVIS platform.

The electron flux, Figure 3.55, was integrated for every energy, $0.04 \text{ MeV} < E_e < 4 \text{ MeV}$, in order to obtain an estimate of the count rate in the detectors, see Table 3.30. Again, a 50% margin policy was followed to take into account errors in estimates due to the detection of electrons inside the complex volume of the SR + THOR + other P/L.

| | Average flux ($\text{cm}^{-2}\text{s}^{-1}$) | Peak flux ($\text{cm}^{-2}\text{s}^{-1}$) |
|----------------------------|---|--|
| Integral flux | 2.96×10^{-2} | 6.22 |
| Integral flux (50% margin) | 4.44×10^{-2} | 9.32 |

Table 3.30: Electron, $0.04 \text{ MeV} < E_e < 4 \text{ MeV}$, background estimated for the THOR orbit.

Keeping in mind that we are neglecting the interaction of electrons with the aluminium enclosure, we present, the total rate of electrons hitting both the CdTe detector and Si detector.

| Detector | Average 50% electrons s^{-1} | Peak 50% electrons s^{-1} |
|--------------|---------------------------------------|------------------------------------|
| THOR_DET_GAM | 3.52×10^{-1} | 7.39×10^1 |
| THOR_DET_PAR | 1.76×10^{-1} | 37 |

Table 3.32: Electron, $0.04 \text{ MeV} < E_e < 4 \text{ MeV}$, background estimated for the THOR detectors

Figure 3.54 shows that the exposure to trapped electrons is limited and, therefore we

only expect a limited exposure time per orbit to the electron flux.

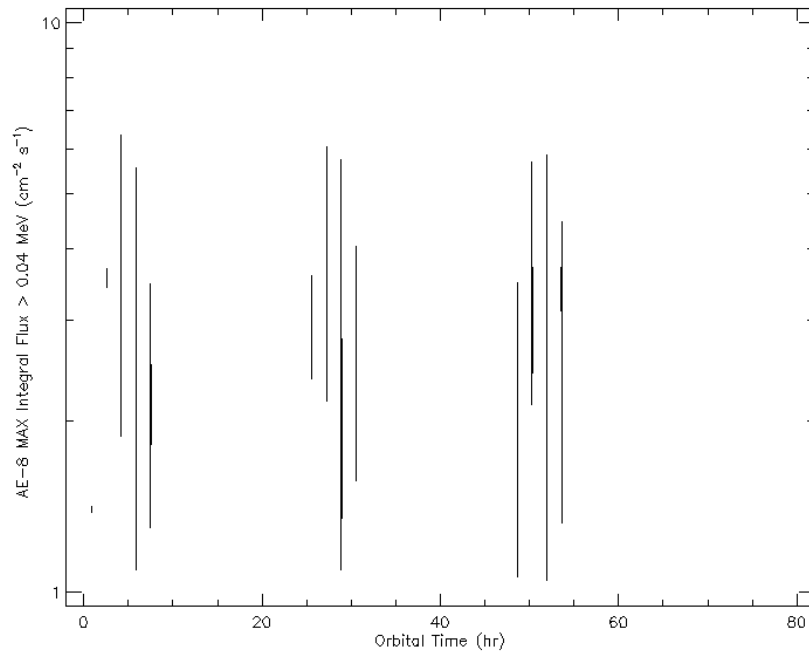


Figure 3.56: THOR orbital electron exposure simulated for 3 days versus the time in orbit, calculated with SPENVIS platform.

Figure 3.56 showcases a simulation of the total amount of time that the payload will be exposed to the electron flux for a total orbit time of three days. The payload will be exposed to the SAA trapped electrons for only 0.97% of the orbit time.

| Parameter | Value |
|---------------------------|-------------|
| Electron Orbital Exposure | 0.97%/orbit |
| Total Time | 838 s/day |

Table 3.33: Total electron orbital exposure.

3.10.3 Proton Environment

The trapped protons environment in the THOR orbit was estimated using the SPENVIS platform from ESA. The model selected was the SAMPEX/PET PSB97 since it estimates more rigorously the proton environment at low altitude than the classic model AP-8 MIN [Heynderickx et al., 1999].

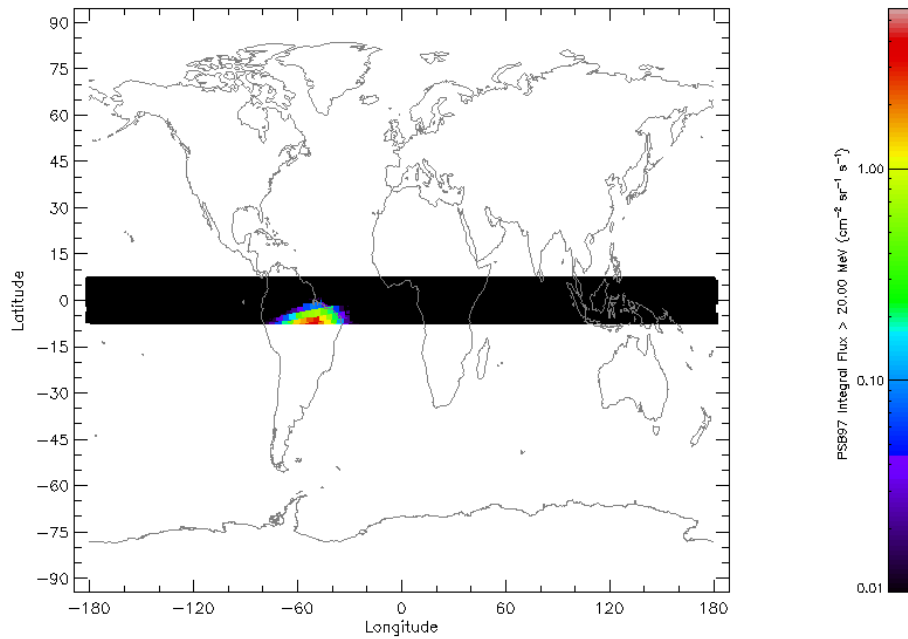


Figure 3.57: THOR orbital exposure to trapped protons versus orbit position. The proton integral flux was calculated using the SPENVIS platform.

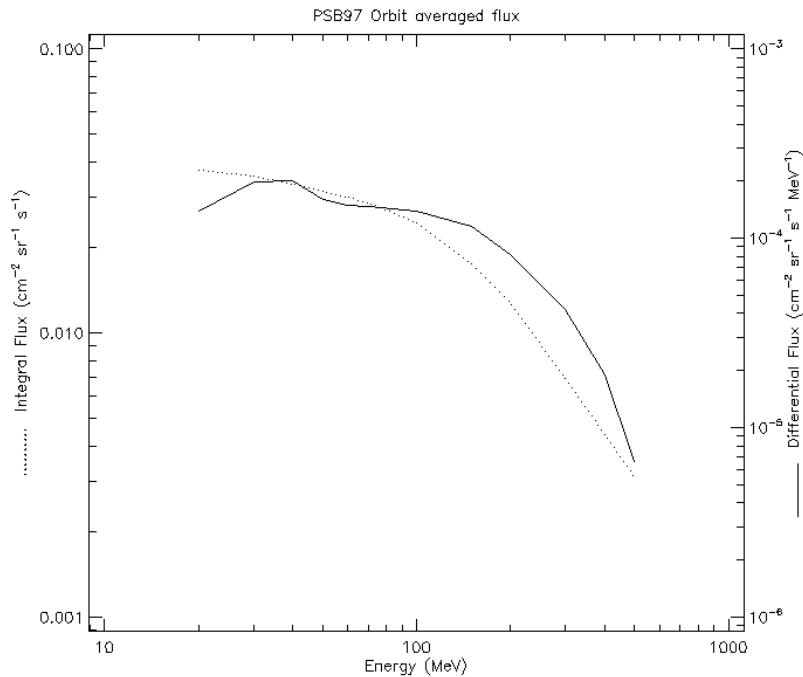


Figure 3.58: Proton Flux for 400km, 6°. Simulated on the SPENVIS platform.

The proton flux, Figure 3.58, was integrated for the energy, $20\text{MeV} < E_p < 500\text{MeV}$, in order to obtain an estimate of the count rate in the detectors. Again, a 50% margin was considered to take into account errors such as, for example, the effective area for detection of protons inside the complex volume of the SR + THOR + other P/L.

| | Average flux ($cm^{-2}s^{-1}sr^{-1}$) | Peak flux ($cm^{-2}s^{-1}sr^{-1}$) |
|----------------------------|---|--|
| Integral flux | 3.54×10^{-2} | 4.81 |
| Integral flux (50% margin) | 5.31×10^{-2} | 7.21 |

Table 3.35: Proton background estimated for the THOR orbit.

Keeping in mind that we are neglecting the interaction of protons with the aluminium enclosure, we present below, the total rate of protons hitting both the CdTe detector and Si detector, assuming the proton flux is omnidirectional: 4π sr.

| Detector | Average 50% protons s^{-1} | Peak 50% protons s^{-1} |
|-----------------|--|---|
| THOR_DET_GAM | 6.03 | 8.20×10^2 |
| THOR_DET_PAR | 4.01 | 5.45×10^2 |

Table 3.37: Proton background estimated for the THOR detectors.

Figure 3.57 shows that the exposure to the trapped protons is also limited, yet higher than to electrons.

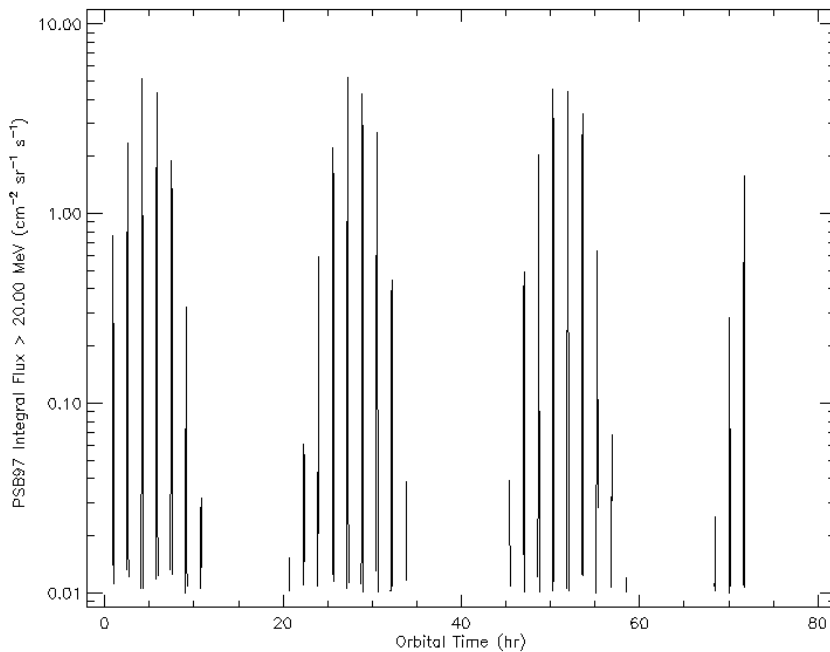


Figure 3.59: THOR orbital Proton exposure simulated for 3 days versus the time in orbit, calculated with SPENVIS platform.

Figure 3.59 showcases a simulation of the total amount of time that the payload will be exposed to the proton flux for a total orbital time of three days. The payload will be exposed to the SAA for 7.29% of the orbit time .

| Parameter | Value |
|---------------------------|-------------|
| Electron Orbital Exposure | 7.29%/orbit |
| Total Time | 6299 s/day |

Table 3.38: Total proton orbital exposure.

3.11 Scientific Data Architecture Definition

To the Scientific data architecture an 8bit per parameter was added, to take into account a possible update in the future. In practice we are overestimating the size of each data package by: $8 \times (\textit{number_of_parameters})$ bits.

3.11.1 RAW Data

The detectors will work on data-driven mode and will output information to a specific file in the OBC at a maximum rate of 53Mbytes/s, with a data transfer speed limit of the USB2.0 protocol. The data driven measurement gives information about all activated pixels. It is read-out immediately and continuously during the exposure time. The detectors give four values for each of the activated pixels (see Table 3.40), which are the output from the functions THOR_F_SCI.G and THOR_F_SCI.P:

| Parameter | Description |
|--------------|---|
| Matrix Index | Pixel ID hit. |
| ToT | Time over Threshold that is related to the energy of the interaction. |
| ToA | Time of Arrival. |
| FToA | Fast Time of Arrival. |

Table 3.40: Output of the functions THOR_F_SCI.G and THOR_F_SCI.P.

This information will be stored in the OBC_MMU with the following format.

| Data Packet | Concept | Value | Memory Consumption (bit) | Total bit | Data Packet Size (Bit) |
|-------------|--------------|-------|--------------------------|-----------|------------------------|
| RAW DATA | Matrix Index | id | 5 | 13 | 89 |
| | Pixel ID | id | 16 | 24 | |
| | ToA | ToA | 14 | 22 | |
| | ToT | ToT | 10 | 18 | |
| | FToA | FToA | 4 | 12 | |

Table 3.42: RAW DATA format to be saved on THOR.MMU.

The Matrix ID value identifies the FB from which the data came while the other values speak from themselves. For every activated pixel from a physics event, the detector transmits all this of data to the OBC.

3.11.2 Enhanced Pre-Processed Data

The RAW DATA coming from the detectors will undergo pre-processing and an enhanced data pre-processement, namely THOR_OBC will apply the calibrations functions, THOR_F_SCI.CAL, as well as the data processing function, THOR_F_DP.DC, to identify which events are being detected. See the diagram of this process in the Figure 3.20. The result of the scientific Data packet is summarized in Sections 3.11.2.1 and 3.11.2.2.

3.11.2.1 Electron and Photon Enhanced Pre-Processed Data

Since there is no direct way to distinguish an electron event from a gamma-ray event, other than comparing the fluxes and energy distributions to existing models, we are going to collect all the RAW Data for every electron/photon identified by the function THOR_F_DC.DP. The data generated by each activated pixel from either a photon or electron event is the following, meaning that for events that activate N pixels, the data generated is $N \times$ the size presented in the Table 3.42.

3.11.2.2 Proton and Heavy ions Enhanced Pre-Processed Data

From previous iterations of this study it was noticed that recording all the raw data from proton interactions the data generated can be up to 2 orders of magnitude higher than the amount of data generated by photons and electrons raw data combined [Sousa, 2023]. To deal with this problem the OBC will generate a set of 5 parameters per proton heavy

ion, that characterize the interaction and allows for the particle reconstruction on ground. See Section for an explanation of these parameters 3.6.6.3. The data collected per event is therefore summarized in the Table 3.44:

| Data Packet | Concept | Value | Memory Consumption (bit) | Total bit | Data Packet Size (Bit) |
|---------------------|---------------------------------|-------|--------------------------|-----------|------------------------|
| PROTON/ ION EPPD | Matrix Index | id | 5 | 13 | 113 |
| | Hit pixel | id | 16 | 24 | |
| | Energy | keV | 18 | 26 | |
| | N ^o activated pixels | int | 10 | 18 | |
| | θ | int | 8 | 16 | |
| | ϕ | int | 8 | 16 | |

Table 3.44: Enhanced Pre-Processed Proton Data format to be saved on THOR_MMU.

3.11.3 Scientific Data String Architecture

As seen in Figure 3.20 the scientific data passes through the data storage functions that associate a proper ID and time stamp to each event in order for each physics event to be easily correlated with the SR attitude data as well as to astronomical events detected by larger space instruments like SWIFT, Fermi or INTEGRAL.

The data strings are based on the outputs of functions THOR_F_DS.ID, THOR_F_DS.TS and THOR_D_DP.DC (see Table 3.45). This data is then stored in the OBC_MMU to be either be sent to the ground segment or to be used to perform scientific calculations on-orbit.

| Description | Data String |
|---------------|--|
| Photon Data | DATA TYPE + DATA SOURCE + EVENT TYPE + EVENT ID + TIMESTAMP + N×RAW DATA |
| Electron Data | DATA TYPE + DATA SOURCE + EVENT TYPE + EVENT ID + TIMESTAMP + N×RAW DATA |
| Proton Data | DATA TYPE + DATA SOURCE + EVENT TYPE + EVENT ID + PROTON ENHANCED PRE-PROCESSED DATA |

Table 3.45: Current design of the THOR scientific data strings.

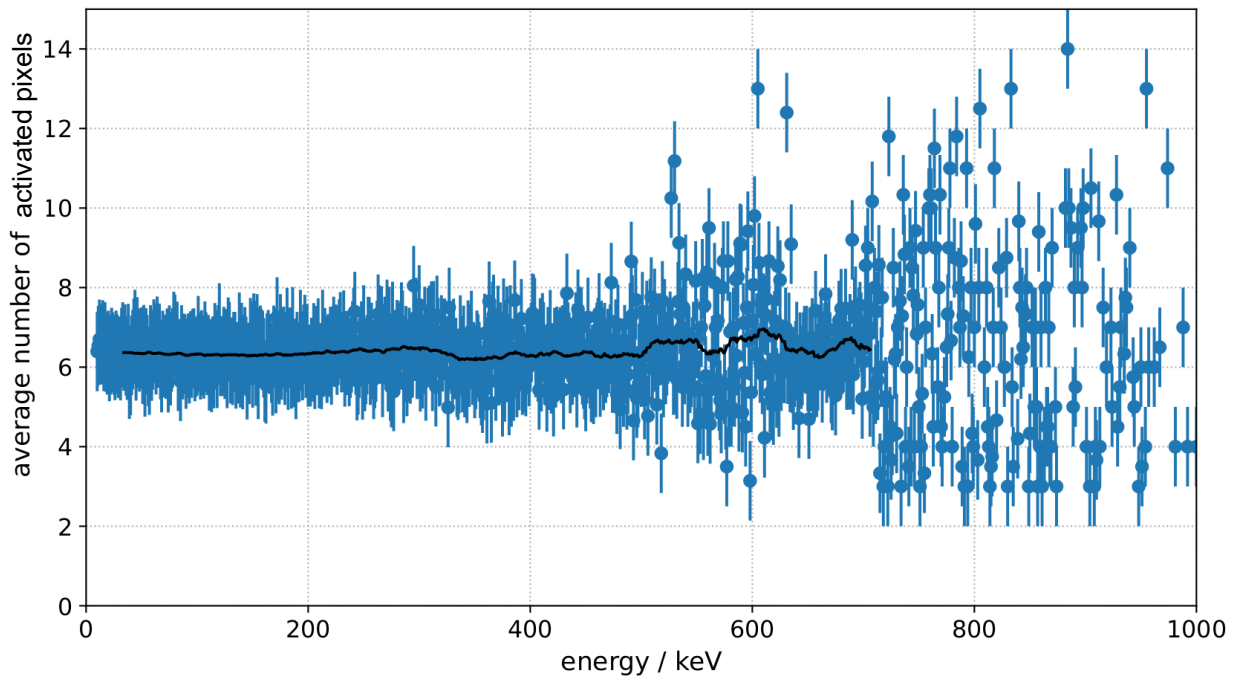


Figure 3.61: Number of activated pixels per event as a function of the incoming photon energy. Credit: Jonathan Flunger

Thus the RAW DATA generated by Gamma-rays arriving at OBC via the interfaces USB2_GAM1, USB2_GAM2, USB2_GAM3 and USB2_GAM4 is the following:

| THOR_DET_GAM | |
|-----------------------|--|
| Gamma-ray count rate | 7.89 s^{-1} |
| Activated pixels rate | 55.23 s^{-1} |
| RAW Data rate | $5.86 \times 10^{-4} \text{ Mbytes/s}$ |

Table 3.46: Orbital gamma-ray scientific RAW data generated by GAM detector.

3.12.1.2 Electron RAW Data

As previously stated we are interested in the worse scenario which, for the electron flux, means using the Integral peak electron flux with 50% margin, $\Phi_{electron} = 9.32 \text{ cm}^{-2} \text{ s}^{-1}$ and also assume all incoming electrons have a maximum energy of 4MeV energy, $E_{electron} = 4 \text{ MeV}$. Thus we are maximizing the total number of activated pixels. It was assumed that the electron flux is omnidirectional: 4π sr.

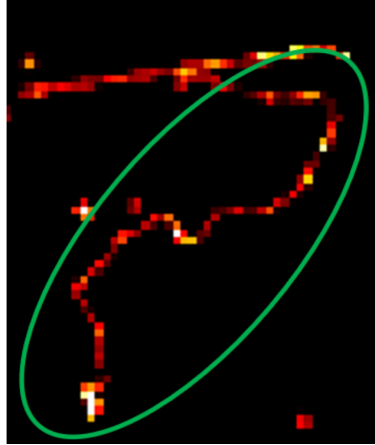


Figure 3.62: Electron interaction highlighted in green. Event captured with the first detector development model - THOR_DET_DM.1

A typical electron event caught by THOR_DET_DM.1 is shown in Figure 3.62. The electrons are light charged particles and, as they travel inside a material, they suffer large deflections as their mass is now equal to the mass of the orbiting electrons with which they will interact. In addition, electron-nuclear Coulomb interactions can sometimes occur and abruptly change electron’s direction [Knoll, 2010]. For this study we assume that, even if the electron mean path is greater than the maximum linear distance allowed inside a single CdTe/Si matrix, the electron path deviation does not cause electrons to leave the detector volume. Note that, in fact, this does not happen in reality.

To obtain an estimate of the number of pixels that are activated per electron interaction one must compute the electron mean range inside both the CdTe and Si semiconductor. To do this the NIST ⁷ [Berger1 et al., 2017] platform was used to get the stopping power value for 4MeV electrons inside CdTe and Si material that were used to estimate the number of activated pixels, showcased on Table 3.47 and 3.48.

| CdTe - Cadmium Telluride | |
|---|---------------|
| Atomic Number (Z) | 48, 52 |
| Density (ρ_{CdTe}) | 5.85 g/cm^3 |
| CSDA range ⁸ $E_{electron} = 4MeV$ | 2.98 g/cm^2 |
| Mean Path $E_{electron} = 4MeV$ | 0.51 cm |
| Pixel Size | 0.0055 cm |
| N ^o activated pixels | 92.71 |

Table 3.47: Characteristics of an electron, $E_{electron} = 4MeV$, interacting with GAM.

⁷<https://www.nist.gov/pml/stopping-power-ran-ge-tables-electrons-protons-and-helium-ions>

⁸Continuous-Slowing-Down Approximation: a very close approximation to the average path length traveled by a charged particle as it slows down to rest, calculated in the continuous-slowing-down approximation. In this approximation, the rate of energy loss at every point along the track is assumed to be equal to the

| Si - Silicon | | |
|---------------------------------|-----------------------|---------------|
| Atomic Number (Z) | | 14 |
| Density (ρ_{Si}) | | 2.33 g/cm^3 |
| CSDA range ⁸ | $E_{electron} = 4MeV$ | 2.41 g/cm^2 |
| Mean Path | $E_{electron} = 4MeV$ | 1.03 cm |
| Pixel Size | | 0.0055 cm |
| N ^o activated pixels | | 188.22 |

Table 3.48: Characteristics of an electron, $E_{electron} = 4MeV$, interacting with PAR

With the average number of activated pixels per electron interaction for either the CdTe and Si semiconductors, one can now compute the expected RAW DATA generated by both THOR_DET_GAM and THOR_DET_PAR that is going to be transmitted to the OBC via the interfaces USB2_GAM1, USB2_GAM2, USB2_GAM3, USB2_GAM4, USB2_PAR2 and USB2_PAR3:

| | THOR_DET_GAM | THOR_DET_PAR |
|-------------------------------------|--------------------------------|--------------------------------|
| Electron Flux ($\Phi_{electron}$) | 9.32 $cm^{-2}s^{-1}$ | |
| Electron Energy ($E_{electron}$) | 4MeV | 4MeV |
| Electron rate over area | 73.9 s^{-1} | 37 s^{-1} |
| Total activated pixels | $6.85 \times 10^3 s^{-1}$ | $6.96 \times 10^3 s^{-1}$ |
| RAW Data rate | $7.27 \times 10^{-2} Mbytes/s$ | $7.38 \times 10^{-2} Mbytes/s$ |

Table 3.49: Orbital Electron Scientific Data generated by each detector.

3.12.1.3 Proton RAW Data

Similarly, to the electron case, the proton flux used was the integral peak flux with the 50% margin also assuming a FoV of 4π . $\Phi_{proton} = 7.21 \times 4\pi = 90.6 cm^{-2}s^{-1}$.

When a proton interacts within a material their deflection as it travels inside the material can be neglected [Knoll, 2010]. The proton only suffers deflections at the end of its trail where its kinetic energy is so small that allows for deflections in its path, see Figure 3.63.

total stopping power. Energy-loss fluctuations are neglected. The CSDA range is obtained by integrating the reciprocal of the total stopping power with respect to energy.

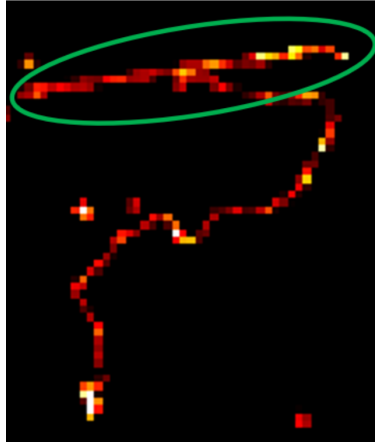


Figure 3.63: Proton interaction highlighted in green. Event captured with the first detector development model - THOR_DET_DM.1

The assumption that we made with the electrons - even if the mean path of the electron is greater than the maximum linear distance allowed inside a single CdTe/Si matrix - can not be made for protons since they move most of their path in a straight line. To get an estimate of the number of pixels that will be activated per proton interaction one can compute the proton mean range inside both CdTe and Si semiconductor. We used the NIST platform was also used to obtain the range for 300MeV protons inside CdTe and Si material an then the number of activated pixels was estimated, as summarized in Table 3.47 and 3.48.

| CdTe - Cadmium Telluride | | |
|---|-------------------------|---------------|
| Atomic Number (Z) | | 50 |
| Density (ρ_{CdTe}) | | 5.85 g/cm^3 |
| CSDA range ⁸ | $E_{proton} = 300MeV$ | 88.5 g/cm^2 |
| Mean Path | $E_{electron} = 300MeV$ | 15.1 cm |
| Pixel Size | | 0.0055 cm |
| N ^o activated pixels (theoretical) | | 2728 |

Table 3.50: Characteristics of a proton, $E_{proton} = 300MeV$, interacting with GAM.

| Si - Silicon | | |
|---|-------------------------|---------------|
| Atomic Number (Z) | | 14 |
| Density (ρ_{Si}) | | 2.33 g/cm^3 |
| CSDA range ⁸ | $E_{electron} = 300MeV$ | 63.9 g/cm^2 |
| Mean Path | $E_{electron} = 300MeV$ | 27.4 cm |
| Pixel Size | | 0.0055 cm |
| N ^o activated pixels (theoretical) | | 4982 |

Table 3.51: Characteristics of a proton, $E_{proton} = 300MeV$, interacting with PAR.

The high mean range for 300MeV protons indicate that we wont be able to detect the overall energy. Nevertheless, the maximum distance that a proton can travel inside the CdTe detector occurs when the proton path coincides with the diagonal of the DP length combined, see Figure 3.64. For the Si detector, coincides with the diagonal of a single Si matrix.

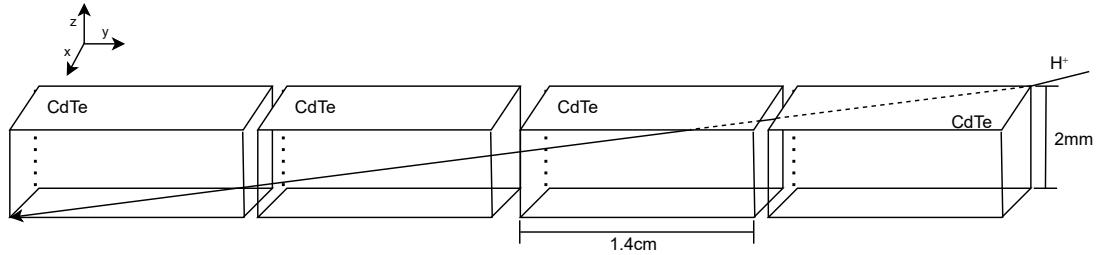


Figure 3.64: Maximum possible distance travelled by a proton in the GAM geometry.

| Detector | Max Length | Max Proton Energy |
|----------|------------|-------------------|
| GAM | ~5.78 cm | ~160MeV |
| PAR | ~1.99 cm | ~65MeV |

Table 3.52: Maximum possible energy detected per proton interaction.

Due to the different geometric scenarios for the proton interaction within the detector, several configurations were studied to predict the worst-case scenario.

CdTe Scenario - A The purpose of this scenario was to simulate the highest possible number of activated pixels. It was assumed that the proton beam (300MeV protons) had an incoming incident angle of 90° , see the Figure 3.65.

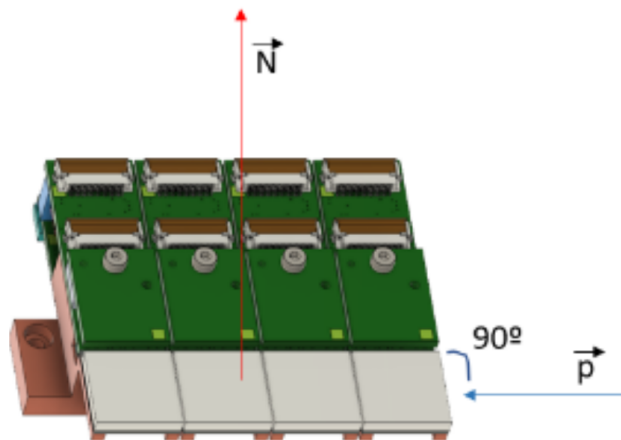


Figure 3.65: Geometry of the incident proton beam, CdTe Scenario A. Only one DP presented in the figure for simplicity.

From the information in Table 3.50, it is estimated that the maximum number of activated pixels is 1024. It is important to note that for this scenario the detection area is limited to the side of the GAM, $4 \times 2\text{mm}$ in height and 1.4cm in length. The proton flux is computed taking this into account $A_{eff-cdte_A} = 1.12\text{cm}^2$. The RAW data generated in this scenario is presented in the Table below:

| | THOR_DET_GAM | THOR_DET_GAM_DP.x |
|-----------------------------------|---------------------------------|--|
| Proton Flux (Φ_{proton}) | | $90.6 \text{ cm}^{-2}\text{s}^{-1}$ |
| Proton Energy (E_{proton}) | | 300MeV |
| Proton rate over $A_{eff-cdte_A}$ | 101s^{-1} | 25.4s^{-1} |
| Total activated pixels | $1.04 \times 10^5\text{s}^{-1}$ | $2.60 \times 10^4\text{s}^{-1}$ |
| RAW Data rate | 1.10 Mbytes/s | $2.76 \times 10^{-1} \text{ Mbytes/s}$ |

Table 3.54: Orbital Proton Scientific Data generated by each detector, CdTe Scenario A.

CdTe Scenario - B The purpose of this calculation was to create a scenario to assess the highest detection area, i.e. $4 \times 1.4 \times 1.4\text{cm}^2 = 7.84\text{cm}^2$. It was assumed that the proton beam (300MeV protons) had an incident angle of 0° , see the Figure 3.66.

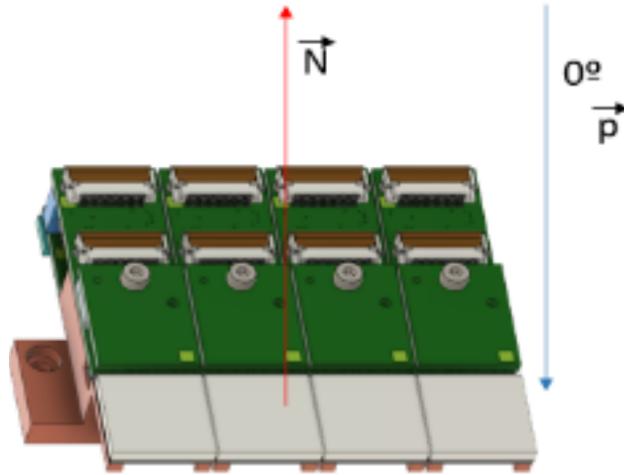


Figure 3.66: Geometry of the incident proton beam, CdTe Scenario B. Only one DP presented in the figure for simplicity.

With the information from Table 3.50, one can conclude that the proton will travel through the 4 detection planes. It was assumed that when the proton interacts with the CdTe/Si it activates 10 pixels, due to the diffusion of the secondary electron cloud in the medium. The RAW data generated in this scenario is presented in the Table below.

| | THOR_DET_GAM | THOR_DET_GAM_DP.x |
|----------------------------------|--------------------------------------|--------------------------------------|
| Proton Flux (Φ_{proton}) | $90.6 \text{ cm}^{-2}\text{s}^{-1}$ | |
| Proton Energy (E_{proton}) | 300MeV | |
| Proton rate over $A_{eff-cdteB}$ | 718s^{-1} | N/A |
| Total activated pixels | $2.87 \times 10^4\text{s}^{-1}$ | N/A |
| RAW Data rate | $3.05 \times 10^{-1}\text{Mbytes/s}$ | $7.62 \times 10^{-2}\text{Mbytes/s}$ |

Table 3.56: Orbital Proton Scientific Data generated by CdTe Scenario B.

Si Scenario - A The purpose of this scenario was to assess the highest possible number of activated pixels. It was assumed that the proton beam (300MeV protons) had an incident angle of 0° , see the Figure 3.67.

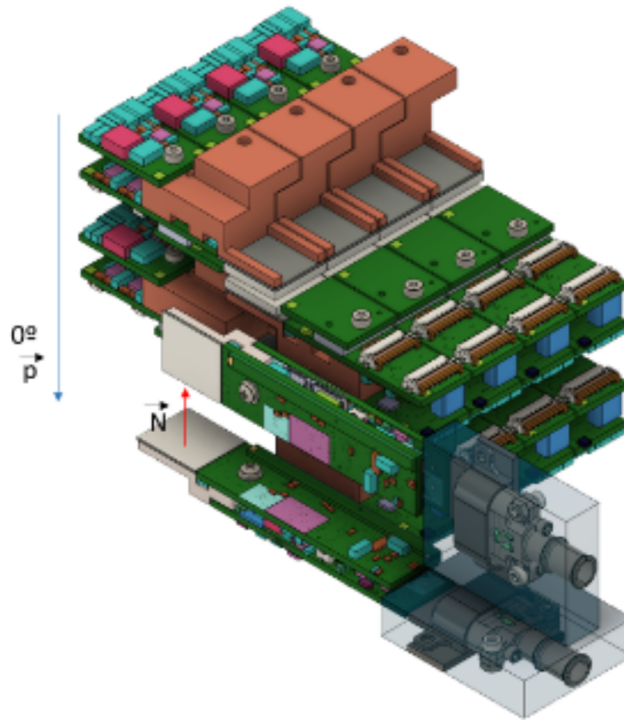


Figure 3.67: Geometry of the incident proton beam, Si Scenario A

From the Table 3.51, one can conclude that the proton will travel through the total transversal length of the THOR_DET_PAR_B.2 (256 pixels) and still interacts within the THOR_DET_PAR_B.3 (10 pixels) giving us a total of 266pixels. It is important to note that for this scenario the detection area is limited to the side of the Si detector i.e. $0.05\text{cm} \times 1.4\text{cm} = 0.07\text{cm}^2$, and the front area of the THOR_DET_PAR.3, i.e. $1.4\text{cm} \times 1.4\text{cm} = 1.96\text{cm}^2$. The proton hit rate is calculated taking this into account $A_{eff-siA} = 2.05\text{cm}^2$. The RAW data generated in this scenario is presented in Table below.

| | THOR_DET_PAR |
|---------------------------------|--------------------------------------|
| Proton Flux (Φ_{proton}) | $90.6 \text{ cm}^{-2}\text{s}^{-1}$ |
| Proton Energy (E_{proton}) | 300MeV |
| Proton rate over A_{eff-sA} | 186s^{-1} |
| Total activated pixels | $4.95 \times 10^4\text{s}^{-1}$ |
| RAW Data rate | $5.25 \times 10^{-1}\text{Mbytes/s}$ |

Table 3.58: Orbital Proton Scientific Data generated by Si Scenario A.

Si Scenario - B The purpose of this scenario was to simulate the highest detection area, with protons colliding with both detectors with a 0° incident angle.

With the information from Table 3.51, one can see that the proton will travel through the thickness of the Si detectors, 0.5mm. It is assumed that when a proton interacts with the Si it activates 10 pixels. A total area of $2 \times 1.96\text{cm}^2 = 3.92\text{cm}^2$. The RAW data generated in this scenario is presented in Table below.

| | THOR_DET_PAR |
|---------------------------------|--------------------------------------|
| Proton Flux (Φ_{proton}) | $90.6 \text{ cm}^{-2}\text{s}^{-1}$ |
| Proton Energy (E_{proton}) | 300MeV |
| Proton rate over A_{eff-sA} | 359s^{-1} |
| Total activated pixels | $3.59 \times 10^3\text{s}^{-1}$ |
| RAW Data rate | $3.81 \times 10^{-2}\text{Mbytes/s}$ |

Table 3.60: Orbital Proton Scientific Data generated by each detector, Si Scenario B.

Conclusion of the Proton Interactions Even though we are assuming the worst possible scenario for every case, it is also assumed that these scenarios happen all at the same time. The Table bellow summarises the proton data generated by the THOR_DET_GAM and THOR_DET_PAR.

| | THOR_DET_GAM | THOR_DET_PAR |
|-----------|-------------------------|--------------------------------------|
| Data Rate | 1.41 Mbytes/s | $5.63 \times 10^{-1}\text{Mbytes/s}$ |

Table 3.61: Total Orbital Proton Scientific Data generated by each detector.

3.12.2 Enhanced Pre-Processed Data Budget

The Enhanced Pre-Processed Data (EPPD) output data packet's are presented on Section 3.11.2.1 and 3.11.2.2.

3.12.2.1 Gamma-ray and Electron EPPD

When the THOR_F_DP.DC function identifies a set of data as a gamma-ray or an electron event, it will add to it the data packets from the THOR_F_DS.ID and THOR_F_DS.TS, this will add extra bits to the data budget present on the previous sections. This data is then recorded on the OBC_MMU at a rate:

| Gamma-ray EPPD Data | |
|---------------------|--|
| Gamma-ray rate | 7.9 s^{-1} |
| Exposure time | 86400 s/day |
| String Data rate | $7.25 \times 10^{-4} \text{ Mbytes/s}$ |
| String Data rate | 113 Mbytes/day |

Table 3.62: EPPD Gamma-ray data rate.

| Electron EPPD Data | | |
|-------------------------------------|--|--|
| | THOR_DET_GAM | THOR_DET_PAR |
| Electron rate ($\Phi_{electron}$) | 73.9 s^{-1} | 37 s^{-1} |
| Exposure time | 838 s/day | 838 s/day |
| String Data rate | $7.40 \times 10^{-2} \text{ Mbytes/s}$ | $7.45 \times 10^{-2} \text{ Mbytes/s}$ |
| String Data rate | 62.0 Mbytes/day | 62.4 Mbytes/day |

Table 3.63: EPPD Electron data rate.

3.12.2.2 Proton/Ion EPPD

When THOR_F_DP.DC function identifies a set of data that represents a proton/ion event it will add to it the data packets from the THOR_F_DS.ID and THOR_F_DS.TS. This data is then recorded on the OBC_MMU at a rate:

| Proton/Ion EPPD Data | | |
|---------------------------------|--|--|
| | THOR_DET_GAM | THOR_DET_PAR |
| Proton rate (Φ_{proton}) | 820 s^{-1} | 545 s^{-1} |
| Exposure time | 6299 s/day | 6299 s/day |
| String Data rate | $2.54 \times 10^{-2} \text{ Mbytes/s}$ | $1.69 \times 10^{-2} \text{ Mbytes/s}$ |
| String Data rate | 160 Mbytes/day | 106 Mbytes/day |

Table 3.64: EPPD Poton/Ion data rate.

3.12.3 Scientific Data Budget

In this section the summary of the data budgets, for the RAW data as well as for the EPPD are presented.

3.12.3.1 RAW data

This is the output data from the the THOR_F_SCI.G and THOR_F_SCI.P.

| | THOR_DET_GAM _DP.x (<i>MBytes/s</i>) | THOR_DET_GAM (<i>MBytes/s</i>) | THOR_DET_PAR (<i>MBytes/s</i>) |
|--------------------------------------|---|-------------------------------------|-------------------------------------|
| I/F ID | USB2_GAMx | N/A | USB2_PARx |
| Gamma-ray Data Rate | 1.46×10^{-4} | 5.86×10^{-4} | N/A |
| Proton Data Rate | 3.52×10^{-1} | 1.41 | 5.63×10^{-1} |
| Electron Data Rate | 1.82×10^{-2} | 7.27×10^{-2} | 7.38×10^{-2} |
| Total Data Rate | 3.70×10^{-1} | 1.48 | 6.37×10^{-1} |
| Total Data Rate (OBC POV) | N/A | 2.12 MBytes/s | |

Table 3.66: Summary of the RAW Scientific Data generated by THOR_DET.

3.12.3.2 Enhanced Pre-Processed Data

This is the output data after being analysed by THOR_F_DP.DC and the THOR_F_DS.TS and THOR_F_DS.ID identifiers.

| | THOR_DET_GAM <i>MBytes/s</i> | THOR_DET_PAR <i>MBytes/s</i> |
|--------------------------------------|--|---------------------------------|
| Gamma-ray Data Rate | 7.25×10^{-4} | N/A |
| Proton Data Rate | 2.54×10^{-2} | 1.69×10^{-2} |
| Electron Data Rate | 7.4×10^{-2} | 7.45×10^{-2} |
| Total Data Rate | 0.1 | 9.14×10^{-2} |
| Total Data Rate (MMU POV) | $1.91 \times 10^{-1} \text{ MBytes/s}$ | |

Table 3.68: Summary of the EPPD generated by THOR_DET.

3.12.4 Data Budget

| | | Margin Policy | |
|--------------------------|--------------|------------------|------------------|
| | | 0% | 25% |
| | | <i>Mbyte/day</i> | <i>Mbyte/day</i> |
| EPPD | Photons | 113 | 141 |
| | Electrons | 124 | 155 |
| | Protons | 266 | 332 |
| HK | Housekeeping | 1.8 | 2.6 |
| TOTAL⁸ | | 240 | 344 |

3.12.5 Mass Budget

| Component | Mass (g) | Margin (15%) | Total (g) | Margin (25%) | Total (g) |
|--------------------|----------|--------------|-----------|--------------|-----------|
| THOR_DET_GAM_DP.FB | 160 | 184 | 5788.1 | 200 | 6291.4 |
| THOR_DET_GAM_RO | 400 | 460 | | 500 | |
| THOR_DET_PAR_B | 26 | 29.9 | | 32.5 | |
| THOR_OBC_GPU | 274 | 315.1 | | 342.5 | |
| THOR_OBC_CB | 184 | 211.6 | | 230 | |
| THOR_PDU | 169 | 195 | | 211.4 | |
| THOR_ENC | 3700 | 4255 | | 4625 | |
| Connectors | 50 | 57.5 | | 62.5 | |
| Cables | 70 | 80.5 | | 87.5 | |

⁸Taking only into account the photon, electron and HK data.

3.12.6 Power Budget

3.12.6.1 Commissioning Power Budget

| Commissioning (worst case) | | |
|-----------------------------------|---------------|------------------|
| Component | Status | Power (W) |
| THOR_DET | Partly ON | |
| THOR_DET_GAM_DP.1 | ON | 4.0 |
| THOR_DET_GAM_DP.2 | | OFF |
| THOR_DET_GAM_DP.3 | | OFF |
| THOR_DET_GAM_DP.4 | | OFF |
| THOR_DET_GAM_RO.1 | ON | 2.0 |
| THOR_DET_GAM_RO.2 | | OFF |
| THOR_DET_GAM_RO.3 | | OFF |
| THOR_DET_GAM_RO.4 | | OFF |
| THOR_DET_PAR_B.1 | | OFF |
| THOR_DET_PAR_B.2 | | OFF |
| THOR_PDU | Partly ON | |
| THOR_PDU_DCDC_GAM.12 | ON | 0.54 |
| THOR_PDU_DCDC_GAM.34 | | OFF |
| THOR_PDU_DCDC_PAR | | OFF |
| THOR_PDU_DCDC_OBC | ON | 0.70 |
| THOR_OBC | ON | |
| THOR_OBC_GPU | | 4.10 |
| THOR_OBC_CB | | 3.65 |
| TOTAL | | 15.0 W |
| TOTAL (15%) | | 17.3 W |

3.12.6.2 Housekeeping

| Housekeeping | | |
|---------------------|---------------|------------------|
| Component | Status | Power (W) |
| THOR_DET | | OFF |
| THOR_DET_GAM_DP.1 | | OFF |
| THOR_DET_GAM_DP.2 | | OFF |
| THOR_DET_GAM_DP.3 | | OFF |
| THOR_DET_GAM_DP.4 | | OFF |
| THOR_DET_GAM_RO.1 | | OFF |
| THOR_DET_GAM_RO.2 | | OFF |
| THOR_DET_GAM_RO.3 | | OFF |
| THOR_DET_GAM_RO.4 | | OFF |
| THOR_DET_PAR.B.1 | | OFF |
| THOR_DET_PAR.B.2 | | OFF |
| THOR_PDU | | Partly ON |
| THOR_PDU_DCDC_GAM | | OFF |
| THOR_PDU_DCDC_PAR | | OFF |
| THOR_PDU_DCDC_OBC | ON | 0.70 |
| THOR_OBC | | ON |
| THOR_OBC_GPU | | 4.1 |
| THOR_OBC_CB | | 3.65 |
| TOTAL | | 8.4 W |
| TOTAL (15%) | | 9.7 W |

3.12.6.3 Observational

| Observational | | |
|----------------------|---------------|------------------|
| Component | Status | Power (W) |
| THOR_DET | | ON |
| THOR_DET_GAM_DP.1 | ON | 4 |
| THOR_DET_GAM_DP.2 | ON | 4 |
| THOR_DET_GAM_DP.3 | ON | 4 |
| THOR_DET_GAM_DP.4 | ON | 4 |
| THOR_DET_GAM_RO.1 | ON | 2.0 |
| THOR_DET_GAM_RO.2 | ON | 2.0 |
| THOR_DET_GAM_RO.3 | ON | 2.0 |
| THOR_DET_GAM_RO.4 | ON | 2.0 |
| THOR_DET_PAR_B.2 | ON | 1.2 |
| THOR_DET_PAR_B.3 | ON | 1.2 |
| THOR_PDU | | ON |
| THOR_PDU_DCDC_GAM | ON | 2.52 |
| THOR_PDU_DCDC_PAR | ON | 0.26 |
| THOR_PDU_DCDC_OBC | ON | 0.81 |
| THOR_OBC | | ON |
| THOR_OBC_GPU | | 10.0 |
| THOR_OBC_CB | | 3.65 |
| TOTAL | | 43.6 |
| Total (15%) | | 50.2 |

3.13 Risk Management

This section was based on the ECSS-M-ST-80C. Each risk was analysed based on the likelihood of happening and the severity of the consequences of each risk scenario. Depending on the risk index (likelihood + severity) the ECSS-M-ST-80C proposes actions to take in order to mitigate, or not, the risk.

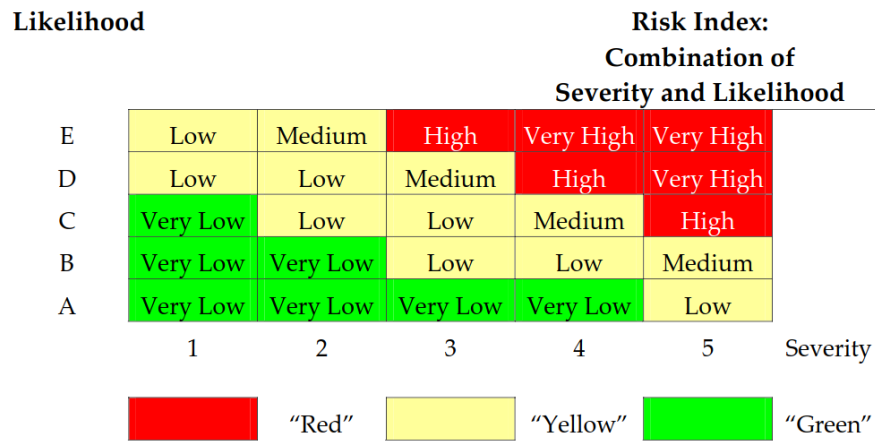


Figure 3.68: Risk Index and magnitude scheme, from ECSS-M-ST-80C.

| Risk index | Risk magnitude | Proposed actions |
|--------------------------------|----------------|---|
| E4, E5, D5 | Very High risk | Unacceptable risk: implement new team process or change baseline – seek project management attention at appropriate high management level as defined in the risk management plan. |
| E3, D4, C5 | High risk | Unacceptable risk: see above. |
| E2, D3, C4, B5 | Medium risk | Unacceptable risk: aggressively manage, consider alternative team process or baseline – seek attention at appropriate management level as defined in the risk management plan. |
| E1, D1, D2, C2, C3, B3, B4, A5 | Low risk | Acceptable risk: control, monitor – seek responsible work package management attention. |
| C1, B1, A1, B2, A2, A3, A4 | Very Low risk | Acceptable risk: see above. |

Figure 3.69: Risk magnitude designations and proposed actions for individual risks, from ECSS-M-ST-80C.

For each risk identified an assessment shall take place where it is judged if the risk is acceptable or unacceptable. According to the assessment a mitigation provision shall be proposed.

On the Table bellow we present the current estimation of the risks within THOR design. The objective of this table is to guide the work flow in order to mitigate these risks before they can even happen.

| ID | System | Item/Failure Mode | Failure Cause and effect | Mission Phase | Criticality Number | Compensating Provisions |
|---------------|--------|---|---|-------------------------------|--------------------|--|
| THOR._RSK.001 | DET | Risk of short circuit between HV and other conductive surface | HV and conductive surface too close / damage the DET bias voltg supply. | Flight | B3 | HV more than 5mm away of conductive surfaces. Monitor the current drawn by the HV bias. |
| THOR._RSK.002 | DET | Vacuum arc between surfaces of CdTe (-500V) and Si (+200V) | Proximity between CdTe and Si surfaces due to DET geometry | Flight/ Testing | D3 | Ensure 5mm of minimum distance between surfaces with voltage levels > Δ300V |
| THOR._RSK.003 | ENC | Structure becoming loose from MPCB | Fixation points not tight enough. Damaging neighbouring P/L's and create space debris | Flight/ Launch | A5 | Provide a mounting procedure to the THOR integration operator. |
| THOR._RSK.004 | ENC | Depressurisation and re-pressurisation may damage the enclosure | High difference of pressures levels inside and outside THOR. May damage THOR and neighboring P/L's. May creat space debris | Flight/ Launch/ Reentry | A5 | Creat venting holes that allow air flow |
| THOR._RSK.005 | COM | USB digital signal prone to EMI | EM environment on SR may induce a loss of communication between OBC and DET. | Flight | C5 | Shielding the cable and connectros on this electrical interface. |
| THOR._RSK.006 | COM | Standard USB connectors on DET side might become loose during launch. | Vibration environment may disconnect the USB plug and lead to a loss of communications of SCI data between DET and OBC | Launch | C5 | Customize the detectors with a click mechanism or screw mechanism. |
| THOR._RSK.008 | DET | Finger Board malfunctioning / ASIC shutdown | ASIC overheating causing inoperability of the Finger Board | Flight | B2 | Perform thermal analysis with the worst possible scenario |
| THOR._RSK.009 | DET-RO | DET Back-end Electronics shutdown, DET FPGA/uC malfunctioning | Overheating that lead to part or full inoperability of DET | Flight | B3 | Perform thermal analysis with the worst possible scenario. |
| THOR._RSK.010 | PDU | 28V input instability | SR cuts THOR power supply and THOR shutdown suddenly | Flight | A5 | Software and hardware development such that it considers a power cut at any time. |
| THOR._RSK.011 | PDU | Malfunctioning of the 12V DC/DC on the PDU | Overheat, shutdown, inoperability of GAM or OBC. | Flight | B5 | Have a double redundancy design at the 12V DC-DC level. Perform thermal simulations to ensure the device does not overheat even in the case where just one DCDC is operating. |
| THOR._RSK.012 | PDU | Malfunctioning of the 5V DC/DC | Overheat, shutdown, inoperability of the Particle Detector array | Flight | B4 | Have a double redundancy design at the 5V DC-DC level. Perform thermal simulations to ensure the device does not overheat even in the case where just one DCDC is operating. |
| THOR._RSK.013 | DET | Operator electric shot with the HV on the detector (-100V to -500V) | Electric shock to the operator | Testing | B1 | Ensure payload enclosure is closed while testing. Only touch the detector when it is powered OFF in case it is not inside an enclosure. |
| THOR._RSK.014 | PDU | Overvoltage in the Input of the PDU, irreversible damage to PDU. | SR 28V unregulated varies between 22-38V | Flight | C5 | Install an Input Voltage Regulator on the PDU |
| THOR._RSK.016 | COM | USB protocol susceptible to EMC noise | EMC environment may induce noise on the low power USB protocol | Flight | C5 | Use shielded cables and connectors as faraday cage. Perform EMC tests as early as possible. |
| THOR._RSK.019 | PDU | If the DC-DC that feed the OBC fails, the rest of the experiment will not shutdown, as of PDU PDR version | DCDC malfunction, overheat, critical failure | Flight | B2 | Redundant DC-DC converters at the OBC level. Put the ON/OFF state of the other DC-DC's as a function of the voltage level of the input of the OBC. In other words, put the I/O expander input voltage as the 12V that goes to the OBC. |
| THOR._RSK.020 | DET | Using the Flight Model on the Grenoble Test, damaging DET while traveling | Mechanical environment, drop of the transportation box | Testing | B5 | When the detector has to travel use personal car. Use extra foam to condition the mechanical environment of the Detector Unit. Move the DET FM as little as possible. Do few long distance travels. |
| THOR._RSK.021 | DET | Miss handling the Detector Unit flight model. Crack the CdTe Crystal. | Dropping the Detector. Hit the CdTe Crystal into a rigid surface. FB may become unusable, detection area decreases. | Testing | C4 | Let ADVACAM assembly the DET in the final configuration in Prague. |
| THOR._RSK.022 | PDU | HV short circuit between the two adjacent FB in the same DP | Implementing REQ-180 and REQ-181 there is an operation mode where half the DP is ON and other half is OFF. Short circuit may occur between -500v and GND and damage the FB electronics. | Flight/ Testing | B4 | Middle FB's shall be seperated by 5mm, see REQ-182. |

Chapter 4

Assembly, Integration, Verification and Testing

In this chapter, we detail the development plan for THOR, divided into two main sections: the payload development philosophy and the individual products development philosophy.

The payload development philosophy pertains to an integrated unit that serves as a reference for the Flight Model. This unit allows to draw conclusions to verify the integrity of the payload design. On the other hand, the individual products development philosophy follows a step-by-step process to ensure each product function is validated.

We provide an overview of these development models and clarify our objectives for each. Additionally, we outline the tests designed for both the individual product and payload development models, explaining the purpose and reasoning behind each test. We also present the results of some tests that have already been conducted.

4.1 Payload Model Philosophy

The payload Model Philosophy was based on the maturity of the development of each subsystem. The payload flight segment is composed of four main products that are developed individually, Detector Unit, Power Distribution Unit, Onboard Computer and Enclosure.

4.1.1 Payload Level Development Models

CAD Model: The development model will be used to verify the physical design of the products, namely DET geometry, as well as compatibility with SR MPCB volume. To ensure that the mechanical interfaces between products, THOR and MPCB and between P/L and the GSE are validated. The model will have a CAD version of each subsystem with the physical dimensions as well as the mechanical interfaces. Two

models will be developed, at PDR and at CDR.

Thermal Model: The development model will be used to qualify the P/L thermal design by performing software thermal analysis taking into account the expected thermal loads on each component as well as the coupling capabilities of the MPCB interface. Two models will be developed by AST: PDR analysis to be performed with the following conditions:

- SR interface at 15°C - to check the stabilized temperature of the P/L components, with the components consuming the Max 15% and nominal 15%;
- SR interface at 40°C - to check see the stabilized temperature of the P/L, with the components consuming the Máx 15% and nominal 15%;
- SR interface at 15°C - to check the stabilized temperature with all the components turned OFF;
- SR interface at 40°C - to check stabilized temperature with all the components turned OFF;

Engineering Model: The development model will be fully representative in form, fit and function of the P/L. This model will be used for functional qualification: verification of both electrical and software interfaces, as well as to perform the tests on TVAC, EMC and Shaker/Shock. The model will be fully equipped except for the THOR_DET_GAM and THOR_DET_PAR. The equipment to be used is:

- 1x THOR_DET_GAM.FB.x (THOR_DET_GAM.FB.DM);
- 1x THOR_DET_GAM.RO.x (THOR_DET_GAM.RO.DM);
- 1x THOR_PDU.DM.2;
- 1x THOR_ENC.EM;
- 1x THOR_OBC_GPU.EM;
- 1x THOR_OBC_CB.EM;
- Dummy weights on CoG of missing products;
- Resistive heaters;

The remaining of the THOR_DET_GAM and THOR_DET_PAR systems shall have a representative weight on the CoG, to simulate the mechanical loads and respective heating elements which will simulate the thermal behaviour. This model will be delivered to ESA, without the detectors, for them to perform the fitting tests to the MPCB.

Flight Model: Fully representative of the flight design. Twin version of the corresponding engineering models that went through rigorous testing.

4.2 Product Level Development Philosophy

Each product has its own development plan due to the technology maturity of each of them. The development models will be used to confirm the design feasibility and the required functions to be performed. The development flow chart until the environmental test campaign is presented in the Figure 4.1.

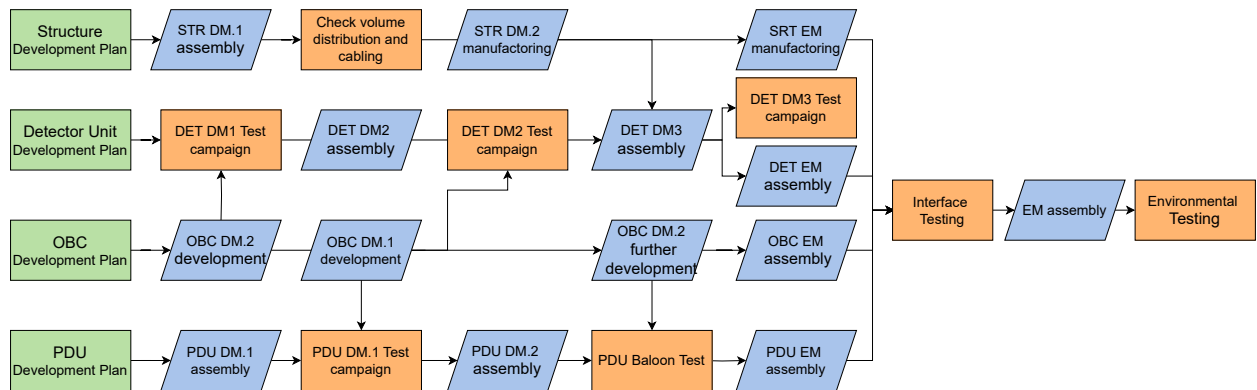


Figure 4.1: Product level development flow chart.

In the following sections the configuration of each development model and the description of every test to be performed will be presented. The Table 4.1 summarizes the representativeness of the development models to be used on each individual test.

| Model | Development Model (DM) | | | | | | | | | | | | | | |
|-----------------------|------------------------|-----|-----|-----|------|-----|-----|-----|------|-----|-----|-----|----|----|--|
| Sub-Model | DM.1 | | | | DM.2 | | | | DM.3 | | | | EM | FM | |
| Product | OBC | PDU | DET | ENC | OBC | PDU | DET | ENC | OBC | PDU | DET | ENC | | | |
| Science | | | | | | | | | | | | | | | |
| TEST_DET_001 | | | X | | X | | X | | | | X | | | X | |
| TEST_DET_002 | | | X | | | | | | | | X | | | X | |
| TEST_LARIX_DET_004 | | | | | | | X | X | | | | | | X | |
| TEST_GRENOBLE_DET_005 | | | | | | | | X | | | X | | | X | |
| TEST_DET_006 | | | X | | | | | X | | | X | | | | |
| TEST_DET_007 | | | X | | X | | X | | | | X | | | X | |
| TEST_DET_008 | | | X | | | | | | | | | | | X | |
| TEST_DET_009 | | | X | | | | X | X | | | X | | | X | |
| TEST_DET_010 | | | X | | | | | | | | | | | | |
| TEST_DET_011 | | | X | | | | X | | | | | | | | |
| TEST_DET_013 | | | X | | | | | | | | | | | X | |
| System | | | | | | | | | | | | | | | |
| TEST_PDU_001 | X | X | | | | | | | | | | | | | |
| TEST_PDU_002 | | X | | | X | | | | | | | | | | |
| TEST_POLLUX_PDU_003 | X | | | | | X | | | | | | | | | |
| Payload | | | | | | | | | | | | | | | |
| TEST_TVAC_EM_001 | | | | | | | | | | | | | X | | |
| TEST_SHAKER_EM_001 | | | | | | | | | | | | | X | | |
| TEST EMC_EM_001 | | | | | | | | | | | | | X | | |
| TEST_LS_CAL | | | | | | | | | | | | | | X | |

Table 4.1: Tests to be performed by each development model.

4.2.1 Detector Unit Development Models

The development model will be used to confirm the design feasibility of the detector. At this stage, each system's performance and integration capabilities will be tested individually. Since ADV is updating the design to meet our requirements, the development models don't have the same form but the function is maintained. The hardware (ASIC, CPU-FPGA and peripherals) is similar and totally representative of the one used on the flight model.

4.2.1.1 First Detector Unit Development Model

The THOR_DET_DM.1 development model validates the performance, operations, and capabilities of the TPX3 ASIC technology. This model is not representative in form nor fit but the core scientific and housekeeping functions remain the same. The electronic is identical to what we'll use in the final flight model.

In terms of configuration, we're using a Minipix TPX-3, 2mm CdTe detector from ADV to validate THOR_DET_GAM and THOR_DET_PAR operations. The model will be integrated with a standard PC and OBC_DM.2 for interface integration tests. The team will also use it to get familiar with the system. We'll test software using Python and C++ APIs and finalize calibration processes for the flight model.



Figure 4.2: Picture of the detector unit first development model, THOR_DET_DM.1.

4.2.1.2 Second Detector Unit Development Model

The next development model, known as the QUAD configuration Advapix TPX3, features a CdTe 2mm unit with 4 CdTe matrices, 4 TPX3 ASICs, and a single RO board. See Figure 4.3. This specific configuration is designed to support more complex detection tasks.

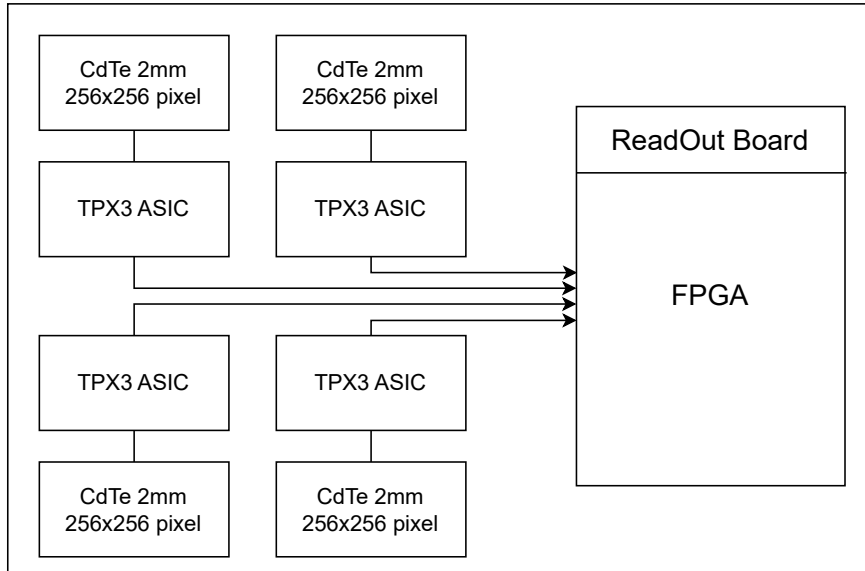


Figure 4.3: Configuration of the detector unit second development model, THOR_DET_DM.2.

To fulfill its purpose, the unit will pair with a standard PC and OBC_DM.2 to assess the handling of DP. It will also serve to refine larger-area detection test procedures. Last but not least, when coupled with the earlier DET_DM.1 as the first layer of a Compton camera, this new setup will validate inter-plane particle and photon detection capabilities. It's designed to work within a tens of microseconds coincidence time.

The delivery for this advanced unit is scheduled for October 2023.

4.2.1.3 Third Detector Unit Development Model

The following development model scales up from the previous designs and is configured as a 2x QUAD Advapix TPX3 with CdTe 2mm units. This setup will feature 8 CdTe matrices, 8 TPX3 Asics, and 2 RO boards to handle more complex detection tasks. See Figure 4.4 for a schematic of the representativeness.

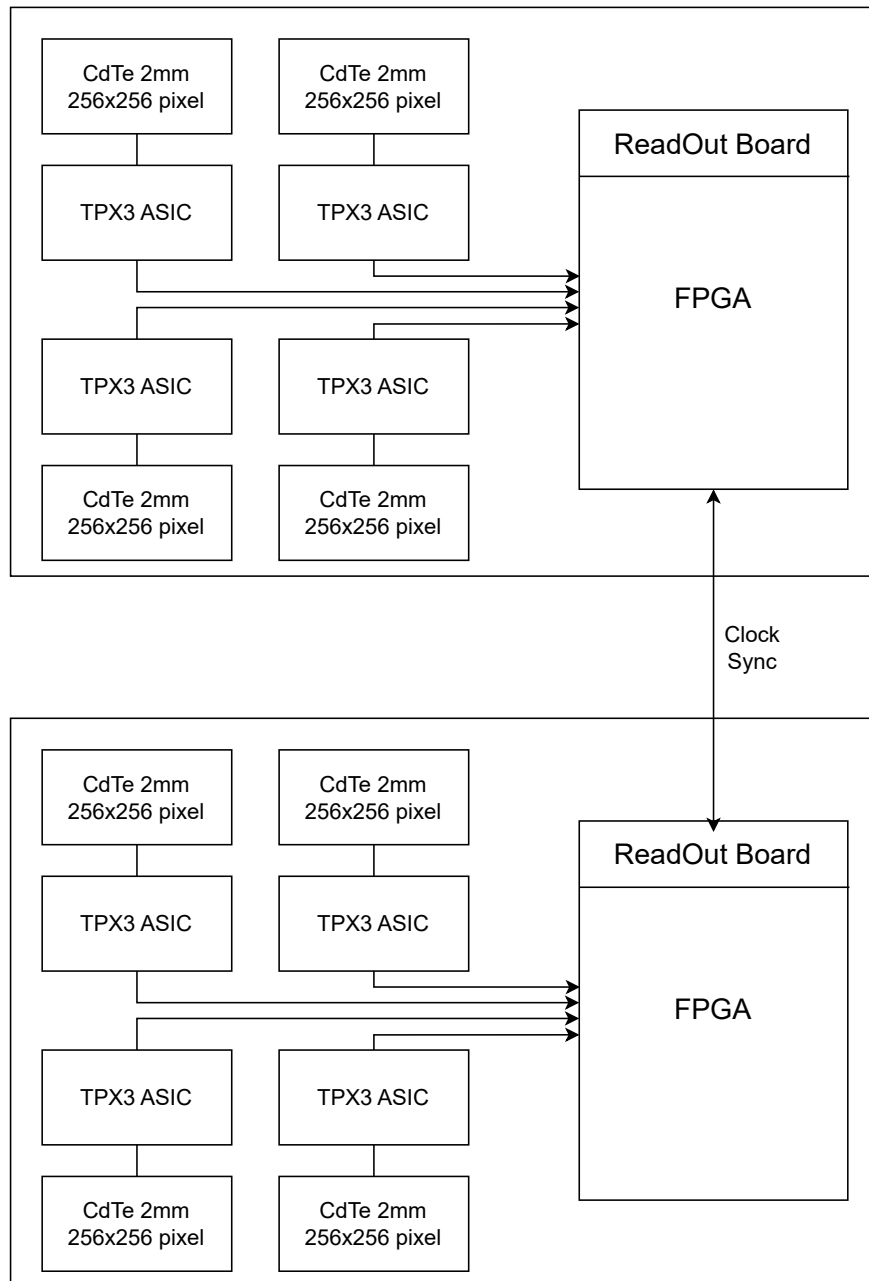


Figure 4.4: Configuration of the detector unit third development model, THOR_DET_DM.3.

This model will work with a standard PC and OBC_DM.2 to evaluate the managing capabilities of multiple detectors. A key objective is to test and confirm the synchronization capabilities between two detectors. Moreover, the model will validate the functionality of a

Compton camera system, specifically achieving a coincidence time as precise as 1.6 nanoseconds. Another objective is to assess polarimetric performance when two detectors are in stacked configuration.

As for the delivery timeline, that's still TBD.

4.2.1.4 Detector Unit Engineering Model

The engineering model will be set up with a single Finger Board (FB) along with a Readout (RO) board, Figure 3.36. We've opted to use just one FB for these tests because they are more intrusive and pose a risk of damaging the bonding of the CdTe detectors. This model is specifically designed for rigorous environmental tests. It will undergo Thermal Vacuum (TVAC), Shaker/Shock, and Electromagnetic Compatibility (EMC) tests. The delivery date is still to be determined.

4.2.1.5 Detector Unit Flight Model

The flight model configuration is outlined in Section 3.8.2. The setup will feature 16 Finger Boards with 2mm CdTe, two particle detectors with 500 μ m Silicon, and four Readout Boards. Currently, the delivery date for this setup is not yet determined.

4.2.2 PDU Development Models

4.2.2.1 First PDU Development Model

The upcoming model serves as a scaled-down version of the final Power Distribution Unit (PDU). This PCB model aims to evaluate the operation of two DC-DC converters, a current monitor and the overcurrent protection system. See Figure 4.5 for a block diagram of the representativeness of the unit.

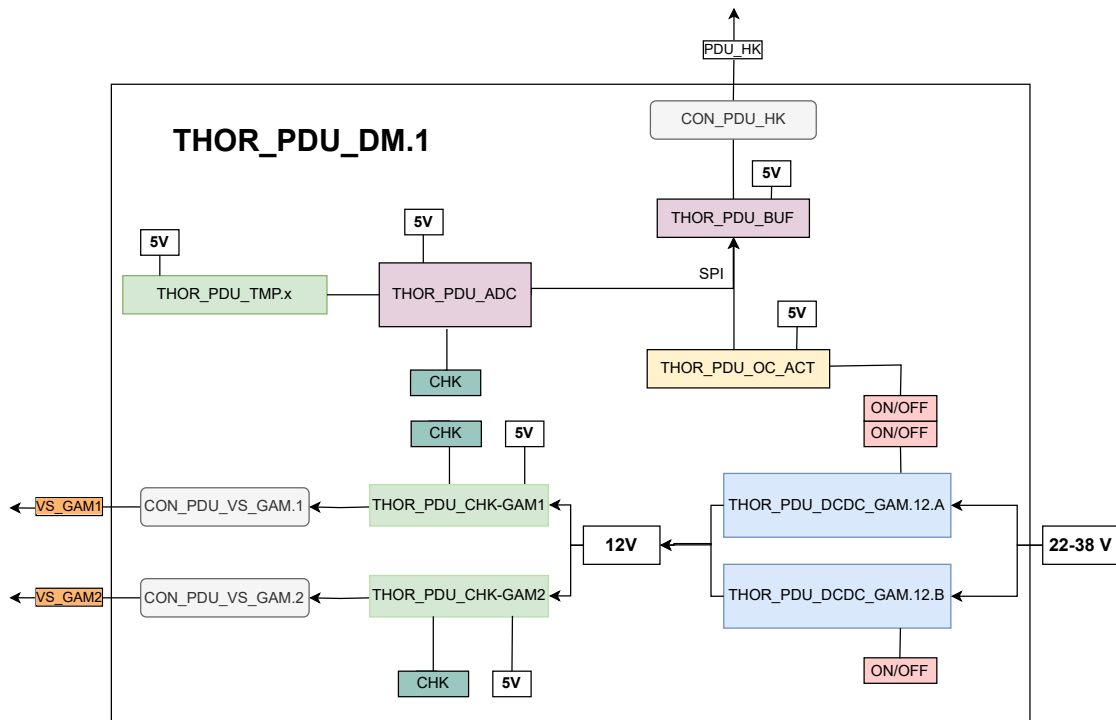


Figure 4.5: Block diagram of the first development model of the PDU, THOR_PDU_DM.1.

This model aims to validate technology readiness levels TRL4 and TRL5, as outlined by ECSS-E-HB-11A. It will also assess the performance and design requirements of the PDU, focusing on both normal operations and failure modes. Tests will be conducted under laboratorial conditions at a temperature of 25°C and pressure of 1 atm (1.01×10^5 Pa), and under vacuum at 25°C and 10^{-2} Pa pressure. Delivery of the model is scheduled for October 2023.

4.2.2.2 Second PDU Development Model

This model is representative of the final design, with the updates resulting from the development and testing of the THOR_PDU_DM.1 model. Meant to be fully representative in form, fit, and function to the Flight Model (FM), this model targets validation at a TRL6 level, as set by the ECSS-E-HB-11A standards. Beyond the design insights from THOR_PDU_DM.1 this model will be subjected to high-altitude balloon flight tests up to 25 km. These tests are designed to simulate the conditions— specifically, temperature and pressure — that the FM will experience in space. During the balloon flight, the model will undergo a comprehensive evaluation of all functions, operational and failure scenarios. Delivery of this model is scheduled for January 2024.

4.2.2.3 PDU Engineering Model

This development model is built from the improvement implied by the THOR_PDU_DM.2 tests, if any. In case there are no design changes the configuration is the same as the THOR_PDU_DM.2. This model aims to achieve TRL7 through TVAC, Shaker, and EMC tests. If during the environmental test campaign any critical design changes are needed, a second version of the EM shall be produced. Depending on the changes, the model may require new environmental tests. The delivery date is still TBD.

4.2.2.4 PDU Flight Model

This model is a twin of the final version of the THOR_PDU_EM.

4.2.3 OBC Development Models

4.2.3.1 First OBC Development Model

This model uses an Arduino board to test and validate the basic functions of the PDU.

4.2.3.2 Second OBC Development Model

This model uses a Jetson AGX Xavier with a standard Carrier Board. Its purpose is to perform integration with the DET API, validate the functional requirements for the OBC, and assess compliance with power consumption limitations. The model was received in January 2023.

4.2.3.3 OBC Engineering Model

This model features a Jetson AGX Xavier Industrial with a Diamond Systems Carrier Board. It is meant to be used during the environmental test campaign. The delivery date is still to be determined.

4.2.4 Enclosure Development Models

4.2.4.1 First Enclosure Development Model

This model is made of cardboard and represents the volume of the P/L PDR design. It's used to check the component distribution and cable management. It was assembled on July 2023.

4.2.4.2 Second Enclosure Development Model

The configuration for this model is still to be determined. Will assemble THOR_DET_DM.1 and THOR_DET_DM.2 in a stacked configuration. It also shall allow a THOR_DET_DM.3 configuration. The model is scheduled for delivery in November 2023.

4.2.4.3 Enclosure Engineering Model

This configuration is the result of the CDR design. At this stage it is expected to be fully representative in form and fit of the Flight Model. If during the environmental test campaign any critical design changes are needed, a second version of the EM shall be produced. Depending on the changes, the model may require new environmental tests. If the changes are not too big (eg.: screw hole 1mm misaligned) the second version of the EM model can then become the FM.

4.3 Test Descriptions

4.3.1 Payload Level Tests

4.3.1.1 Thermal Vacuum Test

During the launch event, THOR will experience a depressurization profile of 2200 Pa/sec until it reaches $\sim 10^{-3}$ Pa, the lower limit of the atmospheric pressure in orbit. The SR baseplates will maintain a working temperature between 15-40°C with a thermal stability of $\pm 5^\circ\text{C}$. A TVAC test will confirm THOR's ability to operate in these conditions. A detailed procedure will be developed once the ICD file from the SR team is provided. The ICD will further specify the thermal interface and include a preliminary concept of operations in which information such as Sun exposure, baseplate temperature, and when THOR will be turned on will be provided.

4.3.1.2 Shaker Test

This test aims to validate THOR's capability to withstand the mechanical environment conditions during the launch and reentry phases aboard the SR vehicle, which includes the Low Frequency Environment (Table 4.2), Random Environment (Figure 4.6), and Shock Environment (Figure 4.7). During the test, accelerometers will be placed in critical locations of the P/L to measure the exact vibration environment. It is convenient to position these accelerometers at the component's interfaces with the enclosure, as well as in critical areas such as near the THOR_DET_GAM.DP.x.FB.x semiconductor since the bonding (electrical connection) between the CdTe and the ASIC pads is fragile. This connection may break,

leading to un-optimal charge transmission between the CdTe and the ASIC making the affected pixel unusable.

| Payload Location | Design Loads (g) | | |
|---------------------------------|------------------|------|------|
| Vertical (Plate 6) ¹ | X | Y | Z |
| | 15 | 3.75 | 12.5 |

Table 4.2: Expected low frequency mechanical environment to be applied to THOR interface with the SR baseplate. The design loads are expressed in units of gravity acceleration, $g=9.8 \text{ m/s}^2$.

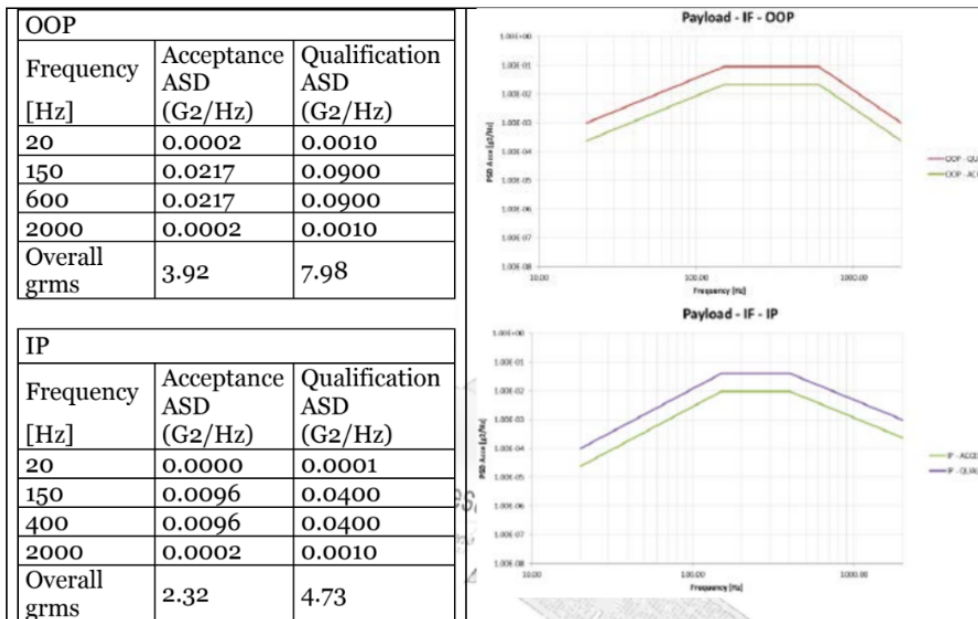


Figure 4.6: Expected random environment to be applied to THOR interface with the SR base plate ,

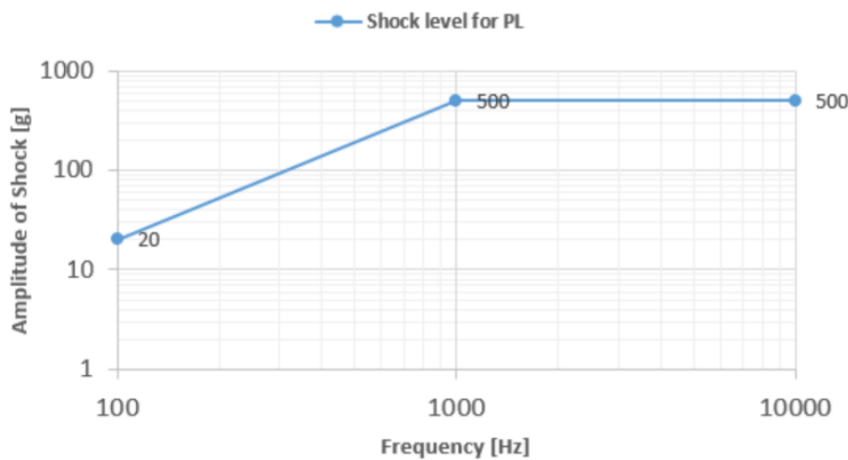


Figure 4.7: Expected shock environment to be applied to THOR interface with the SR base plate. The amplitude of shock is expressed in units of gravity acceleration, $g=9.8 \text{ m/s}^2$.

¹See Figure 3.8

4.3.1.3 Electromagnetic Compatibility Test

This test aims to make sure that THOR payload's electronics are working as expected in the electromagnetic environment inside the MPCB. The test also checks that any electromagnetic perturbation from THOR doesn't disturb other payloads during the flight. We'll use the emission and susceptibility standards outlined in Figure 4.8 as benchmarks.

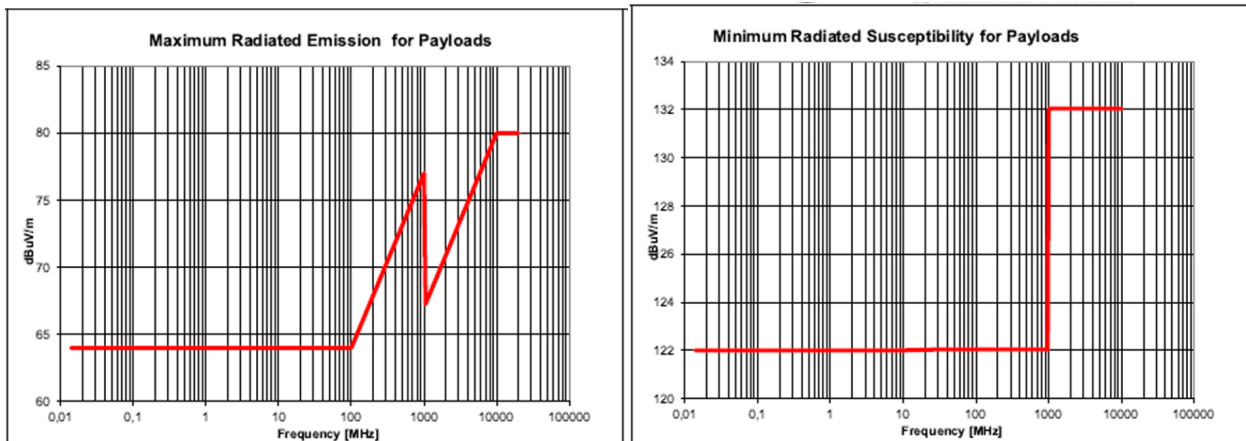


Figure 4.8: EMC environment that THOR shall withstand (right) and emit (left).

This test will be divided in three stages: Radiated emission tests (from 30 MHz up to 18GHz) to study the electromagnetic emissions of THOR; Conducted emission tests (from 9kHz up to 200MHz) to study the emission of lower frequencies (although it is a conducting test the results are related to lower frequency emissions); Radiated immunity tests (from 50MHz up to 3GHz) where THOR will be subject to electromagnetic impulses within these frequencies to verify the nominal operation of the P/L.

4.3.1.4 Pre-integration Calibration

THOR requires a calibration pre-integration on the SR MPCB. The test shall be performed on the same location as the integration of the payload on the SR. The results of this final test will be used to tune the calibration of the Detector Unit. In order to properly perform the calibration, a radioactive source is required (^{137}Cs or ^{22}Na) with activity in the 1–10 μCi interval.

The pre-integration test not only will be useful to calibrate the Detector Unit, giving us a reference point to study the degradation of the detector modules, but also to check for any indication that a malfunction on the Detector Unit may occur during flight, e.g., Finger-Board not working, specific pixels malfunction, etc.). Below the scheduling for the pre-integration test is shown.

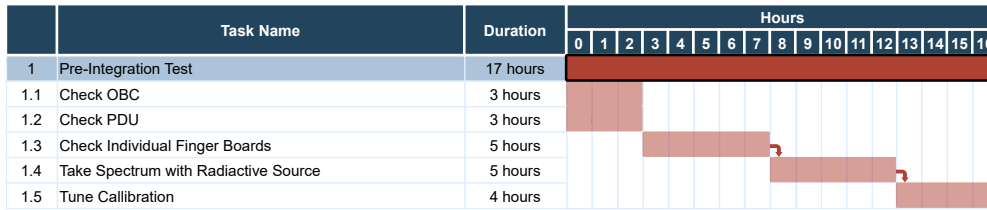


Figure 4.9: Timeline of the pre-integration test.

4.3.2 Detector Unit Tests

4.3.2.1 TEST_DET_001 - Energy Calibration and Energy Resolution

Scope: Preliminary tests showcased that for energies >100keV the factory energy calibrations didn't respond correctly to the energy and therefore a second calibration is required. The main objective of this test is to calibrate the detector response in energy. The second objective is to find the average energy resolution of the detector over the energy range 100 keV–1 MeV. This test will also be used to outline the calibration and energy resolution determination procedure for further development models and even for the flight model. This will be done for the whole detector, and not pixel by pixel as it was done by ADVACAM.

Rational:The detector will be subject to different radioactive sources. Some are available at LIP-Coimbra: ^{133}Ba , ^{137}Cs ; ^{22}Na , and others, namely ^{152}Eu , ^{154}Eu at ICNAS cyclotron facility. The physical set-up of the data collection is similar to all gamma-ray sources. The only consideration to be taken into account is the activity of the gamma-ray source and the distance at which the source is placed from the detector. Lower activity sources were placed closer to the detector than higher activity active ones, to minimize the duration of each run.

Procedure Summary:Place radioactive source a few cm away from the detector, start acquisition, wait a few hours, end acquisition.

Results - THOR_DET_DM.1:²

Calibration results:

The tests were conducted using the following radioactive sources: ^{133}Ba ; ^{137}Cs ; ^{22}Na ; ^{152}Eu and ^{154}Eu .

²The test was carried out by José Sousa and Jonathan Flunger. The data processing was carried out by Jonathan Flunger.

| Isotope | Energy (keV) | Photons per 100 disintegration | Activity (kBq) |
|-------------------|--------------|--------------------------------|------------------------------|
| ^{22}Na | 511.0 | 180.7 ± 0.2 | $51.25 \pm 15\%$ @19/06/2023 |
| | 1274.5 | 99.94 ± 0.13 | |
| ^{133}Ba | 81.0 | 33.31 ± 0.30 | $251.6 \pm 15\%$ @25/08/2020 |
| | 276.4 | 7.13 ± 0.06 | |
| | 302.9 | 18.31 ± 0.11 | |
| | 356.0 | 62.05 ± 0.19 | |
| ^{137}Cs | 661.7 | 85.05 ± 0.29 | $231.2 \pm 20\%$ @19/06/2023 |
| ^{152}Eu | 121.8 | 28.41 ± 0.13 | 18.59 @ 15/04/1993 |
| | 244.8 | 7.55 ± 0.04 | |
| | 344.3 | 26.59 ± 0.12 | |
| | 411.1 | 2.24 ± 0.01 | |
| | 444.0 | 2.80 ± 0.02 | |
| | 778.9 | 12.97 ± 0.06 | |
| | 1408.0 | 20.85 ± 0.08 | |
| ^{154}Eu | 123.1 | 40.4 ± 0.5 | 18.50 @ 01/06/2018 |
| | 247.9 | 6.89 ± 0.07 | |
| | 591.8 | 4.95 ± 0.05 | |
| | 723.8 | 20.05 ± 0.21 | |
| | 873.2 | 12.17 ± 0.12 | |
| | 1274.4 | 34.9 ± 0.3 | |

Table 4.4: Radioactive sources used as well as the used peaks on the calibration and energy resolution tests. Source [Bé et al., 2016]

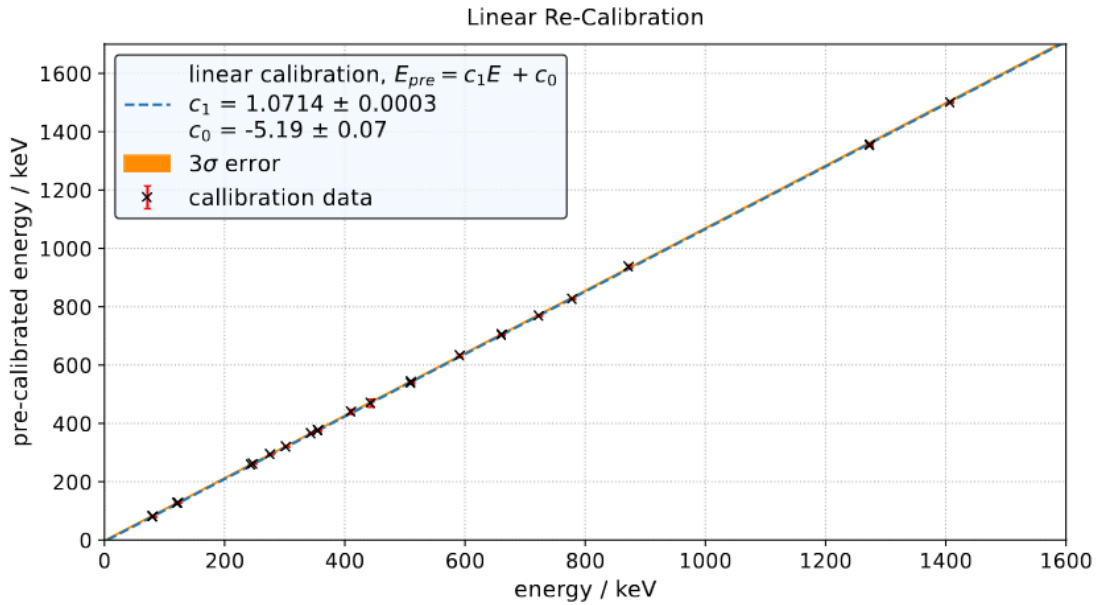


Figure 4.10: Calibration curve of the first detector unit development model. Credit: Jonathan Flunger.

The results show a deviation of the energy response of about 7% which validates the need of this re-calibration procedure.

Energy Resolution Results:

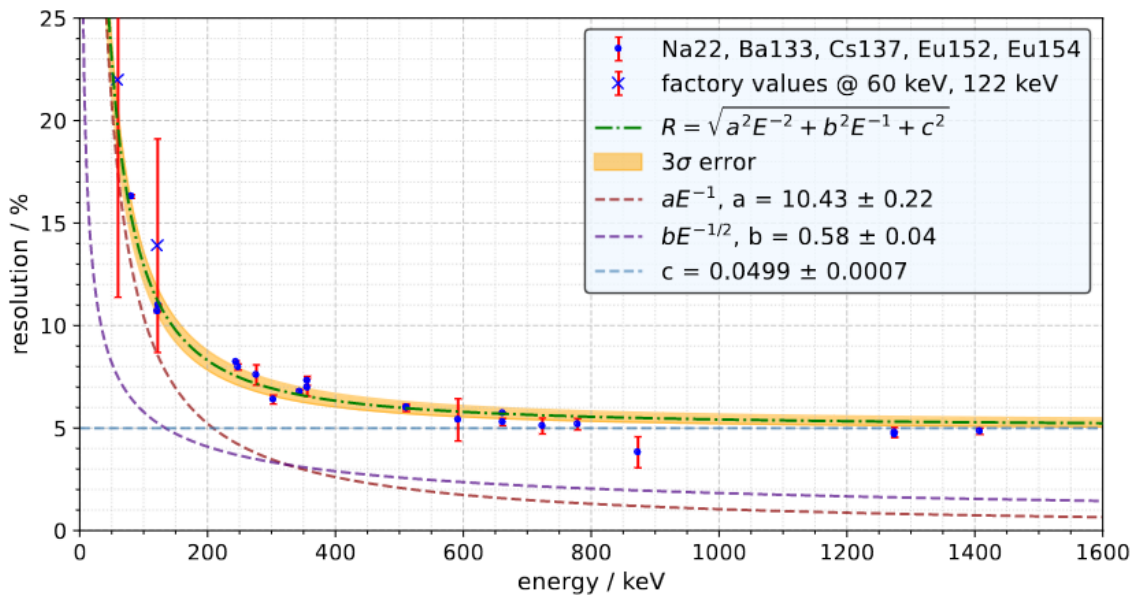


Figure 4.11: Measured energy resolution of the first detector unit development model. Credit: Jonathan Flunger.

| Energy (keV) | Resolution |
|--------------|--------------|
| 100 | 12.93±0.25 % |
| 511 | 5.97±0.1 % |
| 1000 | 5.42±0.08 % |

Table 4.5: Measured resolution of key energies measured with the first development model of the detector unit, THOR_DET_DM.1.

The results of the energy resolution show that for energies below 100keV the resolution is well above 10% but for higher energies the resolution stabilizes on around 5%. The poor energy resolution for lower energies is related to the fact that for lower energies the electronic noise induced on the input of the ASIC which is strongly dependent from the temperature at which the detector was operating. The electronic noise contribution to energy resolution decreases with the energy being its weight represented by the parameter a in the Figure 4.11. Also, the fact that there are statistical fluctuations on the charge generation process, characterized by

$$noise_{intrinsic} = \sqrt{2.35^2 \epsilon F E} \quad (4.1)$$

where ϵ is the energy necessary to create one electron hole pair, F is the Fano factor and E is the photon energy, responsible for a noticeable contribution for lower energies being its weight represented by the parameter b on the Figure 4.11. It should be noted that electronic noise depends on several factors, such as the leakage current through the thickness of the semiconductor (depends on the resistivity), the capacity of the detector (depends on the dielectric constant), etc. The third contribution to the energy resolution includes the effect of the charge collection efficiency, being constant over the energy and its represented by the parameter c in the Figure 4.11. The trade-off between the required charge collection efficiency, the required charge drift time for 3D particle tracking and the leakage current will determine the achievable energy resolution for our detector.

4.3.2.2 TEST_DET_002 - Polarimetry

Scope: Access the polarimetric performances of the CdTe 2mm detector DET_DM.1. Identify single, double and multiple photon events. Access the viability of using the detection of the secondary photon for polarimetry in a single 256x256 CdTe matrix.

Rational: Use the data gathered by the THOR_DET_001 and identify double events and check the geometric distribution of these events on the 2D CdTe matrix.

Procedure Summary: Identify photon events, by characterizing the event by the pixels activated in a 100ns time window. Identify if the event is a Compton by accessing if the event has two distinct cluster of pixels spaced by more than 2 unactivated pixels. Model the planar 2D distribution of the scattered photon.

Results: At this stage it was validated the ability to detect and identify Compton events within a single detector matrix, see Figure 4.12.

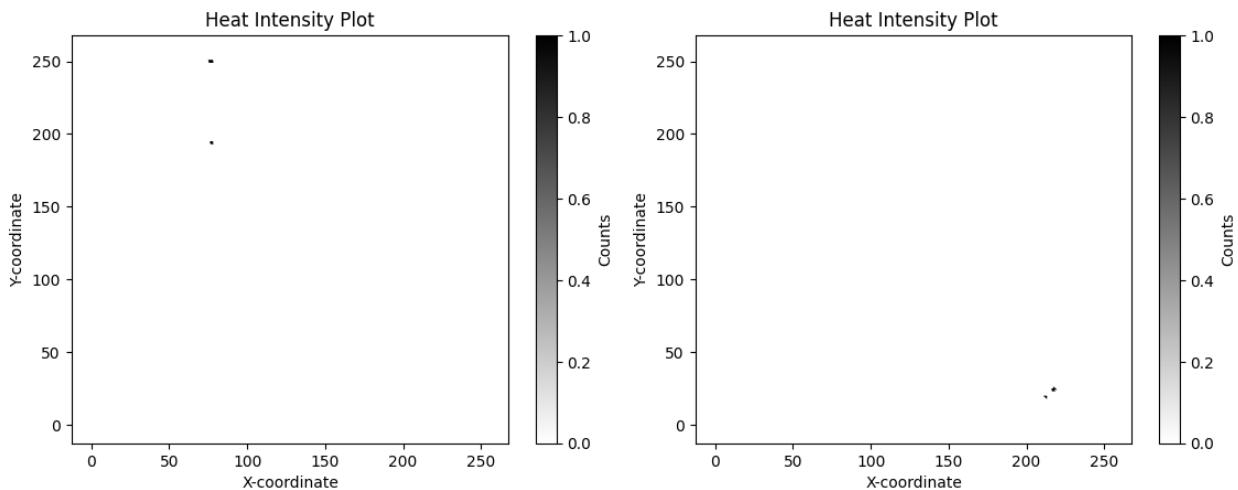


Figure 4.12: Example of two Compton events detected with the preliminary Compton finder algorithm.

A more robust algorithm to identify Compton events is required. At this stage the algorithm treats the two photon interactions as one event and therefore cannot recognize the energy absorbed on the different locations of the matrix. Future iteration of the algorithm shall differentiate the primary absorbed photon from the remitted to then be able to calculate the scattering planar vector direction.

4.3.2.3 TEST_LARIX_DET_004 - LARIX Beamline

Scope: This test will be used to calibrate the detector, energy and baseline polarimetry.

Outline the calibration procedure for the FM. The LARIX beamline produces a collimated gamma-ray beam with energy up to 300keV with a beam size up to $30 \times 30 \text{mm}^2$. To access the scattered Compton photon modulation for an unpolarized beam.

Rational: The squared shaped geometry of the pixels (the material thickness on the diagonal is greater than in the x and y direction) induces an irregular modulation curve that needs to be characterized with the LARIX unpolarized beam. The collimated beam size will be useful to test the detector by sections.

Procedure Summary: Expose the detector to the beamline (few keV up to 300keV). Test different beam attack angles.

Results: Not yet performed.

4.3.2.4 TEST_GRENOBLE_DET_005 - Grenoble Breamline

Scope: Access the polarimetric performances of the detector when subject to a $\sim 99\%$ polarized beam.

Rational: The ESRF facilities opens competitive calls to access their beamlines. In this case we are interested on the beamline ID15A that provides a $\sim 99\%$ polarized beam with photon energies between $\sim 20\text{keV}$ to $\sim 500\text{keV}$.

Procedure Summary: Gather data for different energies and for different attack angles.

Results: Not yet performed. Still have to apply to the call.

4.3.2.5 TEST_ICNAS_DET_006 - Particle Info

Scope: This test has the objective to gather particle information to feed the neural network algorithm that's going to be integrated in the OBSW for active particle identification³. It is expected to access the ICNAS facilities to have access to the $\sim 14\text{MeV}$ proton cyclotron. Radioactive sources that emit alpha particles, e.g. ^{241}Am , are also going to be used.

Rational: Two steps: First, to expose the detector to the cyclotron proton beam. Use absorption material (plastic) between the output of the proton beamline and the detector to have protons with lower energies. For example we can test the detector with proton beams of various energies within $\sim 2\text{-}14\text{MeV}$ range. One can also vary the proton beam attack angle to create different patterns on the detector. Second, to expose the detector to an ^{241}Am source. It is important to note that the heavy alpha particles rapidly lose energy when traveling in air. Therefore, using various distances to the detector surface, it allows testing with various energies of the alpha particle beam, for instance within $\sim 0.5\text{-}4\text{MeV}$ range. Also, by varying the beam attack angle one can create different interaction scenarios on the detector.

Procedure Summary:

Results: Preliminary particle detection validation scrips were developed. Several electrons, protons, muons and alpha particles were detected during the acquisition of a ^{133}Ba

³This algorithms are being developed and tested on an on-going Master's Thesis.

spectrum. The recorded events are the product of atmospheric particle showers and not from the gamma-ray source. The overnight acquisitions with the ^{133}Ba source led us to also detect these background particles, see Figure 4.13 and 4.14.

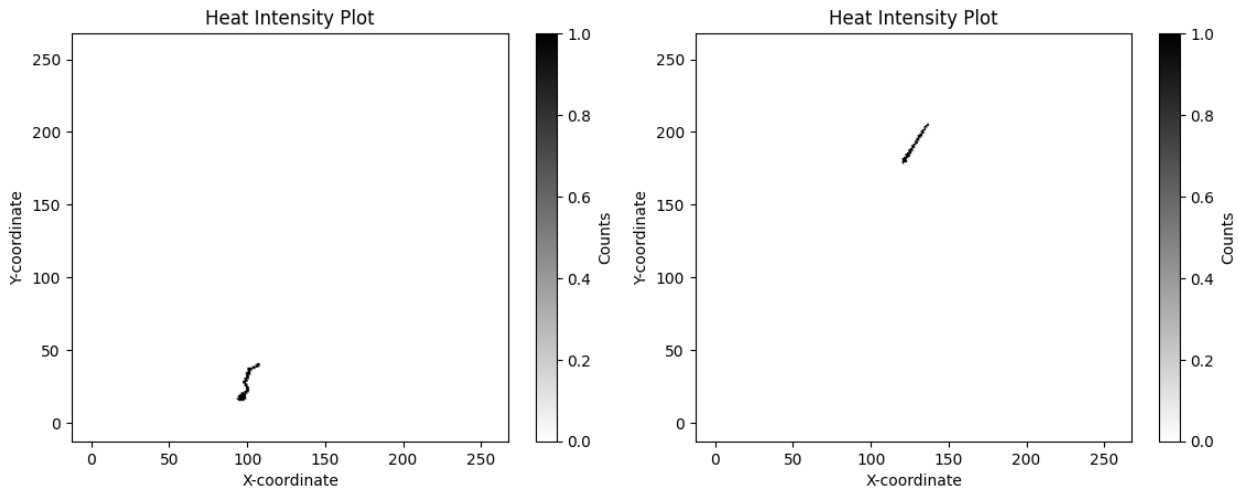


Figure 4.13: Left, example of an electron with 2352keV. Right, example of a proton with 1964keV.

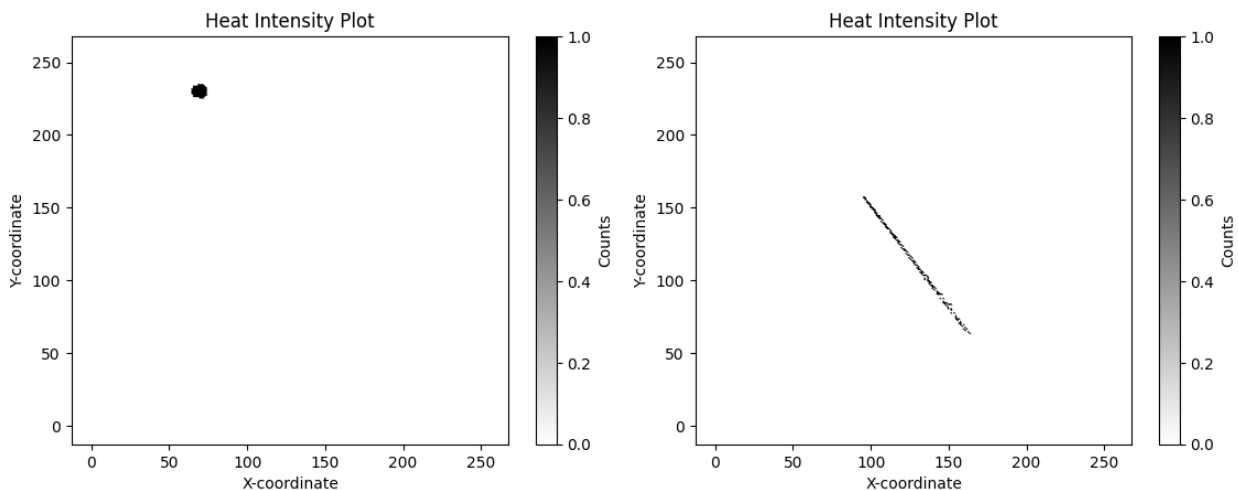


Figure 4.14: Left, example of an alpha with 4595keV. Right, example of a muon with a 2859keV.

4.3.2.6 TEST_DET_007 - Temperature keV

Scope: This test will validate the monitoring of housekeeping data from the detector. This test is also calibrate the response of the ToT regarding the temperature of the ASIC and as a function of the DAC. For different temperatures check the number of noisy pixels.

Rational: The semiconductor detector energy response varies with temperature. The higher the temperature the higher the leakage current and creating an offset at the current that feeds the pre-amplifier on the ASIC. Also the digital to analogue converter (DAC)

that feeds the reference of the comparator which determines the detector threshold is known to change its output with the temperature. Because of these two reasons, the detector requires a temperature calibration.

Procedure Summary: The cold side of a thermoelectric cooler (Peltier cell) element is used to cool down the detector temperature to 10°C. While the hot side of a peltier element is used to heat the detector up to 60°C. Take spectra with different sources (^{133}Ba , ^{137}Cs and ^{22}Na) at temperature steps of 5°C.

Results: Preliminary tests performed at the lab. Calibration of the power supplied to the thermoelectric cooler vs detector temperature already done. See Figure 4.15 for the current setup in the LIP-Coimbra laboratory.

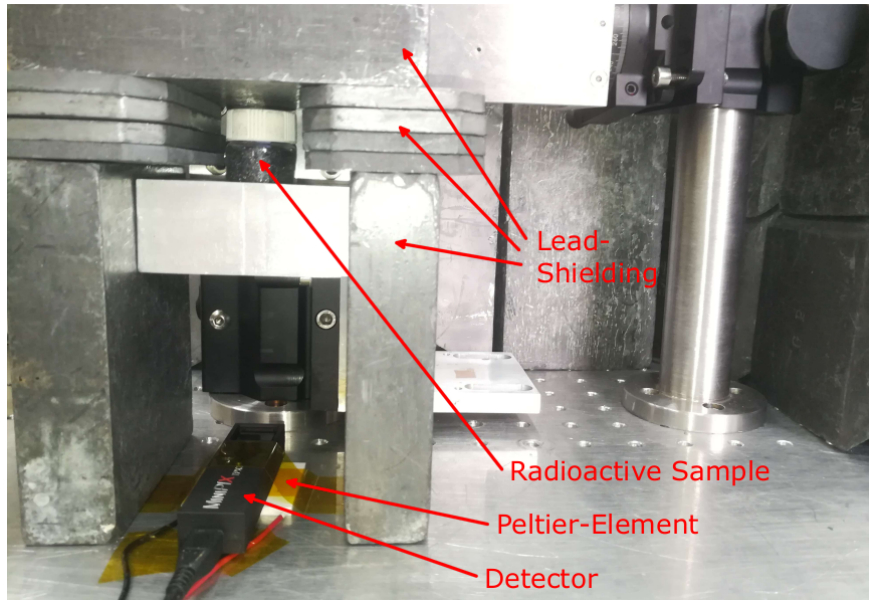


Figure 4.15: Setup in the LIP laboratory. Hot surface in contact with metal table to dissipate the heat. Image credit: Jonathan Flunger.

4.3.2.7 TEST_DET_008 - Efficiency

Scope: Measure the detector intrinsic peak efficiency to detect gamma-rays with energy 100keV - 1MeV.

Rational: The intrinsic peak efficiency, ϵ_{int} , is the ratio between the number of events within the Gaussian shaped energy peak recorded by the detector, N_{total} , over the number of photons of said energy that reach the detector. To measure the detectors intrinsic peak efficiency, the activity of the source must be know, and the set-up geometry must be taken into consideration.

$$\epsilon_{int} = \frac{N_{total}}{a_s \times f_e \times G \times T_{aq}} \quad (4.2)$$

where a_s is the gamma-ray line yield per disintegration, f_e is the source activity, G is the geometric factor and $T_a q$ is the acquisition time. The best set-up is to have a point-like source where the distance between the source and the detector is way greater than the diagonal length of the detector surface, see Figure 4.16. In this case the solid angle subtended by the detector at the source position is calculated in a simple way [Knoll, 2010]. This method is highly dependent on, not only the available sources in the laboratory, but also on their activity (for large distances it may be required several days of acquisition time).

Procedure Summary: Same as TEST_DET_001.

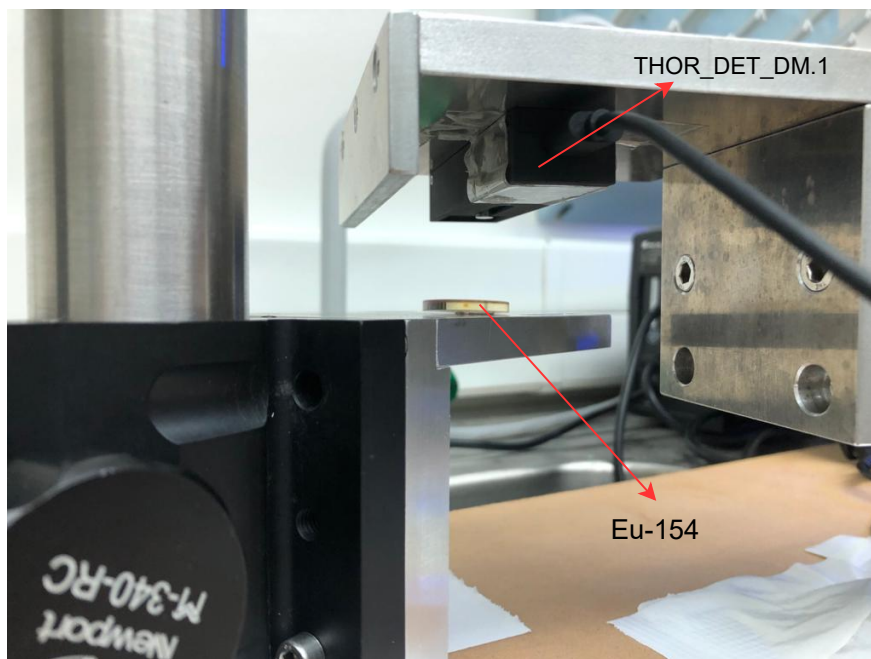


Figure 4.16: Test setup at ICNAS, ^{154}Eu .

Results⁴:

| Energy (keV) | Detection intrinsic peak efficiency |
|--------------|-------------------------------------|
| 100 | 61±29 % |
| 123 | 53±8 % |
| 247 | 8.6±1.4 % |
| 511 | 1.6±0.9 % |
| 724 | 0.66±0.14 % |
| 1000 | 0.36±0.21 % |
| 1274 | 0.23±0.04 % |

Table 4.6: Detection efficiency measured with the first development model of the detector unit, THOR_DET_DM.1.

4.3.2.8 TEST_DET_009 - Charge Drift

Test Procedure ID:

Scope: Modulate the charge drift time as a function of the applied electric field values on the semiconductor.

Rational: Use atmospheric muons that leave a straight trail on the detector. The atmospheric muons travel the whole depth of the detector, generating charge near the cathode and anode at the same instant. With the 1.6ns time resolution, measuring the difference between the charge arrival time at the cathode versus the charge arrival time at the anode one can modulate the charge drift velocity. See Figure 3.34.

Procedure Summary: Let the detector collect data over night.

Results: This test was conceptualized and preliminary verified. For a detected muon event on the ^{133}Ba spectrum, Figure 4.17, with a bias voltage of -500V the electron drift time measured was $t_{drift} = 44.75\text{ns}$.

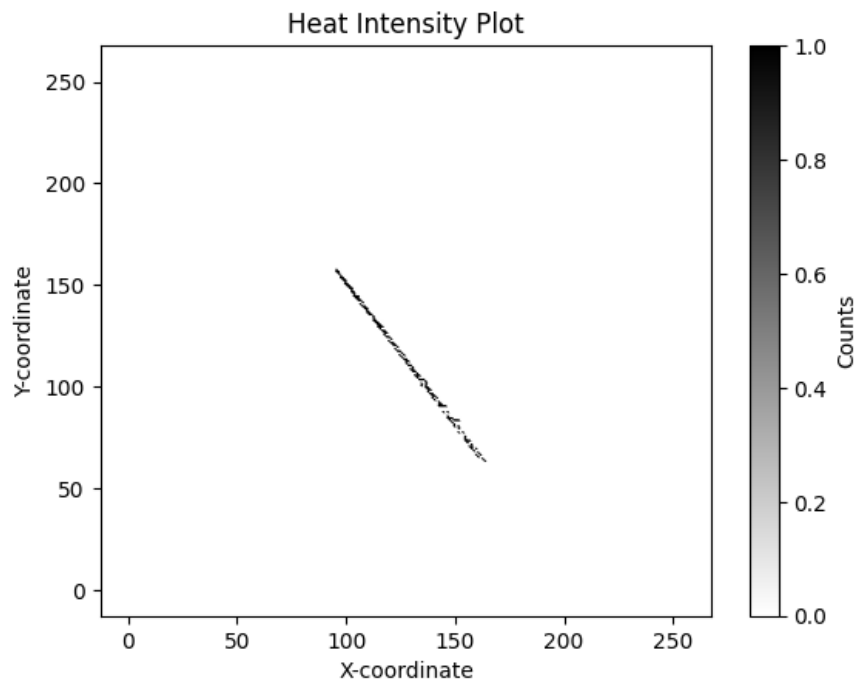


Figure 4.17: Muon captured, CdTe polarized with -500V. Electron charge drift time $t_{drift} = 44.75\text{ns}$.

4.3.2.9 TEST_DET_010 - Compton Electron

Test Procedure ID:

Scope: Measure the scattering angle of the electron on the first Compton interaction.

Rational: With the determination of the scattering angle of the photon it is possible to determine the incoming photon polarization. This property decreases the statistics required to perform polarimetry. Both planar scattering distribution of the scattered photon and the planar scattering distribution of the scattered electron can be used.

4.3.2.10 TEST_DET_011 - Incident Angle Efficiency

Test Procedure ID:

Scope: Study the effect of photons attack angle on the detection efficiency and energy resolution of the detector. The set-up available in the LIP-Coimbra laboratory is presented in the Figure 4.18.

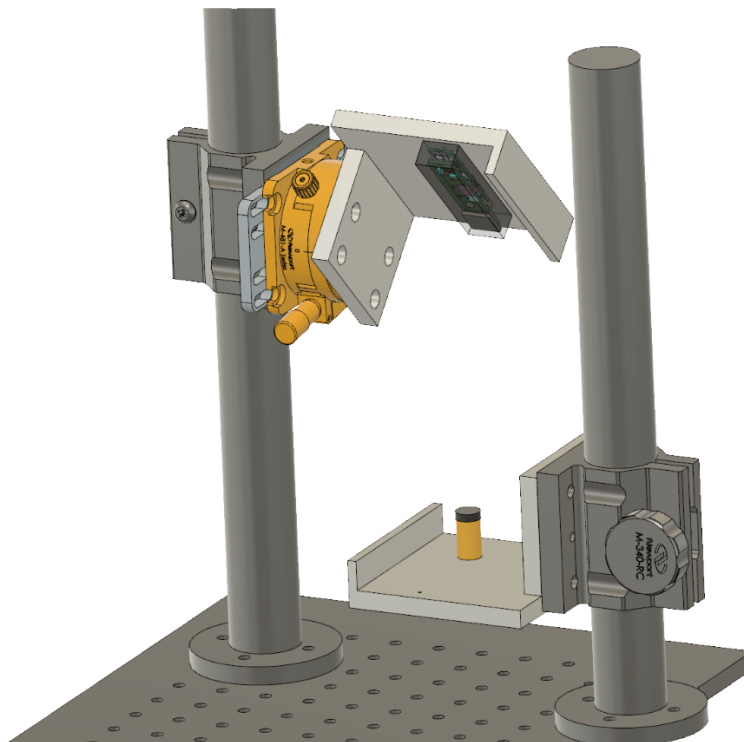


Figure 4.18: Set-up available in the LAB.

4.3.2.11 TEST_DET_013 - Bias Voltage

Test Procedure ID:

Scope: Test the impact of different detector bias voltages on the: a) Detection efficiency, b) Energy resolution, c) Peak shift.

4.3.3 PDU Tests

4.3.3.1 TEST_PDU_001 - First Stage

Test Procedure ID:

Scope: To validate the technology up to a TRL4.

Rational: At this stage the PDU concept is expected to be fully elaborated. Prior testing the performance shall be demonstrated through analysis supported by previous experience. To achieve TRL4 level the PDU shall demonstrate the compliance of functional requirements in laboratory environment, $T=25^{\circ}\text{C}$, $P=1\text{atm}$.

Results: Yet to be performed.

4.3.3.2 TEST_PDU_002 - LIP Vaccum

Test Procedure ID:

Scope: Test the PDU design and components on an environment that the FM will encounter in flight, TRL5.

Rational: To be tested on a LIP vacuum chamber. Place extra temperature sensors in critical components and record their behaviour. Tests every function of the PDU. The electrical connector to the LIP Vaccum chamber will have to have interface SPI (4 pins), +28V, GND (2 pins), I2c for extra TMPs (2 pins): Total 8 pins.

4.3.3.3 TEST_POLLUX_PDU_003 - Pollux Balloon Flight

Test Procedure ID:

Scope: Test the PDU design on an environment that the FM will experience in flight, TRL6.

Rational: To be integrated on the Pollux stratospheric balloon. Will be tested up to an altitude of 25km, vacuum and low temperatures. Either use Balloon OBC or OBC_DM.2 to verify the operations of the PDU in flight. Place extra temperature sensors on critical components such as the DC-DC to calibrate the temperature sensors present on the board.

Chapter 5

Conclusions

With the objective to fully define the THOR payload configuration, operations, scientific capabilities and test plan, this dissertation presents a comprehensive summary of the major design conclusions of the development of THOR up to the PDR. Building upon the current design, the THOR team should explore in more detail each and every topic discussed on this dissertation in order to improve the THOR design and achieve its scientific objectives.

Along the dissertation, we defined the core scientific objectives and created achievable observation requirements that allow the detectors to have enough statistics to characterize terrestrial and cosmic gamma-ray sources of interest. At this stage a total of 18 days of deep sky observation are required to characterize steady gamma-ray sources, e.g. AGN's. During this time the payload will also be searching for transient events like GRB. From the 18 days of deep sky observation, 5 are dedicated to observe the Crab Nebula to calibrate the detectors on orbit as well as to perform spectroscopic, imaging, time variability and polarization measurements. Also in order to observe TGF, it was imposed to the SR team an observational time of 7 days of the Earth atmosphere.

Simulations of the expected gamma-ray and particle fluxes showcased that the payload would generate a total of 628 MBytes/day of scientific data. It was therefore identified the need to have a real time particle identification algorithm on the OBC to distinguish proton/heavy ion events from electron/photon events. Doing this, the payload would generate 341 MBytes/day of scientific data to be downloaded to the LIP-GS (only electron/photon events). Although not yet compliant with the 300MBytes/day requirement imposed by the SR team, the 50% margin applied on the gamma-ray/particle fluxes and the 25% margin applied to the total scientific data budget make this estimation as the worst case scenario. Also, a more detailed simulation scenario is paramount to have a more realistic value, taking into account: 1) the effective area of the detectors; 2) the flux distribution over the particle energies; 3) observation scenarios (SR pointing); 4) Space Rider and other P/L material attenuation. The [Cumani et al., 2019] work should be taken as a reference. The primary

objective of simulating the orbital particle and photon fluxes was to estimate the data generated by the THOR detector system but throughout this study it was noticed that it will be difficult to differentiate events related to low energy electrons from events generated by photons. This will be particularly challenging for the post data processing where one will need to rely on background data rate from similar missions.

The current design of the THOR payload is not compliant with the SR base plate interface, which offers a 58mm x 56mm M6 hole matrix for payloads to secure themselves. Specifically, the 210mm and 275mm spaced M6 holes on the THOR enclosure don't match this base plate interface. Also, the current design of the THOR enclosure has an excessive mass of 3.7kg, which by itself is not compliant with the 3kg total payload mass. Several design changes were discussed with AST in order to mitigate these problems. By rearranging the product distribution within the available volume of the payload we foresee lowering the dimensions of the payload to 232mm x 232mm. The redesign of the TBD detectors' PCB boards will also contribute to the optimization of the available volume. Also by thinning unnecessary enclosure edges, we foresee a cut on the enclosure mass. In case these modifications reveal to have little impact on the overall mass of the payload, possible modifications on the PDU have been identified, e.g. remove redundant components, and a possible change of the OBC that might reduce the overall weight by 300g - 350g. Also, it is important to verify with the SR team and PTSpace margins for the 3kg requirement.

Regarding the design of the PDU, at this stage, the functions to be performed by the unit are already identified and the main components to carry out said function are already selected. Some design changes are yet to be done, for example the interface between the ON/OFF of the DC/DC converters and the I/O expander, where adding a transistor switch, fed from the 12V output of the 12V DCDC and controlled by the I/O expander, should mitigate the incompatibility problem. Also, the fact that the operability of the housekeeping sensors is dependent on the status of the DC/DC that feeds the PAR detectors is not ideal, since when the P/L is in housekeeping mode, the housekeeping sensors of the PDU are turned OFF. For instances, adding a transistor switch to control, via I/O expander, the ON/OFF of the 5V output to the PAR would solve the problem, allowing the 5V DC/DC to be ON all the time, whilst maintaining the function to turn ON/OFF the PAR. The development philosophy outlined allows for the test and identification of similar problems on the future development of the PDU. By developing an increasingly more detailed model and subjecting it to environmental conditions that the unit will encounter in space, the development philosophy is designed in a way that for each new development model subtle design changes can be implemented while maintaining the verification lessons from previous development models.

The development plan outlined in Chapter 4 ensures that products can be developed in

parallel. By having the first development model of the detector unit prior to PDR allowed us to plan and perform several verification and performance tests that showcased the detectors' capabilities which refined the definition of the functions to be performed by the OBC on orbit. Also the hands-on work with the detectors' scientific data gave us insight on how it transmits the data and how the data can be managed by the OBC. Not to forget, it also allowed us to understand the technology of the detector, i.e the 3D particle tracking capabilities, which will come in handy for the IA algorithm, as it adds an extra parameter to input into the neural network decision tree. Finally, from the tests already performed, we were able to outline detailed procedures for the characterization tests to be performed on the detector unit flight model.

References

- [Aartsen et al., 2018] Aartsen, M. G. et al. (2018). Neutrino emission from the direction of the blazar TXS 0506+056 prior to the IceCube-170922a alert. *Science*, 361:147–151. 21
- [Abbott et al., 2016] Abbott, B. P. et al. (2016). Observation of gravitational waves from a binary black hole merger. *Physical review letters*, 116(6):061102. 1, 21
- [Abbott et al., 2017] Abbott, B. P. et al. (2017). Multi-messenger observations of a binary neutron star merger*. *The Astrophysical Journal Letters*, 848(2):L12. 1
- [ALTEC, 2021] ALTEC (09/09/2021). SRS ground segment architecture - powerpoint presentation. 34
- [Angelis and Mallamaci, 2018] Angelis, A. D. and Mallamaci, M. (2018). Gamma-ray astrophysics. *European Physical Journal Plus*, 133. 8
- [Armano et al., 2015] Armano, M. et al. (2015). The LISA pathfinder mission. volume 610. Institute of Physics Publishing. 21
- [Baring et al., 2019] Baring, M. G. et al. (2019). X-ray and gamma-ray polarimetry. *Astro 2010 White Paper*. 1
- [Barthelmy et al., 2005] Barthelmy, S. D. et al. (2005). The burst alert telescope (BAT) on the SWIFT midex mission. *Space Science Reviews*, 120:143–164. 155
- [Bé et al., 2016] Bé, M.-M., Chisté, V., Dulieu, C., Kellett, M., Mougeot, X., Arinc, A., Chechev, V., Kuzmenko, N., Kibédi, T., Luca, A., and Nichols, A. (2016). Table of radionuclides. 8. xxiv, 129
- [Bellazzini and Muleri, 2010] Bellazzini, R. and Muleri, F. (2010). X-ray polarimetry: A new window on the high energy sky. *Nuclear Instruments and Methods in Physics Research Section A: Accelerators, Spectrometers, Detectors and Associated Equipment*, 623(2):766–770. 1rs International Conference on Frontiers in Diagnostics Technologies. 1

- [Berger1 et al., 2017] Berger1, M. et al. (2017). Stopping-power range tables for electrons, protons, and helium ions NIST standard reference database 124. 100
- [Branchesi, 2016] Branchesi, M. (2016). Multi-messenger astronomy: Gravitational waves, neutrinos, photons, and cosmic rays. volume 718. Institute of Physics Publishing. 6, 7
- [Brezin et al., 2014] Brezin, C. et al. (2014). The timepix3 chip: on behalf of the medipix3 collaboration. *tech. rep.* 64
- [Burns et al., 2019] Burns, E. et al. (2019). Gamma rays and gravitational waves. 7
- [Caroli et al., 2018] Caroli, E. et al. (2018). Hard x-ray and soft gamma ray polarimetry with CdTe/CZT spectro-imager. *Galaxies*, 6. 15
- [Cree and Bones, 1994] Cree, M. J. and Bones, P. J. (June 1994). Towards direct reconstruction from a gamma camera based on compton scattering. *IEE Transaction on Medical Imaging*, 13:398–407. 61
- [Creminelli and Vernizzi, 2017] Creminelli, P. and Vernizzi, F. (2017). Dark energy after GW170817 and GRB170817a. *Phys. Rev. Lett.*, 119:251302. 1
- [Cumani et al., 2019] Cumani, P. et al. (2019). Background for a gamma-ray satellite on a low-earth orbit. *Springer Nature Experimental Astronomy*. 87, 141
- [ESA, 2021] ESA (09/09/2021). ESA-STC-SR-TN-2018-002 user guide for the space rider re-usable free flyer platform. 33, 35
- [Filipenko et al., 2014] Filipenko, M. et al. (2014). 3D particle track reconstruction in a single layer cadmium-telluride hybrid active pixel detector. *Eur. Phys. J. C* 74, 3013. 66
- [Heynderickx et al., 1999] Heynderickx, D., Kruglanski, M., Pierrard, V., Lemaire, J., Looper, M., and Blake, J. (1999). A low altitude trapped proton model for solar minimum conditions based on sampex/pet data. *IEEE Transactions on Nuclear Science*, 46(6):1475–1480. 92
- [Hiemstra et al., 2020] Hiemstra, D. M. et al. (2020). Single event effect evaluation of the Jetson AGX Xavier module using proton irradiation. *IEEE Radiation Effects Data Workshop*. 71, 72
- [Hirata et al., 1987] Hirata, K. et al. (1987). Observation of a neutrino burst from the supernova SN1987A. *Phys. Rev. Lett.*, 58:1490–1493. 20
- [Hulsman et al., 2021] Hulsman, J. et al. (2021). POLAR-2: A large scale gamma-ray polarimeter for GRBs. *arXiv*. 20

- [Janka et al., 2007] Janka, H. T., , et al. (2007). Theory of core-collapse supernovae. *Physics Reports*, 442:38–74. 6
- [Kampert et al., 2019] Kampert, K. H. et al. (2019). Multi-messenger physics with the pierre auger observatory. *Frontiers in Astronomy and Space Sciences*, 6. 21
- [Knoll, 2010] Knoll, G. F. (2010). *Radiation Detection and Measurement, 4th Ed.* John Wiley Sons, Inc.. New York, NY, USA. 7, 11, 65, 100, 101, 136
- [Kole, 2018] Kole, M. (2018). Polarimetry with POLAR. 2, 19
- [Kole et al., 2022] Kole, M. et al. (2022). Adding gamma-ray polarimetry to the multi-messenger era. 6, 8, 13, 20
- [Kosmidis et al., 2021] Kosmidis, L. et al. (2021). GPU4S: Embedded GPUs in space latest project updates. 71
- [Kosmidis et al., 2022] Kosmidis, L. et al. (2022). GPU4S (GPUS for space): Are we there yet? 71
- [Kruglansky et al., 2009] Kruglansky, M. et al. (2009). Last upgrades and development of the space environment information system (spenvis). *European Conference on Radiation and Its Effects on Components and Systems*. 87
- [Lei et al., 1997] Lei, F. et al. (1997). Compton polarimetry in gamma-ray astronomy. *Space Science Reviews*. 1, 154
- [Macfadyen and Woosley, 1999] Macfadyen, A. I. and Woosley, S. E. (1999). Collapsars : Gamma-ray bursts and explosions in ”” failed supernovae II. *THE ASTROPHYSICAL JOURNAL*, 524:262–289. 6
- [McEnery et al., 2012] McEnery, J. E. et al. (2012). Fermi gamma-ray space telescope. *Optical Engineering*, 51:011012. 19
- [Moita et al., 2019] Moita, M., Caroli, E., Maia, J., Curado da Silva, R., Auricchio, N., Stephen, J., Páscoa, M., and Trindade, A. (2019). Compton polarimetry with a multi-layer cdte focal plane prototype. *Nuclear Instruments and Methods in Physics Research Section A: Accelerators, Spectrometers, Detectors and Associated Equipment*, 918:93–98. 61
- [Moita et al., 2020] Moita, M., Ferro, L., Caroli, E., Virgilli, E., Curado da Silva, R. M., Auricchio, N., del Sordo, S., Maia, J. M., and Stephen, J. B. (2020). A monte carlo study of a 3d czt spectroscopic imager for scattering polarimetry. In *2020 IEEE Nuclear Science Symposium and Medical Imaging Conference (NSS/MIC)*, pages 1–6. 61

- [Moita, 2019] Moita, M. F. (2019). Polarimeter development for future space gamma-ray telescopes. Tese de doutoramento em engenharia física, ramo de instrumentação, Universidade de Coimbra - Faculdade de Ciências e Tecnologia. 14, 15, 61
- [Murase and Bartos, 2019] Murase, K. and Bartos, I. (2019). High-energy multimessenger transient astrophysics. 5, 6, 7, 21
- [Mészáros et al., 2019] Mészáros, P. et al. (2019). Multi-messenger astrophysics. *Nature Reviews Physics*, 1:585–599. 1, 20
- [Petrovay, 2020] Petrovay, K. (2020). Solar cycle prediction. *Living Reviews in Solar Physics*. 87
- [Sousa, 2023] Sousa, J. (2023). THOR_T_SOFT_DH_003. *THOR-SR internal document*. 96
- [Tavani et al., 2011] Tavani, M. et al. (2011). Discovery of powerful gamma-ray flares from the crab nebula. *Science*, 331:736–739. 6
- [Toma et al., 2009] Toma, K. et al. (2009). Statistical properties of gamma-ray burst polarization. *Astrophysical Journal*, 698:1042–1053. 13
- [Turecek et al., 2018] Turecek, D. et al. (2018). Compton camera based on timepix3 technology. *JINST*. 61
- [Turecek et al., 2020] Turecek, D. et al. (2020). Single layer compton camera based on timepix3 technology. *JINST*. 67
- [Winkler, 1998] Winkler, C. (1998). INTEGRAL: the international gamma-ray astrophysics laboratory. 17
- [W.R.Leo, 1994] W.R.Leo (1994). *Techniques for Nuclear and Particle Physics Experiments, 2nd Ed.* Springer-Verlag, Berlin, Germany. 7, 8

Appendix A

Function Description

A.1 Scientific Data Collection - THOR_F_SCI

The purpose of the THOR_F_SCI (Scientific Data Collection) is to gather data representative of physics events that enable the mission to achieve its scientific objectives, specifically the detection of photons and orbital particles. To ensure comprehensive and accurate data collection, THOR_F_SCI is divided into two main sub-functions: Gamma-ray event detection (THOR_F_SCI.G) and Particle event detection (THOR_F_SCI.P). This functions relies on the do acquisition function already integrated on the detector's API.

THOR_F_SCI.G - The THOR_F_SCI.G sub-function is related to the data generated by a physics event coming from the GAM array. The main objective of this array is to detect gamma-ray events within an energy range of 100 keV to 1 MeV. The GAM is also going to generate data related to particle events. This sub-function ensures that the payload is receiving data from the GAM array. For every activated pixel, the THOR_F_SCI.G sub-function provides the following data:

Inputs:

1. Electrical Interface USBx_GAMx

Outputs (Raw data):

- a) Matrix ID - 13 bit;
- b) Pixel ID - 24 bit;
- c) Energy deposited of the interaction (ToT) - 18 bit;
- d) Time of arrival of the gamma-ray photon (ToA+FToA) - 34 bit.

This function relies on the DO ACQUISITION function already integrated on the detector's API. Further data processing is needed to differentiate between data from particle events and gamma-ray events.

THOR_F_SCI.P - The THOR_F_SCI.P sub-function is related to the data generated by a physics event coming from the PAR array. The main objective of this array is to detect particle events, namely protons and electrons. This sub-function ensures that the payload is receiving data from the PAR array. For every activated pixel, the THOR_F_SCI.P sub-function provides the following data:

Inputs:

1. Electrical Interface USBx.GAMx

Outputs (Raw data):

- a) Matrix ID - 13 bit
- b) Pixel ID - 24 bit;
- c) Energy deposited of the interaction (ToT) - 18 bit;
- d) Time of arrival of the gamma-ray photon (ToA+FToA) - 34 bit

This function relies on the DO ACQUISITION function already integrated on the detector's API. It is important to note that this function does not group the total activated pixels by A particle interaction. Instead, the THOR_F_SCI.P function ensures that if a particle interacts with the detector the detector outputs the ToT and ToA+FToA of every single activated pixel. Further processing is needed to understand the 'track' of each particle and therefore group the activated pixels by physics event.

THOR_F_SCI.CAL - The THOR_F_SCI.CAL sub-function is related to the transformation of the ToT value to keV. This calculation is done in three steps:

1. **Factory Calibration:** The factory calibration is done at the pixel level. For each pixel there are a combination of 4 parameters a, b, c, t that allows us to transform the ToT into keV value.

$$E[\text{keV}] = \frac{ta - b + \text{ToT}}{2a} + \sqrt{\left(\frac{ta - b + \text{ToT}}{2a}\right)^2 - \frac{t(\text{ToT} - b) - c}{a}} \quad (\text{A.1})$$

Yet this calibration revealed to be insufficient.

Inputs:

- (a) THOR_F_SCI.G or THOR_F_SCI.P

(b) a, b, c, t calibration matrices

Outputs:

(a) Energy (keV) - 18 bits.

2. **Spectrum Calibration:** This calibration will be used after the event identification. Upon identifying an event and corresponding energy (calibrated in 1)., this step then re-calibrates the overall energy of the event by summing the energy (keV) deposited on every pixel. The re-calibration curve is the output from the TEST_DET_001.

Inputs:

(a) THOR_F_SCI.CAL-1

Outputs:

(a) Energy (keV) - 18 bits.

3. **Temperature Calibration:** The detector energy response has a temperature dependency. The temperature of reference comes from the CdTe semiconductor that can be read via the detectors' API. This step is to be used right after spectrum calibration (sub-function 2).

Inputs:

(a) THOR_F_SCI.CAL-2

(b) Matrix ID Temperature

Outputs:

(a) Energy (keV) - 18 bits.

The factory per-pixel calibration using the calibration parameter's a, b, c and t its not enough to give precise values of event energy for energies above 100keV, since ADV only uses 3 energy values to perform the calibration.

A.2 Data Processing - THOR_F_DP

THOR_F_DP.DC - This function analyses the Raw data, the outputs of the THOR_F_SCI.G and THOR_F_SCI.P, and characterizes the type of physics event. It distinguishes between different types of interactions, proton/heavy ion events from photon/electron events. Single photon events can be taken for electron events (due to the nature of the interaction), therefore the electron events and single photon events are characterized as the same event type. They will be referenced as Single Events. Since a physics event can activate more than one pixel, this function shall identify the cluster of activated pixels and relate it to a physics event. This function is divided into different steps:

1. **Identify that the data corresponds to an event:** every activated pixel with a ToA+FToA within a time window of $2\mu\text{s}$ (TBD) is considered an event. The algorithm shall be able to use data from the different detector planes. This step can be used as a preliminary way of identifying events.
2. **AI algorithm to identify particles and photons:** this algorithm shall give as an output the clusters of pixels that represent the physics interaction, either Compton, Single event, Proton or Heavy ion. In case the Algorithm identifies a Proton or Heavy ion the output data shall undergo step 3., in the other cases the output of this Function is outlined bellow:

Inputs:

- (a) THOR_F_SCI.G or THOR_F_SCI.P

Output:

- (a) Raw data relative to a Single event and Event type identifier - $N*89$ bits + 11 bits, where N is the number of activated pixels;
 - (b) Raw data relative to a Compton event - either double or multiple - and EVENT type identifier - $M * (N*89 \text{ bits} + 11 \text{ bits})$, where M is the multiplicity o the event and N is the number of activated pixels;
 - (c) Raw data relative to a Proton interaction and Event type identifier - $N*89$ bits + 11 bits;
 - (d) Raw data relative to a Heavy ion interaction and Event type identifier - $N*89$ bits + 11 bits.
3. **Proton and Heavy ion processing:** the main purpose of this step is to reduce the amount of data generated by proton and heavy ion interactions. For each interaction this step characterizes the event by means of 5 parameters, First hit pixel, Energy deposited, n° of activated pixels and particle attack direction (azimuthal angle ϕ , orthogonal angle θ).

Inputs:

- (a) THOR_F_DP.DC-2.c
- (b) THOR_F_DP.DC-2.d

Output for each physics event:

- (a) Hit pixel - 24 bits;
- (b) Energy (Σ ToT) - 26 bits;
- (c) N° activated Pixels - 18 bits;
- (d) Theta (θ) - 16 bits;

(e) Phi (ϕ) - 16 bits.

THOR_F_DP_SL - This function uses the output from the THOR_F_DP_DC-4 as well as the THOR_F_CTR_MMU-h data to perform the source localization on the Galactic Coordinate System. This function relies on Compton Scattering kinematics, Equation 2.2 to assess the possible localization zones of the incoming gamma-rays. This function is divided into different steps:

1. **Select Compton events:** The function reads the output from the THOR_F_DP_DC-2.b and selects only the double events, denominated by D (number of double events). To verify whether the events are real Compton Events the function inputs the data into the Compton Equation 2.2. In case a Compton event is between planes, this process is straight forward and the Compton events acknowledged pass to the step 3. For Compton events within the same detector plane they need to go to the step 2 first.

Inputs:

(a) THOR_F_DP_DC-4

Output of every double event:

- (a) Compton Event ID -
- (b) Hit matrix - $2 * D * 13$ bits;
- (c) Hit pixel - $2 * D * 24$ bits;
- (d) Energy (keV) - $2 * D * 18$ bits;
- (e) ToA+FToA - $2 * D * 34$ bits.

2. **Photon pixel depth determination:** In case the Compton event happens within one detector plane this step is going to determine the Z depth difference between the 2 absorbed photons. It will take into account the bias voltage applied to the detector when the interaction occurred to modulate the internal electric field inside the detector. Comparing the ToA+FToA (resolution of 1.6ns) it is possible to determine the Z depth difference between events and thus determine the photon scattering angle. The events that verify the Compton scattering equation are submitted to the next step.
3. **Compton Cone Determination:** For every Compton event a possible incoming direction cone, with aperture equal to the photon scattering angle θ with its vortex on the straight line that unites the two points where the photons were detected, is created. The surfaces of this constructed cones represent the possible positions of the gamma-ray source. This cone must be represented as a reference to the SR coordinate system.

4. **Reference Normalization:** This step takes the data from the THOR_F_CTR.MMU and makes the coordinate transformation of the cones to the Galactic Coordinate System.
5. **Cone Intersection:** With Compton reconstructed cones referred to the Galactic Coordinate System, this step finds the intersection between the cumulative Compton events and flags potential gamma-ray sources.
6. **Direct Source Localization:** If the SR attitude data shows that the SR is pointed to: Crab Nebula, Sun, Earth - this function shall subtract the background gamma-ray measured in previous orbit, THOR_F_DP.SPEC.2, from the data and assume that the events registered are from the source the SR was pointed to. The function will add a label to the detected gamma-ray events relating them to said source.

THOR_F_DP.PLZ - This function is responsible for calculating the polarization properties of the incoming detected gamma-ray photons. Polarimetry provides valuable information about the emission mechanisms, source geometry, and magnetic field environment of astrophysical objects. Polarization assessments requires cumulative measurements of a gamma-ray source. The THOR_F_DP.PLZ function utilizes the processed data from THOR_F_DP.SL. The function picks a certain gamma-ray source (GRB, Crab Nebula, TGF) and calculates the polarimetric characteristics of the gamma-ray source. This function is divided into different steps:

1. **Polarization Parameters Identification:** From the output of THOR_F_DP.SL this step takes into account only double Compton events. For each Compton event the photon's polar (θ) and azimuthal (η) scattering angles are calculated.
2. **PA Calculation:** The relation of η and Electric field direction of the incoming gamma-ray will lead to an asymmetry in the number of photons scattered in directions parallel and orthogonal to the electric field vector [Lei et al., 1997]. This will create a pattern of activated pixels at the GAM and the preferred direction of the η gives the polarization angle (PA) of the Source.
3. **PD Calculation:** Following the same rationale as the previous step, the polarization degree (PD) is the fraction of photons used to determine the PA over the photons with no polarization information.
4. **Polarization Confidence Estimation:** The function estimates the uncertainties and confidence levels associated with the calculated polarization angles and degrees.

THOR.F_DP.SPEC - This function is responsible for analyzing the energy distribution of the incoming detected gamma-ray photons or particles. Spectroscopy plays a crucial role in understanding various phenomena, such as emission mechanisms, source composition, and physical processes occurring in astrophysical objects. The THOR.F_DP.SPEC can be called to make spectra analysis of different Gamma-ray sources such as: GRB, TGF, Background, Solar Flare, Crab Nebula and other - as well as analysing the in orbit particle spectra: electrons and protons. The function performs the following tasks:

1. **Energy Calibration:** If this function is called to perform the Spectroscopic analysis of the Crab Nebula the function compares the energy read by the detectors and compares it with the expected values. If results are within an acceptable margin there is no need to calibrate the detector. Otherwise, the detector shall be calibrated with new parameter values. If the function is called to perform Spectroscopic analysis of any other Source ID, this step can be ignored.
2. **Background Spectral Analysis:** The background of gamma-rays may vary by more than a factor of two over the 90 min orbit and therefore the OBC shall be monitoring the gamma background environment every 100s [Barthelmy et al., 2005] and register the mean amount of counts and spectra for every 100s section of orbit.
3. **Source ID Spectral Analysis:** This Step uses the output from the THOR.F_DP.SL to make a spectral image of the Source. If it is a continuous source the function can update the new data over the existing one. This involves counting the number of photon events within predefined energy bins (TBD) and normalizing the results to obtain the differential photon flux as a function of energy.
4. **Electron Spectral Analysis:** The function extracts the energy spectra of the detected electrons by constructing a histogram of the calculated initial energy of the electron. This involves counting the number of electron events within predefined energy bins and normalizing the results to obtain the differential electron flux as a function of energy. Also taking into account the SR attitude data, this function can allocate the electron flux and energy distribution to a precise spot in the orbit.
5. **Proton Spectral Analysis:** The function extracts the energy spectra of the detected protons by constructing a histogram of the calculated initial energy of the proton. This involves counting the number of proton events within predefined energy bins and normalizing the results to obtain the differential proton flux as a function of energy. Also taking into account the SR attitude data this function

can allocate the electron flux and energy distribution to a precise spot in the orbit.

THOR_F_DP.GRB - Its primary purpose is to detect Gamma-Ray Burst (GRB) events in the collected pre-processed data. GRBs are extremely energetic and brief flashes of gamma rays that originate from distant cosmic sources. The THOR_F_DP.GRB function processes the data generated by the THOR_F_DP.DC sub-function. The GRB identification function performs the following tasks:

1. **Temporal Analysis:** The function analyzes the time of arrival information from the characterized photon events to search for sudden and brief increases in gamma-ray count rates, which may be indicative of GRB events. It is important to take into account the background event rate 100s prior to the analysed data portion size. The function shall perform an analysis of burst durations between 4ms and 32s. For easier GRB identification, every 64s time interval the OBC shall perform a FFT to check for sudden peaks.
2. **GRB Spectra Analysis:** The function calls the THOR_F_DP.SPEC.3 giving it the data related to the identified GRB.
3. **PA and PD Analysis:** The function calls the THOR_F_DP.PLZ.2 and THOR_F_DP.PLZ.3 to calculate the polarization characteristics of the GRB. If the GRB is long and strong enough (TBD counts/s, time) this function will perform the same PD and PA analysis for specific energy bins (100KeV intervals - TBD).

THOR_F_DP.TGF - Its primary purpose is to detect TGF events in the collected pre-processed data. TGF's are high-energy photons emitted by thunderclouds due to the interaction of cosmic rays with the cloud's electric field. The THOR_F_DP.TGF function processes the data generated by the THOR_F_DP.DC sub-function. The TGF identification function performs the following tasks:

1. **Temporal Analysis:** The function analyzes the time of arrival information from the characterized photon events to search for sudden and brief increases in gamma-ray count rates, which are indicative of TGF events. Threshold (count/s) = TBD

A.3 Data Storage - THOR_F_DS

Different outputs from the functions described above have different data structure when stored in memory.

THOR.F_DS.ID - This function is responsible for correctly identifying and labeling the different types of data. There are three different types of ID's that are attributed to the Data.



Figure A.1: This is the ID data format for the Physics Event data.

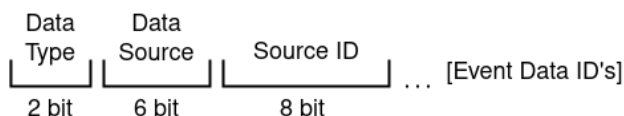


Figure A.2: This is the ID data format for the Source event data.



Figure A.3: This is the Id data format for the Analysis data.

1. **Data Type:** If the data is Housekeeping data or Science. It is a 2 bit header.

| Data Type | Bit Code |
|-------------------|----------|
| Science (SCI) | 11 |
| Housekeeping (HK) | 00 |

Table A.1: Data type identifier.

2. **Data Source:** This ID is a 6 bit header that specifies the source the data came from. Each data source has its own data structure. See Section for a detailed view on the data structure for every data source.

| Data Source | Bit code |
|----------------|----------|
| THOR.F_DP.DC | 100100 |
| THOR.F_DP.SL | 010010 |
| THOR.F_DP.PLZ | 001001 |
| THOR.F_DP.SPEC | 110110 |
| THOR.F_DP.GRB | 011011 |
| THOR.F_DP.TGF | 111111 |
| THOR.F_DP.SF | 000000 |

Table A.2: Data source identifier.

3. **Event Type:** This identifier attributes an 11 bit header to the data from each type of Physics event to distinguish from SINGLE EVENT, COMPTON EVENT AND MULTIPLICITY, PROTON EVENT and HEAVY ION EVENT.

| Event Type | Bit Code |
|------------------------|-------------|
| Single Event | 00000100100 |
| Double Compton Event | 00000110110 |
| Multiple Compton Event | 00000101101 |
| Proton Event | 00000111111 |
| Heavy Ion Event | 00000110111 |

Table A.3: Event type identifier.

4. **Event Index:** At the PDR level all the Physics events identified by the function THOR_F_DP.DC are sequential, from 0 to 2^{40} . This is a 40bit header for each sequential physics event. This index is resets every 24h.
5. **Source ID:** The mission is going to identify different gamma-ray sources which are the products of the following functions: THOR_F_DP.SL, THOR_F_DP.GRB, THOR_F_DP.TGF and THOR_F_DP.SF. Each data source is going to be stored in a different memory directory. For each source an incremental 8 bit index is going to be attributed as an identifier.
6. **Timestamp ID:** Each timestamp has an associated ID. The ID is composed by the first and last Physics Event ID's. The timestamp is a 42bit value.

THOR_F_DS.TS - This function is responsible for assigning time stamps according to the SR time synchronization clock. The THOR_F_DS.TS adds the synchronized time stamp to the events produced by THOR_F_DP. It performs the following tasks:

1. **Acquisition Timestamp:** When the OBC starts an acquisition, this function gives a timestamp at the beginning and end of the acquisition time that can be later used to convert the ToA+FToA to a time scale that has the SR clock as reference.

THOR_F_DS.MMU - This function is responsible for organizing and storing data in the OBC_MMU. At PDR level the development of this function is not critical. However it is critical to ensure that the OBC_MMU has the capacity to save all the Scientific data taken during the flight.

A.4 Power Distribution - THOR_F_PDU

THOR_F_PDU.S - This function executes the need to transform the unregulated 28V supplied by the SR system to the required voltage levels of THOR products and sub-products. It is important to take into account not only the voltage level but also the current for the daughter product/sub-product to operate.

1. **Gamma-Tracker Array** The Gamma-tracker array power supply has to be compliant with the voltage levels presented on REQ-174, 12V for each RO board - 4x 12V outputs in total. Also, each DP consumes up to 10W and therefore the Gamma-tracker Array power supply shall handle 40W of total power supply.
2. **Particle Detector Array** The Particle Detector array power supply shall be compliant with the voltage levels presented on REQ-193, 5V for each board - 2x 5V outputs in total. Also, each board consumes up to 2W and therefore the Particle Detector Array power supply shall handle 4W of total power supply.
3. **Onboard Computer** The Onboard Computer power supply shall be compliant with the voltage levels presented on REQ-091. Although the OBC operations are limited to 10W, a 25W power supply shall be used in case it is required more intense calculations on orbit.

THOR_F_PDU.OC - This function is responsible to provide a fault protection system to the upstream components on the power distribution tree, in order not to be affected if an electrical malfunction happens on a product (ie: short circuit).

THOR_F_PDU.PWR - This function ensures an implementation of a power monitoring system to every major power interface on THOR.

A.5 Control - THOR_F_CTR

THOR_F_CTR.OO - This function is responsible to switch ON/OFF the detectors. This function shall obey the design architecture of the PDU and manage the ON/OFF state of the DC-DC converts that feed the detectors. Taking into account the current design of the PDU - PDR see section about the PDU design - this function can be called in three different ways.

1. **OFF GAM_DP12:** Using this sub-function the OBC sends the command to the THOR_PDU_OC, via SPI, to turn off the THOR_PDU_DCDC_GAM.12.A and THOR_PDU_DCDC_GAM.12.B.

2. **OFF GAM_DP34:** Using this sub-function the OBC sends the command to the THOR_PDU_OC, via SPI, to turn off the THOR_PDU_DCDC_GAM.34.C and THOR_PDU_DCDC_GAM.34.D.
3. **OFF PAR:** Using this sub-function the OBC sends the command to the THOR_PDU_OC, via SPI, to turn off the THOR_PDU_DCDC_PAR.A and THOR_PDU_DCDC_

To turn off all of the THOR_DET, the OBC just needs to use all of the commands above described.

THOR_F_CTR.HK - This function is responsible for the handling of housekeeping data of the payload components. In case the values read measure 15% above or below the threshold value for more than 10 (TBD) consecutive measurements the OBC shall interpret it as an issue and act upon it. The available housekeeping data is presented bellow:

1. **Detector Unit:** Applied to either the GAM and PAR.
 - (a) FB.x Temperature: The temperature can be read in the FB ASIC using the detector API.
 Min Threshold = 0°C
 Máx threshold = 50°C
 - (b) RO.x Temperature: The temperature of the RO CPU via the detector API.
 Min Threshold = -10°C
 Máx threshold = 50°C
 - (c) FB.x Bias voltage: The applied bias voltage to the semiconductor can be read via the detector API.
 Min Threshold = TBD V
 Máx threshold = TBD V
 - (d) FB.x leakage current: The applied bias voltage to the semiconductor can be read via the detector API. Leakage current varies with the FB temperature.
 Min Threshold = TBD μA
 Máx threshold = TBD μA
 - (e) FB.x dead pixels: The pixel ID of a masked pixel can be accessed via the detector API. The OBC can mask noisy pixels.
2. **PDU:**
 - (a) ON/OFF outputs: The DC-DC converters present in the PDU can be controlled via SPI. The ON/OFF state of each DC-DC is dependent on the

current operation mode of the P/L. Also, the state of the DC-DC also depends on the current monitor value of the outputs, and in case a misbehaviour is detected, the OBC shall turn off the respective DC-DC.

- (b) DCDC_XXX temperature monitor: Each DC-DC has designated temperature sensors that communicates via SPI. The sensor requires pre-flight calibration. The calibration can vary between sensors.

Min Threshold = TBD°C

Máx threshold = TBD°C

- (c) VS_GAMx Current Monitor: The PDU has a 12 bit current sensors on each voltage supply to the GAM. The nominal current value is dependent on the operation mode of THOR.

Observational = 0.5 A

Housekeeping = 0 A

Wake-up procedure = 0.5A

- (d) VS_PARx Current Monitor: The PDU has a 12 bit current sensor on each voltage supply to the PAR. The nominal current value is dependent on the operation mode of THOR.

Observational = 0.4 A

Housekeeping = 0A

Wake-up procedure = 0.4 A

- (e) VS_OBC Current Monitor: The PDU has a 12 bit current sensor on each voltage supply to the OBC. The nominal current consumption is dependent on the operations of the OBC, either scientific calculations or data reading from DET. At this stage a detailed operations plan for the OBC has not been developed.

3. OBC:

- (a) GPU temperature: Temperature of the sensor present on the GPU. To monitor and compare with the OBC power consumption to check for inconsistencies.

Min Threshold = -20°C

Máx Threshold = 80°C

- (b) CPU temperature: Temperature of the sensor present in the CPU. To monitor and compare with the OBC power consumption to check for inconsistencies.

Min Threshold = -20°C

Máx Threshold = 80°C

- (c) Operational Mode: The OBC shall record the time at which it changes the operation mode in order to notify the ground segment.

- (d) Memory availability: Manages the OBC_MMU memory availability.

THOR_F_CTR.MMU - This function represents the internal memory available on THOR. This unit shall be able to store all the scientific and housekeeping data to be processed on ground. The data recorded on the MMU shall have double redundancy and be checked frequently for single event anomalies.

1. **Single Events**: This sub function compares the content of the duplicated data distribution within the MMU. The function searches for anomalies created by single events and corrects them.
2. **Memory availability**: This function checks the amount of free memory.

THOR_F_CTR.TCS - This function checks the THOR_F_CTR.HK output to interpret the temperature of each individual component. The nominal working temperature of a component in space may deviate from the one measured in TVAC and simulated on thermal analysis. Thus the function shall adapt the nominal working temperature taking into account the products maximum working temperature advised by the manufacturer. In case a product reaches 95% of the maximum working temperature the OBC shall turn OFF the component to let it cool down to 85% of the maximum working temperature.

A.6 Hold Components - THOR_F_STR

THOR_F_STR.TD - The THOR_F_STR.TD function is responsible for optimizing thermal conductivity between various thermal interfaces within the payload. By ensuring proper thermal coupling, this function enables the components, such as detectors and electronics, to maintain optimal working temperatures.

THOR_F_STR.SC - The THOR_F_STR.SC function ensures mechanical stability of key components such as Detector Unit, OBC, and PDU throughout the mission's launch, operations, and re-entry. It optimizes the internal layout for efficient space utilization while maintaining proper detector geometry. The design also emphasizes ease of assembly, particularly for the Detector Unit, to simplify integration.

THOR_F_STR.IF - The THOR_F_STR.IF function ensures secure and precise placement of the payload in the Multi-Purpose Cargo Bay. It focuses on support plate geometry, MPBC space optimization, and ease of cable routing, aiming for mechanical stability and simplified assembly. Holding points are required to simplify assembly procedures and streamline the overall integration process with the SR vehicle.

A.7 User Operations Control - THOR_F_OP

THOR_F_OP.HK - This function ensures a 'real time' monitoring of the payload HK data on the LIP-GS to understand the health status of THOR. With this data the operator can predict

THOR_F_OP.SCI - To actively perform preliminary analysis such as, particle energy histograms as a function of the orbit, gamma-ray background characterization as a function of the orbit, source localization, GRB finder taking into account larger missions (Integral, Swift, Fermi). To check with the models that OBC is producing and create software updates to improve the on-board models.

THOR_F_OP.IFD - This function ensures a 24/7 connection via Internet with the PGCC in a way that understands the protocol either from PGCC or from the data sent by THOR flight segment.

THOR_F_OP.IFU - From the outputs of the THOR_F_OP.SCI and also from the solution to implement as response to an emergency message, this function implements the solution with the format accepted by PGCC. This function also restructures the command in a way that the OBC can implement the updates.

THOR_F_OP.DISP - To display to the LIP ground operator the HK data and scientific data .

Appendix B

List of Requirements

| | | |
|--------------------|----------------------|---------------------------|
| ID: REQ-001 | Type: Mission | Verification: T, A |
|--------------------|----------------------|---------------------------|

The experiment shall detect Photons with energy between 100keV to 1MeV.

Justification: Energy range where Compton events are predominant.

| | | |
|--------------------|----------------------|---------------------------|
| ID: REQ-002 | Type: Mission | Verification: T, A |
|--------------------|----------------------|---------------------------|

The experiment shall detect Electrons with energy between 5keV and 5MeV.

Justification: Energy of interest to study the electron flux on orbit.

| | | |
|--------------------|----------------------|--------------------------|
| ID: REQ-003 | Type: Mission | Verification: T,A |
|--------------------|----------------------|--------------------------|

The experiment shall detect Protons with energy up to 10MeV.

Justification: Energy of interest to study the proton flux on orbit as well as to study the radiation impact on THOR components.

| | | |
|--------------------|---------------------|--------------------------|
| ID: REQ-005 | Type: Design | Verification: RoD |
|--------------------|---------------------|--------------------------|

The experiment detector shall be of Cadmium Telluride (CdTe).

Justification: Due to high Z, high pixelization potencial, low volume.

ID: REQ-006 **Type:** Design **Verification:** RoD

The CdTe semiconductor shall be pixelized.

Justification: To provide the ability to measure gamma-ray photon polarization.

ID: REQ-008 **Type:** Design **Verification:** RoD, I

The experiment shall have four, stacked, parallel detector planes with an inclination tolerance, between planes, of $\pm 1^\circ$.

Justification: To form a Compton camera and therefor increase the probability of detection compton events.

ID: REQ-010 **Type:** Design **Verification:** RoD, I

The detector planes shall be perpendicular to the \hat{z} axis of the SR-RM Geometric Body Fixed Reference Frame with a tolerance $\pm 1^\circ$.

Justification: When performing data processing we can directly use the SR attitude data.

ID: REQ-017 **Type:** Design **Verification:** RoD, T

The experiment shall weigh less than 3Kg.

Justification: Requirement imposed by PTSpace, otherwise they need to pay more to fly THOR.

ID: REQ-019 **Type:** Design **Verification:** RoD

The OCB shall have an internal memory with a capacity of 32 Gbytes.

Justification: Assures us we can save every photon event already achieving 2 mission objectives.

ID: REQ-022 **Type:** Operational **Verification:** RoD, T

The payload OBC shall send all the Scientific Data to the SR storage system, MMU.

Justification: See justification of REQ-024.

ID: REQ-024 **Type:** Interface **Verification:** RoD

All data on the SR storage system shall be sent to the ground station.

Justification: In case the SR fails reentry we have in the ground segment all the data to achieve the mission objectives.

ID: REQ-030 **Type:** Interface **Verification:** RoD, A

The total data transferred to the SR storage system shall not be greater than 300MByte/day.

Justification: Value negotiated with SR team. SR has limited resources of data transfer to ground.

ID: REQ-033 **Type:** Operational **Verification:** RoD

The experiment shall have two operation modes: Housekeeping - Detector turned off; Observational - Detector turned on.

Justification: KISS, Keep it simple and stupid. Observation taking measurements, Housekeeping if any trouble.

ID: REQ-035 **Type:** Interface **Verification:** RoD, T

The maximum power consumption shall be of 50W.

Justification: Value negotiated with SR team. Limited power to supply the P/L's.

ID: REQ-041 **Type:** Operational **Verification:** RoD

The OBC shall have the capability to shutdown the detector unit.

Justification: To change operation mode and to stop acquisition if any problem arises on the detector.

ID: REQ-048 **Type:** Interface **Verification:** RoD, I

The experiment should be mounted either in N934897 (plate 6) or N934896 (plate 1) location.

Justification: To provide THOR an unobstructed exposure to space.

ID: REQ-049 **Type:** Operational **Verification:** RoD, T

The payload OBC shall perform the synchronization of the time with the SR-MMU whenever the experiment is turned ON.

Justification: To maintain the scientific data as a reference to the SR time for easier integration with the SR attitude data.

ID: REQ-055 **Type:** Design **Verification:** RoD, T

The Finger Boards that make Detection Plane shall be separated by 1mm with a tolerance of 0.5mm.

Justification: To have a geometry as close as to a continuum slab of CdTe as a detector plane.

ID: REQ-056 **Type:** Design **Verification:** RoD, T

The Finger Boards that make up the Detection Plane shall be horizontally align with a tolerance of 1mm

Justification: To have a geometry as close as to a continuum slab of CdTe as a detector plane.

ID: REQ-059 **Type:** Design **Verification:** RoD

The Detector Unit shall be positioned at the top position of the available payload volume.

Justification: To make sure the detector gets an unobstructed view to space.

ID: REQ-060 **Type:** Design **Verification:** RoD, I

The Detection Plane shall have four horizontally displayed CdTe Finger Boards forming a 4x1 array.

Justification: Agreed geometry upon discussions with ADVACAM.

ID: REQ-064 **Type:** Design **Verification:** RoD

OBC shall have at least 1 thread running per detector module.

Justification: Minimum OBC requirement for normal operation of the detectors.

ID: REQ-070 **Type:** Design **Verification:** RoD, T

Whenever the experiment switches its mode of operation the OBC shall record the time of the change.

Justification: To have this information readily available to aid the search of celestial events detected by other satellites.

ID: REQ-071 **Type:** Design **Verification:** RoD, T

Whenever the experiment switches its mode of operation the OBC shall include a message, with the problem identified, in the health monitor data packet.

Justification: To keep the LIP GS up to date on THOR state.

ID: REQ-072 **Type:** Design **Verification:** RoD

The enclosure shall be made of aluminum.

Justification: Low Z, almost transparent (thickness dependent) for photon energies 100keV-1MeV.

ID: REQ-073 **Type:** Design **Verification:** RoD, I

The top plate of the enclosure, above the detector unit, shall have a maximum thickness of 1mm.

Justification: Transmittance photons: 95% @100keV , 97.8% @511keV, 98.3% @1000keV

ID: REQ-075 **Type:** Environmental **Verification:** T

The OBC shall maintain a temperature between -20°C and 80°C throughout the whole flight.

Justification: Temperature of operation of the selected OBC.

ID: REQ-088 **Type:** Design **Verification:** RoD, T

The Gamma-tracker array shall have a maximum power consumption of 40W.

Justification: The detector consumes a lot of power to operate in the best performance mode.

ID: REQ-090 **Type:** Design **Verification:** RoD, T

The Particle-detector array shall have a maximum power consumption of 4W.

Justification: The detector power consumption to operate in the best performance mode.

ID: REQ-091 **Type:** Design **Verification:** RoD

The OBC shall have a 9V-20V voltage supply.

Justification: The input voltage range of the selected OBC.

ID: REQ-093 **Type:** Interface **Verification:** RoD, I

The experiment housing shall have the connector 340105601B06-15-19PN for the power interface.

Justification: Requirement imposed by SR.

ID: REQ-094 **Type:** Interface **Verification:** RoD, I

The experiment housing shall have the connector 3401/001 D-SUB 9 pins, Male for the RS422 communication.

Justification: Requirement imposed by SR.

ID: REQ-095 **Type:** Interface **Verification:** RoD, T

The PDU shall have an input voltage of 22-38V that interfaces with the Power Conector.

Justification: Definition of unregulated 28V from ECSS-E-ST-20-20C.

ID: REQ-099 **Type:** Design **Verification:** RoD

The PDU shall have a 5V/5W voltage output, named VS_PAR

Justification: To supply the hole Particle Detector. 5W limit is compatible with REQ-90

ID: REQ-100 **Type:** Design **Verification:** RoD

The PDU shall have a 9-20V/25W voltage output, named VS_OBC

Justification: Acceptable voltage range and maximum power supply allowed as of the power budget.

ID: REQ-102 **Type:** Design **Verification:** RoD

The PDU input over current protection shall be compliant with the ECSS-E-HB-20-20A.

Justification: Reliable and automatic design to protect over voltage and over current.

ID: REQ-103 **Type:** Design **Verification:** RoD

The PDU shall have dual modular redundancy at the power converts.

Justification: In case a module fails the other is there to replace it. Also useful to distribute the load/heat over two units.

ID: REQ-104 **Type:** Design **Verification:** RoD, T

The PDU shall give feedback to the OBC if the outputs are active within a $\pm 10\%$ normal operational voltage.

Justification: In order for the OBC to have feedback on the misbehaving of downstream components.

ID: REQ-108 **Type:** Design **Verification:** RoD

The OBC shall monitor each of the current output of the PDU with a resolution of 10 bits.

Justification: $2^{10} - 1 = 1023$, $2A/1023 = 2 \times 10^{-3}A$, enough resolution for the current monitor.

ID: REQ-109 **Type:** Design **Verification:** RoD, I

The payload shall have an external pull-pin kill switch connected to the PDU.

Justification: Have a physical switch that allows an automatic turn-on of THOR when pulled. To be used when integrating THOR to the SR.

ID: REQ-110 **Type:** Design **Verification:** RoD, I

The payload shall have an external redundant mechanical kill switch connected to the PDU.

Justification: Have a mechanical switch to control the ON/OFF of THOR during the testing campaign.

ID: REQ-112 **Type:** Design **Verification:** RoD, I

The venting holes shall have a maximum diameter of 3mm

Justification: To block EMI up to 1GHz frequency. Faraday cage

ID: REQ-114 **Type:** Interface **Verification:** RoD

The data sent to the SR MMU shall be of two types: Housekeeping data; Scientific Data

Justification: KISS, Keep it simple and stupid. Different data packets will have different priorities to arrive the LIP GS.

ID: REQ-116 **Type:** Operational **Verification:** RoD, T

The OBC shall save all the scientific data on the internal memory.

Justification: To have access to all of the scientific data gathered. OBC_MMU will be recovered after SR landing.

ID: REQ-117 **Type:** Operational **Verification:** RoD, T

If the OBC internal memory reaches 80% of its capacity a warning message shall be sent to the LIP ground segment.

Justification: In order to LIP operators have time to implement a MMU managment update to send to the OBC. See REQ-118

ID: REQ-118 **Type:** Operational **Verification:** RoD, T

Upon receiving the 80% ocupancy of the OBC internal memory warning LIP ground segment shall send a TC packet specifying what selection of data can be deleted.

Justification: The data already on ground can be deleted from the OBC_MMU

ID: REQ-119 **Type:** Interface **Verification:** RoD

The Housekeeping data transmission delay from the SR MMU to the LIP ground segment shall not be greater than 3,5h, calculated from when the Housekeeping data is received in the SR MMU.

Justification: SR can go up to 1.5h without contact with the SR Ground Segment. SR can have an overload of dama to transmit to GS. This is the minimum acceptable delay since it takes 3.5h of delay to send an uplink command.

ID: REQ-120 **Type:** Interface **Verification:** RoD

The Scientific data transmission delay from the SR MMU to the LIP ground segment shall not be greater than 1 day, calculated from when the Scientific data is received in the SR MMU.

Justification: SCI data is not time sensitive. 1 day is enough to cross check the SCI data with SR attitude data.

ID: REQ-121 **Type:** Interface **Verification:** RoD

The OBC shall communicate with the SR MMU with the RS422 protocol following the electrical requirements specified on TASI-SR-SRS-X-11-IRD-0003

Justification: To communicate with the SR MMU, otherwise we dont have COM's.

ID: REQ-122 **Type:** Design **Verification:** RoD

The identification of the four detection planes shall be numerical, from 1 to 4, beeing 1 the farthest one on the top.

Justification: For easy reference of witch detector plane we are talking about.

ID: REQ-123 **Type:** Design **Verification:** RoD, T

The distance between the detector plane 1 and 2 shall be of 1.8mm +-0.5mm.

Justification: Provides a very good Compton camera configuration between plane 1 and 2 where Compton events can be reconstructed.

ID: REQ-124 **Type:** Design **Verification:** RoD, T

The distance between the detector plane 2 and 3 shall be of 18mm +-0.5mm.

Justification: Good second Compton camera configuration. Given the mechanical dimensions of the FB's this is the best configuration for the second stage.

ID: REQ-125 **Type:** Design **Verification:** RoD, T

The distance between the detector plane 3 and 4 shall be of 1.8mm +-0.5mm.

Justification: Provides a very good Compton camera configuration between plane 1 and 2 where Compton events can be reconstructed.

ID: REQ-126 **Type:** Design **Verification:** RoD

The detector plane 1 shall have the detector's surfaces pointed to the SR negative \hat{z} axis of the SR-RM Geometric Body Fixed Reference Frame with a tolerance $<1^\circ$

Justification: The relative inclination between planes affects the Compton reconstruction geometry. The coincidence with the SR \hat{z} axis allows an easier use of the SR attitude data.

ID: REQ-127 **Type:** Design **Verification:** RoD

The detector plane 3 shall have the detector's surfaces pointed to the SR negative \hat{z} axis of the SR-RM Geometric Body Fixed Reference Frame with a tolerance $<1^\circ$

Justification: Same justification as REQ-126

ID: REQ-128 **Type:** Design **Verification:** RoD

The detector plane 2 shall have the detector's surfaces pointed to the SR positive \hat{z} axis of the SR-RM Geometric Body Fixed Reference Frame with a tolerance $<1^\circ$

Justification: Same justification as REQ-126

ID: REQ-129 **Type:** Design **Verification:** RoD

The detector plane 4 shall have the detector's surfaces pointed to the SR positive \hat{z} axis of the SR-RM Geometric Body Fixed Reference Frame with a tolerance $<1^\circ$

Justification: Same justification as REQ-126

ID: REQ-130 **Type:** Design **Verification:** RoD, I

The detector plane 2 and 3 shall have a Si detector added to one horizontal extremity, having them both added to the same side.

Justification: For an effective monitoring of the particle radiation that allows for a seamless integration with the CdTe data

ID: REQ-132 **Type:** Design **Verification:** RoD, I

The payload's enclosure shall have 4 holding points on the positive \hat{z} face.

Justification: To use during integration between the THOR and the SR.

ID: REQ-139 **Type:** Operational **Verification:** RoD, T

THOR OBC shall update the SR MMU with Scientific data every 24h.

Justification: SCI is not time sensitive. LIP GS requires SCI data to have feedback about the operability of the detector (ie: adjust threshold, calibration).

ID: REQ-140 **Type:** Operational **Verification:** RoD, T

THOR OBC shall update the SR MMU with Housekeeping data every 3.5h.

Justification: Time sensitive data. To provide the LIP GS with regular THOR health report and HK data. Higher frequency than SCI to reduce the down time if a critical error happens.

ID: REQ-141 **Type:** Interface **Verification:** RoD

The SR OBC shall update the THOR-SR MMU with attitude data every 24h.

Justification: In order to perform scientific data analysis on orbit.

ID: REQ-142 **Type:** Operational **Verification:** RoD, T

The OBC, after the wake-up procedure, shall update the SR_MMU with THOR health status, ie: dead pixels, if detectors are nominal, working temperature of components, voltage/current levels.

Justification: Give a general health update to LIP GS operators to understand if THOR is nominal or needs intervention.

ID: REQ-143 **Type:** Interface **Verification:** RoD

In case of an emergency, LIP Ground Segment shall be able to send a Payload Direct Operation Request (PDOR) with an arrival delay of no more than 3.5h.

Justification: To have a maximum payload downtime of 7h.

ID: REQ-144 **Type:** Operational **Verification:** RoD, T

If the communication between the SR MMU and the payload OCB fails the payload OBC shall save all the data, housekeeping and scientific, in the internal memory.

Justification: The OBC shall carry out the scientific operations if possible. Losing COM with SR MMU should not be a reason to stop operations.

ID: REQ-146 **Type:** Design **Verification:** RoD, T

The detector planes shall be in sync within a $2\mu s$ time window.

Justification: To identify the time coincidence of a Compton event it is typically used a $2\mu s$ coincidence time window

ID: REQ-150 **Type:** Interface **Verification:** I

After integrating the THOR-SR P/L in the MPCB the operator shall pull the 'pull-pin' kill switch that will be properly identified with a 'Remove Before Flight tag'

Justification: To ensure that, even though mechanical switch is in OFF state, THOR can be power up when SR turns ON the power lines.

ID: REQ-152 **Type:** Design **Verification:** RoD, I

The top surface of the Silicon detector shall be at least 1cm away from the CdTe top surface.

Justification: To ensure that there will be no arc discharges between the +200V and -500V surfaces.

ID: REQ-154 **Type:** Operational **Verification:** RoD, T

THOR shall be ready, at any time, to be unplugged from the SR power supply.

Justification: When SR enters safe mode it tuns off P/L's power supply without warning.

ID: REQ-156 **Type:** Design **Verification:** RoD

Each Detector Plane shall have an associated independent mechanical part.

Justification: For assembly purposes.

ID: REQ-157 **Type:** Interface **Verification:** RoD, T

The experiment shall be mounted to the Aluminium adaptor using M6 drill with 58mmx58mm spacing.

Justification: Geometrical disposition of the holding points inside the MPCB

ID: REQ-158 **Type:** Design **Verification:** RoD

The experiment housing shall have ETHERNET plug.

Justification: To have full access to THOR OBC during ground testing.

ID: REQ-159 **Type:** Design **Verification:** RoD

THOR enclosure shall have visible LED's that show what components are ON.

Justification: To have an external feedback of the state of THOR during ground testing.

ID: REQ-165 **Type:** Operational **Verification:** RoD, T

THOR shall be able to carry out scientific observations even if THOR OBC loses communication with the SR_MMU

Justification: Losing communications with SR MMU its not critical for the scientific operations of THOR.

ID: REQ-168 **Type:** Environmental **Verification:** RoD, T

THOR shall comply with the mechanical environment of the Vega-C launch, present on the SR-User Guide

Justification: FALTA JUSTIFICAR ESTE REQUIREMENT

ID: REQ-169 **Type:** Mission **Verification:** RoD

The SR shall provide THOR-SR P/L with a total observational time of 5 days of the Crab Nebula within a 10° of margin, taking the the payload's \hat{z} axis as reference.

Justification: Statistics required to perform polarimetric observations of the crab nebula. 10% because the parametric Compton pattern highly depends on the photons attack angle.

ID: REQ-170 **Type:** Mission **Verification:** RoD

The SR shall provide 18 days of deep sky observation time, taking into account the Earth doesn't block more than 20% of the Detector FOV.

Justification: Observational time to search for GRB's (unpredictable) and take enough statistics to identify continuum sources.

ID: REQ-171 **Type:** Mission **Verification:** RoD

The SR shall provide 7 days of Earth atmosphere observation time, with the SR Z-axis pointing to the nadir with a 30° margin, according to the SR-RM Geometric Body Fixed Reference Frame.

Justification: Observational time to search for TGF's (unpredictable). Higher pointing margin because TGF's may occur off-axis (unpredictable).

ID: REQ-172 **Type:** Mission **Verification:** RoD

The SR shall provide 12 h observation time of the Sun with a 30^o margin.

Justification: Sun will be on Solar Maximum. Observational time to catch a direct x-ray solar flare. 30% to ensure x-rays penetrate only the 1mm Al of the enclosure.

ID: REQ-173 **Type:** Interface **Verification:** RoD

Material with an atomic number over $Z \geq 30$ shall not obstruct more than 10% of the detector's field of view.

Justification: Material with high atomic number absorb x-ray and gamma-rays and creat a shadow on the detector FOV.

ID: REQ-174 **Type:** Design **Verification:** RoD

The PDU shall have a 12V/40W voltage output, named VS_GAM

Justification: To supply the GAM with the proper voltage level and power required.

ID: REQ-175 **Type:** Design **Verification:** RoD

The Gamma-tracker array shall have a controllable voltage supply of 12V.

Justification: The detectors don't have an integrated ON/OFF switch. This shall be implemented at the PDU level

ID: REQ-177 **Type:** Design **Verification:** RoD

The PDU voltage output VS_GAM shall be divided into 4 individual outputs, VS_GAMx, being the 'x' the number of the output.

Justification: If a problem happens on one detector plane it can be shutdown while the others keep taking scientific measurements.

ID: REQ-178 **Type:** Design **Verification:** RoD

The PDU voltage output VS_PAR shall be divided into 2 individual outputs, VS_PARx, being the 'x' the number of the output.

Justification: If a problem happens on one particle detector it can be shutdown while the other keep taking scientific measurements.

ID: REQ-180 **Type:** Design **Verification:** RoD, I

Half of the Detector Plane 1, specifically two Finger boards, shall be controlled by the same Readout board as the two adjacent Finger Boards located in the Detector Plane 2.

Justification: To ensure, for power consumption or thermal reasons, that if part of the GAM has to be turned OFF, the compton camera configuration is ensured per RO board.

ID: REQ-181 **Type:** Design **Verification:** RoD,I

Half of the Detector Plane 3, specifically two Finger boards, shall be controlled by the same Readout board as the two adjacent Finger Boards located in the Detector Plane 3.

Justification: See justification of REQ-180

ID: REQ-182 **Type:** Design **Verification:** RoD, I

The middle Finger Boards of the Detector Planes shall be horizontally separated by 5mm.

Justification: To ensure, in case half of the detector plane has to be shut down, the -500V present on the active finger board doesn't create an electric discharge to the 0V on the adjacent inactive finger board.

ID: REQ-183 **Type:** Operational **Verification:** RoD

During pressurization and depressurization the detector shall be in OFF state.

Justification: To ensure that there is no eclectic discharge between the -500V and a conductive surface.

ID: REQ-184 **Type:** Design **Verification:** RoD, I

The surface plane of the Silicon detector on plane 2 shall be parallel to the ZY plane.

Justification: To monitor the particle flux on the X orthogonal direction

ID: REQ-185 **Type:** Operational **Verification:** RoD

The OBC shall monitor the current consumption of the detector unit with the frequency of 2Hz.

Justification: To have regular feedback on the current consumption of the detector unit and have time to act in case there is a misbehaviour.

ID: REQ-186 **Type:** Operational **Verification:** RoD

The OBC shall monitor the voltage levels of the detector's main supply source with the frequency of 2Hz.

Justification: To have regular feedback on voltage supply levels and have time to act in case there is a misbehaviour.

ID: REQ-187 **Type:** Operational **Verification:** RoD

The OBC shall monitor the bias voltage of each detector with a frequency of 1Hz.

Justification: To have regular feedback on the bias voltage and check for electric discharges.

ID: REQ-188 **Type:** Operational **Verification:** RoD

The OBC shall monitor the leakage current of each detector with a frequency of 1Hz.

Justification: To have regular feedback on the noise at the CdTe/Si semiconductor level.

ID: REQ-189 **Type:** Operational **Verification:** RoD

The OBC shall monitor the temperature of the detectors with a frequency of 0.2Hz

Justification: To have feedback on the operational temperature of the detectors. Temperature changes slowly, 5 sec interval is enough.

ID: REQ-190 **Type:** Operational **Verification:** RoD

The OBC shall search for noisy pixels on the raw data every 10 minutes.

Justification: Noisy pixels may appear and saturate the data output of the detectors, making the data produced during that time unusable. Regular checks to mask the noisy pixels.

ID: REQ-191 **Type:** Environmental **Verification:** RoD, T

Each finger board shall dissipate 2W of power passively through the payload's enclosure to maintain an operation temperature between 0°C to 50°C.

Justification: Finger Boards consume 2W maximum. For higher temperatures the noisy pixel density increases, the detector resolution decreases and the semiconductors noise increases.

ID: REQ-192 **Type:** Environmental **Verification:** RoD, T

Each back-end electronics board shall dissipate 2W of power passively through the payload's enclosure to maintain an operation temperature between -10°C to 50°C.

Justification: RO boards consumes 2W and the operation temperature recommended by ADV is between -10°C and 50°C.

ID: REQ-193 **Type:** Design **Verification:** RoD

The Particle-detector array shall have a controllable voltage supply of 4.8 to 5.2V.

Justification: Minimum and Maximum voltage supply levels to supply the particle detectors. Above maximum or below minimum the detectors may be damaged.

ID: REQ-194 **Type:** Design **Verification:** RoD,T

The PDU shall have a overcurrent protection of $2A \pm 5\%$ on the VS_OBC output.

Justification: To ensure the OBC doesn't consume more than the established power budget.

ID: REQ-195 **Type:** Environmental **Verification:** A

The payload's enclosure shall have venting holes in order to comply with the depressurization profiles of 2200 Pa/sec.

Justification: Depressurization profile of the launching phase. Requirement imposed by the SR.

ID: REQ-196 **Type:** Mission **Verification:** RoD

THOR shall be ON during 50 days.

Justification: GRB and TGF's are unexpected, the more time we are active, even though without any specific orientation, the higher is the probability to catch this rare events.

ID: REQ-197

Type: Environmental

Verification: T

THOR shall comply with the EMC susceptibility expected on the MPCB:

- 136 dBuV/m @0 Hz to 1GHz;
 - 127dBuV/m @1GHz to 10GHz;
 - 151dBuV/m @2GHz to 2.3GHz;
 - 140dBuV/m @ 3GHz to 3.8GHz;
 - 151dBuV/m @5.1GHz to 6.1GHz.
-

Justification: Requirement imposed by the SR.

| | | |
|--------------------|----------------------------|------------------------|
| ID: REQ-198 | Type: Environmental | Verification: T |
|--------------------|----------------------------|------------------------|

THOR shall comply with th maximum radiated EMC allowed by the SR:

- 80 dBuV/m @0Hz to 400MHz;
 - 20dBuV/m @400MHz to 500MHz;
 - 80 dBuV/m @ 500MHz to 900MHz;
 - 90 dBuV/m @ 1GHz to 1.1GHz;
 - 25dBuV/m @1.1GHz to 1.2GHz;
 - 90 dBuV/m @ 1.2GHz to 1.6GHz;
 - 25dBuV/m @1.6GHz to 1.7GHz;
 - 90dBuV/m @1.7GHz to 2GHz;
 - 10dBuV/m @2GHz to 2.1GHz;
 - 90dBuV/m @2GHz to 5.5GHz;
 - 65dBuV/m @5.5GHz to 6GHz;
 - 90dBuV/m @ 6GHz to 40GHz.
-

Justification: Requirement imposed by the SR.

| | | |
|--------------------|------------------------|--------------------------|
| ID: REQ-199 | Type: Interface | Verification: RoD |
|--------------------|------------------------|--------------------------|

The first data received by the SR_MMU after the THOR first power up shall be transmitted to the LIP GS with a maximum delay of 2h, counting from the moment the data is transmitted from THOR OBC to SR_MMU.

Justification: Ensures timely validation of payload health and data relay systems, enabling quick, mission-critical decisions and efficient resource allocation.

ID: REQ-200 **Type:** Interface **Verification:** RoD

In case the first downlink message from THOR after the first power up requires ground intervention, a PDOR message shall be sent to THOR with a maximum delay of 1.5h, counting from the moment the LIP GS requests it to the SR GS operators.

Justification: To minimize the downtime keeping in mind

ID: REQ-201 **Type:** Operational **Verification:** RoD

THOR OBC shall switch to housekeeping mode 1h before the power cut.

Justification: OBC to do the final shutdown procedure before reentry.

ID: REQ-202 **Type:** Design **Verification:** RoD

The data sent to the SR MMU shall be PUS compliant.

Justification: For an easier integration with PGCC. PUS has a lot of lessons learned by ESA (Bruno Sousa advice).

ID: REQ-203 **Type:** Operational **Verification:** A

The Observational Mode shall have an availability of 95%.

Justification: To minimize the down time of the scientific observations. From REQ-196 THOR can be in either housekeeping, be-dug or firmware update mode during 2.5days.

ID: REQ-204 **Type:** Design **Verification:** RoD, T

The PDU shall have an input over current protection of $2.5A \pm 5\%$.

Justification: $2.5A \times 22V = 55W$, that its 10% above the REQ-035

ID: REQ-205 **Type:** Design **Verification:** RoD, T

The PDU shall have an over current protection of $0,83A \pm 5\%$ on each VS_GAMx output.

Justification: In case there is a miss behaviour of one detector plane (ie: short circuit) the over current protection ensures that the problem doesn't propagate to other THOR products.

ID: REQ-206

Type: Design

Verification: RoD, T

The PDU shall have an over current protection of 0.5A \pm 5% on each VS_PARx output.

Justification: In case there is a miss behaviour of one particle detector (ie: shortcircuit) the over current protection ensures that the problem doesn't propagate to other THOR products.

Appendix C

Electrical Interfaces Block Diagram

This Appendix showcases a detailed block diagram showcasing the electrical interfaces of the THOR payload.

Appendix D

Connectors' location on THOR products

In this Appendix it is showcased the locations of the electrical connectors on each product.

D.1 GAM Finger Board - THOR_DET_GAM_RO.x.FB.x

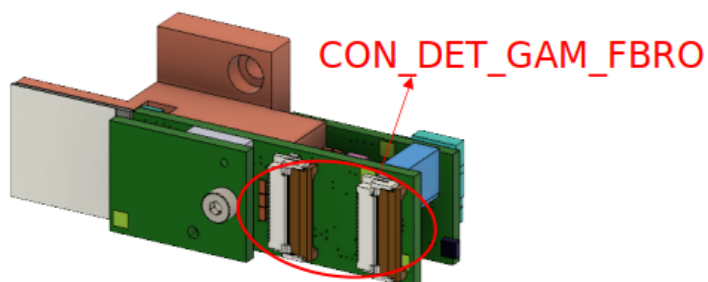


Figure D.1: Finger Board connector location.

D.2 GAM Read Out Board - THOR_DET_GAM_RO.x

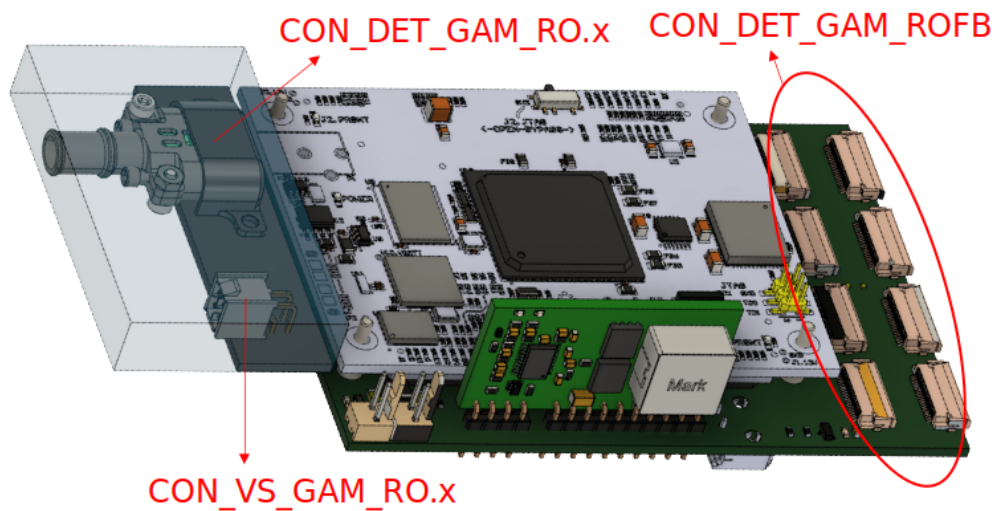


Figure D.2: GAM RO connector location.

D.3 PAR board - THOR_DET_PAR_B.x

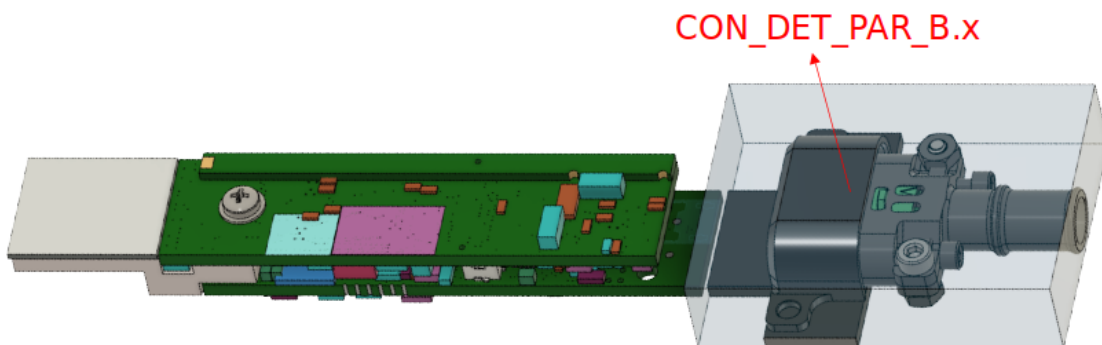


Figure D.3: Particle detector connector location.

D.4 Onboard Computer Carrier Board - THOR_OBC_CB

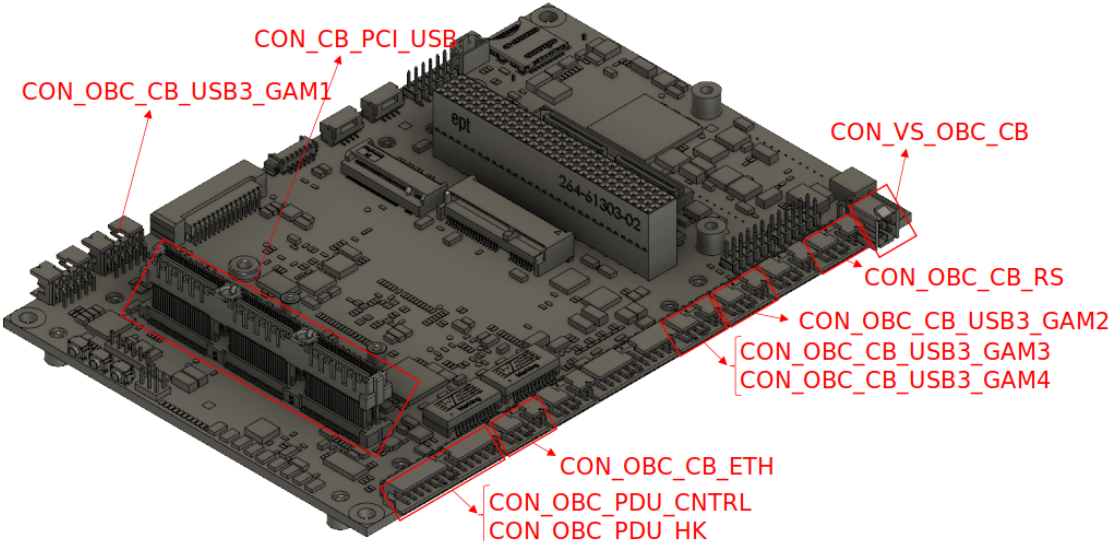


Figure D.4: OBC Carrier Board connector location.

D.5 Power Distribution Unit - THOR_PDU

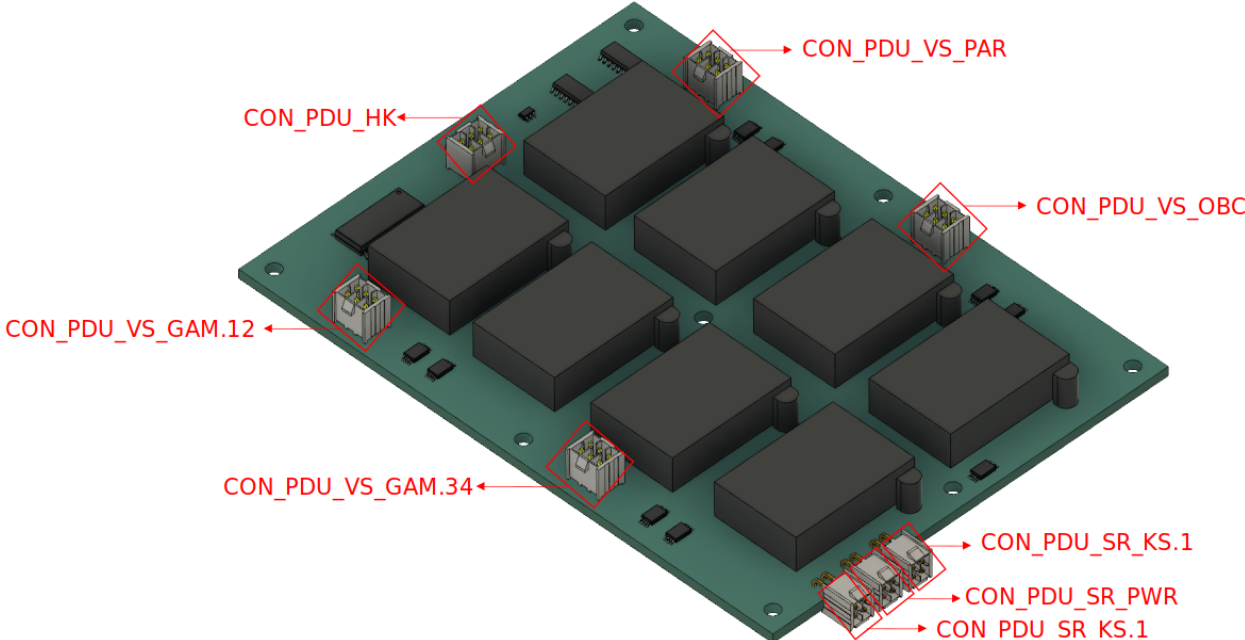


Figure D.5: Power Distribution Unit connector location.

Appendix E

THOR-SR Gantt Chart

In this Appendix we present the Gantt Chart of the project. From the kick-off until the end of the outreach activities. The main milestones are the Requirements Review (6 April 2023), the Preliminary Design Review (27 September 2023), the CDR (15 December 2023), the delivery of P/L software to ESA (2 January 2024), the Engineering Model delivery to ESA (25 March 2024), the Flight Model delivery to ESA (1 July 2024).

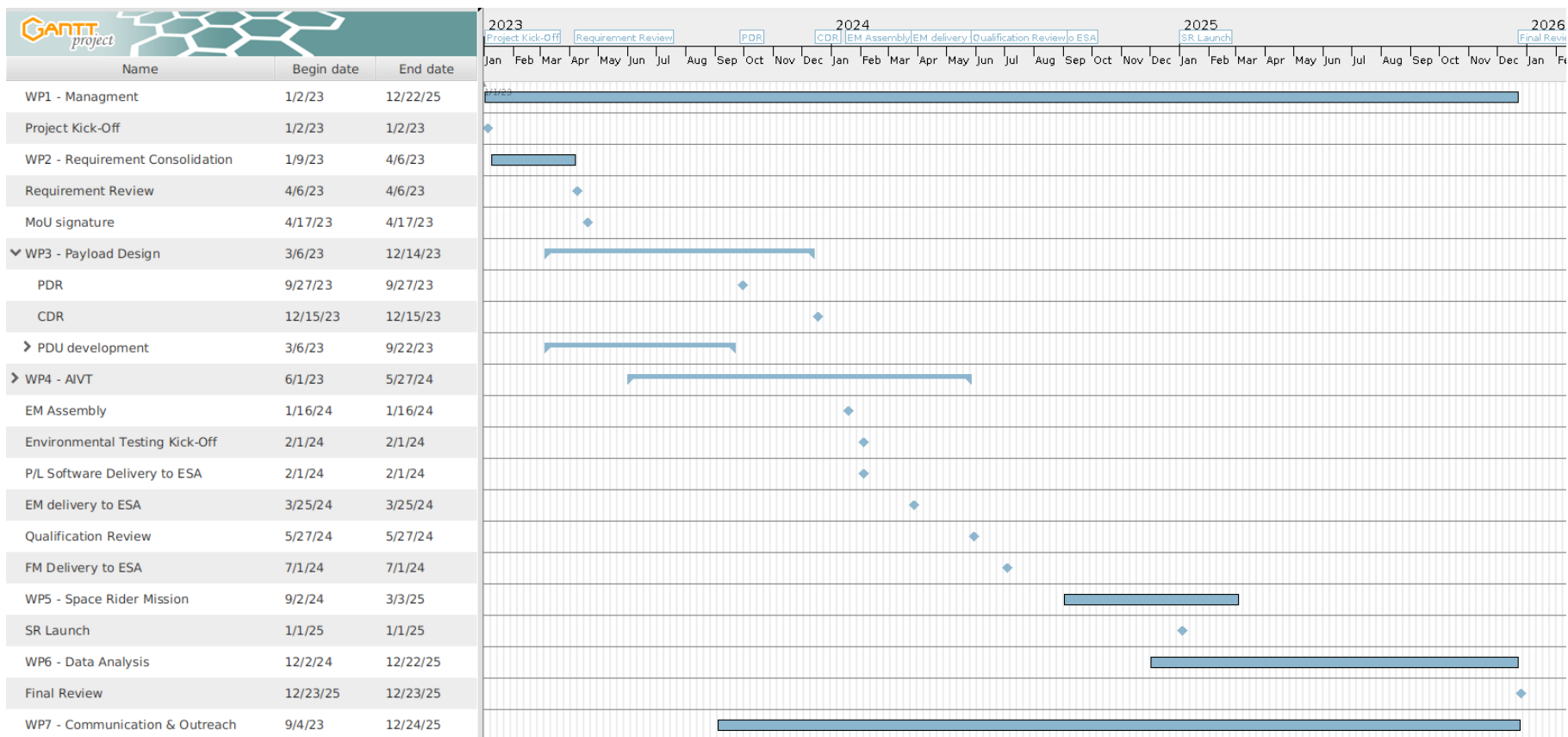


Figure E.1: Last updated on September 2023.

Appendix F

PDR Enclosure design LIP comments

This Appendix showcases the LIP comments to the PDR enclosure design performed by AST. This document showcases if the enclosure PDR design is compliant with the requirements.

ID: THOR_T_AST_SU_002

Date: 03/07/2023

Issue: 2.0

THOR-SR AST Status Update



TGF and High energy astrophysics Observatory for gamma Rays

Prepared by

José Sousa

Document Type

Status Update

Reference

THOR_T_AST_SU_002

Issue/Revision

2.0

Date of Issue

30/07/2023

Status

Approved



LABORATÓRIO DE INSTRUMENTAÇÃO
E FÍSICA EXPERIMENTAL DE PARTÍCULAS
partículas e tecnologia

ID: THOR_T_AST_SU_002

Date: 03/07/2023

Issue: 2.0

APPROVAL

| | | | |
|-------------|---------------------------|------------------|------------|
| Title | THOR-SR AST Status Update | | |
| ID | THOR_T_AST_SU_002 | Revision Number | 1 |
| Author | José Sousa | Date | 03/07/2023 |
| Approved By | José Sousa | Date of Approval | 03/07/2023 |

CHANGE LOG

| Reason for change | Issue Nr | Revision Number | Date |
|--|----------|-----------------|------------|
| Document creation | 1 | 1 | 29/05/2023 |
| Reason for change | Issue Nr | Revision Number | Date |
| AST created the PDR version of the ENC | 2 | 1 | 03/07/2023 |

CHANGE RECORD

| Issue Number | Revision Number | | |
|--|-----------------|-------|--------------|
| Reason for change | Date | Pages | Paragraph(s) |
| Section 2.1 Reference Frame - To standardize the THOR reference Frame | 03/07/2023 | 6 | 2.1 |
| Requirement Verification Matrix with Comments. Created a Status Update ID for every discussion point for easy reference | 03/07/2023 | 7-20 | 3.1 |
| Additional Comments and concerns | 03/07/2023 | 21-22 | 3.2 |
| Added Reference Frame to the image in Annex A | 03/07/2023 | 23 | Annex A |

DISTRIBUTION

| |
|---------------------------|
| Name/Organisational Unit |
| LIP - THOR-SR Team |
| Active Space Technologies |

Table of Contents

| | |
|--|-----------|
| 1. Applicable and reference documents | 4 |
| 2.1 Applicable documents | 4 |
| 2.2 Reference documents | 4 |
| 2.3 Terms, Definitions and Acronyms | 4 |
| 2. Current Status | 6 |
| 2.1 Reference Frame | 6 |
| 3. Requirement Verification | 7 |
| 4. Additional comments | 21 |
| 3.1 Preliminary Thermal Analysis | 22 |
| Annex A. | |
| Detector Unit Requested Configuration | 23 |

1. Applicable and reference documents

2.1 Applicable documents

[AD 1] THOR_T_DDF_002

[AD 2] ADMIN-BZD.2023-PP-0005

2.2 Reference documents

[RD 1] SRIDERUC-AST-MIN-0015

[RD 2] SRIDERUC-AST-RS-0005_1.0_Requirement_Specification-CommentsJoséSou
saTHOR

[RD3] TASI-SR-SRS-X-11-SSS-0046

[RD4] Jetson_AGX_Xavier_Series_Thermal_Design_Guide_TDG-08981-001_v1.3

[RD5] ASY-1000269-A14_THOR_ENC_MAIN

2.3 Terms, Definitions and Acronyms

| | |
|-----|------------------------|
| AB | Adaptation Board |
| ADV | Advacam |
| CB | Carrier Board |
| CDR | Critical Design Review |
| DDF | Design Definition File |
| DET | Detector |
| DP | Detector Plane |
| ENC | Payload Enclosure |
| FB | Finger Board |
| FOV | Field of View |
| GAM | Gamma-ray Detector |

ID: THOR_T_AST_SU_002

Date: 03/07/2023

Issue: 2.0

| | |
|-------|---------------------------|
| GRB | Gamma-Ray Burst |
| HK | Housekeeping |
| HV | High Voltage |
| KS | Kill Switch |
| MPCB | Multi-Purpose Cargo Bay |
| MMU | Mass Memory Unit |
| OBC | OnBoard Computer |
| OBSW | OnBoard Software |
| PDU | Power Distribution Unit |
| PDR | Preliminary Design Review |
| P/L | Payload |
| REQ | Requirement |
| RO | Readout Board |
| SR | Space Rider |
| SU | Status Update |
| SR-RM | SpaceRider Reentry Module |
| TBC | To be Confirmed |
| TBD | To be Defined |
| TC | Telecommand |

2. Current Status

At this stage, the enclosure is ready for PDR. The distribution of the components inside the useful volume is representative of what the final product will look like. ADV is redesigning the PCB's from the THOR_DET_GAM_RO.x. After PDR there will be more comments to adjust the ENC design since we will have direct feedback from ADV. ADV is also redesigning the holding structure of the THOR_DET_GAM_DP.xFB.x, minor changes might appear after PDR.

2.1 Reference Frame

The THOR-SR reference frame is coincident as te SR Reentry module:

- X axis: Red
- Y axis: Green
- Z axis: Blue

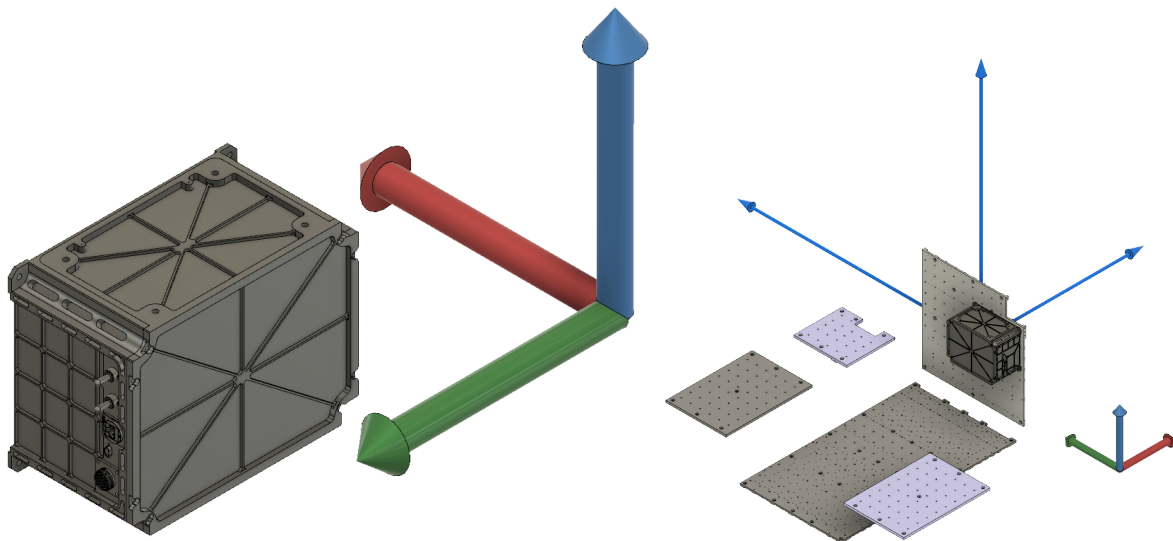


Fig 2.1 a) Visualisation of the THOR reference frame. b) THOR reference frame coincides with the SR reference frame.

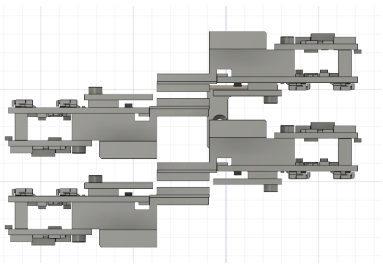
ID: THOR_T_AST_SU_002

Date: 03/07/2023

Issue: 2.0



3. Requirement Verification

| Item ID | REQ ID | Requirement text | Verifica-tion method | Verification Check | LIP Comments |
|---------|--------|---|----------------------|--------------------|--|
| SU1 | 8 | The experiment shall have four, stacked, parallel detector planes with an inclination tolerance, between planes, of $\pm 1^\circ$. | RoD | Compliant | Side View, from :  |
| SU2 | 10 | The detector planes shall be perpendicular to the z axis of the SR-RM Geometric Body Fixed Reference Frame with a tolerance $< 1^\circ$. | RoD, I | Partially | The design is verified. Do the inspection when the ENC and DET_GAM_DP are assembled. |

ID: THOR_T_AST_SU_002

Date: 03/07/2023

Issue: 2.0



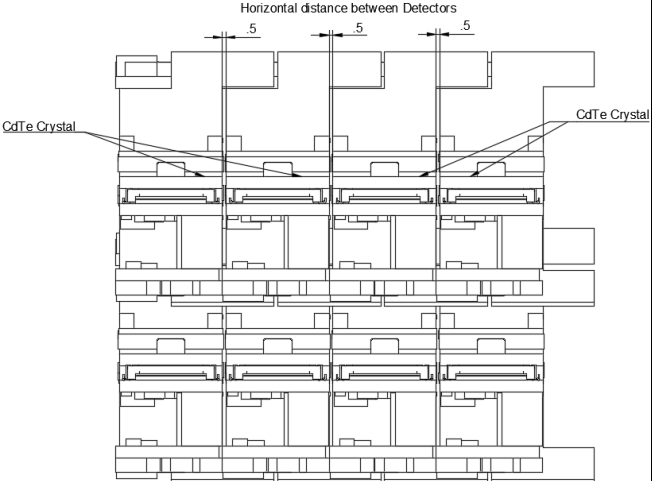
| | | | | | |
|-----|----|---|-----------|---------------|---|
| | | | | | |
| SU3 | 17 | The experiment shall weigh less than 3Kg. | RoD, T | Not Compliant | What is the expected weight of the Enclosure? |
| SU4 | 44 | The payload's enclosure shall dissipate 50W through the SR cold plates. | RoD, A | Not Compliant | Preliminary Thermal Analysis needed. |
| SU5 | 45 | Each finger board shall dissipate 2W of power passively through the payload's enclosure. | RoD, T, A | Not Compliant | LIP will perform a Test to check the Power dissipation of the Units (for CDR). ADV is modifying the firmware to limit the power dissipation to 2W. |
| SU6 | 46 | Each backend electronics board shall dissipate 2W of power passively through the payload's enclosure. | RoD, T, A | Not Compliant | ADV is modifying the firmware to limit the power dissipation to 2W. |



ID: THOR_T_AST_SU_002

Date: 03/07/2023

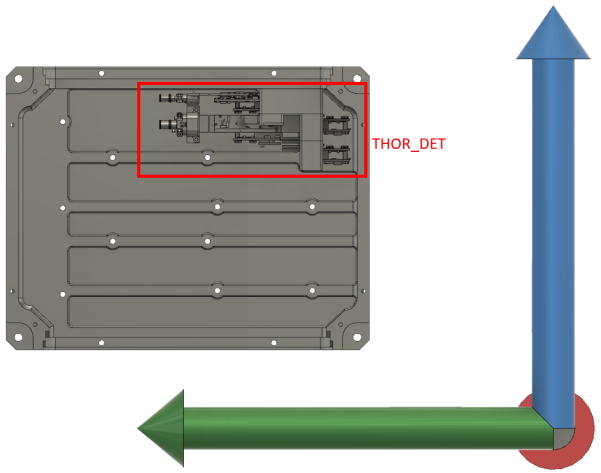
Issue: 2.0

| | | | | | |
|-----|----|--|--------|---------------|---|
| SU7 | 48 | The experiment should be mounted either in N934897 (plate 6) or N934896 (plate 1) location. | RoD, I | Not Compliant | When manufactured, the hole size and distance shall be measured. At the moment it seems that the Holes don't match with the holes in the SR support plates. |
| SU8 | 55 | The Finger Boards that make Detection Plane shall be separated by 1mm with a tolerance of 0.5mm. | RoD | Compliant | RIGHT VIEW:  <p>Also, see REQ-182. The middle finger boards shall be 5mm from each other.</p> |

ID: THOR_T_AST_SU_002

Date: 03/07/2023

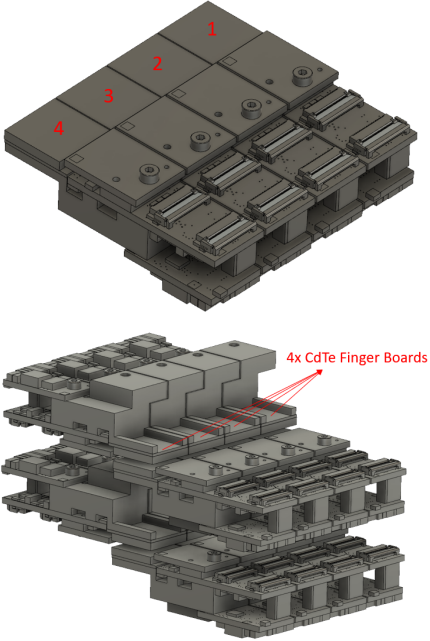
Issue: 2.0

| | | | | | |
|-----|----|--|-----|-----------|--|
| SU9 | 59 | The Detector Unit shall be positioned at the top position of the available payload volume. | RoD | Compliant | Ref axis: X(red), Y(green), Z(blue)  |
|-----|----|--|-----|-----------|--|

ID: THOR_T_AST_SU_002

Date: 03/07/2023

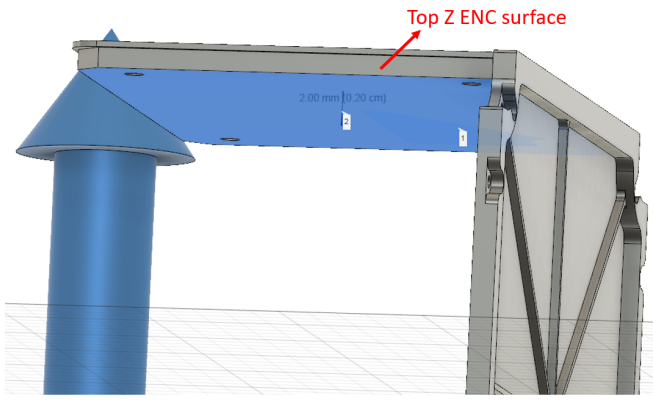
Issue: 2.0

| | | | | | |
|------|----|--|--------|---------------|---|
| SU10 | 60 | The Detection Plane shall have four horizontally displayed CdTe Finger Boards forming a 4x1 array. | RoD, I | Compliant |  |
| SU11 | 72 | The enclosure shall be made of alluminum. | RoD | Not Compliant | |

ID: THOR_T_AST_SU_002

Date: 03/07/2023

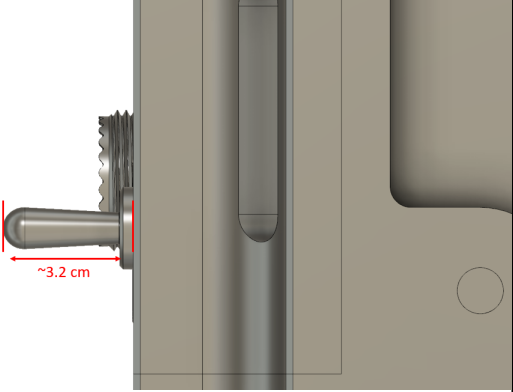
Issue: 2.0

| | | | | | |
|------|----|---|--------|---------------|--|
| SU12 | 73 | The top plate of the enclosure, above the detector unit, shall have a maximum thickness of 1mm. | RoD, I | Not Compliant | The top surface is 2mm. It was mentioned that AST cannot meet this requirement. Please confirm if you can do 1mm.  |
| SU13 | 74 | The detector's RO boards shall maintain a temperature between -10°C and 50°C throughout the whole flight. | T, A | Not Compliant | Min and Máx limits for the working temperature of the RO. Verify this on the Thermal Analysis. |
| SU14 | 75 | The OBC shall maintain a temperature between -20°C and 80°C throughout the whole flight. | T, A | Not Compliant | Min and Máx limits for the working temperature of the OBC. Verify this on the Thermal Analysis. |
| SU15 | 93 | The experiment housing shall have the connector 340105601B06-15-19PN for the power interface. | RoD, I | Compliant | |

ID: THOR_T_AST_SU_002

Date: 03/07/2023

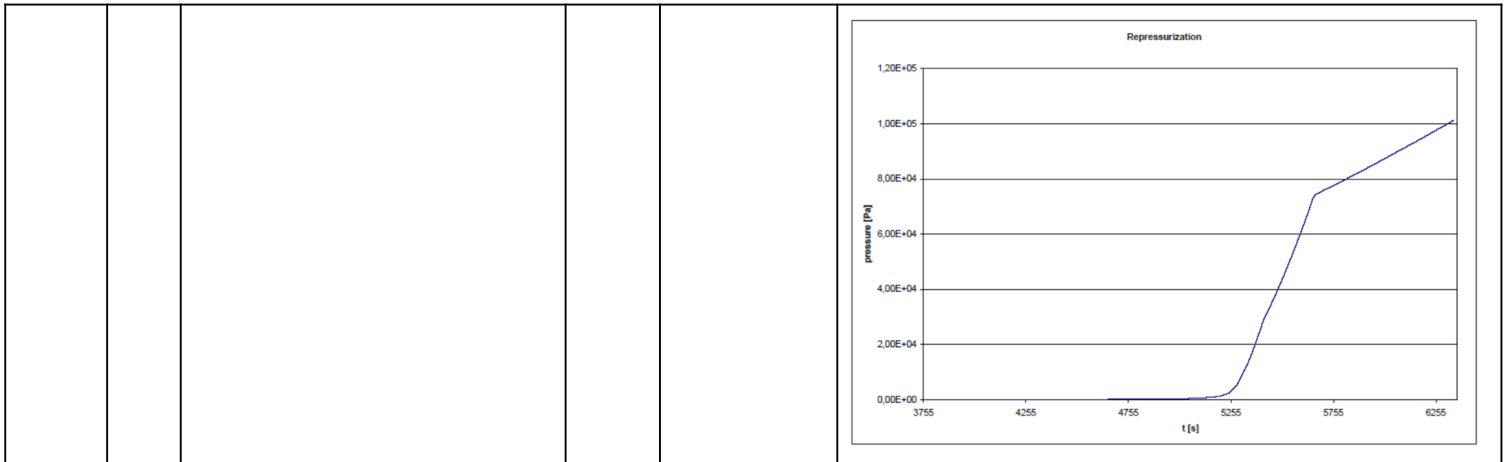
Issue: 2.0

| | | | | | |
|------|-----|--|--------|---------------|---|
| SU16 | 94 | The experiment housing shall have the connector 3401/001 D-SUB 9 pins, Male for the RS422 communication. | RoD, I | Not Compliant | LIP has to check if its the Male version. Mechanical dimensions are verified. |
| SU17 | 109 | The payload shall have an external pull-pin kill switch connected to the IVR/PDU. | RoD, I | Not Compliant | LIP did not yet choose the pull-pin kill switch. |
| SU18 | 110 | The payload shall have an external redundant mechanical kill switch connected to the IVR/PDU. | RoD, I | Not Compliant | LIP might change the connector because it may interfere with neighbouring other payloads.  |
| SU19 | 111 | The payload's enclosure shall have venting holes in order to comply with the pressurization and depressurization profiles present on the Space Rider user guide. | | Compliant | There are a total of 4 venting holes - can you confirm that they are enough to handle the pressurization and de-pressurization profiles of the flight? |

ID: THOR_T_AST_SU_002

Date: 03/07/2023

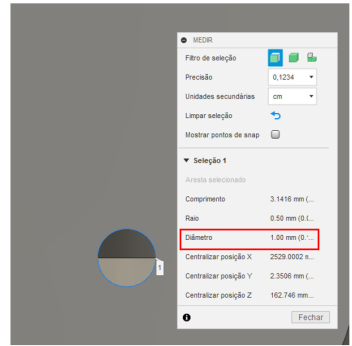
Issue: 2.0



ID: THOR_T_AST_SU_002

Date: 03/07/2023

Issue: 2.0

| | | | | | |
|------|-----|---|--------|---------------|--|
| SU20 | 112 | The venting holes shall have a maximum diameter of 3mm. | RoD, I | Compliant |  <p>They have 1mm diameter.</p> |
| SU21 | 113 | The Finger Boards shall have an operating temperature between 0°C and 50°C. | T, A | Not Compliant | Min and Máx limits for the working temperature of the OBC. Verify this on the Thermal Analysis. The optimal would be 25 - 30°C. |
| SU22 | 122 | The identification of the four detection planes shall be numerical, from 1 to 4, being 1 the farthest one on the top. | RoD | Not Compliant | The DET_GAM_DP.4 is the one further on the top. Rotate 180° on the Y axis. Please label the ENC_DP.x to the according to plane that the enclosure is supporting. |
| SU23 | 123 | The distance between the detector plane 1 and 2 shall be of 1.8mm +-0.5mm. | RoD, T | Compliant | |
| SU24 | 124 | The distance between the detector plane 2 and 3 shall be of 18mm +-0.5mm. | RoD, T | Compliant | |
| SU25 | 125 | The distance between the detector plane 3 and 4 shall be of 1.8mm +-0.5mm. | RoD, T | Compliant | |

ID: THOR_T_AST_SU_002

Date: 03/07/2023

Issue: 2.0

| | | | | | |
|------|-----|---|-----|---------------|---|
| SU26 | 126 | The detector plane 1 shall have the detector's surfaces pointed to the SR negative \hat{z} axis of the SR-RM Geometric Body Fixed Reference Frame with a tolerance $<1^\circ$ | RoD | Not Compliant | It is GAM_DET_DP.1 is pointed on the positive direction of the SR Z axis, see image. See comment on SU22. |
| SU27 | 127 | The detector plane 3 shall have the detector's surfaces pointed to the SR negative \hat{z} axis of the SR-RM Geometric Body Fixed Reference Frame with a tolerance $<1^\circ$ | RoD | Not Compliant | DET_GAM_DP.3 is pointed on the positive direction of the SR Z axis, see image. See comment on SU22. |
| SU28 | 128 | The detector plane 2 shall have the detector's surfaces pointed to the SR positive \hat{z} axis of the SR-RM Geometric Body Fixed Reference Frame with a tolerance $<1^\circ$ | RoD | Not Compliant | DET_GAM_DP.2 is pointed on the negative direction of the SR Z axis, see image. See comment on SU22. |

ID: THOR_T_AST_SU_002

Date: 03/07/2023

Issue: 2.0



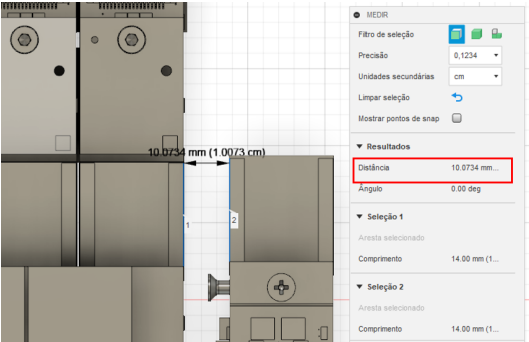
| | | | | | |
|------|-----|---|--------|---------------|--|
| SU29 | 129 | The detector plane 4 shall have the detector's surfaces pointed to the SR positive \hat{z} axis of the SR-RM Geometric Body Fixed Reference Frame with a tolerance $<1^\circ$ | RoD | Not Compliant | GET_GAM_DP.4 is pointed on the negative direction of the SR Z axis, see image. See comment on SU22. |
| SU30 | 130 | The detector plane 2 and 3 shall have a Si detector added to one horizontal extremity, having them both added to the same side. | RoD, I | Compliant | See Annex A. The detectors are switched, the one on top shall be parallel to the ZY plane. |
| SU31 | 131 | The Si detector on plane 2 shall be pointed to the SR positive \hat{z} axis of the SR-RM Geometric Body Fixed Reference Frame with a tolerance $<1^\circ$ | | DELETED | This requirement got deleted. |
| SU32 | 132 | The payload's enclosure shall have 4 holding points on the positive \hat{z} face. | RoD, I | Compliant | Are the holding points removable? The holding/hoisting points are going to be used during integration with SR. They shall be removed for the flight configuration. |



ID: THOR_T_AST_SU_002

Date: 03/07/2023

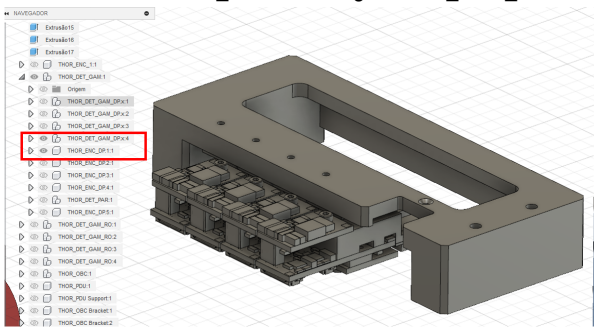
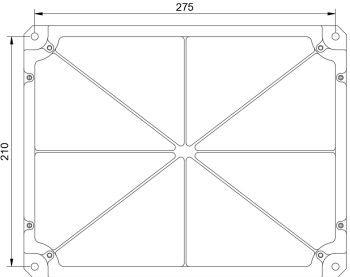
Issue: 2.0

| | | | | | |
|------|-----|---|--------|-----------|---|
| SU33 | 152 | The top surface of the Silicon detector shall be atleast 1cm away from the CdTe top surface. | RoD, I | Compliant |  |
| SU34 | 153 | The surface of the Silicon detector on plane 2 shall be perpendicular to the direction the the negative X axis. | | DELETED | Deleted, See REQ-184 |

ID: THOR_T_AST_SU_002

Date: 03/07/2023

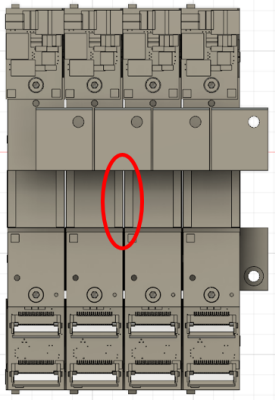
Issue: 2.0

| | | | | | |
|------|-----|---|--------|-----------------|---|
| SU35 | 156 | Each Detector Plane shall have an associated independent mechanical part for mounting purposes. | RoD | Partially - | <p>At the moment the ENC_DP.1 is holding the DET_GAM_DP.4.</p>  |
| SU36 | 157 | The experiment shall be mounted to the Aluminium adaptor using M6 drill with 58mmx58mm spacing. | RoD, I | Not Compliant - | <p>The Distance between the Holding holes are not a multiple of 58. $275/58 = 4,7$ $210/58 = 3,6$</p>  |

ID: THOR_T_AST_SU_002

Date: 03/07/2023

Issue: 2.0

| | | | | | |
|------|-----|--|--------|---------------|---|
| SU37 | 158 | The experiment housing shall have ETHERNET plug for testing purposes. | RoD | Compliant | |
| SU38 | 166 | The P/L shall comply with the mechanical environment of the Vega-C launch, present on the SR-User Guide. | RoD, A | Not Compliant | Mechanical simulations TBD |
| SU39 | 182 | The middle Finger Boards of the Detector Planes shall be horizontally separated by 5mm | RoD, I | Not Compliant | The distance between these middle finger boards (see figure bellow) shall be 5mm, on every Detection Plane  |
| SU40 | 184 | The surface plane of the Silicon detector on plane 2 shall be parallel to the ZY plane. | RoD | Not Compliant | See SU30. |

4. Additional comments

SU41 The code of the PDR version of the enclosure must be THOR_ENC_MAIN. In the document is THOR_EC_MAIN:



SU42 The THOR_DET shall be moved horizontally in the positive Y direction, to be farther away from the negative Y wall (Right wall). The DET shall be more centred.

SU43 The Finger Board mechanical interface may change, I/F ID: MECH_GAM_DP.x.FB.x. ADV is redesigning the module.

SU44 ADV is redesigning the PCB's of the DET_GAM_RO boards instead of having the DET_GAM_RO.x_AB (see 5.4.1.5 from [AD1]). ADV does not expect the dimensions of the DET_GAM_RO.x to change.

SU45 We may select other ENC_KS.x (see Item ID SU18 from this document). It might 'bump' into neighbouring payloads. We will clarify this issue with ESA SR team.

SU46 We will be using the Ethernet plug for testing purposes. It seems like that the plug cannot be used from inside because of the PDU Support Plate.

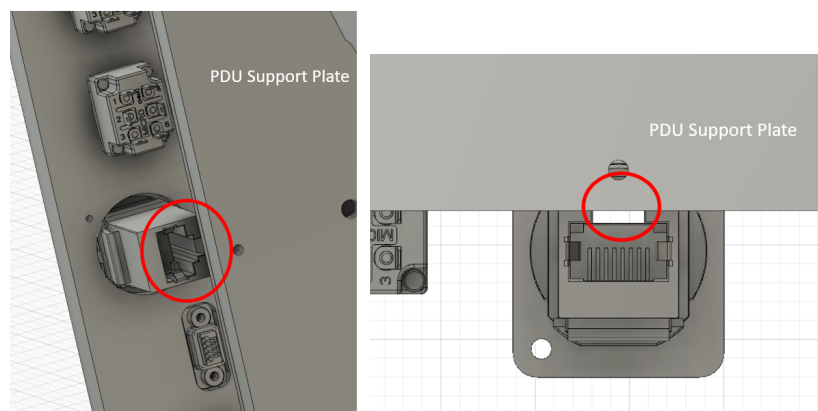
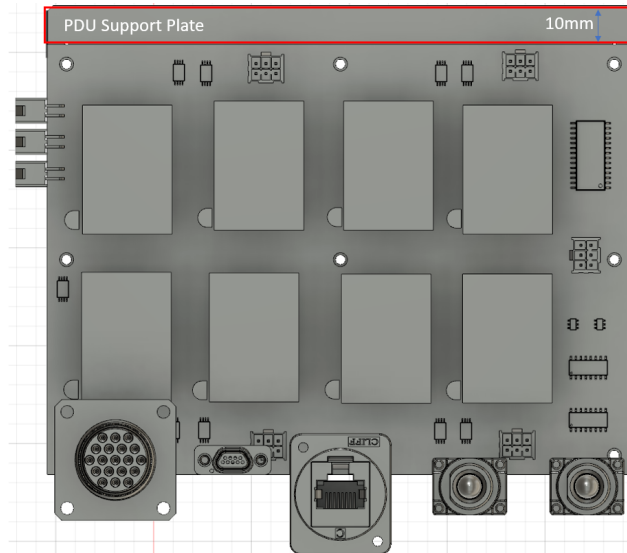


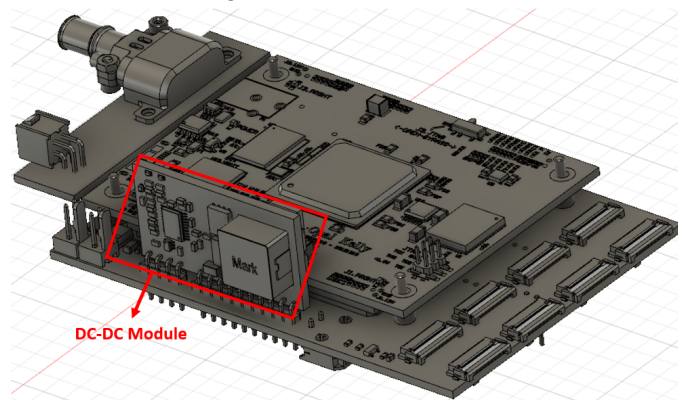
Fig3.1 Ethernet RJ45 plug obstructed

If the PDU Support Plate were 2mm smaller, the obstruction of the Ethernet Plug would be avoided. For instance. The 10mm evidenced on the FigX.x should be reduced to 8 mm or 7mm. Is this viable?

Also note that we can change a little bit the size of the PDU. Tell us if that would be a better solution.



SU47 The DCDC module of the DET_GAM_RO.x boards will be integrated into the main PCB's of the DET_GAM_RO.x. The overall height of the RO boards will decrease.



3.1 Preliminary Thermal Analysis

See [RD3] for the thermal requirements specification for SR. Don't consider the effect of solar exposure. Perform thermal analysis for the following cases (baseline):

One iteration of the thermal analysis is enough for this stage of design.

- SR interface at 15°C - see the stabilized temperature of the P/L components, with the components consuming the Máx 15% and nominal 15%;

ID: THOR_T_AST_SU_002

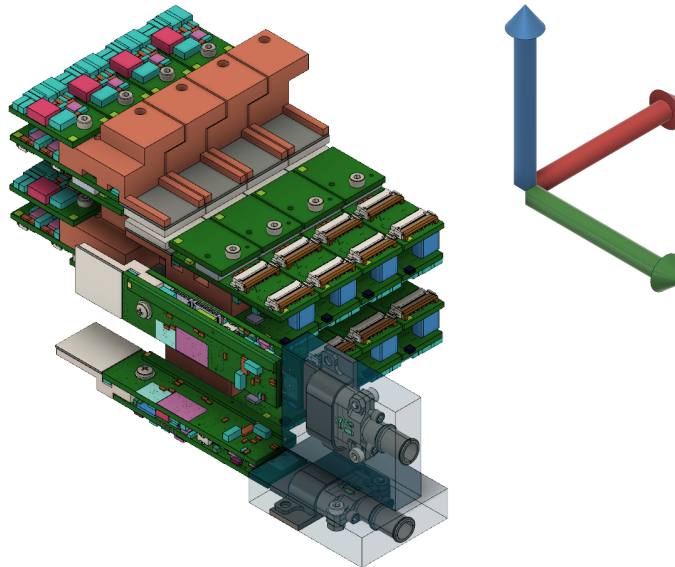
Date: 03/07/2023

Issue: 2.0

- SR interface at 40°C - see the stabilized temperature of the P/L, with the components consuming the Máx 15% and nominal 15%;
- SR interface at 15°C - see the stabilized temperature with all the components turned OFF;
- SR interface at 40°C - see the stabilized temperature with all the components turned OFF;

Annex A.

Detector Unit Requested Configuration



Implementation of the REQ-182 from [AD1] still missing

Appendix G

LIP-AST meeting PDR design discussion

This Appendix showcases the minute of a meeting between LIP and AST discussing the enclosure PDR design. Some design changes were already identified and they will be implemented between PDR and CDR.

ID: THOR_M_AST_D_003

Date: 14/07/2023

Issue: 1.0



LABORATÓRIO DE INSTRUMENTAÇÃO
E FÍSICA EXPERIMENTAL DE PARTÍCULAS
partículas e tecnologia



| | | |
|------------------------------|-------------------------|--------------------|
| Entities: LIP and AST | | |
| Project: THOR-SR | | |
| Local: Online | Date: 14/07/2023 | Time: 10:00 |
| Subject: | | |
| Participants: | | |
| | | |
| | | |
| | | |
| Reference documents: | | |
| [1] THOR_T_AST_SU_002 | | |
| | | |

| Nº | Subject | Action Resp. | Date |
|--------------------------|---|--------------|------|
| MEETING OBJECTIVE | | | |
| | - Efetuar uma revisão ao design e ao vosso feedback no ficheiro (THOR_T_AST_SU_002) | | |

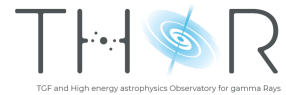
ID: THOR_M_AST_D_003

Date: 14/07/2023

Issue: 1.0



LABORATÓRIO DE INSTRUMENTAÇÃO
E FÍSICA EXPERIMENTAL DE PARTÍCULAS
partículas e tecnologia



| | | | |
|--------------------------|--|--|--|
| | <ul style="list-style-type: none">- Validar componente a componente a sua localização e a necessidade de dissipação em cada um para fechar a caracterização para as análises térmicas.- Rever timeline e deliverables timeline | | |
| DISCUSSION TOPICS | | | |
| DT1 | Nota: AST diz que um requirement é compliant quando o RoD é cumprido. LIP vai ter em consideração nas seguintes iterações do documento 'Status Update' | | |
| DT2 | SU3 [1] <ul style="list-style-type: none">• AST tem uma massa de 3,7kg para a Enclosure - NÃO ACEITAVEL• O budget limite para a Payload TOTAL é de 3kg.• AST propôs diminuir a espessura das paredes para 1mm - pode haver problema com a fabricação - AST vai confirmar.• LIP diz que quanto mais fina a estrutura melhor são as medições científicas.• AST referiu que ainda existe espaço livre não utilizado dentro do volume útil - existe ainda alguma margem de manobra quanto à redistribuição dos produtos e portanto o volume total pode vir a diminuir e conseqüentemente diminuição da massa da estrutura. | | |
| DT3 | SU4 [1] <ul style="list-style-type: none">• AST referiu que o requisito é automaticamente compliant.• Para AST fazer uma boa simulação térmica:<ul style="list-style-type: none">○ Resistência térmica dos integrados;○ Ou LIP fornece dados ou fornece Datasheet e potência dissipada por integrado. | | |

ID: THOR_M_AST_D_003

Date: 14/07/2023

Issue: 1.0



LABORATÓRIO DE INSTRUMENTAÇÃO
E FÍSICA EXPERIMENTAL DE PARTÍCULAS
partículas e tecnologia



THOR
TGF and High energy astrophysics Observatory for gamma Rays

| | | | |
|------|---|--|--|
| | <ul style="list-style-type: none">○ AST necessita de uma BOM dos componentes ativos, potência dissipada e ciclo de operações.● Caso seja necessário arrefecimento ativo, AST propõe utilizar heat pipes para dissipação por contacto nos componentes críticos (fácil implementação). | | |
| DT4 | SU8 [1] <ul style="list-style-type: none">● LIP esclareceu que os .5mm é entre os blocos do semiconductor CdTe (cinzento claro)● LIP vai confirmar com ADV o tamanho real do semiconductor CdTe. | | |
| DT5 | SU11 [1] <ul style="list-style-type: none">● É compliant, a estrutura vai ser de alumínio. | | |
| DT6 | SU16 [1] <ul style="list-style-type: none">● LIP confirmar qual a espessura required pelo fabricante para a estrutura da enclosure. | | |
| DT7 | SU17/18 [1] <ul style="list-style-type: none">● Para modelo de engenharia esses vão ser os kill switches.● Para o FM, eles vão mudar. | | |
| DT8 | SU26/35 [1] <ul style="list-style-type: none">● Ter atenção à numeração dos subprodutos da estrutura. | | |
| DT9 | SU36 [1] <ul style="list-style-type: none">● Por causa do ponto DT2 o tamanho vai mudar para 232x232 mm² | | |
| DT10 | SU47 [1] <ul style="list-style-type: none">● LIP esclareceu que a distancia vertical das Readout boards vai desaparecer, sendo esse modulo integrado nos PCB's principais. | | |

ID: THOR_M_AST_D_003

Date: 14/07/2023

Issue: 1.0



LABORATÓRIO DE INSTRUMENTAÇÃO
E FÍSICA EXPERIMENTAL DE PARTÍCULAS
partículas e tecnologia



| NEXT MEETING | | | |
|--------------|--|--|--|
| | | | |
| | | | |
| MoM SUMMARY | | | |
| | | | |

| ACTION ITEMS | | | | |
|--------------|--------|------|--------------|--------|
| Nº | Action | Date | Action Resp. | Status |
| 01 | | | | |
| | | | | |